ISSN 2542-1565

Vol. 15 2022 No. 02

GEOGRAPHY ENVIRONMENT SUSTAINABILITY

«The journal GEOGRAPHY, ENVIRONMENT, SUSTAINABILITY was founded in 2008 by Russian Geographical Society, the Lomonosov Moscow State University Geography Department, and the Russian Academy of Sciences Institute of Geography. Since that time the journal publishes **4 issues per year**, containing original research papers and reviews. The journal issues are open source and distributed through subscriptions, library exchanges of leading universities, and via the website through the world»

FOUNDERS OF THE JOURNAL: Russian Geographical Society, Faculty of Geography, Lomonosov Moscow State University and Institute of Geography of the Russian Academy of Sciences

The journal is published with financial support of the Russian Geographical Society.

The journal is registered in Federal service on supervision of observance of the legislation in sphere of mass communications and protection of a cultural heritage. The certificate of registration: ПИ № ФС77-67752, 2016, December 21.

PUBLISHER
Russian Geographical Society
Moscow, 109012 Russia
Novaya ploshchad, 10, korp. 2
Phone 8-800-700-18-45
E-mail: press@rgo.ru
www.rgo.ru/en

EDITORIAL OFFICE
Lomonosov Moscow State University
Moscow 119991 Russia
Leninskie Gory, 1,
Faculty of Geography, 1806a
Phone 7-495-9391552
Fax 7-495-9391552
E-mail: ges-journal@geogr.msu.ru
www.ges.rgo.ru

DESIGN
Layout designer: Tereshkin Anton
Moscow, 115088,
26 Simonovsky Val str., bldg. One
Phone: +7 (903) 108-04-44
E-mail: smile.tai@gmail.com

DOI prefix: 10.24057

Format A4 (210x297mm)

"GEOGRAPHY, ENVIRONMENT, SUSTAINABILITY" is the only original English-language journal in the field of geography and environmental sciences published in Russia. It is supposed to be an outlet from the Russian-speaking countries to Europe and an inlet from Europe to the Russian-speaking countries regarding environmental and Earth sciences, geography and sustainability. The main sections of the journal are the theory of geography and ecology, the theory of sustainable development, use of natural resources, natural resources assessment, global and regional changes of environment and climate, social-economical geography, ecological regional planning, sustainable regional development, applied aspects of geography and ecology, geoinformatics and ecological cartography, ecological problems of oil and gas sector, nature conservations, health and environment, and education for sustainable development.

OPEN ACCESS POLICY. "GEOGRAPHY, ENVIRONMENT, SUSTAINABILITY" is an open access journal. All articles are made freely available to readers immediately upon publication. Our open access policy is in accordance with the Budapest Open Access Initiative (BOAI) definition - it means that articles have free availability on the public internet, permitting any users to read, download, copy, distribute, print, search, or link to the full texts of these articles, crawl them for indexing, pass them as data to software, or use them for any other lawful purpose, without financial, legal, or technical barriers other than those inseparable from gaining access to the internet itself.

Date of publication: June 30st, 2022.

EDITORIAL BOARD

EDITORIAL OFFICE

CONTENTS

RESEARCH PAPER

TRAIL IMPACTS IN A TROPICAL RAINFOREST NATIONAL PARK

Erika S. De Almeida[1], Richieri A. Sartori[2]*, André S. Zaú[1]
[1]Federal University of the State of Rio de Janeiro, Av. Pasteur 296, Urca Rio de Janeiro, RJ, 22290-250, Brazil
[2]Pontifical Catholic University of Rio de Janeiro (PUC-Rio), Rua Marquês de São Vicente, 225, Gávea - Rio de Janeiro, RJ, 22451-900, Brazil
***Corresponding author:** richierisartori@puc-rio.br
Received: April 2nd, 2021 / Accepted: April 24th, 2022 / Published: June 30th, 2022
https://DOI-10.24057/2071-9388-2021-036

ABSTRACT. Generally considered a sustainable economic activity, tourism can generate environmental deterioration due to a lack of planning. In this case, the edge effect is utilized to assess the degree of human interference in the environment. Although the Atlantic Forest is known as a hotspot because of its high species richness and endemism, it is also a threatened biome. In this context of anthropogenic pressure, our work assesses the edge-interior gradient in the regenerating forest based on the physical characteristics of vegetation and floristic composition, in addition to providing overall guidelines to effectively assist in its management. For this study, 30 plots of 25 m^2 (10 m x 2.5 m) equally distributed among the edges of trails and locations 20 and 40 m away from them were established, with the greatest length measured parallel to the edge of the tracks. Overall, 443 individuals of 122 species were investigated. More than 60 of them were endemic to Brazil, 13.3% were threatened and 9.1% were widely distributed species. Some species were present at all distances from the trails, others co-occurred, but the majority were exclusive to a single plot category. Differences in species diversity were also observed with an increasing trend in dominance at the edges of trails along with a decreased richness at the same distance.

KEYWORDS: trail disturbance, ecotourism, edge effect, forest fragmentation, habitat modification, Tijuca Forest

CITATION: Almeida E.S., Sartori R.A., Zaú A.S. (2022). Trail Impacts In A Tropical Rainforest National Park. Geography, Environment, Sustainability, 2(15), 5-12.
https://DOI-10.24057/2071-9388-2021-036

ACKNOWLEDGEMENTS: We thank Vinicius Gomes da Costa for help in all fieldworks in TNP. We also thank Alice Sá Rego de Azevedo, Aline Silva Machado, Gláucia Maria Alves de Oliveira e Gustavo Alves Cunha Martins for help in fieldwork. A special thanks to Andrew Merchant (University of Sydney) for helpful comments on the manuscript. We would also like to thank the staff of ICMBio (Instituto Chico Mendes de Conservação da Biodiversidade) who works in Tijuca National Park. This work was partially supported by Brazilian science foundation FAPERJ (Fundação de Amparo à Pesquisa do Estado do Rio de Janeiro), and CNPq/UNIRIO (Conselho Nacional de Desenvolvimento Científico e Tecnológico). ICMBio authorization 15160. Conflicts of interest: none.

Conflict of interests: The authors reported no potential conflict of interest.

INTRODUCTION

Tourism is an extremely important economic activity that experiences significant growth (Dushkova and Ignatieva 2020; Geffroy et al. 2015; Lu and Nepal 2009). Meanwhile, the same authors as well as Montagnini and Jordan (2005) give evidence that inadequate tourism administration aggravates environmental deterioration. Consequently, the utilization of public space together with ecotourism requires appropriate zoning (Pickering and Hill 2007; Sun and Walsh 1998; Walter 2013; Zaú 2014).

Trail impact is defined here as an alteration in any component of the environment, be it partial or total, that modifies interaction between species and the ecosystem dynamics. These disturbances directly or indirectly affect both man and the environment (Montagnini and Jordan 2005).

The Atlantic Forest is known for its elevated species diversity and endemism and is already an eminently threatened forest (e.g. Laurance 2009; Myers et al. 2000; Ribeiro et al. 2009; Teixeira et al. 2009). It is a hotspot biome that currently barely covers 12% of its original area with less than 20% of the fragments larger than 50 ha (Metzger 2009; Ribeiro et al. 2009). Brokaw (1985) indicates that subtle changes in the Atlantic Forest could provoke numerous diffuse transformations in the forestry dynamics. In this case, interconnected microclimatic alterations will occur every time when a natural or anthropogenic forest clearing is opened (e. g. Harper et al. 2005; Kapos 1989). The areas within these gaps of the canopy, as a result, have their solar incidence amplified (Nobis and Hunziker 2005).

Another problem concerns forest edges. Showed by Harris (1980) and Murcia (1995), the edge effect is a phenomenon that occurs at the interface of distinct biomes, and its study is used to evaluate the anthropogenic impact of trails or linear clearings for road and powerline infrastructure in a forest (e.g. Goosem 1997; Pohlman et al. 2007; Spellerberg 1998). According to the studies conducted in tropical forests, edges frequently show these effects due to differentiation and edge-interior vegetation gradients, especially in

relation to microenvironmental conditions (Kapos 1989), vegetal structure, biotic composition, and its interactions (e. g. Bierregaard et al. 2001; Laurance and Yensen 1991). Unfortunately, environmental transformation along the lines integrated into ecotourism still lacks knowledge and clarity in understanding the dynamics as a whole (Zaú 2014).

Due to the lack of knowledge on the existence or magnitude of the impact of walking trails in the mentioned conditions, the objectives of this work were to evaluate the regenerating forest stratum, aiming to contribute to planning activities and management of conservation units. This paper seeks to answer the following questions: Are there trail-associated alterations in the shrubby/arboreal-regenerating stratum? What are the most appropriate indicators for efficiently evaluating and monitoring the impact of public use: vegetation physical parameters or species composition?

METHODOLOGY

Study Site

The investigated area is an Atlantic Forest fragment of Tijuca National Park (TNP) (22º55'-23º00'S, 43º11'-43º19'W, Rio de Janeiro, Brazil – Figure 1). It is located inside the urban city center of Rio de Janeiro and is currently the most visited National Park, in Brasil with more than three million visitors each year (Parque Nacional da Tijuca, 2017). Moreover, TNP is a Conservation Unit of Full protection with an area of about four thousand hectares, and an altitude range from 80 m up to 1,021 m (ICMBIO 2008). According to the Köppen classification, it is characterized by a Humid Tropical climate, with «Tropical Monsoon (Am)» up to an altitude of 500 m, and a «Temperate climate, without dry season (Cf)» above this altitude (Coelho-Netto et al. 2007). Mean annual precipitation generally exceeds 2,000 mm, while the mean temperature is 23.8 ºC and relative humidity is 72% (Zaú 2010). Furthermore, the Massif is formed by gneiss, granite and blocks with intensely leached soils and the predominance of latosol, lithosol and cambisol in the mid-upper part of the area, and podzolic soil in the lower part (Coelho-Netto et al. 2007).

Sampling Design And Data Collection

30 plots of 10 m x 2.5 m were established in the sector «A» of TNP for sampling shrubby/arboreal-regenerating components, which included all the individuals with the stem diameter at breast height (DBH, about 1.3 meters from soil) between 10 mm and 50 mm. The plots were always defined in the hillside stretch above the tracks with the greatest length measured parallel to their edge. The allocation of sampling units was based on a random raffle of pre-defined locations which were identified as feasible for sampling from the baseline cartographic analyses (Instituto Pereira Passos 2004). To avoid spatial pseudo replications (Hurlbert 1984) and minimize sampling distortion, the locations were situated at least 50 m away from rivers and water springs, roads and clearings. Ten plots were defined on the edge of trails (0 m), ten within 20 m of the trails, and ten within 40 m of the trails, with the last category considered as the forest's interior (Harper et al. 2005; Laurance et al. 2002).

Data Analysis

After collecting all the data, several variables were defined to run statistical analysis of each plot: height (m), basal area (mm^2; calculation done from DBH), the density of alive/dead individuals (individuals per m^2), number of tillers, width of the trail (m), declivity (º), slope/trail orientation and altitude (m). The statistics package «R» (R Development Core Team 2020) was used to form Venn's diagrams. Additionally, GraphPad Prism v.6 (Graphpad 2012) was applied to conduct normality and homoscedasticity tests, as well as for univariate statistics comparisons. In the latter, the variables with parametric characteristics had ANOVA counter measures, whilst the remaining were submitted to the non-parametric equivalent – Kruskal-Wallis «H» test. PAST v4.03 (Hammer et al. 2001) was used to compare data between the different sampled distances, estimate diversity and perform multivariate analysis.

RESULTS

Species Response

Overall, 122 different species distributed among 68 Genus and 34 Families were found from 443 investigated individuals. The species can be divided into two groups: A - *infrequent,* with 58 species that were observed at only one plot out of 30; and B - *frequent*, with 64 species. Taking both groups into account, 51 species were detected at the edge of trails (T0), 67 species – at 20 m (T20), and 68 species – in the forest's interior (T40). Some species were noticed at all distances, few others co-occur, but the majority are exclusive to a single plot category. In the *frequent* group, there was a total of two species from T0, five species from T20, and 11 species from T40 (Fig. 2).

Fig. 1. In the left: the location of the city of Rio de Janeiro with Tijuca National Park in red; In the right: Tijuca National Park boundaries. «X» marks the location of unit samples. Font: http://earth.google.com. 2022

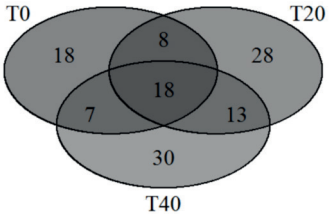

Fig. 2. Venn's diagram with all species found at each distance

The main species (n = 36), *Eriotheca pentaphylla (Vell. & K.Schum.)* A.Robyns, was dominant at T0 and T20 and appeared at only one plot of T40. The third (n = 23), 11th (n = 9), 19th (n = 7) and 20th (n = 7) most prevalent species, *Faramea occidentalis (L.) A.Rich., Erythroxylum citrifolium A.St.-Hil., Myrcia splendens (Sw.) DC.* and *Blepharocalyx salicifolius (Kunth) O.Berg*, respectively, were absent from T0. On the other hand, the 7th most frequent species (n = 12), *Bathysa stipulata (Vell.) C.Presl*, was found only at T0, whilst the 12th most prevailing species (n = 9), *Eugenia batingabranca Sobral*, appeared only at T20. The 13th (*Eugenia florida DC.*) and 15th (*Swartzia simplex (Sw.)* Spreng.) were absent from T40, and 14th (*B. mendoncaei*) was missing from T20 (Appendice). Finally, the 20 most common species represented 59.1% of all individuals (n = 262) and the standing dead individuals corresponded to 6.1% (n = 27).

Analyzing floristic composition, we recognized a total of 110 species, with the other 12 being classified at the genus level. Furthermore, no exotic species were found and 70 species were endemic to Brazil, which corresponds to 63.6% of the total. Additi onally, we also identified two native species from the Amazon, which although they are native to Brazil, are not native to the Atlantic Forest biome: *Coupeia subcordata Benth*. ex Hook.f and *F. occidentalis* (L.) A. Rich. Also, based on Oliveira-Filho & Fontes (2000), nine supertramp species were recognized (n = 40): *Cabralea canjerana* (Vell.) Mart., *Endlicheria paniculata* (Spreng.) J.F.Macbr., *E. citrifolium, E. florida, Guapira opposita* (Vell.) Reitz, *Guarea guidonia* (L.) Sleumer, *Matayba guianensis Aubl., Maytenus communis Reissek, Roupala brasiliensis Klotzsch*. The average species density for each plot category was slightly different with 0.204 species/m^2 for the edge of trails, 0.268 species/m^2 for 20 m, and 0.272 species/m^2 for the interior of the forest (T40).

Six of the identified species were included in the IUCN Red List of Threatened Species (2017): two with «Lower Risk» which are «conservation dependent», three «Vulnerable» and one «Endangered». Also, two species were listed in IBAMA's National Official List of Threatened Species (MMA 2014): one was classified as «Vulnerable», and one as «Endangered» whose presence in this list is constant (Annex 1).

Descriptive And Univariate Analyses

The tracks referring to the studied sections of Tijuca National Park have a minimum width of 0.79 m and a maximum of 2.21 m. Therefore, their average width of 1.28 m (±0.34) shows 26% variation (n=30[1]).

In terms of physical characteristics, the studied shrub/arboreal-regenerating stratum reflects an evolved maturity stage of cover from the same community (Zaú 2010). The average altitude and slope inclination are typical attributes of the regional mountainous relief (Tab. 1; Fig. 3). However, no significant differences in the investigated characteristics were noticed when comparing the physical aspects of the studied segments and the environmental attributes between the assessed intervals (T0, T20 and T40). According to the Kruskal-Wallis H test for medians of abundances, we cannot say that there are significant differences between the three distances analyzed, despite the borderline value of «p» (H=5.084; Hc-tie corrected=5.964; p=0.0507).

In contrast, the Shannon diversity t-test applied for sample units at different distances, reveals significant differences when comparing T0 (the edge of trails) with T20 (t=-3.655; p≤0.001) and T40 (t=-2.939; p=0.004). However, no significant differences were found when comparing T20 and T40 (t=0.653; p=0.514).

Multivariate Analyses

The Non-Metric Multidimensional Scaling (NMDS) using Euclidean distance as a similarity measure for the abundance data of the total number of species in each plot category showed a valid result (stress=0.1567) (Fig. 4). The analysis produced a graphic representation of the first three axes (or coordinates), which «explain» about 86% of the distribution of sampling units in multidimensional space. Axes 1 and 2, which are graphically represented, «explain» 75% of the data distribution. Axis 3 (not graphically represented) «explains» another 11%, and other axes, not measured individually, are responsible for the remaining 14% of data variability. (Fig. 5).

The similarity analyses carried out from 9999 permutations do not allow us to state that there are significant differences between the sets of species and their abundance at various distances to the trails (T0; T20; T40) (ANOSIM with the measured distance by the Bray-Curtis index: R=-0.0042; p=0.5072; NPMANOVA with the distance measured by the Bray-Curtis index: F=1.034; p=0.3979). Additionally, no significant differences were identified in the floristic composition when examining the regenerating stratum at the three distances (Attachment 1).

Table 1. Average physical characteristics of individuals from regenerating stratum and average environmental characteristics at the locations of sample units. Tijuca National Park, Rio de Janeiro, RJ. 2013. In which: H = height; BA = basal area; AD = absolute density; TD = tiller density; DD = density of dead individuals standing; Dcl. = slope declivity; Alt. = altitude; SD = standard deviation; CV = coefficient variation; n = number of sample repetitions

	H (m)	BA (mm)	AD (ind. m^2)	TD (ind. m^2)	DD (ind. m^2)	Dcl. (º) 28	Alt. (m) 621
Average (±SD) =	3.35 (±1.27)	504.11 (±451.57)	0.62 (±0.20)	0.11 (±0.07)	0.02 (±0.03)	(±9)	(±114)
Minimum =	1.40	38.48	0.28	0.00	0.00	5	474
Maximum =	7.50	1,963.50	1.04	0.32	0.12	40	893
CV (%) =	38	90	32	69	164	31	18
n =	443	443	30	30	30	30	30

[1]Each mean was composed of six measurements.

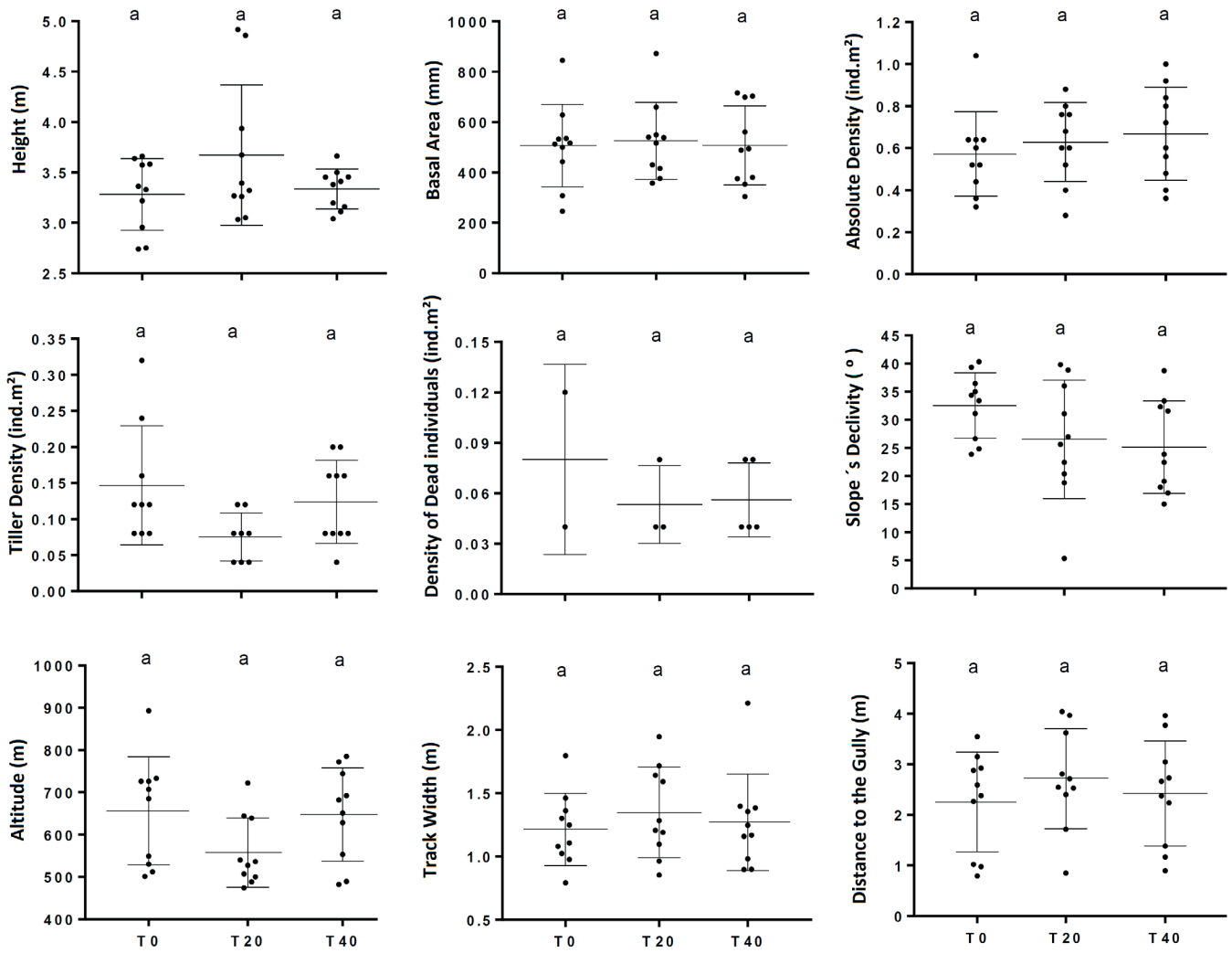

Fig. 3. Characteristics of individuals from regenerating stratum and average environmental characteristics at the locations of sample units. Tijuca National Park, Rio de Janeiro, RJ. 2013. In which: A) height (m); B) basal area (mm); C) absolute density (ind./m²); D) tiller density (ind./m²); E) density of dead individuals standing (ind./m²); F) slope declivity (º); G) altitude (m); H) track width (m); I) distance to the gully (m)

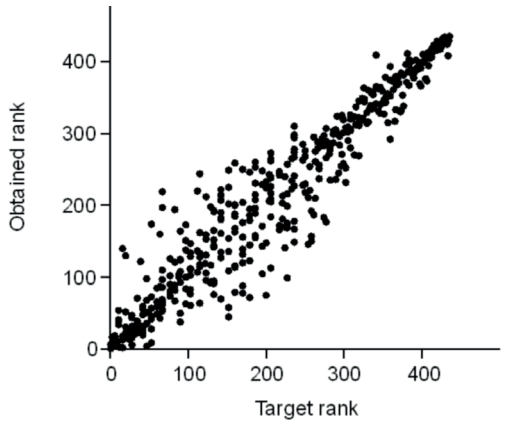

Fig. 4. Shepard stress plot of Non-Metric Multidimensional Scaling (NMDS) from the Euclidian distance, considering abundance data of the regenerating stratum in each sample unit (n=10 per distance), at the edge of trails (0 m); 20 and 40 m of the trails. Stress = 0.1567. Tijuca National Park, Rio de Janeiro, RJ. 2013

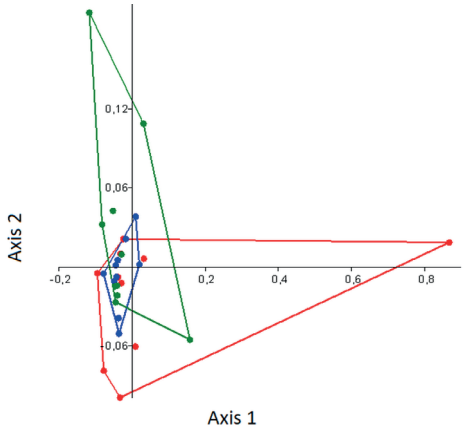

Fig. 5. Non-Metric Multidimensional Scaling (NMDS) from the Euclidian distance, considering abundance data of the regenerating stratum in each sample unit (n = 10 per distance) where in red are values from the edge of trails; in blue for 20 m; and in green for the interior of the forest. Stress = 0.1567; Axis 1 = 0.5435; Axis 2 = 0.2107; Axis 3 = 0.1079. Tijuca National Park, Rio de Janeiro, RJ. 2013

Despite this, we observed a difference between the curves of species accumulation at the edge of trails (T0) and at the distances T20 and T40 (Fig. 6). Differences were also found in the Shannon (H') and Brillouin alpha diversity indices when comparing the abundance of individuals of different species at various distances from the trails (Fig. 7).

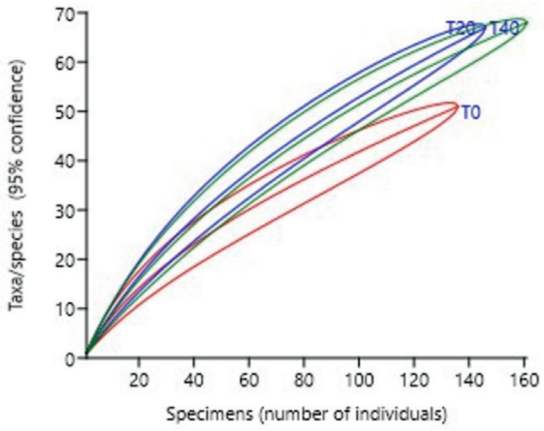

Fig. 6. Rarefaction or accumulation curves of the number of individuals by the number of species at different distances from the trails (T0 in red; T20 in blue; T40 in green). The center curves for each color represent the data for each distance. Polygons of the same colors bordering the center lines represent 95% confidence intervals. Tijuca National Park, Rio de Janeiro, RJ. 2013

DISCUSSION

Based on the analysis of physical variables, no harmful impact on the vegetation structure was detected at the regenerating stratum of the studied stretches as a consequence of the park's public use. However, the lack of differences could be integrated with a larger set of variables, which can occasionally diverge from the examined parameters.

As it was noticed in other studies (e.g. Giulietti et al. 2005; Guedes-Bruni et al. 2009; Murray-Smith et al. 2009; Myers et. al. 2000; Oliveira-Filho and Fontes 2000) and evidenced in this investigation, high floristic diversity is common in multifaceted ecosystems such as the Atlantic Forest. Although certain distinction in the investigated physical components was found, floristic composition implies a relative impact. Shannon diversity «t» tests, Rarefaction Curves and Alpha Diversity Analyzes for Shannon (H') and Brillouin indices, comparing the abundance of individuals of different species at various distances from the trails (T0, T20, T40) suggest that there are differences in the sets of

Table 2. Permutation index of species diversity indicators of the regenerating stratum (dap ≥ 1.0 ≤ 5.0 cm) for various distances from the edge. Tijuca National Park, RJ

Permutation index	T0	T20	Perm p(eq)	T0	T40	Perm p(eq)	T20	T40	Perm p(eq)
Taxa S	51	67	0.02*	51	68.00	0.06	67	68	0.95
Individuals	136	146	<0.00*	136	161.00	<0.00*	146	161	<0.00*
Dominance	0.06	0.03	<0.00*	0.1	0.04	0.01*	0.0	0.0	0.16
Shannon H	3.4	3.9	<0.00*	3.4	3.8	0.01*	3.9	3.8	0.57
Evenness e^H/S	0.6	0.7	<0.00*	0.6	0.6	0.24	0.7	0.6	0.22
Simpson Index	0.94	0.97	<0.00*	0.9	1.0	0.01*	1.0	1.0	0.16
Menhinick	4.4	5.5	0.03*	4.4	5.4	0.07	5.5	5.4	0.76
Margalef	10.2	13.2	0.01*	10.2	13.2	0.05*	13.2	13.2	1.00
Equitability J	0.86	0.92	<0.00*	0.9	0.9	0.08	0.9	0.9	0.21
Fisher alpha	29.6	47.94	0.05*	29.6	44.4	0.1	47.9	44.4	0.72
Berger-Parker	0.16	0.07	<0.00*	0.2	0.1	0.02*	0.1	0.1	0.10

The reduced dominance, together with the verified high species richness, are characteristics of a complex ecosystem in a well developed or mature successional stage (Tab. 2). Conversely, considering all distances, Chao 2 richness estimator indicates the existence of 187 species (SD = ±20.9), with a minimum of 166 species, which confirms the richness elevation model found in this study. Moreover, Jackknife 1 shows a value of 172.7 (SD = ±7.4), Jackknife 2 displays 193.3 and the Bootstrap value is 145.6.

species that are found in the vicinity of the trails compared to the other distances. The NMDS corroborates this result as it showed different distributions for each plot category regardless of the overlap among the three distances (Fig. 4). Furthermore, 18 unique species were found in the edge plots, i.e., ten species less than at 20 m and 12 species less than in the forest interior.

The most frequent species from this study (Eriotheca pentaphylla) dominated in T0 and T20 and was present

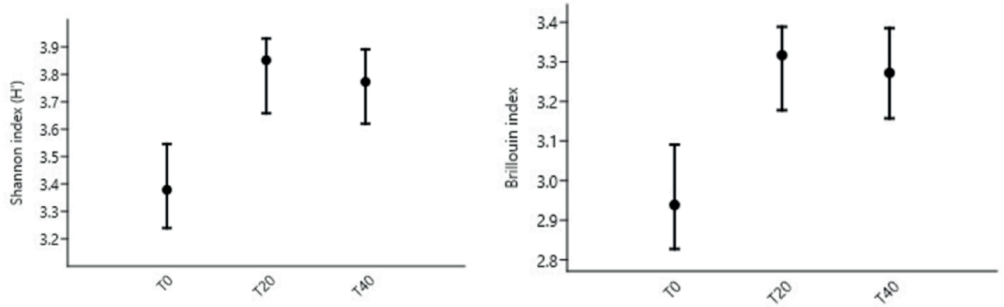

Fig. 7. Shannon (H') and Brillouin alpha diversity indices comparing the abundance of individuals of different species at various distances from the trails (T0, T20, T40). Tijuca National Park, Rio de Janeiro, RJ. 2013

at only one plot of T40. According to Fischer (1997), this could be due to its silky fibers, which promote high wind (aerodynamic) and water dispersion (lasts up to seven days floating), and maintain humidity in seeds. This could increase survival rates and intensify the number of individuals within the forest. Furthermore, the third most prevalent species was absent from the edge of trails, while the 7th most frequent species existed solely at the edge. No individuals of the 20th most frequent species were found at T40, where Simpson's dominance index is 1.6 times smaller than at the edge of trails. The value at the edges is approximately 2.2 times greater than at a 20 m distance. This can be attributed to trampling next to trails, which may impact plant tissue and result in a general decline in the reproduction of plants and their abundance (Wolf and Croft 2014). Additionally, as described by Pickering and Hill (2007), depending on the resistance and resilience of plants to trampling, the impact can extend even to modifications in the species richness (Bassett et al. 2005; Spellerberg 1998; Wolf and Croft 2014).

Machado (2012) found that there is a substantial difference when comparing the edges above and below roads at the same park. According to his study, as well as the study of Lugo & Gucinski (2000), the areas below roads are characterized by elevated water and sediments flow and higher light incidence, causing a notorious proliferation of exotic species, lower density, and greater dominance. On the other hand, Lugo and Gucinski (2000) explain that the presence of exotic species can be minimized by increasing management during the first years of settlement or by benefiting the development of mature vegetation, thus reducing local disturbance. Consequently, it is indispensable to extend these management techniques to tracks.

Moreover, as Forman and Alexander (1998) claim for roads, fauna tends to avoid linear openings, which act as a barrier and separate populations. Openings also affect the hydrological runoff of a forest, leaching out soil and generating high sedimentation downhill (Forman and Alexander 1998). Spellerberg (1998) and Pickering and Hill (2007) also cited a derivative impact of roads and trails on the transfer of spores along the openings, which increases the risk of pathogenic dispersal and could affect the most threatened species. Visitors can potentially also play the role of dispersers, disseminating seeds along tracks (Pickering and Mount 2010). This could explain the results we found for dominance, which has a slightly higher value at the edge (1.6 - 2.2 times) than in the other two plot categories (interior and T20, respectively).

Besides, the amount of light that penetrates the canopy and reaches the ground can affect ecological dynamics (Bréda 2003; Brokaw 1985). In this context, canopy openings in forest ecosystems can lead to changes in local microclimate (Pohlman et al. 2007), erosion, light availability and, consequently, growth, productivity, water consumption and composition of flora (e.g. Bréda 2003; Kunert et al. 2015). Hence, the assessment of canopy opening should also be included in the analysis of environmental impacts.

CONCLUSION

In conclusion, we did not find any evidence that proves differences in terms of structure when evaluating the regenerating tree and shrubby vegetation. However, differences in species diversity were identified when comparing the edges of trails (T0) with other distances further away (T20 and T40). This implies a disparity in species composition and distribution at the edges and therefore indicates at least a relative impact of trails in the studied site. Additionally, an increasing trend in species dominance was found in sector «A» trails of TNP for the sub-forest layer at the edges of trails with a corresponding decrease in species richness at the same distance. However, we perceive that in order to discern the effects of anthropogenic origin in complex and dynamic environments more accurately, there must be a more profound knowledge of fauna and flora richness, with the species composition being a key analysis in these types of studies. Also, seedlings and trees (DAP <10 mm and >50 mm) should be taken into account in order to have wide-ranging results on forestry composition and its impacts.

The current research also acknowledges that it is fundamental to have an accurate record of daily hikers of each track separately. Subsequently, we suggest that other sectors and segments with a large number of visitors and/or great environmental instability should be thoroughly and frequently examined and monitored. We also point out the importance of recovery and/or constant management of certain segments, possibly in alliance with hikers themselves (i.e. through an eventually developed app). This is especially crucial after heavy rain or strong wind, as some stretches we passed presented fallen trunks, marshes, intense erosion and exotic species (notably jackfruit – Artocarpus heterophyllus Lam., Dracaena fragrans (L.) Ker-Gawl., Bambusa vulgaris Schrad ex Wendl., and Coffea Arabica L.). In general, the emphasis of conservation should be on the greatest forest remnants, as suggested by Ribeiro et al. (2009).

Finally, we believe it is crucial to rigorously consider the Conservation Unit's management plan. Furthermore, in order to perpetuate the prevailing status of the regenerating forest stratum, we suggest that the actual number of visitors on the park's trails should not be increased without an accurate investigation of their carrying capacity. The width of trails should also be preserved and new activities should not be incorporated into the trails without more detailed surveys on their impact.

REFERENCES

Bassett I.E., Simcock R.C. and Mitchell, N.D. (2005). Consequences of soil compaction for seedling establishment: Implications for natural regeneration and restoration. Austral Ecology, 30, 827-833, DOI: 10.1111/j.1442-9993.2005.01525.x.

Bierregaard Jr. R.O., Gascon C., Lovejoy T.E., and Mesquita R.C.G. (Ed.). (2001). Lessons from Amazonia: the ecology and conservation of a fragmented forest. Michigan: Sheridan Books, 475.

Bréda N.J. (2003). Ground-based measurements of leaf area index: a review of methods, instruments and current controversies. Journal of Experimental Botany, 54(392), 2403-2417, DOI: 10.1093/jxb/erg263.

Brokaw N.V.L. (1985). Gap-phase regeneration in a tropical forest. Ecology, 66(3), 682-687, DOI: 10.2307/1940529.

Coelho-Netto A.L., Avelar A.S., Fernandes M.C., and Lacerda W.A. (2007). Landslide susceptibility in a mountainous geoecosystem, Tijuca Massif, Rio de Janeiro: The role of morphometric subdivision of the terrain. Geomorphology, 87(3), 120-131, DOI: 10.1016/j.geomorph.2006.03.041.

Convention on International Trade in Endangered Species of Wild Fauna and Flora (CITES). Checklist of CITES Species. Retrieved Jun. 2017, from http://checklist.cites.org/#/en.

Dushkova D. and Ignatieva M. (2020). New trends in urban environmental health Research: from geography of diseases to Therapeutic landscapes and healing gardens. Geography, Environmental, Sustentability, 13(1), 159-171.

Fischer E.A. (1997). The role of plumes in Eriotheca pentaphylla (Bombacaceae) seed survival in south-eastern Brazil. Journal of Tropical Ecology, 13(1), 133-138.

Forman R.T.T. and Alexander L.E. (1998). Roads and their major ecological effects. Annual Review of Ecology and Systematics, Palo Alto/CA, 29(1), 207-231, DOI: 10.1146/annurev.ecolsys.29.1.207.

Giulietti A.M., Harley R.M., Queiroz L.P., Wanderley M.G.L., and Van Den Berg C. (2005). Biodiversity and Conservation of Plants in Brazil. Conservation Biology, 19(3), 632-639, DOI: 10.1111/j.1523-1739.2005.00704.x.

Goosem M. (1997). Internal fragmentation: the effects of roads, highways, and powerline clearings on movements and mortality of rainforest vertebrates. Tropical forest remnants: ecology, management, and conservation of fragmented communities. University of Chicago Press, Chicago, 241-255.

Graphpad Software. (2012). Graphpad Prism 6.exe. Version 6.00. San Diego, California, USA: GRAPHPAD SOFTWARE. Plataforma Windows. Retrieved 26 Jul. 2013, from http://www.graphpad.com/prism/Prism.htm.

Geffroy B., Samia D.S.M., Bessa E. and Blumstein T. (2015). How nature-based tourism might increase prey vulnerability to predators. Trends in Ecology & Evolution, 30(12), 755-765, DOI: 10.1016/j.tree.2015.09.010.

Guedes-Bruni R.R., Silva A.G., and Mantovani W. (2009). Rare canopy species in communities within the Atlantic Coastal Forest in Rio de Janeiro State, Brazil. Biodiversity and Conservation, 18(2), 387-403, DOI: 10.1007/s10531-008-9497-y.

Hammer O., Harper D.A.T. and Ryan P.D. (2001). PAST: Paleontological Statistic software: package for education and data analysis. Palaeontologia Electronica, 4(1), 9.

Harper K.A., Macdonald E., Burton P.J., Chen J., Brosofske K.D., Saunders S.C. and Esseen P. (2005). Edge influence on forest structure and composition in fragmented landscapes. Conservation Biology, 19(3), 768-782, DOI: 10.1111/j.1523-1739.2005.00045.x.

Harris L.D. (1988). Edge effect and conservation of biotic diversity. Conservation Biology, 2(4), 330-332, DOI: 10.1111/j.1523-1739.1988.tb00196.x.

Hurlbert S.H. (1984). Pseudoreplication and the design of ecological field experiments. Ecological monographs, 54(2), 187-211, DOI: 10.2307/1942661.

ICMBio. (2008). Plano de manejo [Management plan]. Parque Nacional da Tijuca. Rio de Janeiro. Retrieved 22 Jul. 2013, from http://www.corcovado.org.br/manejo.php.

Instituto Pereira Passos. (2004). Floresta da Tijuca: Mapa Turístico Plani-Altimétrico [Tijuca's Forest: Touristic Plani-Altimetric Map]. Rio de Janeiro. Escala 1:7.500.

The IUCN Red List of Threatened Species. (2017). Retrieved Jun. 2017, from http://www.iucnredlist.org/.

Kapos V. (1989). Effects of isolation on the water status of forest patches in the Brazilian Amazon. Journal of Tropical Ecology, 5(2), 173-185, DOI: 10.1017/S0266467400003448.

Kunert N., Aparecido L.M.T., Higuchi N., Dos Santos J. and Trumbore S. (2015). Higher tree transpiration due to road-associated edge effects in a tropical moist lowland forest. Agricultural and Forest Meteorology, 213, 183-192, DOI: 10.1016/j.agrformet.2015.06.009.

Laurance W.F. (2009). Preface: Conserving the hottest of the hotspots. Biological Conservation, 142, 1137, DOI: 10.1016/j.biocon.2008.10.011.

Laurance W.F., Lovejoy T.E., Vasconcelos H.L., Bruna E.M., Didham R.K., Stouffer P.C., Gascon C., Bierregaard R.O., Laurence S.G and Sampaio E. (2002). Ecosystem decay of Amazonian forest fragment: a 22-year investigation. Conservation Biology, 16(3), 605-618, DOI: 10.1046/j.1523-1739.2002.01025.x.

Laurance W.F. and Yensen E. (1991). Predicting the impacts of edge effects in fragmented habitats. Biological Conservation, 55(1), 77-92, DOI: 10.1016/0006-3207(91)90006-U.

Lugo A. and Gucinski H. (2000). Function, effects and management of forest roads. Forest Ecology and Management, Amsterdam, 133(3), 249-262, DOI: 10.1016/S0378-1127(99)00237-6.

Lu J. and Nepal S.K. (2009). Sustainable tourism research: an analysis of papers published in the Journal of Sustainable Tourism. Journal of Sustainable Tourism, 17(1), 5-16, DOI: 10.1080/09669580802582480

Machado A.S. (2012). Efeitos de borda de estradas sobre a comunidade arbóreo-arbustiva de um trecho urbano de Floresta Atlântica [Edge effects of roads on the arboreal-shrub community of an urban stretch of the Atlantic Forest]. 82 p. Dissertation tasys (Master degree in Botany) – Botanical Garden of Rio de Janeiro Research Institute.

Metzger J.P. (2009). Editorial: Conservation issues in the Brazilian Atlantic forest. Biological Conservation, 142, 1138-1140, DOI: 10.1016/j.biocon.2008.10.012.

Millennium Ecosystem Assessment. (2005). Ecosystems and human well-being: biodiversity synthesis. Island Press.

Ministério do Meio Ambiente - MMA. (2014). Lista Nacional Oficial de Espécies da Flora Ameaçadas de Extinção [National Official List of Endangered Species of Flora]. Retrieved Jun. 2017, from http://www.mma.gov.br/biodiversidade/especies-ameacadas-de-extincao/atualizacao-das-listas-de-especies-ameacadas.

Montagnini F. and Jordan C.F. (2005). Tropical Forest Ecology: The Basis for Conservation and Management. Netherlands: Springer Berlin.

Murcia C. (1995). Edge effects in fragmented forests: implications for conservation. Trends in Ecology and Evolution, 10(2), 58-62, DOI: 10.1016/S0169-5347(00)88977-6.

Murray-Smith C., Brummitt N.A., Oliveira-Filho A.T., Bachman S., Moat J., Lughadha E.M.N. and Lucas E.J. (2009). Plant Diversity Hotspots in the Atlantic Coastal Forests of Brazil. Conservation Biology, USA, 23(1), 151-163, DOI: 10.1111/j.1523-1739.2008.01075.x.

Myers N., Mittermeier R.A., Mittermeier C.G., Da Fonseca G.A.B. and Kent J. (2000). Biodiversity hotspots for conservation priorities. Nature, Londres, 403(6772), 853-858, DOI: 10.1038/35002501.

Nobis M. and Hunziker U. (2005). Automatic thresholding for hemispherical canopy-photographs based on edge detection. Agricultural and Forest Meteorology, 128(3), 243-250, DOI: 10.1016/j.agrformet.2004.10.002.

Oliveira-Filho A.T. and Fontes M.A.L. (2000). Patterns of Floristic Differentiation among Atlantic Forests in Southeastern Brazil and the Influence of Climate. Biotropica, 32(4b), 793-810, DOI: 10.1646/0006-3606(2000)032[0793:POFDAA]2.0.CO;2.

Parque Nacional Da Tijuca. (2017). Retrieved Jun. 2017, from http://www.parquedatijuca.com.br.

Pickering C. and Hill W. (2007). Impacts of recreation and tourism on plant biodiversity and vegetation in protected areas in Australia. Journal of Environmental Management, 85, 791-800, DOI: 10.1016/j.jenvman.2006.11.021.

Pickering, C. and Mount A. (2010). Do tourists disperse weed seed? A global review of unintentional human-mediated terrestrial seed dispersal on clothing, vehicles and horses. Journal of Sustainable Tourism, 18(2), 239-256, DOI: 10.1080/09669580903406613.

Pohlman C.L., Turton S.M. and Goosem M. (2007). Edge effects of linear canopy openings on Tropical rainforest understory microclimate. Biotropica, 39(1), 62-71, DOI: 10.1111/j.1744-7429.2006.00238.x.

R Development Core Team (2020). R: a language and environment for statistical computing. R Foundation for Statistical Computing, Vienna, Austria. ISBN 3-900051-07-0, http://www.R-project.org.

Ribeiro M.C., Metzger J.P., Martensen A.C., Ponzoni F.J. and Hirota M.M. (2009). The Brazilian Atlantic Forest: How much is left, and how is the remaining forest distributed? Implications for conservation. Biological Conservation, 142(6), 1141-1153, DOI: 10.1016/j.biocon.2009.02.021.

Ruhanen L., Weiler B., Moyle B.D. and McLennan C.J. (2015). Trends and patterns in sustainable tourism research: a 25-year bibliometric analysis. Journal of Sustainable Tourism, 23(4), 517-535, DOI: 10.1080/09669582.2014.978790.

Municipal Secretary of Environment - SMAC. Caracterização Ambiental: Espécies ameaçadas de extinção [Environmental Characterization: Threatened species of extinction]. Retrieved Jun. 2017, from http://portalgeo.rio.rj.gov.br/protocolo/Indicadores_capitulos/[20-IA_Part2_IndAmbientais_CaractAmb_2-4].pdf.

Spellerberg I. (1998). Ecological Effects of Roads and Traffic: A Literature Review. Global Ecology and Biogeography, Oxford, 7(5), 317-333, DOI: 10.1046/j.1466-822x.1998.00308.x.

Sun D. and Walsh D. (1998). Review of studies on environmental impacts of recreation and tourism in Australia. Journal of Environmental Management, 53, 323-338, DOI: 10.1006/jema.1998.0200.

Teixeira A.M.G., Soares-Filho B.S., Freitas S.R. and Metzger J.P. (2009). Modeling landscape dynamics in an Atlantic Rainforest region: Implications for conservation. Forest Ecology and Management, 257, 1219-1230, DOI: 10.1016/j.foreco.2008.10.011.

Walter P.G. (2013). Theorising visitor learning in ecotourism, Journal of Ecotourism, 12:1, 15-32, DOI: 10.1080/14724049.2012.742093.

Wolf I.D. and Croft D.B. (2014). Impacts of tourism hotspots on vegetation communities show a higher potential for self-propagation along roads than hiking trails. Journal of Environmental Management, 143, 173-185, DOI: 10.1016/j.jenvman.2014.04.006.

Zaú A.S. (2010). Composição, estrutura e efeitos de bordas lineares na comunidade arbustiva-arbórea de um remanescente urbano de Mata Atlântica no sudeste do Brasil [Composition, structure and linear edge effects in the shrub-tree community of an urban remnant of the Atlantic Forest in south-eastern Brazil]. 229 p. Tesis (PhD in Botany) - Instituto de Botanical Garden of Rio de Janeiro Research Institute.

Zaú A.S. (2014). A conservação de áreas naturais e o Ecoturismo [Natural areas conservation and ecotourism]. Revista Brasileira de Ecoturismo, 7, 290-321.

Zaú A.S., Freitas G.P. and Oda G.A.M. (2015). Do visitors attract or repel vertebrates in an urban park in the Brazilian Atlantic Forest? Revista Brasileira de Ecoturismo, 8(5), 543-555.

RESEARCH PAPER

THE ROLE OF LATE HOLOCENE LANDSCAPE EVOLUTION IN AFFECTING SETTLEMENT DISTRIBUTION IN BOROBUDUR BASIN, CENTRAL JAVA, INDONESIA

Arif Ashari
Universitas Negeri Yogyakarta, Colombo Street 1, Yogyakarta, 55281, Indonesia
***Corresponding author:** arif.ashari@uny.ac.id
Received: January 23rd, 2020 / Accepted: April 24th, 2022 / Published: June 30th, 2022
https://DOI-10.24057/2071-9388-2020-013

ABSTRACT. Human life has never been separated from the interaction with the surrounding physical environment, especially landscape conditions. In this paper, the role of landscape evolution in influencing the distribution of settlements in the Borobudur Basin, is investigated. The data were collected through observations, remote sensing, documentations, and literature studies. The data were analysed using analytical-descriptive analysis and spatial analysis supported by geographic information system (GIS) analysis. GIS analysis employing average nearest neighbour and buffer analysis. The results of this study indicate that the landscape evolution affects the distribution of settlements as a form of community adaptation to physical environmental conditions in the Borobudur Basin. The distribution of settlements can be traced from the time of Hindu-Buddhism based on the existence of past relics in the form of temples. At present time, the settlements are scattered as hamlets which are grouped in several villages in the Borobudur Basin. Based on the existence of 20 temples located next to the ancient river valleys, the distribution of past settlements mainly follows the pattern of river valleys. The pattern of past settlements is random, correlates with the paleochannel distribution pattern which is also random. This is possibly due to the reason of obtaining resources and a factor of belief (faith or reliance). The pattern of the current settlement distribution is spreading and is more evenly distributed in the Borobudur Basin. The settlements develop to a wider area outside the paleochannel, not only limited to the paleochannel. Instead of far more numerous population, this distribution pattern is also caused by landscape changes that enable them to build settlements more widely. In summary, this study provides new insight into evidence of the influence of landscape evolution due to geomorphic processes on the distribution of settlements. Traditional intelligence encourages humans to choose the best location for settlement.

KEYWORDS: landscape evolution, settlement distribution, Borobudur Basin, human adaptation

CITATION: Ashari A. (2022). The Role of Late Holocene Landscape Evolution in Affecting Settlement Distribution in Borobudur Basin, Central Java, Indonesia. Geography, Environment, Sustainability, 2(15), p 13-22
https://DOI-10.24057/2071-9388-2020-013

ACKNOWLEDGEMENTS: The author thank the various parties who have helped both during the process of data collection and data analysis. Special thank go to Maulana Azkaa Salsabila, B.Ed. who assisted in performing data analysis and mapping. Also, the author acknowledge to the editors and reviewers who have provided suggestions for improving this paper to meet the publication standards.

Conflict of interests: The authors reported no potential conflict of interest.

INTRODUCTION

The Borobudur region in Central Java has been widely known mainly due to the existence of the Borobudur Temple which was designated as a UNESCO world heritage and international tourist destination. However, as an area that has long been occupied by residents and become the centre of cultural development, there is a lot of other information that can be revealed from this region. The existence of various ancient sites provide clues about how the model of lives in the past look like. In addition, it reveals the life of people at the present time that are widely spread in various villages in the Borobudur region. The community life from time to time in this region is definitely inseparable from the condition of the physical environment of the residence, especially the characteristics of the landscape. With their ability to think, humans are able to adapt to the characteristics of the landscape where they live to afford the best life conditions. Due to this situation, geomorphological changes that occur throughout the geological period may correlate with the characteristics of life between generations in the Borobudur region. One of them is the selection of residential locations that can be viewed from the settlement distribution patterns.

Like Java island in general, the Borobudur region has complex geomorphological conditions resulted from the combination of endogenous and exogenous processes. The endogenous process are the tectonism and the influence of volcanic activity around this region. Meanwhile, exogenous processes are influenced by wet-tropical climates with high temperatures and rainfall. Physiographically, the Borobudur region is a basin surrounded by three andesitic volcanoes. The existence of volcanic activity greatly influences the landscape evolution that occur in this region. Gomez et al.

(2010) explain that a large volcano eruption that occurred in ~119,000 BP and ~31,000 BP produced clastic volcanic deposits that covered the Borobudur Basin with more than 10 meters thick. Among the volcanoes that surround the Borobudur Basin, Merapi Volcano with its activities provide the greatest effects (Newhall et al. 2000).

Murwanto and Purwoarminta (2015) say that the Borobudur Basin was formerly a lake that experienced a siltation. The siltation process takes place in stages which are divided into three periods of the lake, namely the Late Pleistocene, Early Holocene, and Late Holocene. Lake siltation is caused by volcanic activity, tectonics, mass movements, and human activities. Tectonic activity plays a role in silting the southern part of Borobudur lake (Murwanto et al. 2014). This indicates the influence of tectonic factors on the landscape evolution in the Borobudur region. Mass movements show the influence of climate, whereas human influence is a form of adaptation to changes in landscape conditions. The changes of landscape conditions require attention because they give a lot of influences on various aspects of the earth's surface, especially human life. Landscape changes and its influence on the lives of people in the Borobudur area, in particular, need to be investigated and informed as a reflection for the present and future lives considering this region has a high cultural value, becomes a world tourist destination, and is occupied by many residents.

The existence of Borobudur temple and other temples in the Borobudur region shows that this region has developed as a centre of civilization since the past time. Degroot (2009) explains that the area between Merapi and Sumbing Volcano was the centre of a strong kingdom in Central Java in between 8th and early 10th centuries. The main temples in the Borobudur area such as Borobudur, Mendut, and Pawon temples were built between 760 - 812 AD indicating the initial period of civilization in Central Java. This tells that the Borobudur area has long been inhabited by the community. In addition, over the past few centuries since the development of the civilization there have been various changes in the physical conditions of the landscape in the Borobudur Region. At this time, Borobudur basin which was geologically included in the Late Holocene Epoch (recent), the last part of Borobudur Lake that had existed since the Late Pleistocene began to disappear (Gomez et al. 2010; Murwanto 2015; Murwanto and Purwoaminta 2015). With regard to this, it is interesting to know thoroughly about how the ability to adapt of the community to deal with the changes of the physical environment therefore it produces a model of life for each generation.

This paper aims at investigating the role of landscape evolution in influencing the distribution of settlements in the Borobudur Basin and the distribution of past settlements related to the condition of the physical environment of the landscape at that time. Population settlement is indicated by the existence of the temple. It is assumed that people who used temples as a place of worship and/or work for taking care the temples might live next to the temple. Determining the location of the temple should take into account the condition of the landscape. There are several requirements to consider in building the temples namely reliefs, availability of groundwater and surface water, contours, and soil conditions such as colour, odour, appearance, taste, fertility, touch, surface flatness, and plant characteristics which grow on it (Darini 2013; Harto 2005). Moreover, the condition of the landscape and the distribution of settlements that exist today need to be revealed.

MATERIALS AND METHODS

This research employed a geographic approach, namely the spatial approach and emphasis on geographical themes in the analysis especially the themes of location, place, and human-environment interaction. The spatial approach was enhanced with the discussion on temporal aspects that were specifically used to analyse paleogeographic conditions. The author combined data collection and data analysis techniques by analysing field data and field investigations. The data consisted of primary and secondary data. Primary data were collected from field observations, namely geomorphological data while secondary data were gathered from previous research and documented data in the publication of statistical data and maps. Geomorphological data include morphology, morphogenesis, morphochronology, and morphoarrangement.

Other primary data gathered from the field are location of temple, settlement, important geomorphological units that indicate changes in landform conditions, and settlements that have toponyms related to past landscape conditions. Temple location data and settlement location are combined with secondary data obtained from previous publications and topographic maps.

Data collection techniques employed in this study are observation, remote sensing image interpretation, literature study, and documentation. Observations were carried out to obtain primary data, utilized the geomorphological survey method. Sampling for observation in the Borobudur Basin was performed purposively on geomorphological units which provided traces of landscape evolution. Remote sensing images interpretation was intended to obtain geomorphological data and distribution of settlement data. Geomorphological data were obtained from the interpretation of Landsat imagery while settlement data were gathered from Quickbird imagery. Literature studies were carried out to obtain secondary data on temple distribution, rock age, and past geomorphological conditions. Meanwhile, documentation was carried out to obtain population data, settlements, and geological conditions collected from BPS data, Geological Maps, and Topographical Map (Table 1).

An analytical descriptive analysis was supported by a geographic information systems (GIS) analysis. In addition, spatial analysis was used to answer research problems. The analysis began by identifying the condition of past landscapes and investigated the distribution of the temple affected by the culture of the people in the past. The GIS analysis which utilized the average nearest neighbour analysis technique was intended to know the type of temple distribution. The type of distribution is indicated by the nearest neighbour value obtained from the analysis. To determine the type of distribution patterns, the z-score and p-value are used as an indicator (Nirwansyah et al. 2015). The z-score and p-value indicate the nature of the relationship between points and their area boundaries as described by Clark and Evans (1954). There are three types of distribution patterns, namely clustered, dispersed, and random. After investigating the temple distribution pattern, the next step is performing spatial analysis to know the physical environmental factors which influence the distribution of the temple. The influence of the physical environment on the temple are indicated by the location of the temple against certain landscape units. After undergoing this analysis process, the influence of past landscape conditions on the distribution of the temple as an indicator of settlement can be described. The same step is repeated to analyse the influence of landscape conditions on the current distribution of settlements. The final step is comparing the past conditions and current conditions (Fig 1)

Table 1. Data Types, Data Collection Methods, Instruments, and Data Sources

No	Data	Data collection methods	Instrument/data sources
1	Landform	Field observation	GPS, observation sheet, digital camera
		Remote sensing image interpretation	Landsat Imagery, Quickbird Imagery
2	Slope	Field observation	Yallon, abney level, roll meter
		Documentation	*Peta Rupabumi Indonesia* (Indonesian Topographical Map)
3	Relief unit	Field observation	Yallon, abney level, roll meter
		Documentation	*Peta Rupabumi Indonesia*
4	Rock type	Field observation	Geological compass, GPS
		Documentation	Geological Map Sheet Magelang and Semarang
5	Paleolandscape	Literature Study	Gomez et al (2010), Newhall et al (2000), Murwanto (2015), Murwanto and Purwoarminta (2015), Murwanto et al (2004)
6	Settlement distribution	Documentation	*Peta Rupabumi Indonesia*
7	Temple distribution	Literature Study	Degroot (2009)

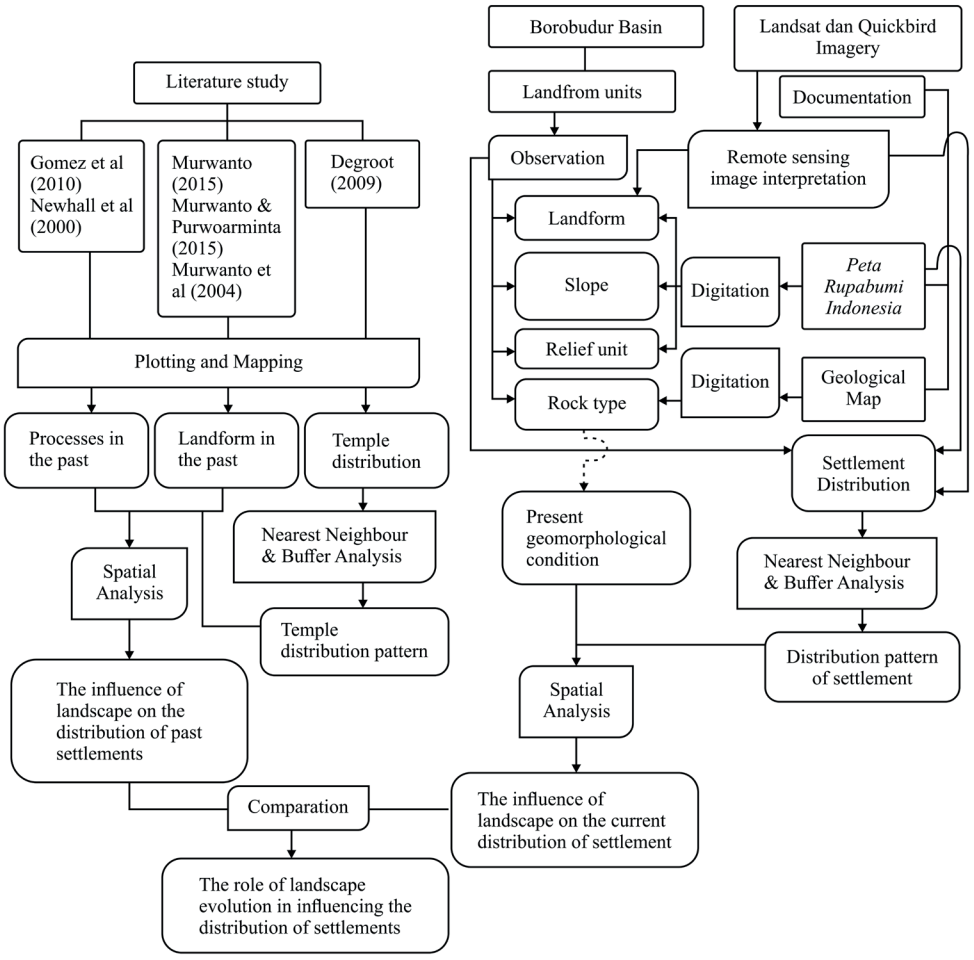

Fig. 1. Research procedure

The Study Area

This research was conducted in the Borobudur Basin area, Central Java. The total area is 65 km2. Physiographically, the study area is bordered by escarpment of the Menoreh Mountains in the south and west, the volcanic foot of the Sumbing volcano in the north, and the volcanic foot of the Merbabu and Merapi volcanoes in the east (Fig 2). The boundaries of the Borobudur Basin area in this study was determined by referring to the ancient Borobudur Lake region during the late Pleistocene published by Murwanto and Purwoarminta (2015) and Murwanto (2015). It's assumed that the Borobudur Basin in the Late Pleistocene period was a landscape of lakes which then experienced an evolution along with the commencement of the historical period of occupancy by the community. After the community occupancy period began, this region continued to be occupied by different generations till the present time. Murwanto and Purwoarminta (2015), as well as Murwanto (2015), determine the boundaries of the

Borobudur Ancient Lake region based on the presence of black clay. Murwanto (2015) explained that black clay deposits are swamp deposits which are indicated by the presence of pollen from swamp community vegetation. The black colour itself derives from high carbon content (Murwanto & Purwoaminta 2015). Furthermore, Murwanto and Purwoarminta (2019) also explained that in addition to the lacustrine sediment outcrop, evidence of ancient lakes around Borobudur can also be revealed by geomorphological features.

The study area is administratively located in Magelang Regency which consists of six subdistricts, namely Mertoyudan, Mungkid, Muntilan, Borobudur, Tempuran, and Salaman. The population in 2021 was approximately 475,502 people. Based on the Geological Map Yogyakarta Sheet Year 1995 by Raharjo et al. (1995), the research area is composed of various types of rocks, including alluvium, young Merapi volcanic deposits, Merbabu volcanic deposits, young Sumbing volcanic deposits, volcanic breccias, and andesites. Murwanto et al. (2004) explain that, Quaternary deposits of lacustrine and volcaniclastic are dominated in the Borobudur region.

RESULTS AND DISCUSSION

The Borobudur Basin's Chronicle: A Review of the Paleogeography

Borobudur Basin is well-known due to the existence of Borobudur Temple which is designated as a UNESCO World Heritage and become international tourist destination. Moreover, this region has rich historical heritages, both geological history and the history of civilization. Borobudur Temple is not the only temple in the Borobudur Basin area. There are 17 other temples in the Borobudur Basin area which are restricted as this study area. However, the structure of the temples is not always complete. Degroot (2009) states that the Borobudur region is one of the core temple-heritage regions in Central Java. Borobudur area, as part of the Progo Valley region is the zone with the highest density of temple remains. The Borobudur region in the past was a Hindu-Buddhist centre in Central Java, and even various evidences show that this region was the former capital of Central Java at that time. Among the two main temple-regions, Borobudur and Prambanan, the ancient kingdom was closer to Borobudur. Borobudur Basin has undergone changes of landscape conditions for a long time. At the Late Pleistocene, a long time before the development of civilization that produced a cultural heritage of temples, this region was a lake landscape.

The lake landscape in the Borobudur Basin has developed since the Late Pleistocene which lasted until Recent. As the time went by, the lake was narrowing and eventually became a plain (Murwanto and Purwoaminta 2015). At the Late Pleistocene, the lake was very wide which then became narrower due to the influence of volcanic, tectonic, and deposition activities (Murwanto and Purwoaminta 2019). Furthermore, volcanic and tectonic activities continued to occur in the beginning of the holocene therefore they buried and lifted the lake. The community began to inhabit this area and manage the land for agriculture, thereby it increased the process of erosion and sedimentation (Murwanto 2015; Murwanto and Purwoaminta 2015). During the drying process, two separate lakes were formed. Borobudur Hill and the other two stand as islands in between (Murwanto et al. 2004).

Gomez et al. (2010) describe that there are several generations of paleolake in the Borobudur Basin. The formation of paleolakes most likely derived from the blockage of hydrographic network by volcanic materials. The volcanic process related to the formation of paleolake possibly occured 31,000 years BP from Merapi Volcano. There are similarities and differences between this view and that of Van Bemmelen (1949) stating that the activity of Merapi Volcano contributes to the formation of paleolake, but this volcanic activity has occurred in the Pleistocene far from the time proposed by Van Bemmelen in 1006. In historical times, the last period of paleolake had

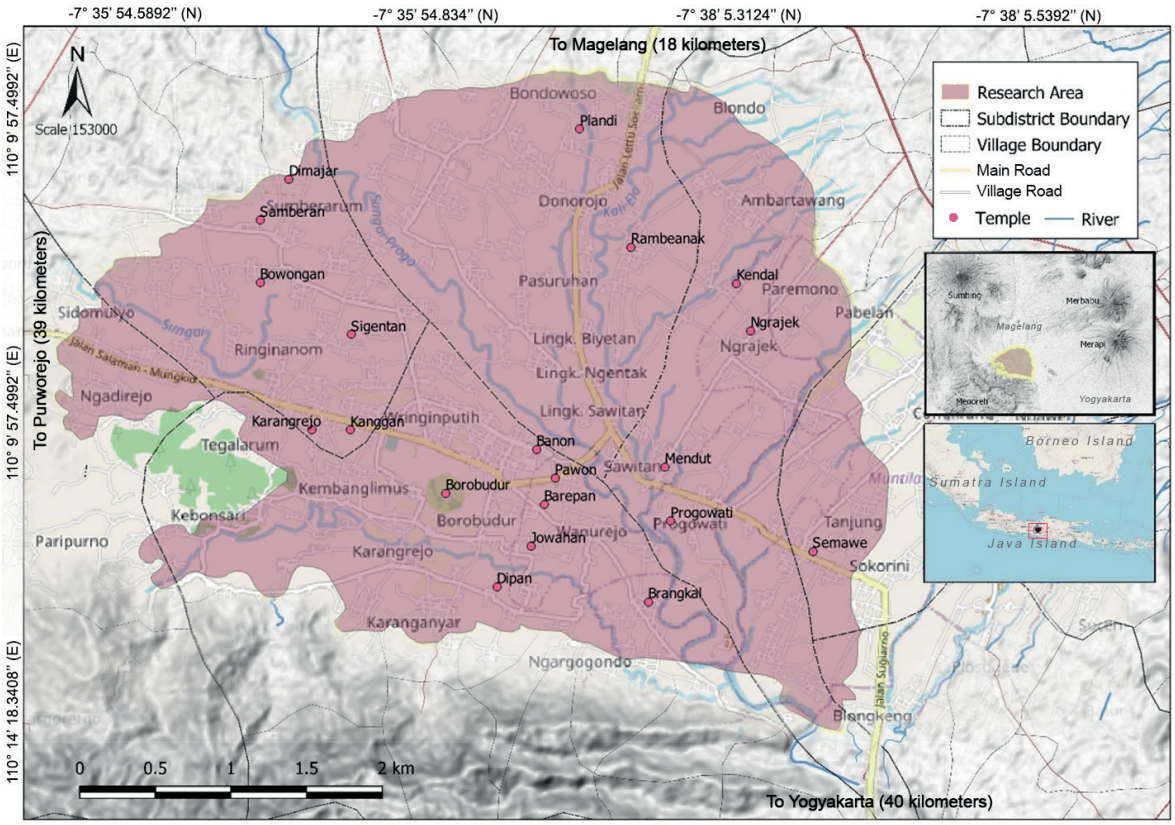

Fig. 2. The Study Area

experienced a shrinkage. This provides information that there was paleolake in the Borobudur region when the civilization began to develop. It was not the first paleolake but a paleolake which has undergone evolution since its initial formation in the Late Pleistocene. Futhermore, Gomez et al. (2010) explain that the presence of early paleolake can be identified from 27,640 years BP lacustrine deposits with a mixture of millimeters to centimeters of clastic pumice and other pyroclastic materials. Paleolake had existed permanently for 20,000 years around the Sileng River, or the entire southern part of the Borobudur Basin, until the historical period. In the Sileng area as a main area, the lake possibly did not dry up for a very long time (Murwanto et al. 2004). Paleolake is not entirely limited to paleochannel but it spreads over a large area at the intersection between the Elo River and the Progo River (Gomez et al. 2010). The development of paleolake in the Borobudur Basin since the Late Pleistocene was greatly influenced by the geographical setting in this region. Geomorphologically, Borobudur Basin is a basin surrounded by volcanoes and Menoreh Mountains. This condition determines the geomorphological process that takes place from time to time since the Late Pleistocene, thus causing the siltation and disappearance of paleolake. The quaternary volcanic which borders Borobudur Basin plays the most important role in the evolution of paleolake in the Borobudur Basin (Murwanto 2015).

The volcanism process has been very influential in the Borobudur area for long time. In relation to the paleolake, all of these volcanic activities influence the development of paleolake. Merbabu Volcano produce an important eruption that influence the development of the Borobudur basin, which produces lahar that lines the andesite blocks. Meanwhile, Sumbing volcanic results are beleived to produce pyroclastic deposits in the Progo River in the northern part of the basin. Sumbing Volcano and also Merapi Volcano have produced pyroclastic flows that are transported reaching a distance of 30 km and enclose short-aged lakes in the Borobudur Basin (Gomez et al. 2010). The activities of Merapi Volcano which have greater intensity and impact than other volcanoes become the main factors that contribute to the disappearance of Borobudur Lake (Newhall et al. 2000). The role of volcanism which is very strong seems to be more dominant than climate variation factors in causing the disappearance of Borobudur Lake. This condition is different from the process of lake sedimentation in other regions with non-volcanic landscapes (Romashkin and Williams 1997; Zolitschka 1998; Sapelko et al. 2019) or volcanic areas accompanied by strong tectonism influences (Liu et al. 2015). However, the role of human activity factors in land use that causes lake sedimentation shows similarities with other regions (Ahn et al. 2006).

Paleolandscape conditions and its influence on the selection of community residence locations

Borobudur area has been occupied for a long time and become one of the centres of ancient civilization in Central Java. The most monumental relics as evidence of past civilizations is temples that were built from the 8th century to the mid-10th century, including the Borobudur Temple, Mendut Temple, and Pawon Temple (Degroot 2009). There are 20 temples in this study area. The temple as a relic of the past can be used as a proxy to identify the existence of the settlements and their distribution.

Temples as a symbol of belief definitely correlate with the lives of people who have settled in the region. In building the temple, the area around the temple was functioned as a place for settlements. Therefore, in choosing the construction site of the temple, various factors are considered such as resource availability and land stability (Kramrisch 1946) for the sake of building good settlements and meeting the basic needs of people living in the area. The observations that have been carried out on 26 temples in the Progo Valley show that the location of the temples are next to springs or rivers. Moreover, the land has a dark texture and is generally located on the fluviovolcanic plains (Ashari 2015). The relationship between the temple and the people living around can be viewed from various activities during the construction phase of the temple (Darini 2013; Harto 2005).

The existence of the temple indicates the existence of community settlements in the area. Community settlements are possibly located next to the temple. During the construction of temples in the 8th century, a settlement as a permanent city which had good arrangements for water management infrastructure was not found in Central Java, as it was found in the Hindu-Buddhist period in East Java several centuries later (Wirjomartono et al. 2009). Thus, the community settlement was close to the temple and had a simple layout. An ancient settlement between the 6th century and the 10th century found in the Liyangan site also indicated the connection between the temple and settlements. Spatial structures in the ancient Liyangan neighbourhood show the existence of residential, worship, and agricultural areas (Riyanto 2015).

When community settlements developed in the 8th century, the Borobudur Basin area was still a lake landscape. This lake landscape in the history of Borobudur Basin evolution is the last generation of paleolake in this region. Compared with paleolake which was firstly developed in the Late Pleistocene, paleolake in this period has undergone many changes, especially shrinking the lake area and increasing intensive sediment deposition, thereby reducing the area of the lake. Gomez et al. (2010) explain that paleolake in the Borobudur basin had existed up to the historical time. Paleolake in this period was limited to paleochannel gullies. Spatial analysis of the distribution of temples in the Borobudur Basin shows that the temples were mostly built next to this paleochannel. The number of temples based on the distance from the paleochannel are as follows: two temples at a distance of 100 meters, six temples at a distance of 200 meters, 9 temples at a distance of 300 meters, 12 temples at a distance of 500 meters, 15 temples at a distance of 800 meters, and 18 temples at a distance of 1000 meters (Figure 3). Two other temples located at a distance of more than 1000 meters from the paleochannel turned out to be located near the present river. The spread of this temple shows that past settlements developed close to river gullies which might be part of the paleolake edge.

Gomez et al. (2010) analyse the relationship between the distribution of the temple and the river. The results of the analysis indicate that there is a link between the temple and following the river network. This further strengthens the existence of the link between the temple – as settlement representation – and river gullies, both paleochannel as part of paleolake and actual river. The landscape condition in the past which was dominated with lakes and swamps limited the selection of settlement locations. This might contribute to the limited development of settlements around the paleochannel. The toponym of Bumisegoro and Sabrangrowo hamlets (Murwanto 2015) affirmed the existence of the swamp landscape at that time. In addition to physical conditions, settlements that are located next to the river are possibly due to people's motivation in obtaining resources (and transportation infrastructure?). Besides, a factor of belief also contribute to the relationship between the temple and the river (Darini 2013; Harto 2005; Kramrisch 1946). In summary, the evolution of the lake landscape at that time has created a landscape condition in such a way that the people who occupy their territory might adapt to that condition.

Based on the results of the average nearest neighbour analysis conducted on 20 temples in the study area, the pattern of temples distribution in the Borobudur Basin is random. The random pattern is influenced by the distribution of paleochannel which is also random in the boundaries of the study area. The z-score shows that the distribution of paleochannel in the study area is very random. The results of the analysis which indicate a random distribution of temples are aline with the distribution

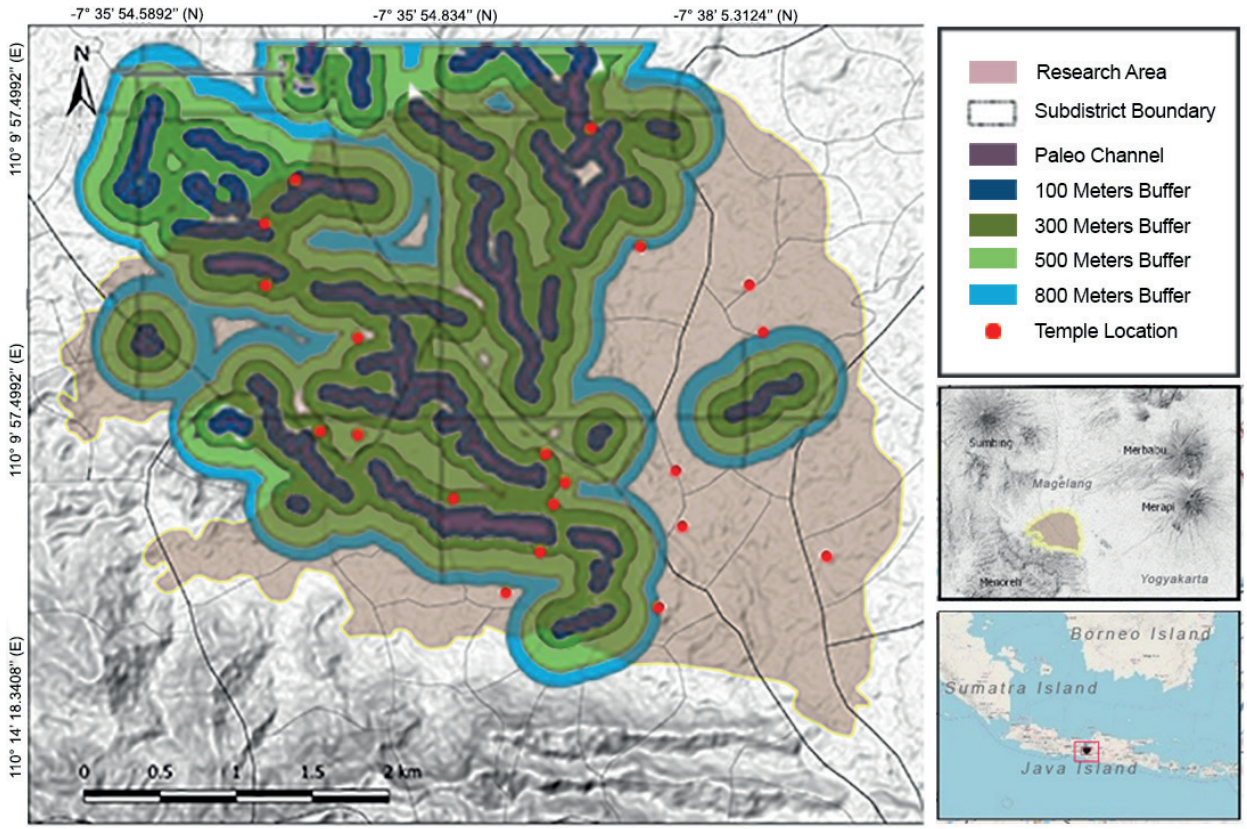

Fig. 3. Buffering analysis of temple distance from paleochannel

of paleochannel which are also random, supporting each other with the results of buffering analysis in which the temples were built close to the paleochannel. Although in general the spread of the temple in all research areas is random, the z-score on the temple's distribution pattern which is negative shows a slight tendency to be cluster patterns. Viewed in a narrow scope in the area around the paleochannel, for example in a 800 meter buffer, the spread of the temple does indeed show a tendency to cluster (Fig. 4).

The pattern of ancient settlements in the Borobudur Basin of which the distribution pattern is random becomes the main finding of this analysis result. Furthermore, based on the results of the buffering analysis, this random settlement pattern correlates with the paleochannel distribution pattern which is also random in nature. The author predicts that the distribution of settlements which tends to be located next to the paleochannel is due to the existence of water resources and the factor of belief. This condition is similar to that of found by Singh et al. (2017) which shows that urban areas that developed in the Bronze-age of Indus Civilization spread around the big Himalayan river due to the existence of water resources. The distribution of settlements develops along the paleochannel which is currently inactive, but the location was the provider of water resources to meet the needs of the community in the past. Ancient settlements built near rivers due to water sources availability is also shown by Lu et al. (2019) in Songshan Mountain, China, and Wilkinson (1998) in the Balikh Valley, Syria, in which the development of settlements correlates with water resources availability in the region over a very long period of time.

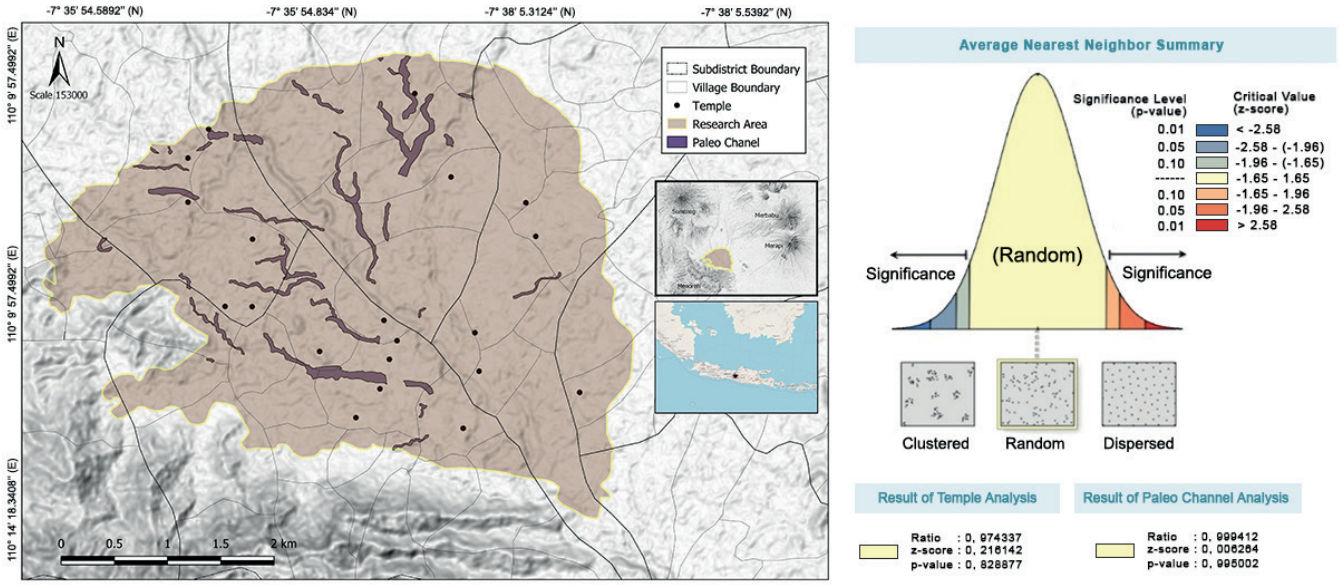

Fig. 4. Left: distribution of temples in the research area (after Gomez et al 2010 and Murwanto 2015). Right: results of average nearest neighbour for temple analysis and results of average nearest neighbour for paleochannel analysis

Why aren't ancient settlements dispersed distributed in the Borobudur Basin? It seems that the topographic barrier in the form of a swamp in the area is a factor that inhibit settlements from being widely distributed. This condition is the same as that of expressed by Lü et al. (2019) where fluvio-lacustrine aggradation is characterized by an increase of flood which causes uninhabitable hydrological and geomorphic conditions. This condition further influenced the pattern of settlement development which was then located along the basin. A similar situation is explained by Kidder (2006) in which the increase of flood volume in river valleys foster people to abandon the ancient settlements and push them to move to new or more suitable locations. Honegger and Williams (2015) also explain that climate changes that cause changes of the conditions in the Nile River, influence the development of settlements in the region. Meanwhile, Smith et al (2021) showed that in addition to natural factors, demographic and political factors also influenced the shift of settlements in the river valley.

Environmental conditions dealing with suitability of settlement locations as well as spatial and temporal changes are factors that influence settlement patterns in the Borobudur Basin. This condition is also found in other places, including areas with different climatic and landscape environmental characteristics. Climate change, as explained by Kidder (2006), Honegger and Williams (2015), Li et al. (2017), Lü et al. (2019), and Nikulina (2019) becomes a factor that greatly determine the changes of environmental conditions which later on influence the development of settlement. Bolikhovskaya et al. (2010) describe relatively similar conditions, based on the finding that climate evolution in the lower Volga region during the holocene, is closely related to changes in climatic conditions in the region. Slightly different conditions are found in the Borobudur Basin in which the very active volcanic activity of the various volcanoes around the Borobudur Basin becomes a very influential factor in the change of the landscape in this region.

The Condition of Landscape and Distribution of Actual Settlements

The Borobudur Basin has now developed as a form of alluvial plains. Some rivers that cross this region greatly contribute to the development of the present landform. As a plain landform, the Borobudur Basin currently has a topographical impression as a flat land (Fig. 5) Viewed from the morphoarrangement aspects, the position of the Borobudur Basin which is surrounded by volcanoes and Menoreh Mountains also influences the development of current landforms, although the geomorphological processes that take place at this time are different from that of the past. The deposition of massive volcanic materials do not occur in the modern era. This is due to the reduction in volcanic activity in today's era. Among several volcanoes that surround the Borobudur Basin, Merapi Volcano is the only volcano that is still active in the last few centuries. However, the volcanoes around the Borobudur Basin still become a source of material deposited in this region. Human factors that utilize land for agriculture also play a role in influencing the denudation process in the upstream area, thereby increasing the amount of sediment deposited through the river.

The conditions of different settlements are also found in the today's era as it was in the beginning of civilization

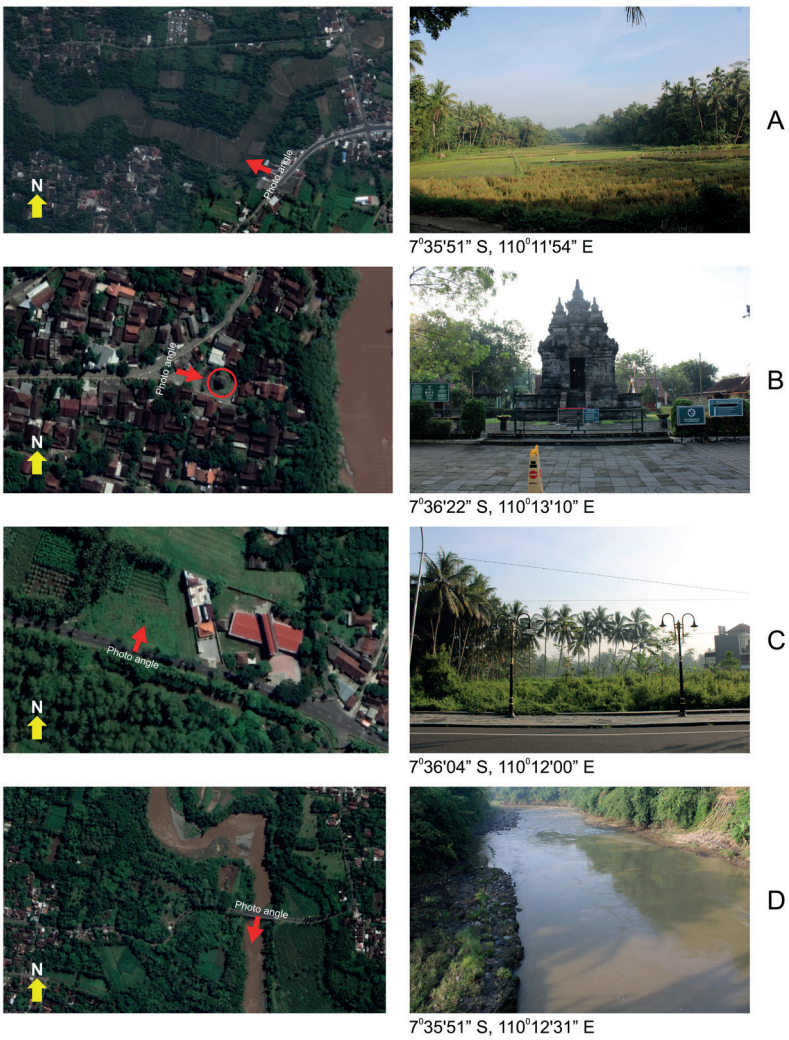

Fig. 5. Geomorphological conditions of several locations in the Borobudur Basin. A: palaeochannel in Wringinputih Village. B: Pawon Temple, located on the edge of the present river valley and 650 meters from paleochannel. C: flat-sloping topography around Borobudur hill. D: fault structure in breccia rocks in the Progo River (Source: Field data 2002 and Google Earth 2020)

in the 8th century. In the 8th century, the settlements developed around the paleochannel and spread randomly in the Borobudur Basin whereas in the modern era settlements were relatively dispersed (uniformly). In summary, community settlements in the modern era currently occupy various parts of the Borobudur Basin area and are not limited to certain areas (Fig. 6).

The uniform distribution of settlements in the Borobudur Basin is also influenced by landscape conditions in this time. Geomorphological conditions of Borobudur Basin in the form of alluvial plains allow a more widely settlements development. Compared with the final period of paleolake which was still in the form of swamps, the current conditions enhance the development of settlements more evenly in various regions. The changes of landscape conditions from time to time in the Borobudur Basin have influenced the way of life of the community, especially in utilizing land for residential locations. Another important factor which influences the development of settlements more broadly in modern times is the high population. As stated in the previous section, there were approximately 475,502 people living in the Borobudur Basin area in 2021. The high number of population require high needs of land both for settlements and agriculture. This factor supported with the geomorphological conditions encourage the development of settlements in various parts of the Borobudur Basin.

Based on the observations of remote sensing images and topographic maps, the author have identified settlement units in the research area. The current area of settlements is 28% of the total area of the study area. The buffering analysis results show that 72% of residential units are located in an area of 800 meters from paleochannel and 28% outside the paleochannel area. This condition provides information that the settlements develop to a wider area outside the paleochannel. The current settlements are not only limited to the paleochannel which in the past became the centre of a residential area. Viewed from the distribution and density of paleochannel in the study area (see Fig. 3), areas with a distance of 800 meters from paleochannel have covered most of the study area which is 82%. The rest is only 18% of the total area included in the area outside the 800 m distance from the paleochannel. This 18% turned out to be 28% of residential units currently. Based on the spread of the temple, the area outside the 800 meters of the river (paleochannel and actual river) is only 17% of the temple.

It is generally known that the changes of the lake environment into alluvial plains greatly contribute to the development of settlements area distribution from the past to the present time. Interestingly, viewed from the distribution of the paleochannel, there is a linkage between the spread of the temple and the current distribution of settlements (see Fig. 4 and Fig. 6) in which the current settlements develop from the expansion of past settlements. The development of settlements in the present time does not take place without order. There is a possibility that the past settlements, may become a starting point for the development of settlements in the later periods. The changes of landscape that provide more space for the development of settlements and the increasing number of people have caused settlements to develop more widely from their initial point. The expansion of residential areas takes place in stages along with shrinking paleolake. In the area near Mendut Temple to the capital city of Magelang Regency, the traces of paleolake were found from 1163-1251 AD (Gomez et al. 2010). The area includes the last part of Paleolake in the Borobudur Basin so that new settlement expansion probably began in the period after that year. The expansion of settlements that developed after the end of the paleolake period differs up to 4 centuries from the heyday of Hindu-Buddhist civilization that built the Borobudur Temple.

The slight different percentage of the number of temples and residential units in each buffer area of the paleochannel further strengthens that the past settlements became the node for the development of settlements in the future. For example, there were 45% of the temples as indicators of past settlements and 54% of the current settlements in a buffer area of 300 meters from the paleochannel. When the buffer distance was expanded to 800 meters, it turned out that there were 75% of temples and 72% of settlements. This condition shows that the spread of the temple tends to be close to the paleochannel while the distribution of settlements is wider. However, there is no contradictory data showing that the temple area is very localized and modern residential areas are dispersed distributed. The development of settlements can occur because paleolake is increasingly shrinking into an alluvial plain (Fig. 7).

The changes of landscape conditions become a factor which influences the settlement development. As explained by Lu et al. (2017), the selection of settlement location is greatly determined by Landform. Lü et al. (2019)

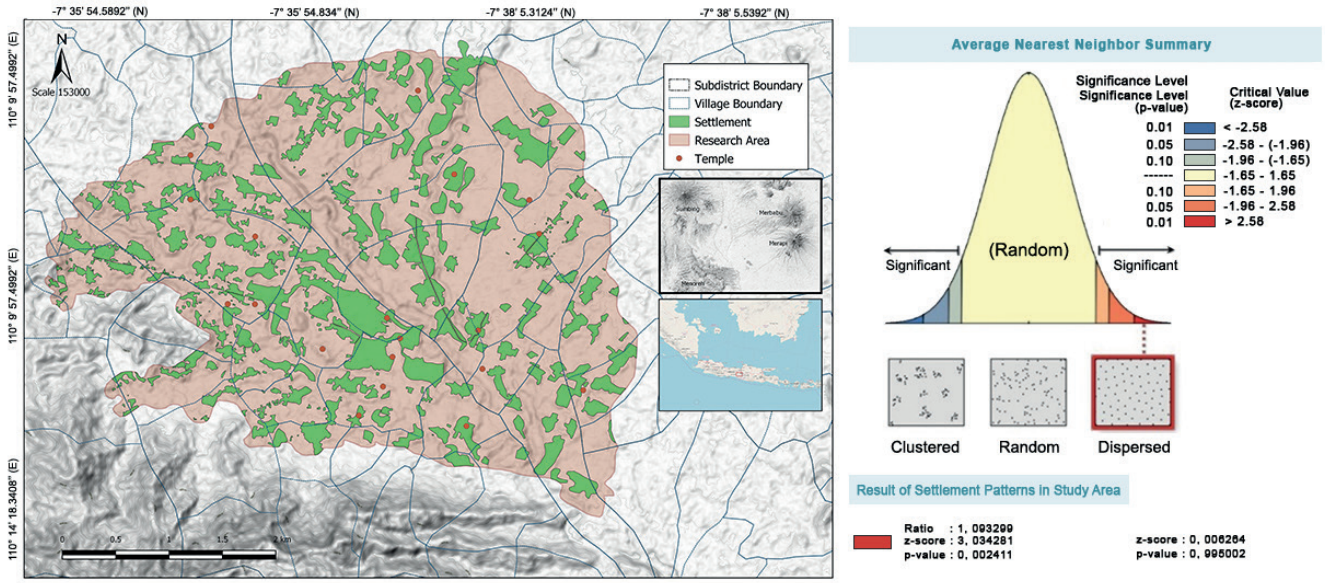

Fig. 6. Distribution of settlements in the study area (left) and results of the average nearest neighbour analysis showing dispersed settlement patterns in the study area (right)

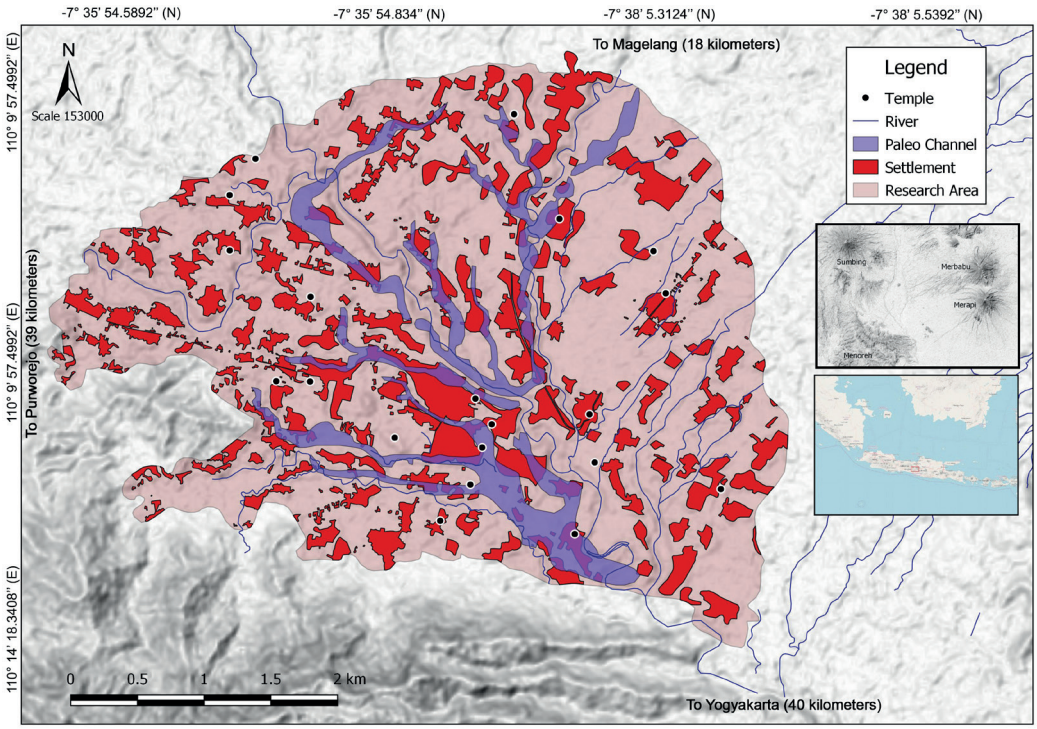

Fig. 7. The distribution of settlements to paleolake. Some residential units overlap against paleolake which indicate the development of settlements after the physical environment changes from the lake to an alluvial plain

explain that the characteristics of human activity deal with local and regional geomorphic changes. Geomorphic changes that occurred in the Borobudur Basin has fostered the development of a dispersed pattern settlement, formerly the pattern was random which was limited to the area around the palaeochannel. The same conditions are also found in various landscape in the world, for example the activities of residents in the Mississippi River valley (Kidder 2006) or the occupation of past inhabitants during the Nile River shrinkage (Honegger and Williams 2015). The findings from Walker et al. (1997) explain that humans try to adapt to the geomorphic processes that take place to decide the location of their settlements. In certain cases, the characteristics of landforms and geomorphological processes determine the type of developed settlement (Stafford and Creasman 2002). This study doesn't investigate the types of settlements in the Borobudur basin, but it is still limited to the spatial distribution pattern of settlements in the Borobudur basin dealing with the evolution of the landscape in the region.

The changes of favorable landscape conditions will further encourage the development of settlements and their distribution over a wider area. Lu et al (2017) say that landforms have a fundamental role in relation to the selection of residential locations. In Songshan Mountain, China, the selection of residential locations is involved over time. Lu et al. (2019) further explain that the development of settlements in Songshan Mountain occurred after the incised river period which made settlements on the river terraces safer from the effects of flooding. Compared with these two findings, the different landform conditions and geomorphic processes in the Borobudur Basin causes different settlement development characteristics. In the Borobudur Basin region, the settlements are growing and dispersed distributed due to the influence of geomorphic evolution in the form of sedimentation in the lake environment.

CONCLUSIONS

The evolution of the landscape that took place in the Borobudur basin during the Holocene period influenced various aspects, one of which was the life of the people in the area which was indicated by the selection of residential locations. The variation of temporal distribution shows that the changes of landscape affect the selection of settlement locations by communities across generations. The evolution of landscapes that provide opportunities for the development of settlements encourages the spatial distribution of settlements into a wider and more dispersed distributed area which differ from the conditions when there are still many natural obstacles. In the Borobudur area, this is indicated by the distribution of settlements which are dispersed distributed in the present times with landscapes in the form of alluvial plains, whereas in the past the distribution of settlements developed randomly under the influence of the landscape at that time in the form of lakes and swamps.

For evaluation purposes, this study is still limited to the comparison of spatial distribution of past settlements, using proxies for temple distribution, and current settlements related to the changes of landscape that occur. Further study on how the pattern and progress of the settlements development from time to time is required. Various relics that enrich the world's cultural heritage may be explored further. Moreover, the current spatial distribution of settlements can be used to give information to support the development, especially increasing accessibility to health, education, resources, and economic equality.

REFERENCES

Ashari A. (2015). The Local Genius of Pre-Modern Javanese Communities in the Progo Valley in Recognizing Landscapes for Settlements: Overview of Geoarchaeological Studies. In Nasiwan, ed., The Dilemma of Building Indonesian Humans: Choosing Between Global Demands or Local Wisdom. Yogyakarta: FISTRANS Institute, 366–377. (in Bahasa Indonesia)

Bemmelen R.W.Van. (1949). The Geology of Indonesia. Vol IA General Geology of Indonesia and Adjacent Archipelagoes. The Haque: Government Printing Office.

Bolikhovskaya N.S. and Kasimov N.S. (2010). The Evolution of Climate and Landscapes of the Lower Volga Region During the Holocene. Geography, Environment, Sustainability, 3(2), 78-97

Clark, P.J., and Evans, F.C. (1954). Distance to nearest neighbor as a measure of spatial relationships in populations. Ecology 35(4), 445-453

Darini R. (2013). Sejarah Kebudayaan Indonesia Masa Hindu-Buddha. Yogyakarta: Penerbit Ombak (in Bahasa Indonesia).

Degroot V. (2009). Candi, Space and Landscape: A Study on the Distribution, Orientation and Spatial Organization of Central Javanese Temple Remains. Leiden: Leiden University. Available at: https://books.google.com/books?id=u2HzduME8OcC&pgis=1. [Accessed 16 Okt. 2013]

Gomez C., Janin M., Lavigne F., Gertisser R., Charbonnier S., Lahitte P., and Murwanto H. (2010). Borobudur, a basin under volcanic influence: 361,000 years BP to present. Journal of Volcanology and Geothermal Research 196, 245–264, DOI:10.1016/j.jvolgeores.2010.08.001.

Harto D.B. (2005). Tata Cara Pendirian Candi Perspektif Negarakertagama. Jurnal Imajinasi, 1(2), 1–18 (in Bahasa Indonesia).

Honegger M. and Williams M. (2015). Human occupations and environmental changes in the Nile valley during the Holocene: The case of Kerma in Upper Nubia (northern Sudan). Quaternary Science Reviews, 130, 141-154, DOI:10.1016/j.quascirev.2015.06.031.

Kidder T.R. (2006). Climate Change and the Archaic to Woodland Transition (3000-2500 Cal B.P.) in the Mississippi River Basin. American Antiquity, 71(2), 195-231, DOI: 10.2307/40035903.

Kramrisch S. (1946). The Hindu Temple. Vol I. India: University of Calcuta.

Li H., Liu F., Cui Y., Ren L., Storozum M.J., Qin Z., Wang J., and Dong G. (2016). Human settlement and its influencing factors during the historical period in an oasis-desert transition zone of Dunhuang, Hexi Corridor, northwest China. Quaternary International, DOI:10.1016/j.quaint.2016.11.044.

Liu Y-Q., Kuang H-W., Peng N., Xu H., Zhang P., Wang N-S., and An W. (2015). Mesozoic basins and associated paleogeographic evolution in North China. Journal of Palaeogeography, 4(2), 189-202, doi:10.3724/SP.J.1261.2015.00073.

Lu P., Wang H., Chen P., Storozum M.J., Xu J., Tian Y., Mo D., Wang S., He Y., and Yan L. (2019). The impact of Holocene alluvial landscape evolution on an ancient settlement in the southeastern piedmont of Songshan Mountain, Central China: A study from the Shiyuan site. Catena, 183(2019) 104232.

Lü J., Douwen M., Zhuang Y., Jiang J., Liao Y., Lu P., Ren X., and Feng J. (2019). Holocene geomorphic evolution and settlement distribution patterns in the mid-lower Fen River basins, China. Quaternary International, 521, 16-24, DOI:10.1016/j.quaint.2019.05.032.

Murwanto H., Gunnell Y., Suharsono S., Sutikno., and Lavigne F. (2004). Borobudur monument (Java, Indonesia) stood by a natural lake: chronostratigraphic evidence and historical implications. The Holocene, 3, 459-463.

Murwanto H. and Purwoarminta A. (2015). Reconstruction of Borobudur Ancient Lake with a Spatiotemporal Approach. Limnotek, 22, 106–117 (in Bahasa Indonesia with English summary).

Murwanto H. and Purwoarminta A. (2019). The Ancient Borobudur Lake, History, and Its Evidences to Develop Geo-archeotourism in Indonesia. Indonesian Journal on Geoscience, 6(1), 103-113.

Murwanto H., Purwoarminta A., and Siregar D.A. (2014). Effect of tectonic and landslides on landform changes in the southern part of Borobudur Ancient Lake. Jurnal Lingkungan Dan Bencana Geologi, 5, 143-158 (in Bahasa Indonesia with English summary).

Newhall C.G., Bronto S., Alloway B., Banks N.G., Bahar I., Del Marmol M.A., and Wirakusumah A.D. (2000). 10,000 Years of explosive eruptions of Merapi Volcano, Central Java: Archaeological and modern implications. Journal of Volcanology and Geothermal Research, 100, 9–50, DOI:10.1016/S0377-0273(00)00132-3.

Nikulina A.V. (2019). GIS-based analysis of settlement patterns for the central Baraba Lowland (Western Siberia, Rusia) in relation to climatic conditions of the Middle-Late Holocene. Journal of Archaeologica Science: Reports 24, 302-312, DOI:10.1016.j.jasrep.2019.01.018.

Nirwansyah A.W., Utami M., Suwarno.S., Hidayatullah T., 2015. Analisis pola kejadian sebaran longsorlahan di Kecamatan Somagede dengan Sistem Informasi Geografis (Analysis of the distribution pattern of landslide events in Somagede Sub-District with Geographic Information Systems). Geoplanning 2(1), 1-9.

Riyanto S. (2015). Liangan Site: Variety of Data, Chronology, and Spatial Aspects. Berkala Arkeologi, 31, 33–58 (in Bahasa Indonesia with English summary).

Romashkin P.A. and Williams D.F. (1997). Sedimentation history of the Selenga Delta, Lake Baikal: simulation and interpretation. Journal of Palaeolimnology, 18, 181-188.

Rychagov G.I., Korotaev V.N., and Chernov A.V. (2010). History of Formation Palaeo-Deltas of Lower Volga Deltas. Geography, Environment, Sustainability, 3(1), 4-15

Sapelko T., Pozdnyakov S., Kuznetsov D., Ludikova A., Ivanova E., Guseva M, and Zazovskaya E. (2019). Holocene sedimentation in the central part of Lake Ladoga. Quaternary International, 524, 67-75, DOI: 10.1016./j.quaint.2019.05.028.

Singh A., Thomsen K.J., Sinha R., Buylaert J-P., Carter A, Mark D.F., Mason P.J., Densmore A.L., Murray A.S., Jain M., Paul D., Gupta S. (2017). Counter-intuitive influence of Himalayan river morphodynamics on Indus Civilisation urban settlements. Nature Communications, 8 1617, DOI:10.1038/s41467-017-01643-9.

Smith M.E., Hare, T.S., Montiel, L., Sherfield, A., Huster, A. (2021). Settelement pattern and urbanization in the Yaupetec Valley of Central Mexico. Open Archaeology, 7, 378-416.

Stafford C.R. and Creasman S.D. (2002). The Hidden Record: Late Holocen Landscapes and Settlement Archaeology in the Lower Ohio River Valley. Geoarchaeology: An International Journal 17(2), 117-140.

Walker I.J., Desloges J.R., Crawford G.W., Smith D.G. (1997). Floodplain Formation Processes and Archaeological Implications at the Grand Banks Site, Lower Grand River, Southern, Ontario. Geoarchaeology: An International Journal, 12(8), 865-887.

Wilkinson T.J. (1998). Water and Human Settlement in the Balikh vlley, Syria: Investigations from 1992-1995. Journal of Field Archaeology, 25, 63-87.

Wirjomartono B., Sukada B.A., Sudrajat I., Tjahjono G., Widodo J., Prijotomo J., and Saliya Y. (2009). Indonesian Cultural History: Architecture. Jakarta: Raja Grafindo Persada (in Bahasa Indonesia).

Zolitschka B. (1998). A 14,000year sediment yield record from western Germany based on annlually laminated lake sediments. Geomorphology, 22, 1-7.

RESEARCH PAPER

TRANSFORMED WETLANDS AND URBAN RESILIENCE: A CASE STUDY FROM BELLANWILA – ATTIDIYA WETLAND SANCTUARY, SRI LANKA

Munagamage S. Gayani[1], Deepthi D. Wickramasinghe[1], Harsha D. Dahanayake[1], Yugani N. Weerasinghe[1*]
[1]Department of Zoology and Environment Sciences, Faculty of Science, University of Colombo, Colombo 07(00700), Sri Lanka
***Corresponding author:** yuganinayanathara@gmail.com
Received: March 17th, 2021 / Accepted: April 24th, 2022 / Published: June 30th, 2022
https://DOI-10.24057/2071-9388-2021-028

ABSTRACT. Urbanization is a major issue that threatens natural habitats. However, carefully planned anthropogenic activities give the opportunity to transform urban natural habitats to offer new services to cities. In this study, we assessed the impact of land-use conversions on the spatial status of Bellanwila - Attidiya wetland sanctuary in the Colombo district, Sri Lanka. The Bellanwila - Attidiya wetland provides many ecosystem services but is highly vulnerable to the rapid land use and land cover changes that comes with urbanization. Multi-temporal remote sensing images were analyzed for the years 2005, 2009, and 2015 to study the changes in land use/land cover features of the wetland. The social perception of the ecosystem services was assessed by conducting semi-structured interviews with the residents. During the study period, parts of the wetland had been transformed into residential areas (10.1%) and open water systems (8.6%). Urban expansion and the construction of a storm water management system were found to be the main causes for these changes. The community perception revealed that the wetland has deteriorated, and that the ecosystem services had been altered due to the land use/land cover changes. The anthropogenic transformation of part of the wetland into a flood retention area and the addition of infrastructure for recreational purposes have added value to the wetland complex and therefore opportunities for new ecosystem services have emerged. Our findings shed light on the need for inclusive urban planning mainstreaming community perceptions. It also highlights the benefits of transforming urban spaces into anthropogenic landscapes that blends with nature to offer ecosystem services and enhance community resilience.

KEYWORDS: wetlands, ecosystem services, land use change, community perception, GIS

CITATION: Gayani M.S., Wickramasinghe D.D., Dahanayake H.D., Weerasinghe Y.N. (2022). Transformed Wetlands and Urban Resilience: a Case Study From Bellanwila – Attidiya Wetland Sanctuary, Sri Lanka. Geography, Environment, Sustainability, 2(15), p 23-30
https://DOI-10.24057/2071-9388-2021-028

ACKNOWLEDGEMENTS: The authors acknowledge the logistical and financial support of the Department of Zoology and Environment Science, University of Colombo to carry out this work.

Conflict of interests: The authors reported no potential conflict of interest.

INTRODUCTION

Wetlands represent important natural capital that delivers many Ecosystem Services (ES) including provisioning, regulating, supporting, and cultural services (Millennium ecosystem assessment 2005). Yet, these ecosystems have been threatened throughout the world due to different human-induced activities such as fragmentation, pollution, overexploitation, and urbanization. Land Use/Land Cover (LULC) changes are identified as the main driver that affects the degradation of wetlands (Gagné and Fahrig 2007; Jurn et al. 2018). Dynamics in physical, chemical, and biological features that are associated with the wetland ecosystems can affect the proper functioning of the system while disrupting the services it offers to the community (Ehrenfeld 2000; Zhan et al. 2020). For instance, alterations in land use associated with wetlands can result in fluctuations in biodiversity profile, hydrology, and connectivity of habitats which led to changes in the benefits obtained from the wetland ecosystems (Yurek et al. 2016; Roy-Basu et al. 2020).

Urban wetlands have been identified as one of the most threatened ecosystem types in the world due to their intensive interaction with the surrounding landscape which is dominated by humans (Ehrenfeld 2000). As they are the intersections between wetlands and municipal landscapes, these fragile ecosystems are affected by many anthropogenic activities in different degrees (Khatri and Tyagi 2014). This may lead to a decline in the degree of the ES derived from the wetland and it could affect human well-being (Millennium ecosystem assessment 2003). On the other hand, urban wetlands provide several habitats for different groups of flora and fauna while maintaining comparatively high biodiversity as species have been restricted to these areas due to habitat fragmentation and urbanization, and degradation of the quality of the wetland systems may adversely affect their survival.

The benefits obtained from wetlands are influenced by the perceptions of people based on the location, beliefs, values, cultural and socioeconomic status of the landscape (Willock et al. 1999; Urgenson et al. 2013; Hein et al. 2006;

Cowling et al. 2008). Especially, communities that are living close to the ecosystems such as rain forests, wetlands have a higher appreciation regarding the ES-derived from the natural systems (Sodhi et al. 2010; Abram et al. 2014; Muhamad et al. 2014) Therefore, investigations on urban wetlands with the surrounding human-dominated landscape are essential to understand the patterns and processes associated with the ecosystem and the benefits they offer to communities (McInnes 2014). However, there are limited studies that focus on ES derived from urban wetlands to the communities. Therefore, consideration of the community perception is needed as it is important to understand the attitudes of urban dwellers on the benefits they receive from these habitats, in the view of management and conservation of wetlands (Grimm et al. 2000; Alberti et al. 2003).

The present study focuses on Bellanwila – Attidiya Wetland Sanctuary, which is known as one of the most significant wetlands located in a major urban agglomerate in South Asia (Hettiarachchi et al. 2014). The sanctuary is in the wet zone which, together with the Western Ghats in India, is considered as one of the 34 global biodiversity hotspots (Mittermeier et al. 2004). This Sanctuary is listed under the highly-threatened wetlands in the Colombo district and declared as a protected area by the Department of Wildlife Conservation Sri Lanka (Kotagama and Bambaradeniya 2006). BirdLife International has declared this wetland as an Important Bird and Biodiversity Area (IBA) in 2004 (Karunarathna et al. 2010).

According to the National Wetland Directory of Sri Lanka (2006), Bellanwila – Aththidiya wetland system maintains high biodiversity. *Nymphaea* spp., *Syzygium* spp. and *Pandanus* spp., and several species of grasses including *Cynodon dactylon* and sedges including *Fimbristylis* spp., *Eleocharis* spp. have been recorded as the noteworthy flora in the wetland (IUCN and CEA 2006).

Considering the fauna, previous studies have been reported 77 species of butterflies, 37 species of dragonflies with 5 nationally threatened species, 15 species of nationally threatened and endemic amphibians, 30 species of reptiles, 27 species of reptiles, and 33 species of freshwater fish species in the study site (Nanayakkara 1998; Goonethilake et al. 2001; Maduranga 2005). As reported in the various studies the most dominant vertebrate group in the Bellanwila – attidiya area is birds including both resident and migratory species (Karunarathne et al. 2010). The vegetation type and the aquatic areas create suitable habitats for a variety of birds such as herons, egrets, cormorants, kingfishers, pelicans, etc. as this area is an important breeding habitat of native birds, as well as for the migratory birds and it is also a preferred feeding and resting habitat of several species. This site has been used by several species of rare winter migrants including globally threatened *Pelecanus philippensis* (IUCN and CEA 2006; Karunarathne et al. 2010). Further, uncommon waterbird species such as *Rallus striatus, Porzana fusca, Gallicrex cinerea, Phalacrocorax carbo, Rostratula benghalensis* have been recorded in the study area (IUCN and CEA 2006).

In the past few decades, urban expansion, and other associated LULC changes such as landfilling for development, land clearing, flood control systems, etc. have resulted in severe pressure on the Bellanwila – Attidiya Wetland Sanctuary as well as the ES it served (Flower et al. 2019). Yet, studies on LULC changes through integrating remote sensing tools with the perceptions of local communities concerning urban wetlands are lacking. Therefore, this kind of study can provide useful insights regarding the requirement for the success of participatory approaches to the management of urban wetlands. In this context, the present study was carried out to investigate the changes in LULC of Bellanvila – Attidiya Wetland Sanctuary, from 2005 to 2015. The study also attempts to understand the perception of residents of the area on land-use changes and the ES they obtain from the wetland.

MATERIALS AND METHODS

Study site

Bellanvila-Attidiya Wetland, bearing IUCN status as a sanctuary, which is located at 6° 52′ 0″ N and 79° 52′ 0″ E to 6° 48′ 0″ N and 79° 56′ 0″ E within the Kesbewa Divisional Secretariat Division (DSD), a local administrative division in Colombo District in Western Province, Sri Lanka (Fig. 1.a). The study area consists of an extent of 372 ha within the Kesbewa DSD which carries a high population (244,062) in the district. This study has been conducted based on five "Grama Niladari Divisions (GND)" which are subunits of local administrative divisions within the Colombo district (Fig. 1.b).

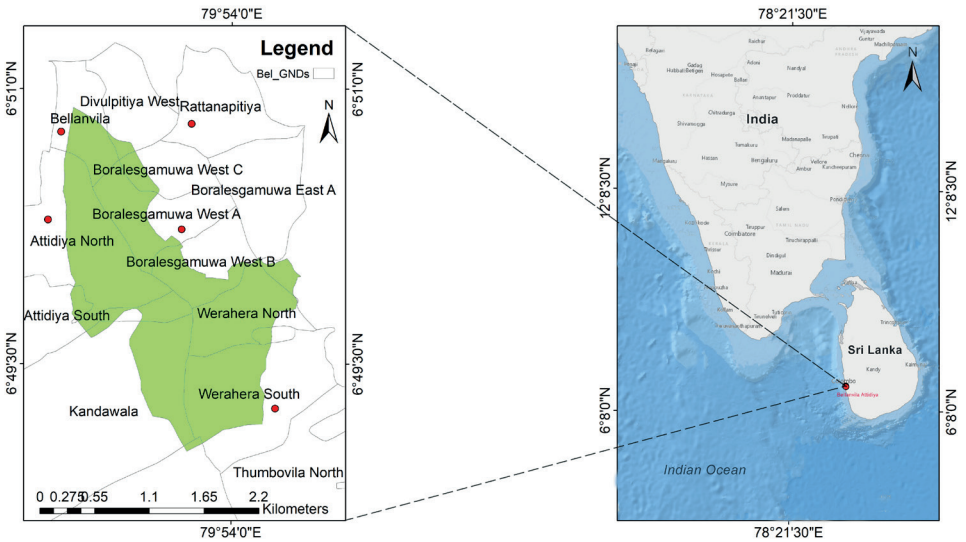

Fig. 1. Map of the study site, (a) local administrative divisions covering the study site in Colombo District in Western Province, and the GNDs in which the study has been conducted denoted by red dots. (b) Location of the study area in the Sri Lanka

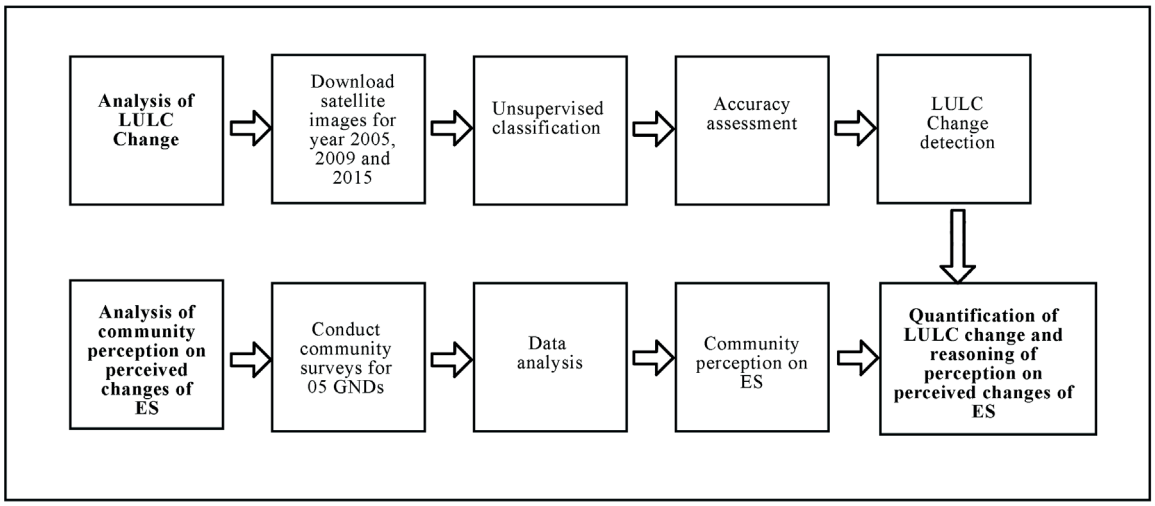

Fig. 2. Summary of methods used to analyze LULC change and community perception on perceived changes of ES

Analysis of LULC change

Multi-temporal satellite images for the years 2005, 2009, and 2015 were downloaded from the Earth Explorer USGS website (https://earthexplorer.usgs.gov/) to assess the LULC Changes (Reis, 2008). A collection of land images from Landsat 4-5 TM (dated 13/02/2005, path 141, row 55) Landsat 4-5 TM (dated 08/02/2009, path 141, row 55), and Landsat 8 OLI/TIRS (dated 08/01/2015, path 142, row 54) were used to generate the study maps. The cloud cover for the downloaded satellite images was selected at 10% or less. The composite band images were prepared for the downloaded satellite images and the masking tool in the ArcGIS (Version 10.3) software was used to extract the study area. The unsupervised classification method was utilized to identify the temporal LULC changes for the study area (Lillesand et al. 1998; Dewan & Yamaguchi 2008; Karnieli and Rozenstein 2011). Five LULC types were defined for this study and presented in Table 1. Different band combinations for the images were used for the identification of different LULC categories during the classification process (NASA 2011). The features of the LULC classification on the images were verified using Google earth pro software during this study. The change detection method was used, and changes were calculated in percentage for the analysis of the transformation of land categories into other categories (Dewan & Yamaguchi 2008).

Analysis of community perception on perceived changes of ES

A social survey was carried out using a semi-structured interview based on a questionnaire focusing on the community perception of the wetland. The people who have been living in the Bellanwila- Attidiya wetland sanctuary area since on or before 2005 were interviewed. Questions in the questionnaire were designed to collect data on the community perception of perceived changes of the ES derived from the wetland. The questions were designed as multiple-choice questions where the residents had to choose the most suitable answer which described their perception. The survey data were analyzed by using the statistical package of social sciences (SPSS 20.0) software and the Minitab 17.0 statistical software and RStudio (Version 21.0).

RESULTS

Analysis of LULC change

The LULC change analysis for the period 2005–2015 revealed that open areas and settlements have increased while thick vegetation, soft vegetation, and water bodies have decreased (Table 2 and 3; Fig. 3). According to the data analysis, human settlements have been increased by 31.12% while open water areas have been increased by 4.07% between 2005–2009 (Table 2). These values show a significant increase comparing the other LULC classes. From 2009 to 2015, the highest LULC change was recorded for the human settlements (30.37%) and it has been decreased compared to LULC in 2005–2009 (Table 3). The second highest LULC change has been recorded in open water areas (5.65%) and it has been significantly increased compared to the LULC changes in 2009–2015. The major reason for the conversion of the wetland area into open water areas is the flood management scheme that has been implemented in this area.

According to the LULC map, the pattern of urban pressure on the wetland demonstrates three distinct models (Fig. 3). However, the intensity of land use alterations in association with urban transformation and stormwater management program that was carried out during 2005–2009 was restricted to the perimeter of the wetland boundary. In contrast, during the period 2009–

Table 1. LULC class types identified in the Bellanwila – Attidiya wetland sanctuary

LULC class	Description
Water bodies	Areas covered with water bodies
Settlement	Residential areas and areas with infrastructure
Wetland soft vegetation	Marshlands with bushes, grass, or waterly plants
Thick vegetation	Areas with thick vegetation cover
Open areas	Open land areas

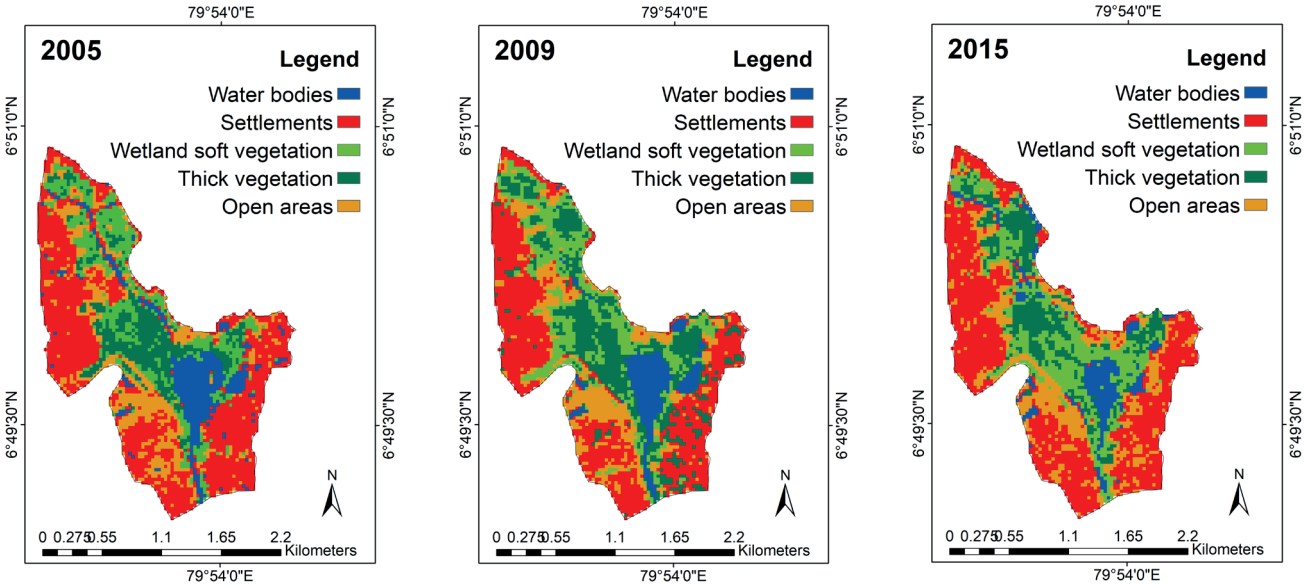

Fig. 3. Human-induce LULC conversions in the Bellanwila – Attidiya Wetland Sanctuary for the period (a) 2005 (b) 2009 (c) 2015

Table 2. LULC conversions between 2005–2009

2009										
2005	Row Labels	Open area		Settlement		Soft vegetation		Thick vegetation		Water bodies	
		ha	%	ha	%	ha	%	ha	%	ha	%
	Open area	33.75	8.88%	15.47	4.07%	12.20	3.21%	3.43	0.90%	0.26	0.07%
	Settlement	20.79	5.47%	118.29	31.12%	7.19	1.89%	15.36	4.04%	2.47	0.65%
	Soft vegetation	3.70	0.97%	1.83	0.48%	25.39	6.68%	29.78	7.84%	1.15	0.30%
	Thick vegetation	2.03	0.53%	0.18	0.05%	17.96	4.73%	26.57	6.99%	0.50	0.13%
	Water bodies	0.15	0.04%	0.96	0.25%	6.69	1.76%	7.21	1.90%	26.75	7.04%
	Grand Total	60.42	15.90%	136.73	35.97%	69.43	18.27%	82.35	21.67%	31.13	8.19%

ha – hectare

Table 3. LULC conversions between 2009–2015

2015										
2009	Row Labels	Open area		Settlement		Soft vegetation		Thick vegetation		Water bodies	
		ha	%	ha	%	ha	%	ha	%	ha	%
	Open area	30.98	8.14%	21.51	5.65%	3.49	0.92%	1.67	0.44%	2.83	0.74%
	Settlement	18.27	4.80%	115.55	30.37%	1.53	0.40%	0.38	0.10%	1.45	0.38%
	Soft vegetation	12.24	3.22%	5.85	1.54%	29.48	7.75%	17.62	4.63%	4.20	1.10%
	Thick vegetation	6.95	1.83%	11.01	2.89%	29.49	7.75%	31.87	8.38%	2.97	0.78%
	Water bodies	2.02	0.53%	1.90	0.50%	7.40	1.95%	1.35	0.36%	18.43	4.84%
	Grand Total	70.46	18.52%	155.82	40.96%	71.40	18.77%	52.89	13.90%	29.87	7.85%

ha – hectare

2015, the conversions have moved into the core areas of the wetland indicating the severity of pressure on land.

Analysis of community perception on perceived changes ES

The community survey was carried out focusing on five GNDs of Kesbewa DSD, i.e., Bellanwila, Boralesgamuwa West A, Rattanapitiya, Attidiya North, and Werahara South. Fifty-seven residents between the age of 20-90 years old have been interviewed for this study. There were 46% of females and 54% of males in the study group and the majority (99.95%) were permanent residents in this area. Perceptions of the residents reflect their experiences on land-use changes, causes, and ES they derive from the wetland (Fig. 4).

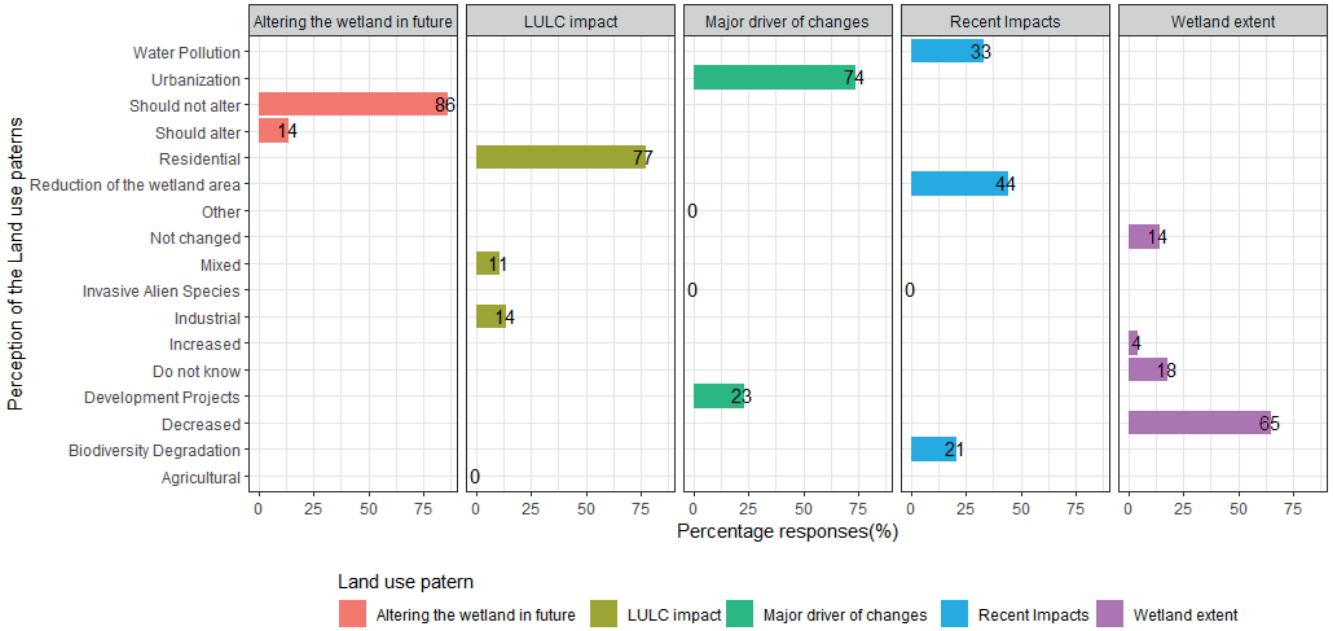

Fig. 4. Summary of the respondent's perception of land–use patterns

Although this ecosystem is a sanctuary, some human-induced activities that would not harm the environment are allowed by the law. While a series of questions were presented to the respondents, significant findings concerning the changes in ES are presented below.

Question 1: What happened to the extent of the wetland area during the past decade?

Sixty-five percent of respondents stated that the extent of wetland areas has been significantly decreased during the past decade.

Question 2: What is the major reason for the reduction of the extent of the wetland area?

According to 77% of the residents, the expansion of the residential areas was identified as the major reason for the reduction of the extent of the wetland. In contrast, 14% of the residents believe that the wetland area is reducing due to the increasing industrial activities in the vicinity.

Question 3: In your opinion, what is the most recent major damage to the wetland?

The reduction of the wetland area was identified as the major damage that happened in the recent past as indicated by 43.86% of the residents, while 33% of them believe that it is the degradation of the quality of the water due to the pollution. Moreover, 74% of the residents believe that urbanization is the major driver of wetland pattern and process change while 23% of the residents are under the opinion that it is the development projects that were taken place in the area.

Question 4: What happened to the ES-derived from the wetland over the past 10 years?

According to the results of the community survey, ten years ago more than 56% of the residents have at least obtained a single provisioning service including water or food from the wetland. In contrast, 84% of the respondents are obtaining none of the provisioning services as in the previous times. (Fig. 5). Nearly half of the respondents believe that water was clean ten years ago compared to now indicating water pollution in the wetland area. Interestingly, 14 % of residents believe that services related to recreation have been increased compared with the recent past due to the alternation of sanctuary landscapes.

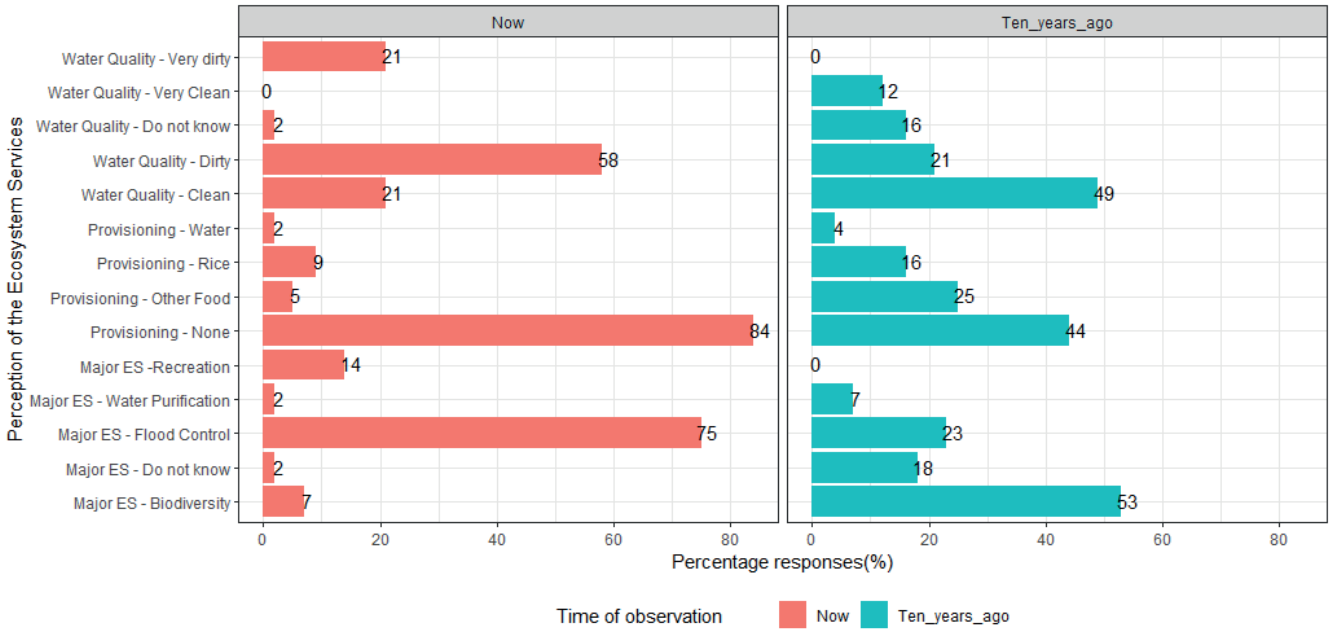

Fig. 5. Percentage responses of the identified ES provided 10 years ago and the present (n = 57)

DISCUSSION

Understanding the link between ES (Ecosystem Services) and human wellbeing is becoming a major research area worldwide as it recognizes the benefits people gain from nature which supports achieving sustainable development goals (Karki et al. 2018). Against this backdrop, this study presents an overview of LULC change in the Bellanwila – Attidiya wetland sanctuary, Sri Lanka between 2005 to 2015 and the perceptions of the local community on the provisioning of several ES by the sanctuary.

The ESs are indispensable to the well-being of people everywhere on the globe because it is essential in assuring the sustainable livelihood of the community (Islam et al. 2015). In the recent past, the anthropogenic transformation of natural ecosystems has been increasingly evident which either contributes to enhancing or reducing the ESs these habitats provide. For instance, transforming a wetland into a rice field will affect the natural water balance of the habitat, yet it may enhance food security. Urban areas are one of the most dynamic landscapes with ever-increasing human activities (Ricaurte et al. 2017). In many parts of the world, the changes in land use have not restricted only to the city area but gradually encroaching the suburbs as well as remaining natural habitats (Bengtsson et al. 2003; McDonagh 2007).

A wide array of problems emerge as anthropogenic activities rise in urban areas affecting ecosystems. In particular, rapid urbanization has been recognized as a key contributor to the degradation of ecosystem quality. The LULC changes have been identified as one of the main drivers of changes in different ecosystems and their services worldwide (Gaglio et al. 2015; Wang et al. 2015; Karki et al. 2018). Unplanned changes and unsustainable land-use practices in urban areas create significant impacts on natural ecosystems which affects the multi-functionality of these habitats (Seto et al. 2010; Zorrilla-Miras et al. 2014). Sri Lanka has been undergoing rapid urbanization over the past few decades resulting in alterations and changes in the ecosystems in time and space. For instance, the built-up area in Colombo, the capital city, has undergone a seven-fold increase from 1995 to 2017 (UN-HABITAT 2018). Similarly, there has been a significant reduction in green spaces in Colombo during the recent past (Li and Pussella 2017).

Results of the present study reveal a significant change in LULC in the study area. During the study period, areas that were covered with thick and wetland vegetation in and around the wetland sanctuary have been transformed into settlements and open water areas. The percentage transformation of the wetland to residential areas was10.1% and open water systems was 8.6%. Nearly 77% of the residents thought that the expansion of the residential areas was the foremost reason for the reduction of the wetland area. They were not aware of the actual extent of the transformation of open water areas. The major cause for the increase of open areas is the stormwater management program, the Weres River Project, which has been established to avoid flash floods, inundation, and damage to the land. This project is a part of a large wetland and canal network in Colombo flood mitigation. Under this flood management program, some areas of the wetland were dredged to remove sediments and to increase water holding capacity, and new connections were made to link isolated ponds. The area around the sanctuary is rapidly transforming into an urban landscape with high human density and commercial capacity. Thus, new or improved infrastructures are needed to avert the adverse impacts of floods. As expected, the floodwater retention capacity of the wetland has been increased due to these transformations and development under the Weres river project.

Less than half of the communities interviewed (43.86%) believe that the reduction of the wetland is the major damage that happened in the recent past. In contrast, 33% of them believe that the pollution of water is the major damage. Also, it's worth noting that half of the respondents believe that the water was clean ten years ago than today. Wetland has been providing ESs to fulfill community needs: more than half of the respondents indicated that wetland provided food items and water in the past. A majority (84%) of the respondents stated that they do not obtain any provisioning services from the wetland when compared to the previous time.

On the other hand, even though some ESs have been diminished due to the loss of natural wetlands as mentioned by the communities, new opportunities have emerged. According to the results of the analysis of the community perception regarding the changes of perceived ES, people have experienced a significant loss of ES such as provisioning services including food and water from the wetland system while gaining increased cultural services such as wetland parks and walkways. Some parts of the areas surrounding eh wetland sanctuary have been developed as walking pathways and serve as a recreational area for different entertaining activities. It is important to note that at least only a comparatively low proportion (14 %) interviewed, believe that services related to recreation have been increased compared to the past. However, the majority of the people have understood the increase of regulatory service of the wetland as a flood-controlling area compared to the past 10 years, but the perception of the biodiversity has been notably declined.

In this regard, understanding the impacts of LULC change is essential for mitigating the consequences of human-environment interactions (Hasan et al. 2020), and these changes should be accurately quantified to understand the impacts of the changes on the ecosystems as well as the community well-being. The results of the present study reveal that although the natural habitats were affected depriving the ES to the community due to different intensities of LULC changes, the new developments could contribute to enhancing urban resilience to floods as well as offering opportunities for physical well-being. Few studies have so far highlighted the community perception on the transformation of urban natural habitats to anthropogenic land or waterscapes. As inadequate information and knowledge limit good urban governance, city planners need to take proper steps to conserve and restore urban natural habitats to establish ESs, while taking careful consideration of community views.

CONCLUSION

The present research attempts to examine changes in LULC and the impacts of urban expansion on Bellanvila – Attidiya wetland sanctuary. This wetland is situated in a rapidly expanding urban area, yet delivered many services to the residents for decades. The results reveal that during the period 2005 to 2015, the sanctuary and the adjacent areas have undergone a rapid change in LULC. Most prominent changes are reflected in built up areas which has increased in size by expanding into the wetland marshy areas replacing vegetation. However, the open water area of the wetland has increased. The thick vegetation has decreased

in extent from 21.67% to 13.90%. The alternation of natural wetland results in changes in ecosystem services it offers to the residents. For instance, more than 80% of residents have indicated that the wetland currently does not offer any provisioning services it provided 20 years ago.

However, the transformation of a part of wetland into a storm water management pond and subsequent infrastructural development have provided new services in the recent past. Residents believe that opportunities for leisure and recreational activities that are being currently provided by the wetland contribute positively to urban resilience and community wellbeing. Our findings offer new insights into urban management and indicate the benefits of transforming urban spaces into landscapes that blend with nature and reduce developmental pressure. Our study highlights the essential need to pay attention to community views in effective and inclusive urban planning.

REFERENCES

Abram N.K., Meijaard E., Ancrenaz M., Runting R.K., Wells J.A., Gaveau D., Pellier A. and Mengersen K. (2014). Spatially Explicit Perceptions of Ecosystem Services and Land Cover Change in Forested Regions of Borneo. Ecosystem Services, 7(C), 116-127, DOI: 10.1016/j.ecoser.2013.11.004.

Alsharif A.A.A., Pradhan B., Mansor S. and Shafri H.Z. (2015). Urban expansion assessment by using remotely sensed data and the relative Shannon Entropy Model in GIS: a case study of Tripoli. Theoretical and Empirical Researches in Urban Management, 10(1), 55-71.

Amaleeta N. (2006). Bellanwila-Attidiya: in a state of daunting disgrace! The Nation (Sri Lanka). Available via www.nation.lk/2006/08/27/eyefea2.html. Accessed 27 August 2006.

Bengtsson J., Angelstam P., Elmqvist T., Emanuelsson U., Folke C., Ihse M., Moberg F. and Nyström M. (2003). Reserves, Resilience and Dynamic Landscapes. AMBIO: A Journal of the Human Environment, 32(6), 389-396, DOI: 10.1579/0044-7447-32.6.389.

Cowling R.M., Egoh B., Knight A.T., Reyers B., Rouget M., Roux D. and Welz A.S. (2008). An Operational Model for Mainstreaming Ecosystem Services for Implementation. Proceedings of the National Academy of Sciences, 105(28), 9483-9488.

Ehrenfeld J.G. (2000). Evaluating wetlands within an urban context. Ecological Engineering, 15(3-4), 253-265, DOI: 10.1016/S0925-8574(00)00080-X.

Gaglio M., Aschonitis V.G., Gissi E., Castaldelli G. and Fano E.A. (2017). Land-use change effects on ecosystem services of river deltas and coastal wetlands: a case study in Volano–Mesola–Goro in Po river delta (Italy). Wetlands Ecology and Management, 25(1), 67-86, DOI: 10.1007/s11273-016-9503-1.

Gagné S.A., and Fahrig L. (2007). Effect of landscape context on anuran communities in breeding ponds in the National Capital Region, Canada. Landscape Ecology, 22, 205, DOI: 10.1007/s10980-006-9012-3.

Goonatilake W.L.D.P.T.S.D.A., Perera L.J.K.R. and Gabadage D.E. (2001). Amphibians of Bellanwila-Attidiya Sanctuary. Loris, 22(5), 10-14.

Grimm N.B., Grove J.G., Pickett S.T.A. and Redman C.L. (2000). Integrated Approaches to Long-Term Studies of Urban Ecological Systems. BioScience, 50(7), 571-584, DOI: 10.1641/0006-3568(2000)050[0571:IATLTO]2.0.CO;2.

Hasan S.S., Zhen L., Miah M.G., Ahamed T. and Samie A. (2020). Impact of land-use change on ecosystem services: A review. Environmental Development, 100527.

Hein L., Van Koppen K., De Groot R.S. and Van Ierland E.C. (2006). Spatial Scales, Stakeholders and the Valuation of Ecosystem Services. Ecological Economics, 57, 209-228, DOI: 10.1016/j.ecolecon.2005.04.005.

Hettiarachchi M., Morrison T.H., Wickramsinghe D., Mapa R., De Alwis A. and McAlpine C.A. (2014). The eco-social transformation of urban wetlands: A case study of Colombo, Sri Lanka. Landscape and urban planning, 132, 55-68.

Islam G.T., Islam A.S., Shopan A.A., Rahman M.M., Lázár A.N. and Mukhopadhyay A. (2015). Implications of agricultural land-use change to ecosystem services in the Ganges delta. Journal of environmental management, 161, 443-452, DOI: 10.1016/j.jenvman.2014.11.018.

Jurn K., Lavallee J. and King L. (2018). Environmental destruction in the new economy: Offshore finance and mangrove forest clearance in Grand Cayman. Geoforum, 97, 155-168.

Karki S., Thandar A.M., Uddin K., Tun S., Aye W.M., Aryal K. and Chettri N. (2018). Impact of land use land cover change on ecosystem services: a comparative analysis on observed data and people's perception in Inle Lake, Myanmar. Environmental Systems Research, 7(1), 25.

Karunarathna D.S., Amarasinghe A.T., Gabadage D.E., Bahir M.M. and Harding L.E. (2010). Current Status of Faunal Diversity in Bellawila-Attidiya Sanctuary, Colombo District – Sri Lanka. Taprobanica, 2(1), 48-63.

Khatri N. and Tyagi S. (2014). Influences of natural and anthropogenic factors on the surface and groundwater quality in rural and urban areas. Frontiers Life Sciences, 8(1), 23-39, DOI: 10.1080/21553769.2014.933716.

Kotagama S. and Bambaradeniya C. (2006). An Overview of the Wetlands of Sri Lanka and Their Conservation Significance. IUCN Sri Lanka and the Central Government Authority, National Wetland Directory, Colombo, Sri Lanka.

Liu T. and Yang X. (2015). Monitoring land changes in an urban area using satellite imagery, GIS, and landscape metrics. Applied Geography, 56, 42-54.

Maduranga H.G.S. (2005). Ichthyofauna of Bellanwila-Attidiya Sanctuary and its environs in Colombo, Sri Lanka. Tiger paper, 32(1), 26-32.

McDonagh J. (2007). Theories of Urban Land Use and their Application to the Christchurch Property Market. Property and Land Economy Institute of New Zealand Newsletter.

McInnes R. (2014). Recognizing wetland ecosystem services within urban case studies. Marine and Freshwater Research, 65(7), 575, DOI: 10.1007/s13157-016-0849-1.

Millennium Ecosystem Assessment (2003). Ecosystems and human well-being; a framework for assessment. Island Press, Washington, DC, USA.

Millennium Ecosystem Assessment (2005). Ecosystems and Human Well-Being: Synthesis. World Health Organization. Island Press., Washington DC, USA.

Mittermeier R., Robles-Gil P., Hoffmann M., Pilgrim J., Brooks T., Goettsch-Mittermeier C., and Fonseca G. (2004). Hotspots Revisited: Earth's Biologically Richest and Most Endangered Terrestrial Ecoregions. Conservation International, 392.

Muhamad D., Okubo S., Harashina K., Parikesit B., and Takeuchi K. (2014). Living Close to Forests Enhances People's Perception of Ecosystem Services in a Forest-Agricultural Landscape of West Java, Indonesia. Ecosystem Services, 8(C), 197-206.

Nanayakkara G.L.A. (1988). Checklist of the Reptiles inhabiting the Bellanwila-Attidiya Marshes. Young Zoologists' Association of Sri Lanka Occasional paper, 4, 6.

Newman E., Kennedy M., Falk D. and McKenzie D. (2019). Scaling and Complexity in Landscape Ecology. Frontiers Ecology and Evolution, 7, 293, DOI: 10.3389/fevo.2019.00293.

Nicholls R.J. (2004). Coastal flooding and wetland loss in the 21st century: changes under the SRES climate and socio-economic scenarios. Global Environmental Changes, 14(1), 69-86, DOI: 10.1016/j.gloenvcha.2003.10.007.

Ricaurte L.F., Olaya-Rodríguez M.H., Cepeda-Valencia J., Lara D., Arroyave-Suárez J., Finlayson C.M. and Palomo I. (2017). Future impacts of drivers of change on wetland ecosystem services in Colombia. Global Environmental Change, 44, 158-169.

Roy-Basu A., Bharat G., Chakraborty P. and Sarkar S. (2020). Adaptive co-management model for the East Kolkata wetlands: A sustainable solution to manage the rapid ecological transformation of a peri-urban landscape. Science of Total Environment, 698, 134-203, DOI: 10.1016/j.scitotenv.2019.134203.

Seto, K. C., Golden, J. S., Alberti, M., and Turner, B. L. (2017). Sustainability in an urbanizing planet. Proceedings of the National Academy of Sciences, 114(34), 8935-8938.

Sodhi N.S., Lee T.M., Sekercioglu C.H., Webb E.L., Prawiradilaga D.M., Lohman D.J., Pierce N.E., Diesmos A.C., Rao M.K. and Ehrlich P.R. (2010). Local People Value Environmental Services Provided by Forested Parks. Biodiversity Conservation, 19, 1175-1188, DOI: 10.1007/s10531-009-9745-9.

Tscharntke T., Klein A.M., Kruess A., Steffan-Dewenter I. and Thies C. (2005). Landscape perspectives on agricultural intensification and biodiversity-ecosystem service management. Ecology Letters, 8, 857-874, DOI: 10.1111/j.1461-0248.2005.00782.x.

Todd P.A., Heery E.C., Loke L.H.L., Thurstan R.H., Kotze D.J., and Swan C. (2019). Towards an urban marine ecology: characterizing the drivers, patterns, and processes of marine ecosystems in coastal cities. Oikos, 128, 1215-1242, DOI: 10.1111/oik.05946.

Tuomisto H.L., Scheelbeek P.F.D. and Chalabi Z. (2017). Effects of environmental change on agriculture, nutrition, and health: A framework with a focus on fruits and vegetables. Wellcome Open Research, 2, 21, DOI: 10.12688%2Fwellcomeopenres.11190.2.

Urgenson L.S., Prozesky H.E. and Esler K.J. (2013). Stakeholder Perceptions of an Ecosystem Services Approach to Clearing Invasive Alien Plants on Private Land. Ecology and Society, 18(1), 26-39, DOI: 10.5751/ES-05259-180126.

UN-HABITAT. (2018). The State of Sri Lankan Cities Report. 18 April 2018, Colombo, Sri Lanka. Retrieved from https://unhabitat.org/is-sri-lanka-one-of-the-least-urbanised-countries-on-earth

Villamor G.B., Palomo I., Santiago C.A.L., Oteros-Rozas E. and Hill J. (2014). Assessing stakeholders' perceptions and values towards social-ecological systems using participatory methods. Ecological Processes, 3(1), 1-12, DOI: 10.1186/s13717-014-0022-9.

Wang Z., Wang Z., Zhang B., Lu C. and Ren C. (2015). Impact of land use/land cover changes on ecosystem services in the Nenjiang River Basin, Northeast China. Ecological Processes, 4(1), 1-12, DOI: 10.1186/s13717-015-0036-y.

Willock J., Deary I.J., Edwards-Jones G., Gibson G.J., McGregor M.J., Sutherland A., Dent J.B., Morgan O. and Grieve R. (1999). The Role of Attitudes and Objectives in Farmer Decision making: Business and Environmentally Oriented Behavior in Scotland. Journal of Agricultural Economics, 50, 286-303, DOI: 10.1111/j.1477-9552.1999.tb00814.x.

Willis C. (2015). The contribution of cultural ecosystem services to understanding the tourism–nature–wellbeing nexus. Journal of Outdoor Recreation and Tourism, 10, 38-43, DOI: 10.1016/J.JORT.2015.06.002.

Yurek S., DeAngelis D., Trexler J., Klassen J. and Larsen L. (2016). Persistence and diversity of directional landscape connectivity improve biomass pulsing in simulations of expanding and contracting wetlands. Ecological Complexity, 28, 1-11.

Zhan P., Liu Y., Wang H., Wang C., Xia M., Wang N., Cui W., Xiao D. and Wang H. (2020). Plant litter decomposition in wetlands is closely associated with phyllospheric fungi as revealed by microbial community dynamics and co-occurrence network. Science of Total Environment, 753, 142-194, DOI: 10.1016/j.scitotenv.2020.142194.

Zorrilla-Miras P., Palomo I., Gómez-Baggethun E., Martín-López B., Lomas P.L. and Montes C. (2014). Effects of land-use change on wetland ecosystem services: A case study in the Doñana marshes (SW Spain). Landscape and Urban Planning, 122, 160-174, DOI: 10.1016/j.landurbplan.2013.09.013.

RESEARCH PAPER

PREDICTION OF WILDFIRES BASED ON THE SPATIO-TEMPORAL VARIABILITY OF FIRE DANGER FACTORS

Almaz T. Gizatullin[1*], Natalia A. Alekseenko[1,2]
[1]Lomonosov Moscow State University, Leninskie Gory, 119991, Moscow, Russia
[2]Institute of Geography, RAS, Staromonetniy pereulok, 119017, Moscow, Russia
***Corresponding author:** almazgiz1995@yandex.ru
Received: December 27th, 2021 / Accepted: April 24th, 2022 / Published: June 30th, 2022
https://DOI-10.24057/2071-9388-2021-139

ABSTRACT. Most methods in the field of wildfire prevention are based on expert assessment of fire danger factors. However, their weights are usually assumed constant for the entire application area despite the geographical and seasonal changes of factors. This study aimed to develop a wildfire prevention method based on partial and general fire danger ratings taking into account their spatio-temporal variability. The study was conducted for Krasnoyarsk territory, Orenburg region and the Meschera lowland as the most forest, steppe and peat fire dangerous regions of Russia respectively. Surface temperature, moisture, vegetation structure, anthropogenic load, topography and their variation over subzones and in time were used as fire danger factors. They were evaluated by measuring parameters such as radiobrightness temperature, Normalized Difference Water Index (NDWI), Normalized Difference Vegetation Index (NDVI), Soil-Adjusted Vegetation Index (SAVI), distance to settlements and roads, elevation, slope and aspect. Materials from the Terra/Aqua, Sentinel-3, Landsat-8, Sentinel-2 satellites, ASTER Global Digital Elevation Model and Open Street Maps vector layers were used in the study. Correlation between these parameters and the actual fires in 2016-2018 was analyzed. Linear relationships were established, and correlation coefficients, equations of partial ratings and prevention 90%-threshold values were identified. On their basis, the parameter weights were computed to integrate them into the general fire danger rating. The developed method was validated using data over 2019. The results showed 67% confidence and 61% reliability of fire prevention along with the spatio-temporal patterns of fire danger factors. The method is recommended for preventing wildfires within the study areas and can be extend to similar regions.

KEYWORDS: wildfire prediction, remote sensing, fire danger

CITATION: Gizatullin A.T., Alekseenko N.A. (2022). Prediction of Wildfires Based on the Spatio-Temporal Variability of Fire Danger Factors. Geography, Environment, Sustainability, 2(15), p 31-37
https://DOI-10.24057/2071-9388-2021-139

ACKNOWLEDGEMENTS: The study was supported by State Assignment № AAAA-A19-119022190168-8.

Conflict of interests: The authors reported no potential conflict of interest.

INTRODUCTION

Fire danger is a key indicator in the prevention of wildfires. It is estimated based on weather variables influencing the fire conditions (Camia and Amatulli 2009) and the health of vegetation, which acts as the main fuel (Yebra et al. 2013; Sofronova and Volokitina 2017). With methodological advances, various national fire danger rating systems were developed, including American National Fire Danger Rating System (Deeming et al. 1972; Burgan 1988), Canadian Fire Weather Index (Van Wagner 1987), Russian Nesterov (Nesterov 1949) and Australian (McArthur 1967) Fire Danger Index, etc. These systems mainly use ground meteorological observations at weather stations and forest inventory data.

The development of remote sensing technologies has led to the use of satellite datasets with larger spatial coverage and higher temporal resolution. Estimation of fire danger based on remote sensing data is performed using visible and infrared imagery, which characterize major fire danger factors (Chuvieco and Congalton 1989). It is commonly used to assess live and dead fuel moisture content (Chuvieco et al. 2003; Arganaraz et al. 2016), temperature (Chuvieco et al. 2004), topography (Eskandari et al. 2020), and anthropogenic load (Suresh Babu et al. 2016). The usual practice is to define fire prevention zones by assigning certain weights to the classes of all fire danger factors according to their influence on fire probability (Jaiswal et al. 2002; Xu et al. 2005). Combining all factors into a general fire danger parameter is usually conducted using GIS operations such as overlay and raster algebra (Akbulak et al. 2018; Yankovich et al. 2019), with the recent addition of machine learning, neural networks (Bui et al. 2018) and big data (Piralilou et al. 2022) technologies. Modern methods have advanced to using ensembles of different techniques with the selection of the most optimal and accurate results (Rosadi and Andriyani 2021).

In Russia, methods for fire prevention and fire danger assessment are currently developed for three major areas:

– Institute of Space Research of the Russian Academy of Sciences (RAS) developed technologies for improving the Remote Monitoring Information System of the Russian Federal Forestry Agency, which is aimed at predicting pyrogenic tree mortality (Bartalev et al. 2017), stochastic simulation of fire ignition and propagation (Khvostokov et al. 2016) and mapping of fire danger classes

based on remote sensing products (Plotnikova and Ershov 2015) for the Central and European parts of Russia as well as its entire territory;

– The Siberian branch of RAS devoted its studies to enhancing fire danger classes and developing local and regional scales for Siberian forests (Sofronova et al. 2008; Volokitina et al. 2016);

– Far-Eastern branch of RAS developed methods for predicting fires based on vegetation combustibles (Zubareva 2018) and evaluating grass fire danger (Glagolev 2018) for Far-Eastern regions.

However, despite the great number of methods and their regional and local corrections, almost all of them have a major shortcoming – the key parameters describing fire danger factors (threshold values, weights, etc.) are assumed to be constant for large territories, while in fact they are characterized by significant spatial (geographical and scale) and temporal (seasonal) variability. This leads to a rough and inaccurate assessment of fire danger: for example, one temperature threshold value for a large meridional territory can perform well for the middle part of the area, overestimate the danger in the south and underestimate it in the north. Another shortcoming concerning Russian territory is that the Nesterov index, which mainly uses ground meteorological data and ignores the huge potential of remote sensing and other spatial products, is usually applied at the official level.

The aim of this study was thus to develop a method for preventing wildfires based on fire danger estimation, which would rely on the general principles of existing systems (Gizatullin et al. 2019) and take into account the spatio-temporal variability of fire danger factors. The study was conducted in the most fire dangerous regions of Russia – Krasnoyarsk Territory, Orenburg Region and the Meschera lowland, using Terra/Aqua, Sentinel-2,3 and Landsat-8 images, ASTER GDEM elevation model and OpenStreetMap layers.

MATERIALS AND METHODS

The study area

The study areas were selected based on the number of fire cases and the spatial variability of fire conditions and fuels in Russia, which is characterized by the type of wildfire: forest, steppe and peat. Sample analysis included an overlay of landcover maps (Ogureeva and Kotova 2013) with FIRMS hotspot (fire points) layers (Hanston et al. 2014, https://firms.modaps.eosdis.nasa.gov/). It was demonstrated that during the last decade (in 2010-2018), the largest number of forest, steppe and peat fires was observed in the Krasnoyarsk territory, Orenburg region, and the Meschera lowland respectively. The study areas were divided into zones of homogeneous vegetation (Fig. 1) corresponding to different types of forests, steppes and peatland which determine the possible fuel (based on Furaev et al. 2016; Pavleychik 2016; Medvedeva et al. 2019).

Krasnoyarsk territory is characterized by a high forest cover – more than 70% of the region area or 160 million hectares. The forests of the region have a large meridional extent and can be divided into seven forest zones (Fig. 1a) with different natural pyrological conditions. The area is characterized by the prevalence of coniferous tree species along with fire dangerous moss and lichens, lowland (0-200m) and tableland (500-700m) topography, and a heavy continental climate with the maximum temperature (+25…40°C) and consequently the largest number of fires observed in summer due to lightning ignition (based on Sofronov and Volokitina 1990 with authors' updating). In addition, the region has a population of about 2.8 million people, concentrated in its southern part. However, the middle and northern parts are also characterized by a high anthropogenic fire load due to the development of oil and gas fields and pipelines installation. Under these conditions, several million hectares of forest burn annually within the region as more than 700 thousand MODIS hotspots were registered here from 2010 to 2018.

In Orenburg region, the main pyrological factors include the dominance of dry steppe vegetation (sheep fescue, needlegrass, artemisia, etc.), heavily continental arid climate with a shortage of liquid precipitation and significant variation in topography (segments of the Southern Urals). Anthropogenic factors of fire ignition are a population of 1.9 million people, agriculture development and a great number of grass fires in the spring during a sharp temperature increase by 10-20°C. From 2010 to 2018, about 140 thousand MODIS hotspots were registered in the region.

The Meschera lowland is located within Moscow, Ryazan and Vladimir regions and is characterized by a continuous

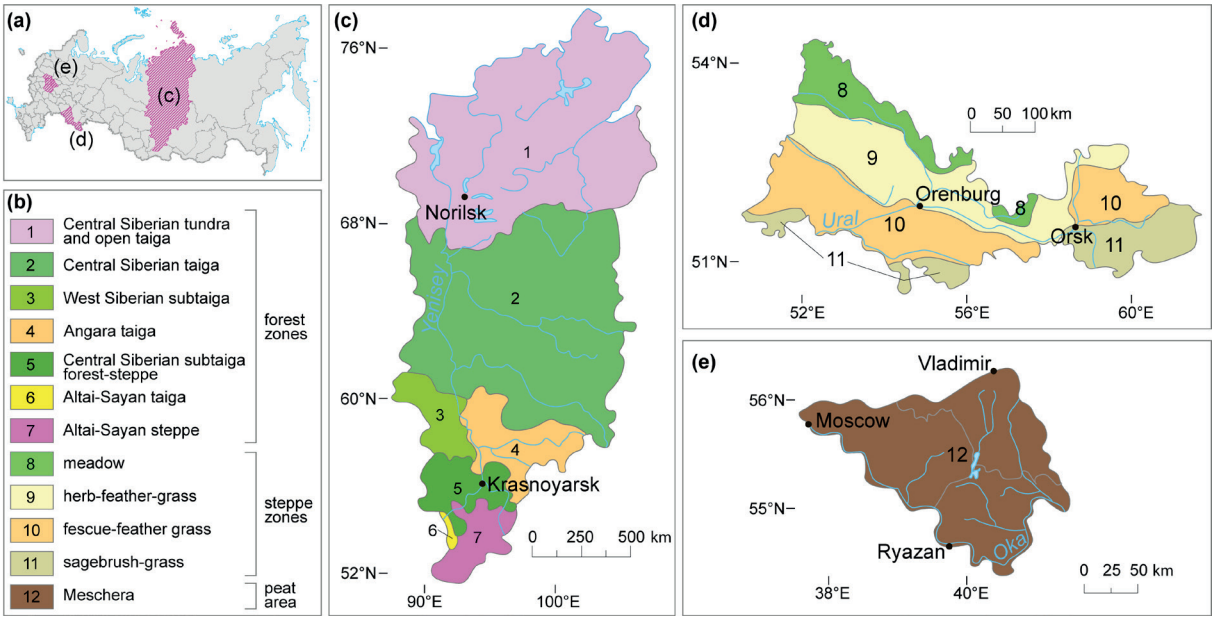

Fig. 1. Spatial units of the study areas: (a) Overview map (b) Legend (c) Krasnoyarsk territory (d) Orenburg region (e) Meschera peat area

spread of dry peatlands. The fire vulnerability of the region is determined by its high population density (more than 150 people per km^2) and consequently great anthropogenic load, as well as the presence of drained peatland locations with low moisture. The region is known for the fires of 2010 during the summer heat wave, while 7.4 thousand MODIS hotspots were also determined here from 2010 to 2018.

Data

In the study, we used only data that met the requirements of spatial reference, regular updating and open access, which makes it possible to reproduce the developed method for further studies and use it for similar purposes.

Fire data. Previously mentioned FIRMS MODIS and VIIRS hotspots with confidence values greater than 95% were used as a reference sample of fires from 2010 to 2019. This sample was divided into several parts:

– 2000-2018 – to select the regions of Russia with the most fires in the last decade for further study (as was mentioned in the Study areas section);

– 2016-2018 – for estimating fire danger parameters based on the available remote sensing data of the selected satellites;

– 2019 –to test and validate the developed fire prevention method in near-real-time conditions.

For Krasnoyarsk territory, 2016-2019 ground data from the regional forest fire center (http://www.lpcentr.ru/) was additionally applied.

Remotely sensed data. To identify the changes in fire danger factors during the considered period, we used atmospherically corrected satellite products over 2016-2019 with different spatial and temporal resolution: MODIS (Moderate Resolution Imaging Spectroradiometer, Aqua/Terra, 250/500 meters, 0.5-2 days), SLSTR (Sea and Land Surface Temperature Radiometer, Sentinel-3, 500/1000 meters, 1.5 days), OLI/TIRS (Operational Land Imager/Thermal Infrared Sensor, Landsat-8, 30/100 meters, 16 days) and MSI (Multispectral Instrument, Sentinel-2, 10/20/60 meters, 5 days). Satellite data were derived from the USGS EarthExplorer service (https://earthexplorer.usgs.gov/). During the processing, they were divided into two complementary spatial levels: regional (MODIS and SLSTR, resampled to a base resolution of 500 m, available 1-2 times a day for all the study areas) and local (OLI/TIRS and MSI, resampled to a base resolution of 30 m, more accurate sensors, but available only once every 5-14 days).

Digital elevation model. The ASTER GDEM (Advanced Spaceborne Thermal Emission and Reflection Radiometer Global Digital Elevation Model) Version 3 was also obtained from the USGS EarthExplorer service to characterize the topography of the areas, including elevation, slope and aspect parameters. Its spatial resolution is 1" (~30 meters), vertical accuracy (RMSE) – 8.52 meters, and it covers the area between 83°N and 83°S, which is crucial for the territory of Russia.

Map layers. Feature layers for settlements and roads located in the study areas were extracted from OpenStreetMap (https://www.geofabrik.de/data/download.html) to estimate the anthropogenic load.

METHODS

To achieve the main goal of the study, a mixed methodological approach was used. Quantitative methods of GIS, raster algebra and mathematical statistics were applied to process the input spatial data, calculate fire danger parameters, investigate their correlation with the observed fires and evaluate the applicability of the developed method. But to interpret the results and make some conclusions, qualitative expert methods were included in the study.

Fire danger parameters. Fire danger parameters were defined in this study as parameters that are related to the fire danger factors and can be used to quantify them. The structure of the forest, steppe and peat vegetation was described using vegetation indices – Normalized Difference Vegetation Index (NDVI; Rouse 1973) and Soil Adjusted Vegetation Index (SAVI; Huete 1988), which were applied for complete and partial projective cover respectively. These parameters are calculated based on two stable spectral bands – red (R) and near-infrared (NIR). Normalized Difference Water Index (NDWI; Gao 1996) was also used to evaluate surface moisture based on the near-infrared and shortwave infrared (SWIR) bands. These indices were computed using the following formulas:

$$NDVI = (B_{NIR} - B_R) / (B_{NIR} + B_R) \quad (1)$$

$$SAVI = (B_{NIR} - B_R) / (B_{NIR} + B_R = 0.5) \times (1 + 0.5) \quad (2)$$

$$N_{DWI} = (B_{NIR} - B_{SWIR}) / (B_{NIR} + B_{SWIR}) \quad (3)$$

where B_R, B_{NIR} and B_{SWIR} correspond to reflectance in channels 1, 2 и 5 of MODIS, 2, 3, 4 of SLSTR, 4, 5, 9 of OLI and 4, 8a, 10 of MSI.

The surface temperature was derived from the MO/YD11 (MODIS) and LST (SLSTR) thermal products and was also calculated from the thermal channels 10 and 11 of TIRS using QGIS (Quantum Geographic Information System). Topography was expressed in terms of morphometric parameters – true altitude, slope and aspect, derived from ASTER GDEM.

The anthropogenic load was determined as a normalized back-weighted function of the distance to settlements and roads. One of the main causes of fires is an anthropogenic factor. Therefore, a simple assumption was used: lower distance to settlements and roads as places of possible human presence corresponds to the higher fire danger. The weights of normalized distance values were calculated for different features using the ranked method: 0.91 for settlements and 0.09 for roads. Finally, the anthropogenic load (*AL*) was computed by the following formula:

$$MML = 0.91 \times D_S / D_{Smax} + 0.09 \times D_R / D_{Rmax} \quad (4)$$

where D_S – distance to settlements, D_R – distance to roads, D_{Smax} and D_{Rmax} – maximal values of distance to settlement and roads respectively, for normalization.

All fire danger parameters were divided into two types according to their variability:

– variable – NDVI, SAVI, NDWI and surface temperature, which vary within a day and over longer time intervals and were estimated using remotely sensed data for 2016-2018 and 2019;

– constant – topography parameters and anthropogenic load, which are characterized by negligible temporal changes and were determined once using the elevation model and feature layers.

Correlation of variable fire danger parameters with the actual fires. 4,590 actual fires were extracted from the fire data for 2016-2018, when all the used satellites were operational. To analyze the occurrence of these fires, we introduced the conditional probability of ignition P as a linear function of time. The zero probability was fixed at the time T1: 7 days before the fire at the regional level (when using frequent MODIS and SLSTR data) and 30

days at the local level (rare OLI/TIRS and MSI). **These time intervals allowed to gain a sufficient number of points and analyze trend lines.** The threshold probability of 90%, characterizing a potential fire, was defined as the value of the maximum difference in the parameter before the fire – at the time T2. As a result, the conditional probability of ignition P was found by interpolating between (T1, 0) and (T2, 90).

To determine the correlation between variable parameters V (NDVI, SAVI, NDWI and surface temperature t) and the value of P, we built their regional 7-day and local 30-day time series and established linear relationships between them (example in Fig. 2). To take into account the spatio-temporal variability of the fire danger factors, the analysis was performed in each of the 12 spatial units (seven forest zones, four steppe zones and one peat area) of the study areas for each of the 7 fire season months, from April to October. Finally, the linear transition equations P(V), correlation coefficients r and 90%-threshold values Vthreshold were derived for each variable parameter and 84 space-time units on two spatial levels. All these values were published at https://preventfires.github.io/.

Correlation of constant fire danger parameters with the actual fires. The constant fire danger parameters (C) within the study areas were divided into 8 equal topography (true altitude, slope, aspect) and anthropogenic load (L) classes. Based on these classes, the statistical probability of ignition S, which was defined as the ratio of the number of fires in the current class to the total number of fires, was calculated for the 84 space-time units and two spatial levels mentioned above (the values are presented on https://preventfires.github.io/).

RESULTS

The derived transition equations and 90%-threshold values of variable parameters can be used to prevent wildfires in the study areas over the fire season: if at least one indicator is greater than its threshold value, then this location can be interpreted as a fire point. For example, the temperature threshold value for the Meschera peat area in July is 51.5°C on a regional level and 55.1°C on a local level, while in June it is 41.5°C and 42.3°C respectively. Thus, the conditional probabilities *P* of NDVI, SAVI, NDWI and surface temperature represent partial ratings of fire danger.

However, the main principle of the existing systems is the weighted combination of partial ratings into a general fire danger rating. In our case, variable and constant parameters were combined at the highest hierarchical level. As the significance of variable parameters is larger compared to constant parameters due to the temporal updatability, their weights were ranked as 0.66 and 0.33 respectively. At the next level, the NDVI, SAVI, NDWI and temperature weights were established based on the correlation coefficient *r*, while statistical probability was used to determine the weights for topography and anthropogenic load factors. As a result, the equation of the general fire danger rating *G* within each space-time unit was as follows:

$$G = 2/3\sum_{i=1}^{n}\frac{r_i}{\sum r_{V-P}}\circ P(V_i) + 1/3\sum_{j=1}^{m}\frac{S_j}{\sum S(C)} \quad (5)$$

where *n*, *m* – the number of significant ($r > 0.7$) variable and constant parameters. For example, for the Altai-Sayan taiga May unit this equation was as follows:

$$G = 0.28P(NDVI) + 0.39P(t) + 0.33S(L) \quad (6)$$

The weights of fire danger parameters that were used to generate equations for other space-time units as well as other result values from this study were published at https://preventfires.github.io/. The obtained general fire danger rating was used to divide the territory into 2 classes: fire points and no-fire area. If the value of the rating was greater than 0.9 or 90%, then the pixel was attributed to the fire point class, otherwise – to the no-fire class.

The workflow of the wildfire prevention method is shown in Fig. 3. It was validated by monitoring the study areas from April to August 2019. The fire points obtained using the developed method were compared with the reference FIRMS fire data of the same period (Table 1). To evaluate the applicability of the method, two metrics were used:

– reliability – the ratio of truly prevented (observed) fire points to all prevented (potential) fire points, this metric demonstrates the plausibility of the method results;

– confidence – the ratio of observed fire points, registered by the method, to all observed (real) fire points, this metric indicates how much the method results relate to the real situation.

Overall, the reliability of the method was 61%, and its confidence was 67%. These values were reached due to the spatio-temporal sampled variability of threshold values, equations and weights of fire danger partial and general parameters. It was also improved by combining the results of two spatial levels: regional data has large territorial coverage and high temporal resolution, but local data is more spatially detailed and accurate in identifying the fire danger parameters. There were common cases, when fires were not prevented by MODIS/SLSTR data, but prevented by OLI/TIRS/MSI data, and cases, when a fire was prevented on both levels.

However, the one weakness of the method is a sufficiently great number of falsely prevented points. It is planned to correct this in further studies.

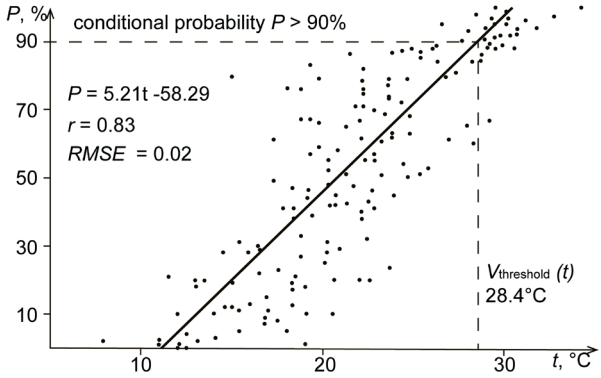

Fig. 2. Correlation between surface temperature t and conditional probability of ignition P in the case of the Altai-Sayan taiga forest area in May

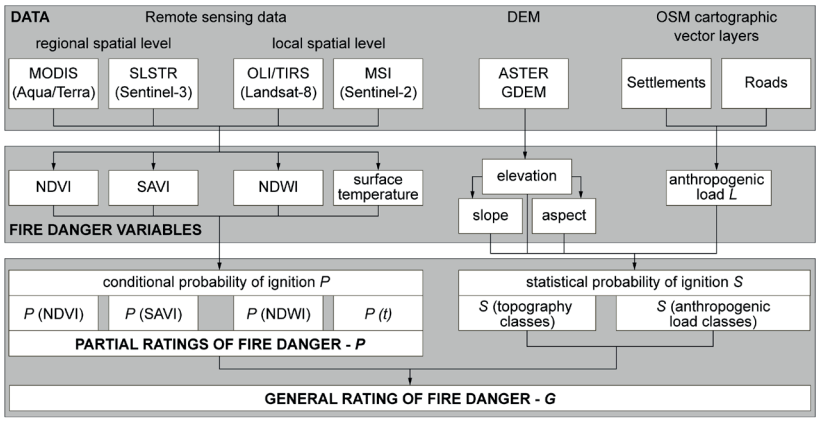

Fig. 3. Wildfire prevention by computing partial and general fire danger ratings

Table 1. Results of the fire prevention method validation

Parameter	Krasnoyarsk territory	Orenburg region	Meschera lowland	In total
Number of potential fires	201	60	41	302
Occured of them	119	37	29	185
Reliability, %	59	62	71	61
Number of occured fires	98	25	20	143
Prevented of them	64	15	17	96
Confidence, %	65	60	85	67

DISCUSSION

The proposed method is based on the spatio-temporal variability of fire danger factors, which was achieved by dividing the study areas into space-time units. To confirm that, changes in the threshold values of variable fire danger parameters were analyzed.

In Krasnoyarsk Territory, it was found that informative parameters with $r > 0.7$ were NDVI and surface temperature (Fig. 4a, b). The threshold values reached a maximum in June and July, during the flowering phenological phase and the highest surface heating. In Orenburg region, SAVI, NDWI and surface temperature were found to be informative. The time variation of SAVI showed a maximum in May, which corresponds to the phenological season in the steppes (Fig. 4c). Temperature threshold variation (Fig. 4d) was similar to the trend in the Krasnoyarsk forests. The NDWI changes (Fig. 4e) were inversely related to the temperature curve with a negative peak displacement towards August, when the surface moisture is minimal. The largest number of informative parameters (NDVI, SAVI, NDWI and surface temperature) was found in Meschera. Their variation (Fig. 4f) corresponded to the general trends described above with a difference only in values. Spatially, threshold values varied monotonically from North to South, which indicates the zonal variability of surface temperature, vegetation and consequently fire danger factors.

These trends led to the following conclusions. The dependence of fire danger on vegetation indices is complex. The higher index value usually corresponds to more live green vegetation, which limits the fire ignition. However, in our case, the inverse quantitative trend was identified as the higher index value indicates a larger amount of available fuel, which changes both zonally and seasonally. Surface temperature and moisture are inversely proportional and change in accordance with the air temperature curve, which creates conditions for ignition.

The significance of constant fire danger parameters represented by statistical probabilities was also great. The largest number of wildfires were observed in areas with slightly sloping surfaces (1…3°), southern aspect (South, South-East, South-West) and high anthropogenic load. These patterns allow to prevent fires in areas with these classes of constant parameters. It proves that the inclusion of constant fire danger factors in the analysis is crucial, particularly when variable parameters do not reach threshold values.

To summarize, we had the following policy implications. The revealed spatial and temporal trends of threshold values, especially zonal and seasonal, justified the relevance of the discrete approach to fire danger assessment based on space-time units (zones and months). The obtained values of correlation coefficient (in most cases higher than 0.7) and statistical probability allowed to establish the relations between fire danger factors and integrate them in the general fire danger parameter for the study areas.

CONCLUSIONS

As a result of the study, we developed the wildfire prevention method that is distinguished by original and advantageous features:

– the method involves multidimensional discrete adaptive modelling of significant fire danger factors – NDVI and SAVI as vegetation fuel factor; NDWI as water content factor; surface temperature as thermal factor; elevation, slope and aspect as topography factor; and distance to settlements and roads as anthropogenic load factor;

– the identification of possible fire points was performed both analytically, based on partial ratings (each variable factor has a threshold value and can independently characterize a potential fire), and synthetically by normalized-weight integration of parameters into the general rating;

– the fire prevention was enhanced by the use of heterogeneous regional and local data, which complement each other at two different spatial levels;

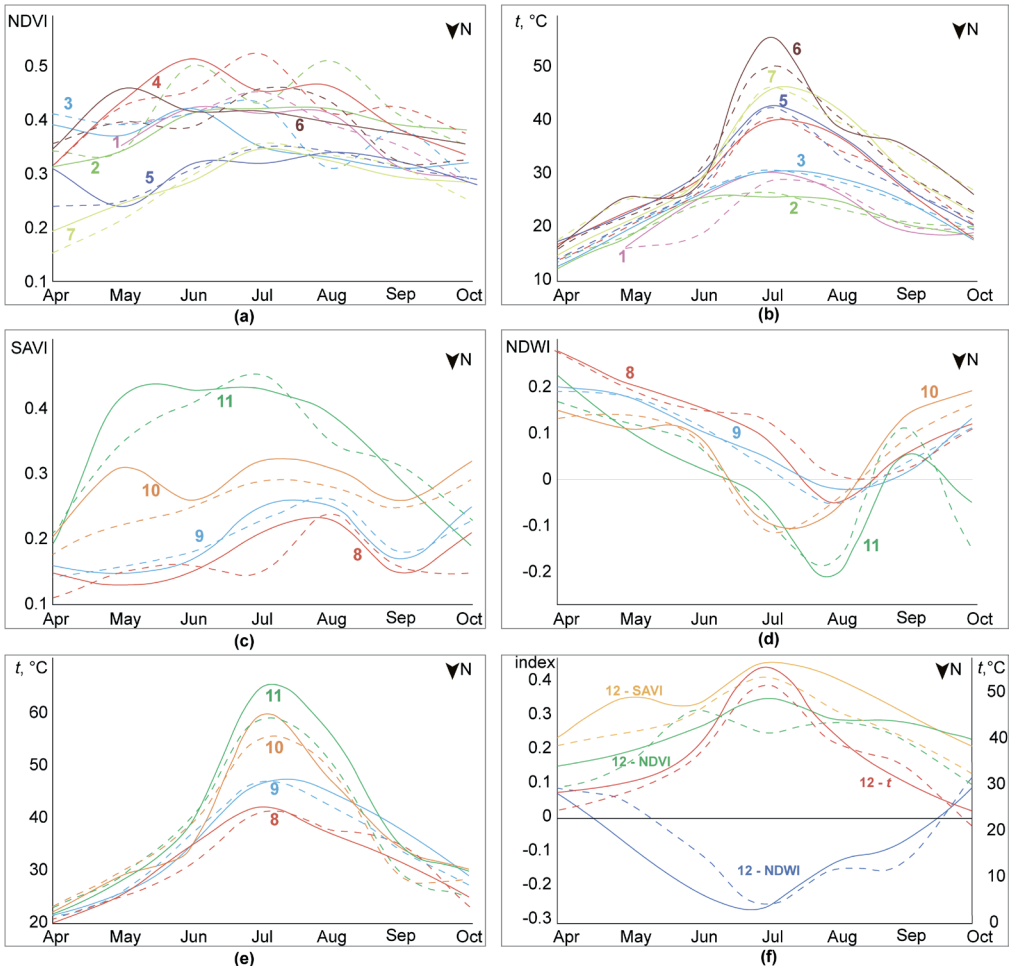

Fig. 4. Temporal variation in threshold values of variable fire danger parameters: (a) NDVI, (b) surface temperature in Krasnoyarsk, (c) SAVI, (d) NDWI, (e) surface temperature in Orenburg region, (f) in Meschera. The subzones are presented in Fig. 1, solid lines reperesent OLI/TIRS and MSI values, dashed lines – MODIS and SLSTR

– the main feature is the establishment of the key parameters (threshold values, equations and weights) for different space-time units (forest, steppe and peat zones and months), which makes it possible to improve fire prevention based on the spatio-temporal differentiation of fire danger factors.

All of this indicates the validity of the method for solving scientific and practical problems in similar study regions, which was confirmed by the relevant validation results with the confidence and reliability values above 60%. Further studies will be devoted to improving the prevention by extending fire danger parameters for the study areas by including deviation spring, relative greenness (Cheret and Denux 2011), etc.

REFERENCES

Akbulak C., Tatli H., Aygun G., and Saglam B. (2018). Forest fire risk analysis via integration of GIS, RS and AHP: The Case of Canakkale, Turkey. International Journal of Human Sciences, 15(4), 2127-2143, DOI: 10.14687/jhs.v15i4.5491.

Arganaraz J., Landi M., Bravo S., Gavier-Pizzaro G., Scavuzzo C., and Bellis L. (2016). Estimation of Live Fuel Moisture Content From MODIS Images for Fire Danger Assessment in Southern Gran Chaco. IEEE Journal of Selected Topics in Applied Earth Observations and Remote Sensing, 9(12), 5339-5349, DOI: 10.1109/JSTARS.2016.2575366.

Bartalev S., Stytsenko F., Khvostikov S., and Loupian E. (2017) Methodology of post-fire tree mortality monitoring and prediction using remote sensing data. Current problems in remote sensing of the Earth from space, 14(5), 176-193 (in Russian with English summary).

Bui D., Le H., and Hoang N. (2018). GIS-based spatial prediction of tropical forest fire danger using a new hybrid machine learning method. Ecological Informatics, 48, 104-116, DOI: 10.1016/j.ecoinf.2018.08.008.

Burgan R. (1988). 1988 Revisions to the 1978 National Fire-Danger Rating System. Asheville, NC: U.S. Department of Agriculture, Forest Service, Southeastern Forest Experiment Station, DOI: 10.2737/SE-RP-273.

Camia A. and Amatulli G. (2009). Weather Factors and Fire Danger in the Mediterranean. In: E. Chuvieco, ed., In Earth Observation of Wildland Fires in Mediterranean Ecosystem. Berlin: Springer., 71-82, DOI: 10.1007/978-3-642-01754-4_6.

Cheret V. and Denux J. (2011) Analysis of MODIS NDVI Time Series to Calculate Indicators of Mediterranean Forest Fire Susceptibility. GIScience & Remote Sensing, 48(2), 171-194, DOI:10.2747/1548-1603.48.2.171.

Chuvieco E. and Congalton R. (1989). Application of remote sensing and geographic information systems to forest fire hazard mapping. Remote Sensing of the Environment, 29, 147-159, DOI: 10.1016/0034-4257(89)90023-0.

Chuvieco E., Aguado I., Cocero D., and Riano D. (2010). Design of an empirical index to estimate fuel moisture content from NOAA-AVHRR images in forest fire danger studies. International Journal of Remote Sensing, 24(8), 1621-1637, DOI: 10.1080/01431160210144660b.

Chuvieco E., Cocero D., Riano D., Martin P., Martinez-Vega J., de la Riva J., and Perez F. (2004). Combining NDVI and surface temperature for the estimation of live fuel moisture content in forest fire danger rating. Remote Sensing of Environment, 92(3), 322-331, DOI: 10.1016/j.rse.2004.01.019.Deeming J. (1974). The National fire-danger rating system. Fort Collins, Colo: Rocky Mountain Forest and Range Experiment Station, Forest Service, U.S. Dept. of Agriculture, DOI: 10.5962/bhl.title.98707.

Eskandari S., Pourghasemi H., and Tiefenbacher J. (2020). Relations of land cover, topography, and climate to fire occurrence in natural regions of Iran: Applying new data mining techniques for modeling and mapping fire danger. Forest Ecology and Management, 473, 1-15, DOI: 10.1016/j.foreco.2020.118338.

Furaev V., Tsvetkov P., Furaev I., and Zlobina L. (2016). Conditions of fire origin and spreading in forest regions of Krasnoyarsk krai. Conifers of the boreal area, 35(1-2), 66-74 (in Russian with English summary).

Gao B. (1996). NDWI — A normalized difference water index for remote sensing of vegetation liquid water from space. Remote Sensing of Environment, 58(3), 257-266, DOI: 10.1016/S0034-4257(96)00067-3.

Gizatullin A., Alexeenko N., Moiseeva N. (2019). Development of the preventive natural fire danger assessment algorithm using remote sensing data. Geodesy and Cartography, 80(1), 102-109 (in Russian with English summary), DOI: 10.22389/0016-7126-2019-943-1-102-109.

Glagolev V. (2018). Predicting the Emergence and Spread of Grass Fires – on the example of Jewish Autonomous Region. Regional problems, 21(2), 86-91 (in Russian with English summary). DOI: 10.31433/1605-220X-2018-21-2-92-96.

Hanston S., Padilla M., Corti D., and Chuvieco E. (2013). Strengths and weaknesses of MODIS hotspots to characterize global fire occurrence. Remote Sensing of Environment, 131, 152-159, DOI: 10.1016/j.rse.2012.12.004.

Huete A. (1988). A soil-adjusted vegetation index (SAVI). Remote Sensing of Environment, 25(3), 295-309, DOI: 10.1016/0034-4257(88)90106-X.

Jaiswal R., Mukherjee S., Raju K., and Saxena R. (2002). Forest fire risk zone mapping from satellite imagery and GIS. International Journal of Applied Earth Observation and Geoinformation, 4(1), 1-10, DOI: 10.1016/S0303-2434(02)00006-5.

Khvostikov S., Bartalev S., and Loupian E. (2016). Stochastic wildfire model based on Monte-Carlo method and remote sensing data integration. Current problems in remote sensing of the Earth from space, 13(5), 145-156 (in Russian with English summary).

McArthur A. (1967). Fire behaviour in eucalypt forests. Canberra: Forestry and Timber Bureau.

Medvedeva M., Vozbrannaya A., Sirin A., and Maslov A. (2019). Potential of different multispectral satellite data for monitoring abandoned fire hazardous peatland and rewetting effectiveness. Current problems in remote sensing of the Earth from space, 16(2), 150-159 (in Russian with English summary), DOI: 10.21046/2070-7401-2019-16-2-150-159.

Nesterov V. (1949). Forest burnability and methods of its determination. Moscow: Goslesbumizdat (in Russian).

Ogureeva G. and Kotova T. (2013). Biogeographic maps for geospatial analysis of environmental potential of Russia. Geobotanical mapping, 136-144, DOI: 10.31111/geobotmap/2013.136.

Pavleychik V. (2016). Long-term dynamics of natural fires in the steppe regions (case study- of the Orenburg region). Bulletin of Orenburg State University, 6(194), 74-80 (in Russian).

Piralilou S., Einali G., Ghorbanzadeh O., Nachappa T., Cholamnia K., Blaschke T., and Chamisi P. (2022). A Google Earth Engine Approach for Wildfire Susceptibility Prediction Fusion with Remote Sensing Data of Different Spatial Resolutions. Remote sensing, 14, 1-26. DOI: 10.3390/rs14030672.

Plotnikova A. and Ershov D. (2015). The method to update maps of forest natural fire danger levels using satellite-derived thematic products. Current problems in remote sensing of the Earth from space, 12(1), 181-189 (in Russian with English summary).

Rosadi D. and Andriyani W. (2021). Prediction of forest fire using ensemble method. Journal of Physics: Conference Series, 1918, DOI: 10.1088/1742-6596/1918/4/042043.

Rouse J., Haas R., Deering D., Schell J., Harlan J. (1973). Monitoring the vernal advancement and retrogradation (green wave effect) of natural vegetation. Greenbelt: NASA Goddard Space Flight Center.

Sofronov M. and Volokitina A. (1990). Pyrological zoning in the taiga zone. Novosibirsk: Nauka, the RAS Siberian branch (in Russian).

Sofronova T., Volokitina A., and Sofronov M. (2008). Assessing the Fire Hazard from Weather Conditions in Mountain Forests of the Southern Baikal Region. Geography and Natural Resources, 29(2), 163-168 (in Russian with English summary).

Sofronova A. and Volokitina A. (2017). Assessment of fire hazard for forest sites at the territory of oil and gas complexes using Earth remote sensing data. Siberian Journal of Forest Science, 5, 84-94 (in Russian with English summary), DOI: 10.15372/SJFS20170508.Suresh Babu K., Roy A., and Prasad P. (2016). Forest fire danger index based on modifying Nesterov Index, fuel, and anthropogenic activities using MODIS TERRA, AQUA and TRMM satellite datasets. Proceedings of the SPIE 9877, Land Surface and Cryosphere Remote Sensing III, 98771A, DOI: 10.1117/12.2222738.

Van Wagner C. (1987). The development and structure of the Canadian Forest Fire Weather Index System. Ottawa: Canadian Forestry Service Headquarters.

Volokitina A., Sofronova T., and Korets M. (2016). Regional scales of fire danger rating in the forest: improved technique. Siberian Journal of Forest Science, 2, 52-61 (in Russian with English summary).

Xu D., Dai L., Shao G., Tang L., and Wang H. (2005) Forest fire risk zone mapping from satellite images and GIS for Baihe Forestry Bureau, Jilin, China. Journal of Forestry Research, 16(3), 169-174, DOI: 10.1007/BF02856809.

Yankovich K., Yankovich E., and Baranovckiy N. (2019). Classification of Vegetation to Estimate Forest Fire Danger Using Landsat 8 Images: Case Study. Mathematical Problems in Engineering, 2019, 1-14, DOI: 10.1155/2019/6296417.

Yebra M., Dennison P., Chuvieco E., Riano D., Zylstra P., Raymond H., Danson F., Qi Y., and Jurdao S. (2013). A global review of remote sensing of live fuel moisture content for fire danger assessment: Moving towards operational products. Remote Sensing of Environment, 136, 455-468, DOI: 10.1016/j.rse.2013.05.029.

Zubareva A. (2018). Evaluation methods of vegetation fire risks. Regional problems, 21(2), 92-96 (in Russian with English summary). DOI: 10.31433/1605-220X-2018-21-2-92-96.

RESEARCH PAPER

EFFICACY OF SYNTHETIC SEDIMENT GRAPH DEVELOPED USING VARIOUS MODIFIED TIME-AREA METHODS

Azadeh Katebikord[1], Seyed H. Sadeghi[1*] and Vijay P. Singh[1, 2]

[1] Department of Watershed Management Engineering, Faculty of Natural Resources and Marine Sciences, Tarbiat Modares University, Noor, 46417-76489, Iran

[2] Department of Biological and Agricultural Engineering & Zachry Department of Civil & Environmental Engineering, Texas A&M University, College Station, TX 77843-2117, USA

***Corresponding author:** sadeghi@modares.ac.ir

Received: September 25th, 2021 / Accepted: April 24th, 2022 / Published: June 30th, 2022

https://DOI-10.24057/2071-9388-2021-109

ABSTRACT. Suspended sediment (SS) is an essential indicator for assessing watershed health. However, the temporal variation of SS, called sediment graph (SG) using readily available data, is not always considered, particularly in un-gauged watersheds, which are many in developing countries. Since field measurements of SS are time-consuming and costly, the synthetic SG seems to be a promising alternative. Therefore, it is essential to have reliable SS data for watershed management. This study aimed at simulating SGs through conceptual analysis of soil erosion and sediment yield at the watershed scale. To that end, soil erosion, sediment yield, and sediment routing were modeled using 38 storm events collected during 2011 and 2019 at the Galazchai Watershed in West Azerbaijan Province, Iran. Initially, the Time-Area Method (TAM) was applied, and then two strategies were considered to improve the TAM performance, including RUSLE and sediment delivery ratio (SDR) using gradient ratio and WaTEM/SEDEM methods. Comparing simulated SGs with recorded ones showed that the SDR-based method had the lowest relative error in time to peak and base time, but the peak value had the highest relative error. Results also showed that TAM developed using the spatially distributed travel time method had a better performance than the channel longitudinal profile method. Overall, TAM could not simulate the temporal variation of sediment and needs further research.

KEY WORDS: fluvial behavior, sediment modeling, soil erosion, temporal distribution, watershed modeling

CITATION: Katebikord A., Sadeghi S.H., Singh V.P. (2022). Efficacy of Synthetic Sediment Graph Developed using Various Modified Time-Area Methods. Geography, Environment, Sustainability, 2(15), p. 38-57
https://DOI-10.24057/2071-9388-2021-109

ACKNOWLEDGEMENTS: The corresponding author was partially supported by the Agrohydrology Research Group of Tarbiat Modares University (Grant No. IG-39713), Iran. The authors warmly credit Dr. Raoof Mostafazadeh, Dr. Pari Saeidi, and Dr. Mostafa Moradi Dashtpagerdi for providing the first data bank of rainfall storm occurrences.

Conflict of interests: The authors reported no potential conflict of interest.

INTRODUCTION

Soil erosion is a severe menace to soil and water resources. Soil erosion of watershed areas leads to suspended sediment (SS) and its transport by flow and sediment yield (Golosov et al. 2014; Sadeghi and Singh 2017). The spatio-temporal analysis of sediment yield is needed for watershed management, especially for soil and water conservation and watershed health assessment (Sadeghi et al. 2019; Hazbavi et al. 2020; Mirchooli et al. 2021). The amount of SS produced in a watershed depends on the distribution and duration of precipitation, sediment availability, flow velocity, geomorphology, land cover and human activities (Seeger et al. 2004; Messina and Biggs 2016; Rahaman and Solavagounder 2020; Sokolov et al. 2020; Waiyasusri and Wetchayont 2020; de Paula et al. 2021). Most watershed management studies provide general estimates of soil erosion using empirical or non-distributed models such as Universal Soil Loss Equation (USLE), Revised Universal Soil Loss Equation (RUSLE), and Water Erosion Prediction Project (WEPP) (Wischmeier and Smith 1978; Sadeghi and Mizuyama 2007; Srivastava et al. 2020; Zheng et al. 2020).

The pattern of SS variation during hydrological events, especially flood events, has already been considered (e.g., Rovira and Batalla 2006; Sadeghi et al. 2008b; Zheng et al. 2013; Sadeghi and Zakeri 2015; Sadeghi and Singh 2017; Rymszewicz et al. 2018; Zhan et al. 2019; Qiao et al. 2020). Since the SS load accounts for a significant portion of the total sediment load at the storm scale, the sediment load estimation from individual storms is of particular importance (Xie et al. 2017). Accordingly, the temporal distribution of the SS load as sediment graph (SG) at a storm-scale was considered (Sadeghi and Singh 2005; De Girolamo et al. 2015), based on sufficient sampling during each event (Rovira and Batalla 2006; Choubin et al. 2018; Ruben et al. 2020).

Different methods have been developed to estimate sediment yield at different temporal and spatial scales and provide synthetic SGs (Singh et al. 2008; Bhunya et al. 2010; Banasik and Hejduk 2014; Trinh et al. 2018). In estimating the temporal variation of SS for a storm, the Instantaneous Unit Hydrograph (IUH) has been used to produce Instantaneous Unit Sediment Graph (IUSG) and then provide SG (Banasik

and Mitchell 2008; Sadeghi et al. 2008; Bhunya et al. 2010; Banasik and Hejduk 2014). Other methods, such as regression analysis (Sadeghi and Saeidi 2010), power model (Bhunya et al. 2010), two-parameter gamma distribution function (Singh et al. 2013), and SCS-CN method with IUSG (Gupta et al. 2019), have also been used for deriving the synthetic SG. The SG has been simulated using hydrograph (Saeedi et al. 2016). Using 25 measured SGs from 2011 to 2015 in the Galazchai Watershed, Iran, Saeedi et al. (2016) simulated SG based on hydrograph with the allometric concept and fitted bivariate regression equations. Their results showed that the temporal components were more accurate than other components.

The spatial distribution of contributory areas in runoff generation was done using the time-area method (TAM) by Clark (1945). This method was then applied by Kothyari et al. (1994, 1996) to fluvial studies at the watershed scale. Noting the uncertainties of TAM in the estimation of SG (Kothyari et al. 1994, 1996; Du et al. 2009; Raisi et al. 2010; Sadeghi et al. 2015), Kothyari et al. 1994) divided the Karso watershed, India, into several segments based on TAM and used USLE to calculate erosion in each section, and then calculated the sediment transported to the watershed outlet with the sediment delivery ratio (SDR) derived from the slope ratio of the two consequent sections. Kothyari et al. (1997) also estimated instantaneous sediment variation for individual storms in 12 small watersheds in India by employing the kinematic wave method and sediment-based mapping, Kothyari et al. (2002), Sadeghi and Tofighi (2003), Raisi et al. (2010), Khaledi Darvishan et al. (2010) reported that the TAM was less than accurate. Her and Heatwole (2016) simulated sediment yield for three storm events in the Owl Run Watershed in the US using the HYSTAR model based on two time-area sediment routing methods and sediment transport capacity. Li et al. (2017) successfully examined monthly changes in sediment discharge and its amount in a watershed located in the karst areas of China. Mahoney et al. (2018) investigated the temporal and spatial variations of sediment production in the Upper South Elkhorn Watershed in Kentucky, USA. They found that the sediment production in different parts of the watershed was in proportion to the extent of their connection during the year. Gupta et al. (2019) modeled the SG for small watersheds using soil moisture under four different conditions in six watersheds, and the estimated values were compared with observed values and the Bhunya et al. (2010) Sediment Graph Model (BSGM). Ruben et al. (2020) used Acoustic Sediment Estimation Toolbox (ASET) to calculate SS transport in the Paraná River in Argentina to obtain temporal and spatial variations of SSC. Bajirao et al. (2021) validated the ANN and ANFIS Artificial Intelligence models to simulate the daily SSC of the Koyna River in India and showed that data preprocessing with wavelet significantly improved the model prediction. Yadav et al. (2021) used GA-MOO-ANN, ANN, MLR, and SRC models to estimate the suspended sediment at 11 gauging stations of the Mahanadi River, India from 1990 to 2010, and showed that the GA-MOO-ANN model was better than other models.

Despite the importance of temporal variation of SS load, SGs are not available in many watersheds. Therefore, a simple method based on readily available SG at the watershed scale is needed. To that end, TAM, due to its simplicity and easy availability of data, is desirable. However, it requires improvement, so TAM was derived from different approaches at the watershed scale. Hence, this study calculated isochrones using spatially distributed travel time and channel longitudinal profile methods using two methods, viz. Hadley et al. (1985) and WaTEM/SEDEM method to calculate the SDR for the increased accuracy of the TAM method in estimating the synthetic SG.

MATERIALS AND METHODS

Study area

The study was conducted in the Galazchai Watershed due to reliable information and input data (i.e., Sadeghi et al. 2015; Moradi Dashtpagerdi et al. 2019). The Galazchai Watershed (ca. 103 km^2, 37° 01' and 37° 09' N, and 44° 56' and 45° 35' E) is located in West Azerbaijan Province, Iran, as one of the sub-watersheds of the diminishing Urmia Lake. The general view of the study watershed is shown in Fig. 1. The mainstream is 19.3 km long. The mean slope is 32%, and the elevation varies from 1492 to 3273 m above mean sea level. The watershed is in a semiarid climate with a mean annual temperature of 11.8°C and mean annual precipitation (1981–2010) of 482 mm. The mean annual discharge of the Galazchai River is 1.64 m^3 s^{-1}, and the mean annual water yield is 51.72 million m^3, and the highest observed mean annual discharge was recorded at 7.24 m^3 s^{-1} (Sadeghi et al. 2015). Rangeland is the dominant vegetation of the area (≈ 87%). In many flat areas, land use is agriculture and orchard (≈ 11%). Most of the agricultural lands are distributed in the vicinity of the main outlet and upstream of the watershed (Sadeghi et al. 2015).

Methodology

Data Collection

In this study, TAM was used to prepare a synthetic SG. For this purpose, flow and SS data were also recorded for 38 storm events during 2011 and 2019. The storms from 2011 to 2018 were obtained from previous researches (i.e., Mostafazadeh et al. 2015; Saeedi et al. 2016; Moradi Dashtpagerdi et al. 2019), and the last 4 storms for year 2019 were recorded during the present study. All samplings were made from the onset of the rising flow at the main outlet to the time of flow recession. So that, the suspended sediment sampling was performed at one-hour intervals in each storm event. The water level was simultaneously recorded to estimate flow discharge using the associated stage-discharge relationship. Water samples for the determination of SS concentration were collected through the depth integration method with the help of 2 l-capacity polyethylene flasks. SS concentrations were then determined in g l^{-1} through settling, decantation, and drying processes in the oven at 105°C for 24 h (Putjaroon and Pongboon 1987; Walling et al. 2001; Sadeghi and Saeidi 2010).

Development of Isochrones

The watershed was subdivided into isochrone segments by spatially distributed travel time (Welle and Woodward 1986) and channel longitudinal profile methods as in Eq. (1):

$$T_c = \frac{Kc}{I^{0.4}}\left(\frac{nL}{\sqrt{S}}\right)^{0.6} \quad (1)$$

where T_c is the surface flow travel time (min), *Kc* is the unit conversion factor and equals 6.943, I is the rainfall intensity (mm h^{-1}) with a 2-year return period and 24-hour rainfall duration, *n* is the roughness coefficient (Usul and Yilmaz 2002), *L* is the flow length (m), and *S* is the surface slope (m m^{-1}). The digital elevation model was used to calculate the slope and flow direction (FldrGrid) (Sadeghi et al. 2015).

The concentration time was calculated in the channel longitudinal profile method by the Kirpich formula (Sadeghi et al. 2015) as in Eq. (2).

$$T_c = 0.6628 L^{0.77} S^{-0.385} \quad (2)$$

where *Tc* is the concentration time (h), *L* is the stream length (km), and S is the typical slope (m m^{-1}). The principal tributary profiles and contour lines were plotted on the topographic map at a spacing equal to the desired period of 0.5 h to create isochrones on the watershed map. TAH was calculated by computing areas between isochrones drawn by joining the points of intersections with the same time interval. The pattern of isochrone areas with a digital elevation model (DEM) as the background is shown in Fig. 1. DEM with 30 m resolution was downloaded from the Terra satellite ASTER sensor from the USGS. This DEM was used due to its availability for the study area whose precision and validity have been proved and also recommended by Moradi Dashtpagerdi et al. (2019) for the same study watershed.

Soil Erosion Estimation

The RUSLE model was used to compute soil erosion in each isochrone segment, as stated in the general form of Eq. (3) (Renard et al. 1991).

$$E = RKLSCP \quad (3)$$

in which *E* is estimated soil loss (ton ha^{-1}) for each storm, *R* is rainfall erosivity factor (Mj mm ha^{-1} h^{-1}), *K* is soil erodibility factor (ton ha h ha^{-1} Mj^{-1} mm^{-1}), *LS* is slope length and steepness factor, *C* is cover management factor, and *P* is conservation practice factor.

Since no details except the total amount precipitation has been recorded in the weather station nested in the watershed, the calibrated Roose method (Roose 1977) for the region (Sadeghi and Tavangar 2015; Sadeghi et al. 2017) was used to calculate rainfall erosivity (R in Mj mm ha^{-1} h^{-1}) using the amount of rainfall (P in mm) as shown in Eq. (4).

$$R_R = 0.5 + 0.05P \quad (4)$$

In the same vein, no soil study has been conducted for the region to be used for the current research. Meanwhile, the global soil maps do not have an appropriate resolution for the small study watershed. Therefore, a high-resolution soil sampling was made through which 88 soil samples were collected from different parts of the watershed whose details were employed to develop the *K* factor map. After performing relevant experiments to calculate soil texture and organic matter, the value was calculated using soil erodibility nomograph (Foster et al. 1981), and the values were generalized to the watershed surface using the kriging method (Arnaldo et al. 2018). The *L* factor was obtained using Eq. (5) as proposed by Desmet and Govers (1996). The results were then multiplied into S to ultimately obtain the *LS* factor for the Galazchai Watershed.

$$L = \frac{\left(A_{ij-in} + D^2\right)^{m+1} - A_{ij-in}^{m+1}}{D^{m+2} \times x_{ij}^{m} \times 22.13^{m}} \quad (5)$$

where is the contributing area (m^2), *D* is the dimension of each cell (m), and x_{ij}=*sin* a_{ij}+*cos* a_{ij} x a_{ij} is also the flow direction in each cell *ij*. To prepare input maps to SAGA GIS software, the catchment area tool, particular area raster map, and slope map were used (Khorsand et al. 2017). The slope map was obtained using the 9-parameter 2nd order polynomial method (Zevenbergen and Thorne 1987) in SAGA software with radian unit. Also, a multiple flow direction method was used to map A_{ij} due to its ability to simulate convex and concave flows (Desmet and Govers 1996). As shown in Eq. 6, the cover management factor (C) on storm basis was calculated using the Normalized Difference Vegetation Index (NDVI) (Durigon et al. 2014). In this study, the Landsat 8 Operational Land Imager (OLI) and the ETM+ sensor from the USGS site were used to obtain NDVI. Therefore, Landsat OLI was georeferenced and necessary corrections including radiometric and FLAASH atmospheric were consequently conducted. The panchromatic images were also used to increase the

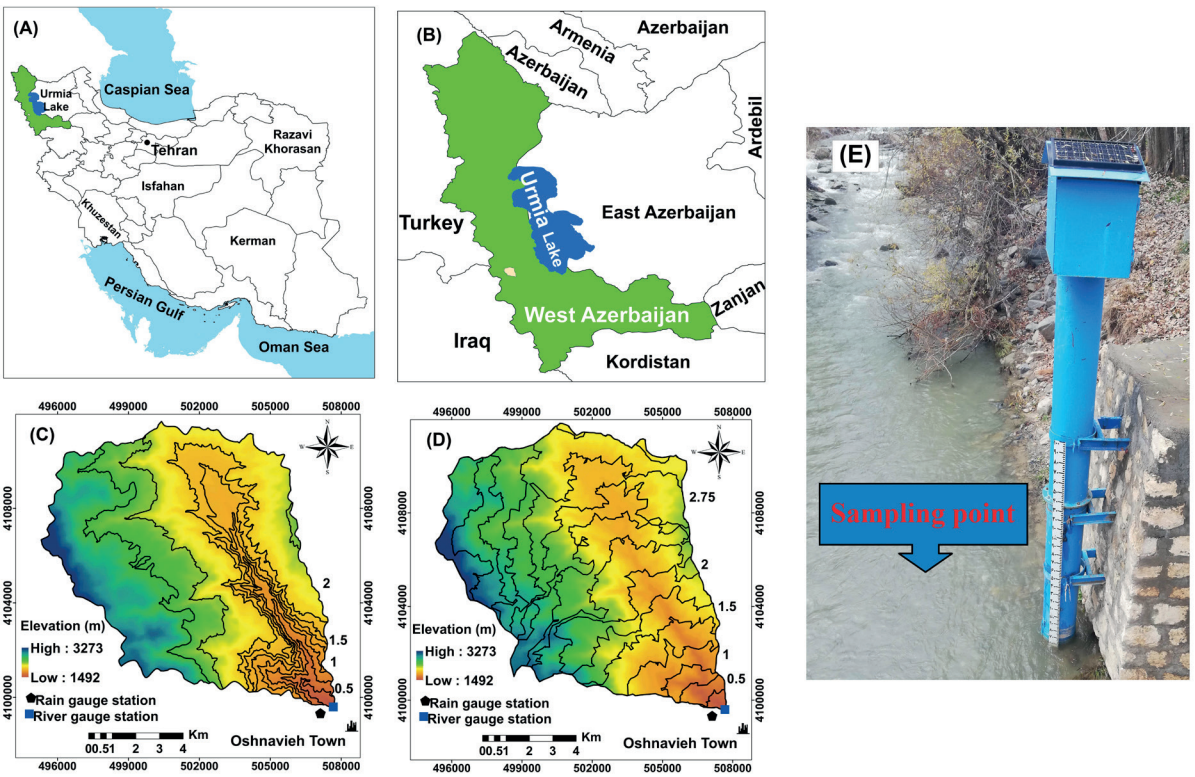

Fig. 1. A general view (A&B), the distribution pattern of the isochrone areas using the channel longitudinal profile (C), and spatially distributed travel time (D) methods with digital elevation model (DEM) as background with 30 m resolution (USGS), and a photo from the river gauge station (E) of the Galazchai Watershed, West Azerbaijan, Iran

resolution of images to 15 m (Hadjimitsis et al. 2010; Zhang et al. 2017). Ultimately, the red and near-infrared bands were used to prepare the NDVI. Since the time scale of a storm has been considered for the study, it was tried to use a satellite image for each storm to calculate the C factor. Nevertheless, due to the proximity of the occurrence date of the storms, the maximum number of six C factors was finally obtained. For example, for storms 35 and 36, a C factor was obtained, and for storms 37 and 38, another C factor was obtained.

$$C = 1 - NDVI / 2 \quad (6)$$

If no conservation practice is done, the P factor was deemed one (Wischmeier and Smith 1978). The land-use effect was also considered to further adjust the P factor to avoid overestimation of the amount of soil erosion (Panagos et al. 2015). Thus, for forest and rangeland, the value of P was one. In agriculture at different slopes, P values were considered 0.1 to 0.33. The maps used to estimate soil erosion using the RUSLE model are shown in Fig. 2. Rainfall erosivity for different storms is summarized in Table 2.

Sediment Routing

Sediment routing between two adjacent isochrone segments was obtained using the SDR concept developed, based on the slope ratio of the giving segment to the receivisng segment (Hadley et al. 1985). If the slope of the upstream isochrone was higher than the downstream, all the erosion that occurred would be transferred to the next segment as sediment, otherwise, SDR was equal to upstream segment slope per downstream segment slope. The temporal variations of sediment yield concerning the time of participation of the isochrone segments to the total sediment were also calculated.

The RUSLE-based WaTEM/SEDEM (i.e., Water and Tillage Erosion Model/Sediment Delivery Model) with similar inputs was also used to estimate SDR (Verstraeten et al. 2002). Sediment transport capacity (STc) was obtained from Eq. (7):

$$STc = ktc \times Eprg = ktc \times R \times K \times \left(LS - 4.12 \times Sg^{0.8} \right) \quad (7)$$

where *ktc* is the transport capacity coefficient, Eprg is the potential gully erosion, *R, K,* and *LS* are the RUSLE

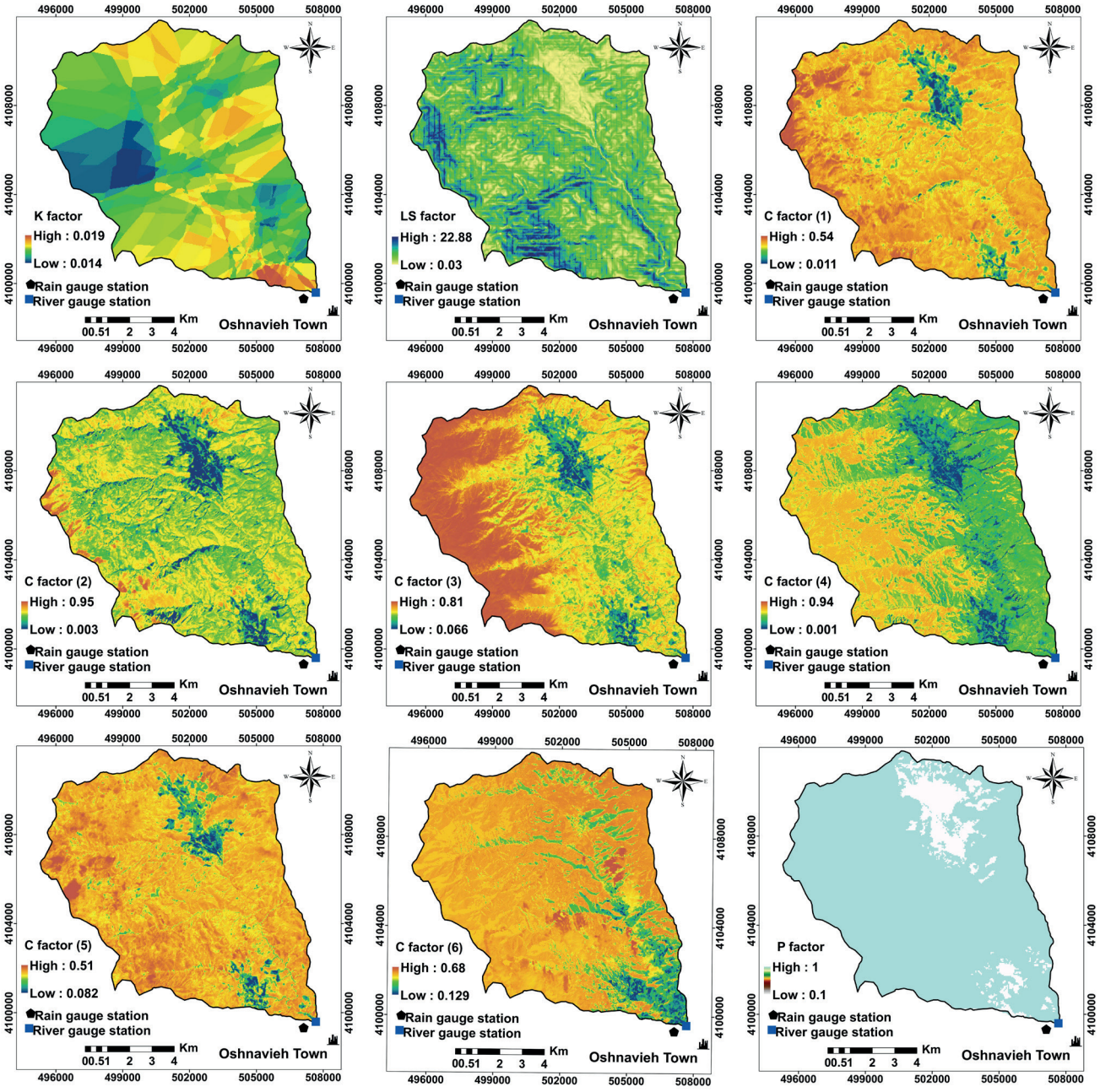

Fig. 2. Map of topography factor (LS), soil erodibility factor (K), Conservation practice factor (P), and cover management factor at different times (C) for the Galazchai Watershed, West Azerbaijan Province, Iran

factors, and *Sg* is the ground slope. The *ktc* is the main coefficient for calibrating the WaTEM/SEDEM model. In many documents (e.g., Quijano et al. 2016; Borrelli et al. 2018), changing this coefficient has been used to calibrate the model. The values of *ktc* should be calibrated for the use of the model. The sediment delivery ratio was calculated using the relationship presented in the WaTEM-SEDEM in GIS. It was determined that *ktc* values less than 0.5 should be checked. Because, when *ktc*>0.5, SDR was much higher than the unacceptable value of one. Therefore, *ktc* values less than 0.5 were examined with intervals of 0.01. The performance of the model was then determined using the median confidence level (*ME*) index (Borrelli et al., 2018). Therefore, by comparing the *ME* value, *ktc*=0.2 was finally considered for the subsequent calculations. After calculating *STc* (i.e., The transport capacity is the maximum sediment mass that can be transported by the overland flow), SDR was obtained using Eq. (8).

$$SDR = STc / SoilErosian \quad (8)$$

Sediment Graph Simulation

After calculating soil erosion in each isochrone and each storm, its temporal distribution was calculated using the lag time of each segment to the outlet and its cumulative contribution to sediment yield. The critical components of synthetic SGs, including base time, time to peak, and SSC peak, were compared with those of the observed SGs. Finally, the total sediment of each storm was

$$V_S = SDR_1E_1 + SDR_1SDR_2E_2 + ... + SDR_1SDR_2...SDR_nE_n \quad (9)$$

obtained using Eq. (9) (Kothyari et al. 1996):

where V_S is total sediment yield (t), SDR_i is sediment delivery ratio for each segment, and E_i is soil erosion in each isochrone segment (t).

Calibration and Validation of Synthetic Sediment Graph

According to the limited number of the recorded storm events, some 70% of the events were used for the calibration stage. The rest 30%, was employed for the validation stage (Dawson et al. 2007; Mohammed et al. 2021). Therefore, 38 storms were divided into two parts, 25 and 13. It is necessary to explain that there were 36 recorded storms at first, so 25 storms for calibration and 11 for validation were considered. Then, two more storms were further collected during the research and added to the validation stage. Data recorded from 2011 to 2014 were used for the calibration, and data recorded last two years of 2018 to 2019 ended at the time of preparation of the current report, and extendable to the near future were used for the validation. The simulated SGs were compared with recorded ones in terms of peak and total sediment volume, base time, and time to peak using absolute (*AE*) and relative (*RE*) errors. The overall performance of the estimated SGs was also assessed using the normalized Nash–Sutcliffe efficiency (NNSE) and root mean squared error (RMSE). These criteria were calculated for both calibration and validation datasets (Dawson et al. 2007; Nossent and Bauwens 2012; Sadeghi and Saeidi 2010). Finally, the best model performance in estimating SG components was selected based on the lowest AE, RE, and RMSE and highest NNSE (Dawson et al. 2007; Sadeghi et al. 2008; Sadeghi and Saeidi 2010). The Normalized Nash-Sutcliffe efficiency (*NNSE*) was employed for a more straightforward interpretation and to show how different methods actually worked. In this regard, Nash-Sutcliffe efficiencies of 1, 0, and -∞ correspond to *NNSE* of 1, 0.5, and 0, respectively (Nossent and Bauwens 2012).

RESULTS

To determine the efficacy of the time-area model (TAM), mean soil erosion was calculated for each storm. The characteristics of the 38 storm events from October 2011 to March 2019, rainfall erosivity, and mean soil erosion of each storm are shown in Table 2. As seen, the lowest and highest erosion rates were 0.02 and 0.047 (ton ha^{-1}), respectively, for the storms dated October 29, 2011, and March 31, 2019.

Then, the channel longitudinal profile and spatially distributed travel time were used to divide the watershed into isochrone segments. Sediment routing was also done by the Hadley et al. (1985) method. Details of each isochrone segment are given in Table one to ten is in the appendix. Therefore, the table numbers in the appendix should be corrected and written from Appendix 1 to Appendix 10. The table numbers will also change in the text of the manuscript. Though it can be rearranged based on the journal system and format too. The tables citations were fixed in the context. The SDR equaling one indicated that all soil eroded in the higher slope segment was transferred to the lower slope segment (Hadley et al. 1985; Kothyari et al. 1996). SDR was also calculated using WaTEM/SEDEM. The SDR results of the two methods for each isochrone segment are shown in Appendix Table 2.

Table 1. NNSE and RMSE results for different methods in two stages of calibration and validation for the Galazchai Watershed, Iran

Methods	Stage	Time to peak (h)		Peak Value (ton)		Base Time (h)		Total sediment (ton)	
		NNSE	RMSE	NNSE	RMSE	NNSE	RMSE	NNSE	RMSE
Hadley/channel longitudinal profile	Calibration	0.31	5.81	0.07	3699.98	0.19	13.91	0.45	3037.54
Hadley/spatially distributed travel time		0.31	5.92	0.30	1506.11	0.21	12.83	0.45	3074.39
WaTEM-SEDEM/channel longitudinal profile		0.31	5.81	0.49	996.77	0.19	13.91	0.45	3080.14
WaTEM-SEDEM/spatially distributed travel time		0.31	5.92	0.48	1027.01	0.21	12.83	0.45	3069.70
Hadley/channel longitudinal profile	Validation	0.29	9.20	0.01	458.18	0.16	17.52	0.44	371.93
Hadley/spatially distributed travel time		0.27	9.60	0.19	109.69	0.18	16.40	0.45	362.35
WaTEM-SEDEM/channel longitudinal profile		0.29	9.20	0.09	161.63	0.16	17.52	0.31	488.08
WaTEM-SEDEM/spatially distributed travel time		0.27	9.60	0.51	51.24	0.18	16.40	0.33	470.17

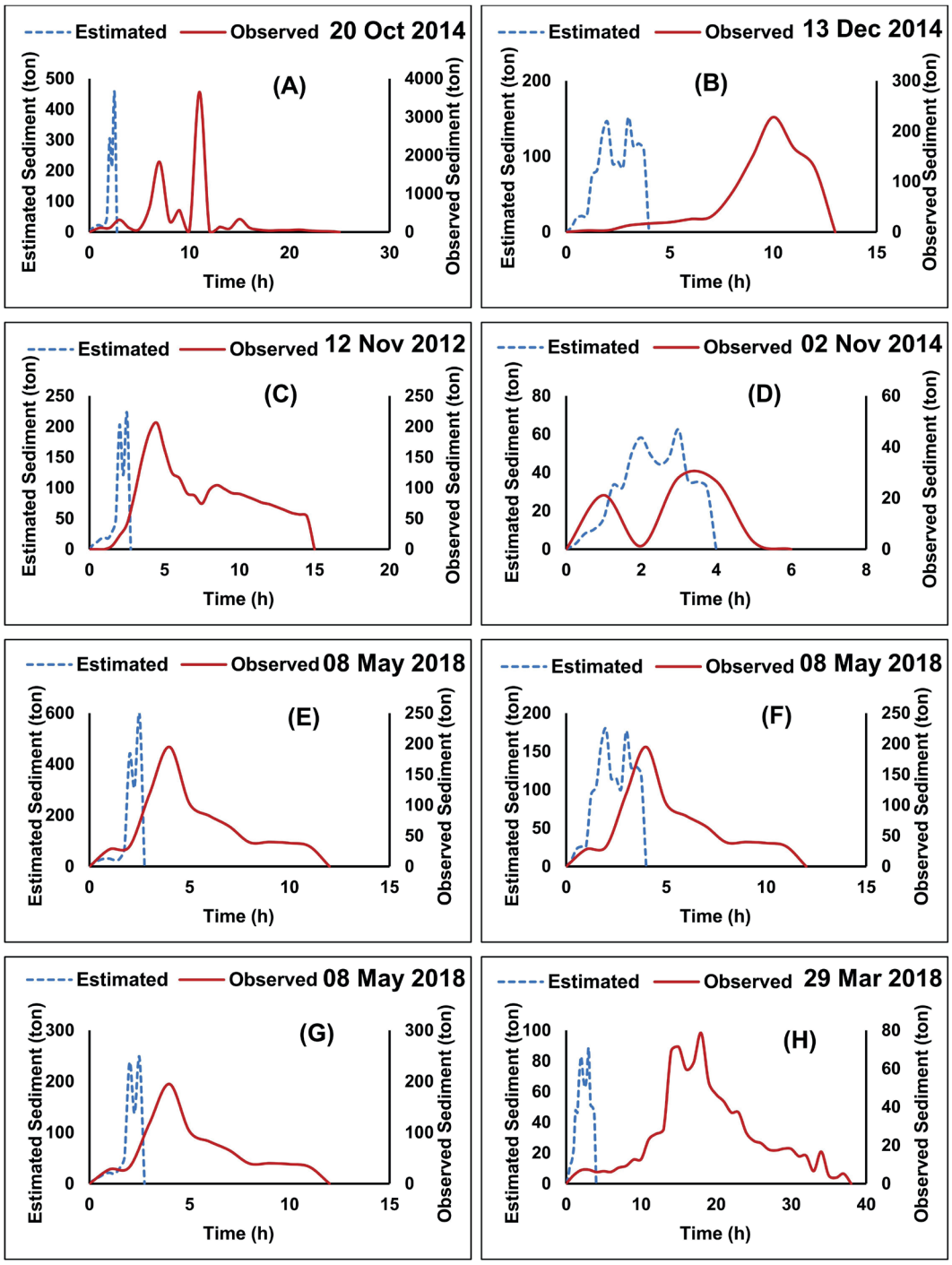

Fig. 3. Sample of synthetic sediment graphs obtained from different methods with the lowest RE in peak value estimation, (A)&(E): channel longitudinal profile and Hadley methods, (B)&(F): spatially distributed travel time and Hadley methods, (C)&(G): channel longitudinal profile and WaTEM/SEDEM, (D)&(H) methods: spatially distributed travel time and WaTEM/SEDEM methods

The results of TAMs derived from the channel longitudinal profile and spatially distributed travel time methods and corresponding sediment estimations are presented in Appendix Tables 3 to 10 for the calibration and validation data sets. Table 1 also shows the NNSE and RMSE results. Finally, sediment graphs were prepared. Fig. 2 shows some examples of synthetic sediment graphs obtained from different methods.

DISCUSSION

This study aimed to prepare synthetic sediment graphs in the Galazchai Watershed using readily available data, based on Kothyari et al. (1994 and 1997) and Kothyari et al. (2002). While they reported the accuracy of TAM in the simulation of SG in a small watershed in India, Sadeghi and Tofighi (2003) and Khaledi Darvishan et al. (2010) observed poor performance of the original TAM. To increase the accuracy in each stage of synthetic sediment graph preparation, the following modifications were made: (a) Soil erosion was calculated using RUSLE with each of its factors computed as accurately as possible. For example, six C factors were calculated for different storms. (b) For calculating the isochrone segments, two methods of longitudinal channel profile (Sadeghi et al. 2015) were used. (c) SDR was calculated using two Hadley et al. (1985) and WaTEM/SEDEM.

The minimum and maximum RE for the estimated peak values were 87.54 % and -161588.7 % for the channel longitudinal profile and Hadley et al. (1985) methods.

Likewise, the minimum and maximum *RE* for the estimated peak values were 33.58 % and -51521.1 % for the spatially distributed travel time and Hadley et al. (1985) methods. At the same time, the minimum and maximum *RE* for estimated peak values equaled -7.53 % and -8825 % for channel longitudinal profile and WaTEM/SEDEM. Ultimately, the least minimum and maximum *RE* for the estimated peak values belonged to the spatially distributed travel time method and WaTEM/SEDEM with respective values of 0.45 % and -3008.9 %. Similarly, the *RE* values ranged from 2.28 to -6273.7; 2.28 to -6273.7; -9.1 to -7026.1; 61.96 to 99.9, and -12.3 to 99.961 associated with channel longitudinal profile and Hadley et al. (1985) methods, spatially distributed travel time and Hadley et al. (1985) methods, channel longitudinal profile and WaTEM/SEDEM approach, and spatially distributed travel time method and WaTEM/SEDEM method, respectively. The negative *RE* values indicated an overestimation of the model. Despite the high error in estimating peak and total sediment, results showed that peak and base times were simulated with lower errors. In addition, the spatially distributed travel time method estimated the peak time and base time with lower error than did the channel longitudinal profile method.

The coefficient of variations varied from 0 to 139.1% for the simulated sediment graph obtained from different methods. Also, the standard deviations for the study criteria were from 0 to 2952.9. The lower coefficients of variation were related to time components, and the highest ones were related to peak value and total sediment. In general, the Hadley et al. (1985) estimates in both channel longitudinal profile and spatially distributed travel time methods in the calibration stage had the highest coefficient of variation and standard deviation. According to Table 11, none of the methods could reasonably estimate the various components of the sediment graph in all the mentioned methods. Results showed that the NNSE values were all less than 0.5, which indicated the low performance of different methods. The highest NSEE value, 0.49, was related to the peak value in the calibration stage, using the WaTEM-SEDEM/channel longitudinal profile method. Likewise, the lowest value of NSEE (i.e., 0.01) was related to the peak value obtained from the Hadley/channel longitudinal profile method in the validation stage. Similarly, the lowest value of RMSE, 5.81, was related to Hadley et al. (1985) and WaTEM-SEDEM/channel longitudinal profile, while the highest value of RMSE (i.e., 3699.98) was associated with the Hadley et al. (1985)/channel longitudinal profile method.

Results showed that in the calibration stage, channel longitudinal profile, WaTEM-SEDEM/channel longitudinal profile, spatially distributed travel time method, and Hadley et al. (1985)/channel longitudinal profile were more efficient for estimating time to peak, base time, peak value, and total sediment. In the validation stage, the estimation of time to peak by the channel longitudinal profile, the base time by the spatially distributed travel time method, the peak value by the WaTEM-SEDEM method/spatially distributed travel time, and the total sediment by Hadley/spatially distributed travel time was better performed.

Scrutinizing Table 2 showed that the WaTEM/SEDEM method reduced the SDR values by about 50% on average. In this method, SDR was calculated separately for each storm, and also factors than slope were considered. However, none of these methods had enabled TAM to simulate sediment graphs accurately. These results are consistent with the results of Sadeghi and Tofighi (2003) and Khaledi Darvishan et al. (2010) but are inconsistent with the results of Kothyari et al. (1994 and 1997) and Kothyari et al. (2002). Estimates of peak value and total sediment were, in most cases, more than observed values. High sediment estimation can be ascribed to the inaccuracy of the RUSLE method in estimating soil erosion in the study watershed because of rigorous topography and non-uniform distribution of rainfall (Khaledi Darvishan et al. 2010; Kothyari et al. 1997).

The time to peak and base time had lower coefficients of variation because these are mainly influenced by the physical characteristics of the watershed. The rest of the sediment graph components showed higher coefficients of variation due to precipitation conditions and other influential factors. These results are consistent with the findings reported by Mostafazadeh et al. (2015). The amount of relative error in estimating the peak values resulting from the WaTEM/SEDEM method had decreased by about 60% on average. The success of WaTEM/SEDEM results has been confirmed by Bezak et al. (2015) and Fang (2020). The ratio between sediment yield and soil erosion depends on many factors, for example, topography, climatic conditions, and geology (Bezak et al. 2015). Therefore, in this study, WaTEM/SEDEM was able to estimate with minor error than the Hadley et al. (1985) method. Besides, while employing WaTEM/SEDEM, SDR was calculated for each storm individually. As shown in Figure 2, although in these examples, different methods were able to estimate the peak value somewhat close to the observed value, they were not successful in simulating the overall sediment graphs shape. This disagreement was due to the effect of TAM structure on the overall shape of sediment graphs.

CONCLUSIONS

The present study synthesized SG using the modified TAM in the Galazchai Watershed, Iran. It can be concluded that, in general, TAM could not adequately simulate the temporal variation of sediment. Therefore, the methods of calculating SDR and isochrones were redefined, and the associated synthetic SGs were computed. The TAM performed better with the channel longitudinal profile method with the spatially distributed travel time method. It also had a better estimate of the time components than the sediment values. Overall, WaTEM/SEDEM performed better than the Hadley et al. (1985) method in SG components simulation.

REFERENCES

Adhami M., Sadeghi S.H.R., Duttmann R. and Sheikhmohammady M. (2019). Changes in watershed hydrological behavior due to land use comanagement scenarios. Journal of Hydrology, 577(July), 124001, DOI: 10.1016/j.jhydrol.2019.124001.

Arnaldo F., Avalos P., Gomes P.V., Leandro M., Silva N. and Oliveira M.S. De. (2018). Digital soil erodibility mapping by soilscape trending and kriging. Land Degradation & Development, 29(9), 3021–3028, DOI: 10.1002/ldr.3057.

Arnold J.G., Srinivasan R., Muttiah R.S. and Williams J.R. (1998). LARGE AREA HYDROLOGIC MODELING AND ASSESSMENT PART I : MODEL DEVELOPMENT. JAWRA Journal of the American Water Resources Association, 34(1), 73–89.

Bajirao T.S., Kumar P., Kumar M. and Elbeltagi A. (2021). Superiority of Hybrid Soft Computing Models in Daily Suspended Sediment Estimation in Highly Dynamic Rivers. Sustainability, 13(2), 542.

Banasik K. and Hejduk A. (2014). Ratio of basin lag times for runoff and sediment yield processes recorded in various environments. IAHS-AISH Proceedings and Reports, 367(December 2014), 163–169, DOI: 10.5194/piahs-367-163-2015.

Banasik K. and Mitchell J.K. (2008). Conceptual model of sedimentgraph from fl ood events in a small agricultural watershed. Annals of Warsaw University of Life Sciences-SGGW. Land Reclamation, 57(39), 49–57.

Bezak N., Rusjan S., Petan S., Sodnik J. and Mikoš M. (2015). Estimation of soil loss by the WATEM/SEDEM model using an automatic parameter estimation procedure. Environmental Earth Sciences, 74(6), 5245–5261, DOI: 10.1007/s12665-015-4534-0.

Bhunya p. k., Jain S.K., Singh P.K. and Mishra S.K. (2010). A simple conceptual model of sediment yield. Water Resources Management, 24(8), 1697–1716, DOI: 10.1007/s11269-009-9520-4.

Borrelli P., Oost K. Van, Meusburger K., Alewell C., Lugato E. and Panagos P. (2018). A step towards a holistic assessment of soil degradation in Europe : Coupling on-site erosion with sediment transfer and carbon fl uxes. Environmental Research, 161(2018), 291–298, DOI: 10.1016/j.envres.2017.11.009.

Chen V.J. and Kuo C.Y. (1986). A study on synthetic sedimentgraphs for ungaged watersheds. Journal of Hydrology, 84(1–2), 35–54.

Choubin B., Darabi H., Rahmati O., Sajedi-Hosseini F. and Kløve B. (2018). River suspended sediment modelling using the CART model: A comparative study of machine learning techniques. Science of the Total Environment, 615, 272–281.

Cimen M. (2008). Estimation of daily suspended sediments using support vector machines. Hydrological Sciences Journal, 53(3), 656–666.

Clark C. o. (1945). Storage and the unit hydrograph. Proceedings of the American Society of Civil Engineer, 69(9), 1333–1360.

Dawson C.W., Abrahart R.J. and See L.M. (2007). HydroTest : A web-based toolbox of evaluation metrics for the standardised assessment of hydrological forecasts. Environmental Modeling & Software, 22(2007), 1034–1052, DOI: 10.1016/j.envsoft.2006.06.008.

De Girolamo A.M., Pappagallo G. and Porto A. Lo. (2015). Temporal variability of suspended sediment transport and rating curves in a Mediterranean river basin: The Celone (SE Italy). Catena, 128, 135–143.

De Paula, D.P., Lima, J.C., Barros, E.L. and Santos, J.D.O. (2021). Coastal erosion and tourism: the case of the distribution of tourist accommodations and their daily rates. Geography, Environment, Sustainability, 14(3), 110-120, DOI: 10.24057/2071-9388-2021-018.

Desmet P.J.J. and Govers G. (1996). A GIS procedure for automatically calculating the USLE LS factor on topographically complex landscape units. Journal of Soil and Water Conservation, 51(5), 427–433.

Du J., Xie H., Hu Y., Xu Y. and Xu C.-Y. (2009). Development and testing of a new storm runoff routing approach based on time variant spatially distributed travel time method. Journal of Hydrology, 369(1–2), 44–54.

Durigon V.L., Carvalho D.F., Antunes M.A.H., Oliveira P.T.S. and Fernandes M.M. (2014). NDVI time series for monitoring RUSLE cover management factor in a tropical watershed. International Journal of Remote Sensing, 35(2), 441–453.

Engman E.T. (1986). Roughness coefficients for routing surface runoff. Journal of Irrigation and Drainage Engineering, 112(1), 39–53.

Fang H. (2020). Impact of land use changes on catchment soil erosion and sediment yield in the northeastern China: A panel data model application. International Journal of Sediment Research, 35(5), 540–549, DOI: 10.1016/j.ijsrc.2020.03.017.

Foster G.R., McCool D.K., Renard K.G. and Moldenhauer W.C. (1981). Conversion of the universal soil loss equation to SI metric units. Journal of Soil and Water Conservation, 36(6), 355–359.

Golosov V.., Zhang X., Qiang T., Zhou P. and He X. (2014). Quantitative assessment of sediment redistribution in the Sichuan hilly basin and the Central Russian upland during the past 60 years. Geography, Environment, Sustainability, 7(3), 39–64.

Gupta S.K., Tyagi J., Singh P.K., Sharma G. and Jethoo A.S. (2019). Soil Moisture Accounting (SMA)based sediment graph models for small watersheds. Journal of Hydrology, 574, 1129–1151, DOI: 10.1016/j.jhydrol.2019.04.077.

Hadjimitsis D.G., Papadavid G., Agapiou A., Themistocleous K., Hadjimitsis M.G. and Retalis A. (2010). Atmospheric correction for satellite remotely sensed data intended for agricultural applications : impact on vegetation indices. 1984, 89–95.

Hadley R.F., Lal R., Onstand C.A., Walling D.E. and Yair A. (1985). Recent developments in erosion and sediment yield studies. Paris. In: International Hydrological Programme, UNESCO.

Hazbavi, Z., Sadeghi, S.H.R., Gholamalifard, M. and Davoudirad, A.A. (2020). Watershed health assessment using pressure-state- response (PSR) framework. Land Degradation and Development, 31, 3-19.

Her Y. and Heatwole C. (2016). HYSTAR Sediment Model: Distributed Two-Dimensional Simulation of Watershed Erosion and Sediment Transport Using Time-Area Routing. Journal of the American Water Resources Association, 52(2), 376–396, DOI: 10.1111/1752-1688.12396

Khaledi Darvishan A., Sadeghi S.H.R. and Gholami L. (2010). Efficacy of Time-Area Method in simulating temporal variation of sediment yield in Chehelgazi watershed , Iran. Annals of Warsaw University of Life Sciences (Land Reclamation), 42(1), 51–60.

Khorsand M., Khaledi Darvishan A. and Gholamalifard M. (2017). Comparison between estimated annual soil lossusing RUSLE model with data from the erosion pins and plots in Khamsan representative watershed. Iranian Journal of Ecohydrology, 3(4), 669–680, DOI: 10.22059/IJE.2016.60376.

Kothyari U. C., Tiwari A.K. and Singh R. (1997). Estimation of temporal variation of sediment yield from small catchments through the kinematic method. Journal of Hydrology, 203(1–4), 39–57, DOI: 10.1016/S0022-1694(97)00084-X.

Kothyari U.C., Tiwari A.K. and Singh R. (1994). prediction of sediment yield. Journal of Irrigation and Drainage Engineering, 120(6), 1122–1131.

Kothyari U.C., Tiwari A.K. and Singh R. (1996). Temporal Variation of Sediment Yield. Journal of Hydrologic Engineering, 1(October), 169–176.

Kothyari UC C, Jain M.K. and Raju K.G.R. (2002). Estimation of temporal variation of sediment yield using GIS. Hydrological Sciences Journal, 47(5), 693–706.

Lee Y.H. and Singh V.P. (2005). Tank model for sediment yield. Water Resources Management, 19(4), 349–362, DOI: 10.1007/s11269-005-7998-y.

Li Z., Xu X., Xu C., Liu M., Wang K. and Yi R. (2017). Monthly sediment discharge changes and estimates in a typical karst catchment of southwest China. Journal of Hydrology, 555, 95–107, DOI: 10.1016/j.jhydrol.2017.10.013.

Mahoney D.T., Fox J.F. and Al Aamery N. (2018). Watershed erosion modeling using the probability of sediment connectivity in a gently rolling system. Journal of Hydrology, 561(April), 862–883, DOI: 10.1016/j.jhydrol.2018.04.034.

Melesse A.M. and Graham W.D. (2004). Storm runoff prediction based on a spatially distributed travel time method utilizing remote sensing and gis. JAWRA Journal of the American Water Resources Association, 40(4), 863–879.

Messina A.M. and Biggs T.W. (2016). Contributions of human activities to suspended sediment yield during storm events from a small, steep, tropical watershed. Journal of Hydrology, 538, 726–742, DOI: 10.1016/j.jhydrol.2016.03.053.

Mirchooli, F., Sadeghi, S.H.R., Khaledi Darvishan, A. and Strobl, J. (2021). Multi-dimensional assessment of watershed condition using a newly developed barometer of sustainability, Science of The Total Environment, 791, 148389, DOI:10.1016/j.scitotenv.2021.148389.

Moore I.D. and Wilson J.P. (1992). Length-slope factors for the Revised Universal Soil Loss Equation : Simplified method of estimation. Journal of Soil and Water Conservation, 47(5), 423–428.

Moradi Dashtpagerdi M., Sadeghi S.H.R. and Moradi Rekabdarkoolai H. (2019). Changeability of simulated watershed hydrographs from different vector scales and cell sizes. Catena, 182, 104097, DOI: 10.1016/j.catena.2019.104097.

Mostafazadeh R., Sadeghi S.H.R. and Sadoddin A. (2015). Analysis of storm-wise sedimentgraphs and rating loops in Galazchai Watershed, West-Azarbaijan. Journal of Water and Soil Conservation, 21(5), 175–190.

Nearing M.A., Foster G.R., Lane L.J. and Finkner S.C. (1989). A process-based soil erosion model for USDA-Water Erosion Prediction Project technology. Transactions of the ASAE, 32(5), 1587–1593.

Nossent J. and Bauwens W. (2012). Application of a normalized Nash-Sutcliffe efficiency to improve the accuracy of the Sobol' sensitivity analysis of a hydrological model. Geophysical Research Abstract EGU General Assembly Conference Abstracts, 14(2011), 237. https://ui.adsabs.harvard.edu/abs/2012EGUGA..14..237N/abstract

Panagos P., Borrelli P., Meusburger K., Zanden E.H. Van Der, Poesen J. and Alewell C. (2015). ScienceDirect Modelling the effect of support practices (P -factor) on the reduction of soil erosion by water at European scale. Environmental Science and Policy, 51(2015), 23–34, DOI: 10.1016/j.envsci.2015.03.012.

Pandey A., Chowdary V.M. and Mal B.C. (2007). Identification of critical erosion prone areas in the small agricultural watershed using USLE , GIS and remote sensing. Water Resources Management Manage, 21(4), 729–746, DOI: 10.1007/s11269-006-9061-z.

Pelton J., Frazier E. and Pickilingis E. (2014). Calculating slope length factor (LS) in the revised Universal Soil Loss Equation (RUSLE).

Qiao L., Liu S., Xue W., Liu P., Hu R., Sun H. and Zhong Y. (2020). Spatiotemporal variations in suspended sediments over the inner shelf of the East China Sea with the effect of oceanic fronts. Estuarine, Coastal and Shelf Science, 234, 106600, DOI: 10.1016/j.ecss.2020.106600

Quijano L., Beguería S., Gaspar L. and Navas A. (2016). Estimating erosion rates using 137Cs measurements and WATEM/SEDEM in a Mediterranean cultivated field. Catena, 138, 38–51.

Rahaman, A.S. and Solavagounder, A. (2020). Natural and human-induced land degradation and its impact using geospatial approach in the Kallar Watershed of Tamil Nadu, India. Geography, Environment, Sustainability, 13(4), 159-175.

Raisi M.B., Sadeghi S.H.R. and Noor H. (2010). Accuracy of Time- Area Method in Sedimentgraph Development in Kojour Watershed. Rangeland, 4(4), 320–333.

Renard K.G., Foster G.R., Weesies G.A. and Porter J.P. (1991). RUSLE: revised universal soil loss equation. Journal of Soil & Water Conservation, 46(1), 30–33.

Rovira A. and Batalla R.J. (2006). Temporal distribution of suspended sediment transport in a Mediterranean basin: The Lower Tordera (NE SPAIN). Geomorphology, 79(1–2), 58–71, DOI: 10.1016/j.geomorph.2005.09.016.

Ruben L.G.D., Szupiany R.N., Latosinski F.G., López Weibel C., Wood M. and Boldt J. (2020). Acoustic Sediment Estimation Toolbox (ASET): A software package for calibrating and processing TRDI ADCP data to compute suspended-sediment transport in sandy rivers. Computers and Geosciences, 140(2020), 104499, DOI: 10.1016/j.cageo.2020.104499

Rymszewicz A., Bruen M., O'Sullivan J.J., Turner J.N., Lawler D.M., Harrington J.R., Conroy E. and Kelly-Quinn M. (2018). Modelling spatial and temporal variations of annual suspended sediment yields from small agricultural catchments. Science of The Total Environment, 619, 672–684.

Sadeghi S.H.R. and Mizuyama T. (2007). Applicability of Modified Universal Soil Loss Equation for prediction of sediment yield in Khanmirza watershed, Iran, Hydrological Science Journal (IAHS), 52(5),1068-1075.

Sadeghi S.H.R. and Saeidi P. (2010). Reliability of sediment rating curves for a deciduous forest watershed in Iran. Hydrological Sciences Journal, 55(5), 821–831.

Sadeghi S.H.R. and Singh J.k. (2005). Development of a synthetic sediment graph using hydrological data. Journal of Agricultural Science and Technology, 7(2005), 69–77.

Sadeghi S.H.R. and Singh V.P. (2017). Dynamics of suspended sediment concentration, flow discharge and sediment particle size interdependency to identify sediment source. Journal of Hydrology, 554(1–2), 100–110, DOI: 10.1016/j.jhydrol.2017.09.006.

Sadeghi S.H.R. and Tavangar S. (2015). Development of stational models for estimation of rainfall erosivity factor in different timescales. Natural Hazards, 77(1), 429–443, DOI: 10.1007/s11069-015-1608-y.

Sadeghi S.H.R. and Tofighi B. (2003). Application of time-area model in preparing sediment rating curve (Case study: Khanmirza River in Karun watershed). Journal of Caspian Agricultural Sciences and Natural Resources, 1(1), 54–66.

Sadeghi S.H.R. and Zakeri M.A. (2015). Partitioning and analyzing temporal variability of wash and bed material loads in a forest watershed in Iran. Journal of Earth System Science, 124(7), 1503–1515.

Sadeghi S.H.R., Mizuyama T., Miyata S., Gomi T. and Kosugi K. (2008). Development , evaluation and interpretation of sediment rating curves for a Japanese small mountainous reforested watershed. Geoderma, 144(2008), 198–211, DOI: 10.1016/j.geoderma.2007.11.008.

Sadeghi S.H.R., Mizuyama T., Miyata S., Gomi T., Kosugi K., Fukushima T., Mizugaki S. and Onda Y. (2008). Determinant factors of sediment graphs and rating loops in a reforested watershed. Journal of Hydrology, 356(3–4), 271–282, DOI: 10.1016/j.jhydrol.2008.04.005.

Sadeghi S.H.R., Mostafazadeh R. and Sadoddin A. (2015). Changeability of simulated hydrograph from a steep watershed resulted from applying Clark's IUH and different time–area histograms. Environmental Earth Sciences, 74(4), 3629–3643, DOI: 10.1007/s12665-015-4426-3.

Sadeghi S.H.R., Saeidi P., Singh V.P. and Telvari A.R. (2019). How persistent are hysteresis patterns between suspended sediment concentration and discharge at different timescales? Hydrological Sciences Journal, 64(15), 1909–1917, DOI: 10.1080/02626667.2019.1676895.

Sadeghi S.H.R., Zabihi, M., Vafakhah M. and Hazbavi Z. (2017). Spatiotemporal mapping of rainfall erosivity index for different return periods in Iran. Natural Hazards, 87(1), 35-56, DOI: 10.1007/s11069-017-2752-3.

Saeedi P., Sadeghi S.H.R. and Telvari A.R. (2016). Sediment graph simulation using Hydrograph. Watershed Engineering and Management, 8(2), 28–41.

Seeger M., Errea M.P., Beguería S., Arnáez J., Martí C. and García-Ruiz J.M. (2004). Catchment soil moisture and rainfall characteristics as determinant factors for discharge/suspended sediment hysteretic loops in a small headwater catchment in the Spanish pyrenees. Journal of Hydrology, 288(3–4), 299–311, DOI: 10.1016/j.jhydrol.2003.10.012.

Singh P.K., Bhunya P.K., Mishra S.K. and Chaube U.C. (2008). A sediment graph model based on SCS-CN method. Journal of Hydrology, 349(1–2), 244–255, DOI: 10.1016/j.jhydrol.2007.11.004.

Singh P.K., Jain M.K. and Mishra S.K. (2013). Fitting a simplified two-parameter gamma distribution function for synthetic sediment graph derivation from ungauged catchments. Arabian Journal of Geosciences, 6(6), 1835–1841, DOI: 10.1007/s12517-011-0473-6.

Sokolov D.I., Erina, O.N., Tereshina M.A. and Puklakov V.V. (2020). Impact of mozhaysk dam on the moscow river sediment transport. Geography, Environment, Sustainability, 13(4), 24-31, DOI: 10.24057/2071-9388-2019-150.

Srivastava A., Brooks E.S., Dobre M., Elliot W.J., Wu J.Q., Flanagan D.C., Gravelle J.A. and Link T.E. (2020). Modeling forest management effects on water and sediment yield from nested , paired watersheds in the interior Pacific Northwest , USA using WEPP. Science of the Total Environment Journal, 701, 134877, DOI: 10.1016/j.scitotenv.2019.134877

Tyagi J. V., Mishra S.K., Singh R. and Singh V.P. (2008). SCS-CN based time-distributed sediment yield model. Journal of Hydrology, 352(3–4), 388–403, DOI: 10.1016/j.jhydrol.2008.01.025.

Usul N. and Yilmaz M. (2002). ESTIMATION OF INSTANTANEOUS UNIT HYDROGRAPH WITH CLARK ' S TECHNIQUE IN GIS. In Proceedings of 2002 ESRI International User Conference. ESRI on-Line, 1–20.

Van Oost K., Govers G. and Desmet P. (2000). Evaluating the effects of changes in landscape structure on soil erosion by water and tillage. Landscape Ecology, 15(6), 577–589.

Van Rompaey A., Bazzoffi P., Jones R.J.A. and Montanarella L. (2005). Modeling sediment yields in Italian catchments. Geomorphology, 65(1–2), 157–169.

Van Rompaey A.J.J., Verstraeten G., Van Oost K., Govers G. and Poesen J. (2001). MODELLING MEAN ANNUAL SEDIMENT YIELD USING A. Earth Surface Processes and Landforms, 26(11), 1221–1236.

Vercruysse K., Grabowski R.C. and Rickson R.J. (2017). Suspended sediment transport dynamics in rivers: Multi-scale drivers of temporal variation. Earth-Science Reviews, 166, 38–52, DOI: 10.1016/j.earscirev.2016.12.016

Verstraeten G., Oost K. Van, Rompaey A. Van, Poesen J. and Govers G. (2002). Evaluating an integrated approach to catchment management to reduce soil loss and sediment pollution through modelling. Soil Use and Management, 18(4), 386–394, DOI: 10.1079/SUM2002150.

Waiyasusri K. and Wetchayont P. (2020). Assessing long-term deforestation in nam san watershed, loei province, Thailand using a dyna-clue model. Geography, Environment, Sustainability, 13(4), 81-97, DOI: 10.24057/2071-9388-2020-14.

Welle P.I. and Woodward D. (1986). Engineering hydrology—Time of concentration. Hydrology Technical Note, No. N4, June 17.

Wischmeier W.H. and Smith D.D. (1978). Predicting rainfall erosion losses: a guide to conservation planning , Issue 537. Department of Agriculture, Science and Education Administration.

Xie H., Shen Z., Chen L., Qiu J. and Dong J. (2017). Time-varying sensitivity analysis of hydrologic and sediment parameters at multiple timescales: Implications for conservation practices. Science of The Total Environment, 598, 353–364.

Yadav A., Chatterjee S. and Equeenuddin S. (2021). Suspended sediment yield modeling in Mahanadi River , India by multi-objective optimization hybridizing arti fi cial intelligence algorithms. International Journal of Sediment Research, 36(1), 76–91, DOI: 10.1016/j.ijsrc.2020.03.018.

Zevenbergen L.W. and Thorne C.R. (1987). quantitative analysis of land surface topography. Earth Surface Processes and Landforms, 12, 47–56.

Zhan W., Wu J., Wei X., Tang S. and Zhan H. (2019). Spatio-temporal variation of the suspended sediment concentration in the Pearl River Estuary observed by MODIS during 2003–2015. Continental Shelf Research, 172, 22–32, DOI: 10.1016/j.csr.2018.11.007.

Zhang X., Estoque R.C. and Murayama Y. (2017). An urban heat island study in Nanchang City, China based on land surface temperature and social-ecological variables. Sustainable Cities and Society, 32, 557–568, DOI: 10.1016/j.scs.2017.05.005.

Zheng F., Zhang X.J., Wang J. and Flanagan D.C. (2020). Assessing applicability of the WEPP hillslope model to steep landscapes in the northern Loess Plateau of China. Soil & Tillage Research, 197(26), 104492, DOI: 10.1016/j.still.2019.104492.

Zheng M., Qin F., Yang J. and Cai Q. (2013). The spatio-temporal invariability of sediment concentration and the flow-sediment relationship for hilly areas of the Chinese Loess Plateau. Catena, 109(2013), 164–176, DOI: 10.1016/j.catena.2013.03.017.

APPENDICES

Appendix Table 1. Details of each isochrone segment and SDR obtained using the Hadley et al. (1985) method for the Galazchai Watershed, Iran

Method	Isochrone NO.	Time of Concentration (min)	Slope (%)	Area (ha)	SDR
Channel longitudinal profile	1	0.25	28.70	91.43	1.00
	2	0.50	34.53	133.69	1.00
	3	0.75	31.90	207.63	0.92
	4	1.00	28.41	270.42	0.89
	5	1.25	24.38	284.55	0.86
	6	1.50	17.82	582.05	0.73
	7	1.75	18.94	939.81	1.00
	8	2.00	24.92	3266.89	1.00
	9	2.25	30.33	1679.44	1.00
	10	2.50	35.31	2722.59	1.00
Spatially Distributed Travel Time	1	0.25	26.70	51.31	1.00
	2	0.50	30.99	132.76	1.00
	3	0.75	31.80	168.48	1.00
	4	1.00	22.91	391.83	0.72
	5	1.25	29.29	615.17	1.00
	6	1.50	29.69	608.41	1.00
	7	1.75	34.01	815.19	1.00
	8	2.00	33.30	959.27	0.97
	9	2.25	26.50	962.88	0.79
	10	2.50	23.95	941.67	0.90
	11	2.75	20.10	1248.58	0.83
	12	3.00	24.12	1363.56	1.00
	13	3.25	27.90	760.55	1.00
	14	3.50	34.13	609.27	1.00
	15	3.75	34.60	562.55	1.00

Appendix Table 2. Characteristics of the storms and details of each isochrone segment and SDR obtained using the WaTEM/SEDEM method for the Galazchai Watershed, Iran

NO.	Date	Rainfall (mm)	Rainfall Erosivity (MJ mm ha^{-1} h^{-1})	Soil Erosion (t ha^{-1})	SDR (Channel longitudinal profile method)										SDR (Spatially distributed travel time method)														
					1	2	3	4	5	6	7	8	9	10	1	2	3	4	5	6	7	8	9	10	11	12	13	14	15
1	29, Oct, 2011	2.42	0.621	0.021	0.551	0.515	0.562	0.593	0.619	0.723	0.709	0.548	0.510	0.478	0.564	0.561	0.607	0.654	0.540	0.490	0.492	0.510	0.570	0.588	0.641	0.576	0.495	0.485	0.470
2	30, Oct, 2011	13.20	1.160	0.039	0.551	0.515	0.562	0.593	0.619	0.723	0.709	0.548	0.510	0.478	0.564	0.561	0.607	0.654	0.540	0.490	0.492	0.510	0.570	0.588	0.641	0.576	0.495	0.485	0.470
3	04, Nov, 2011	13.60	1.180	0.040	0.551	0.515	0.562	0.593	0.619	0.723	0.709	0.548	0.510	0.478	0.564	0.561	0.607	0.654	0.540	0.490	0.492	0.510	0.570	0.588	0.641	0.576	0.495	0.485	0.470
4	05, Nov, 2011	4.62	0.731	0.025	0.551	0.515	0.562	0.593	0.619	0.723	0.709	0.548	0.510	0.478	0.564	0.561	0.607	0.654	0.540	0.490	0.492	0.510	0.570	0.588	0.641	0.576	0.495	0.485	0.470
5	11, Apr, 2012	14.29	1.215	0.041	0.551	0.515	0.562	0.593	0.619	0.723	0.709	0.548	0.510	0.478	0.564	0.561	0.607	0.654	0.540	0.490	0.492	0.510	0.570	0.588	0.641	0.576	0.495	0.485	0.470
6	03, Nov, 2012	8.25	0.913	0.031	0.551	0.515	0.562	0.593	0.619	0.723	0.709	0.548	0.510	0.478	0.564	0.561	0.607	0.654	0.540	0.490	0.492	0.510	0.570	0.588	0.641	0.576	0.495	0.485	0.470
7	11, Nov, 2012	13.50	1.175	0.040	0.551	0.515	0.562	0.593	0.619	0.723	0.709	0.548	0.510	0.478	0.564	0.561	0.607	0.654	0.540	0.490	0.492	0.510	0.570	0.588	0.641	0.576	0.495	0.485	0.470
8	12, Nov, 2012	8.70	0.935	0.032	0.551	0.515	0.562	0.593	0.619	0.723	0.709	0.548	0.510	0.478	0.564	0.561	0.607	0.654	0.540	0.490	0.492	0.510	0.570	0.588	0.641	0.576	0.495	0.485	0.470
9	13, Nov, 2012	14.70	1.235	0.042	0.551	0.515	0.562	0.593	0.619	0.723	0.709	0.548	0.510	0.478	0.564	0.561	0.607	0.654	0.540	0.490	0.492	0.510	0.570	0.588	0.641	0.576	0.495	0.485	0.470
10	14, Nov, 2012	5.18	0.759	0.026	0.551	0.515	0.562	0.593	0.619	0.723	0.709	0.548	0.510	0.478	0.564	0.561	0.607	0.654	0.540	0.490	0.492	0.510	0.570	0.588	0.641	0.576	0.495	0.485	0.470
11	19, Nov, 2012	10.26	1.013	0.034	0.551	0.515	0.562	0.593	0.619	0.723	0.709	0.548	0.510	0.478	0.564	0.561	0.607	0.654	0.540	0.490	0.492	0.510	0.570	0.588	0.641	0.576	0.495	0.485	0.470
12	20, Nov, 2012	3.41	0.671	0.023	0.551	0.515	0.562	0.593	0.619	0.723	0.709	0.548	0.510	0.478	0.564	0.561	0.607	0.654	0.540	0.490	0.492	0.510	0.570	0.588	0.641	0.576	0.495	0.485	0.470
13	25, Nov, 2012	6.40	0.820	0.028	0.551	0.515	0.562	0.593	0.619	0.723	0.709	0.548	0.510	0.478	0.564	0.561	0.607	0.654	0.540	0.490	0.492	0.510	0.570	0.588	0.641	0.576	0.495	0.485	0.470
14	10, Mar, 2014	5.00	0.75	0.025	0.552	0.528	0.571	0.596	0.625	0.720	0.710	0.553	0.516	0.499	0.560	0.569	0.627	0.655	0.544	0.497	0.510	0.521	0.575	0.587	0.644	0.582	0.508	0.509	0.492
15	17, Mar, 2014	4.50	0.73	0.024	0.552	0.528	0.571	0.596	0.625	0.720	0.710	0.553	0.516	0.499	0.560	0.569	0.627	0.655	0.544	0.497	0.510	0.521	0.575	0.587	0.644	0.582	0.508	0.509	0.492
16	18, Mar, 2014	12.50	1.13	0.037	0.552	0.528	0.571	0.596	0.625	0.720	0.710	0.553	0.516	0.499	0.560	0.569	0.627	0.655	0.544	0.497	0.510	0.521	0.575	0.587	0.644	0.582	0.508	0.509	0.492
17	30, Mar, 2014	7.00	0.85	0.028	0.552	0.528	0.571	0.596	0.625	0.720	0.710	0.553	0.516	0.499	0.560	0.569	0.627	0.655	0.544	0.497	0.510	0.521	0.575	0.587	0.644	0.582	0.508	0.509	0.492
18	13, Apr, 2014	4.00	0.70	0.023	0.552	0.528	0.571	0.596	0.625	0.720	0.710	0.553	0.516	0.499	0.560	0.569	0.627	0.655	0.544	0.497	0.510	0.521	0.575	0.587	0.644	0.582	0.508	0.509	0.492
19	18, Apr, 2014	5.50	0.78	0.026	0.552	0.528	0.571	0.596	0.625	0.720	0.710	0.553	0.516	0.499	0.560	0.569	0.627	0.655	0.544	0.497	0.510	0.521	0.575	0.587	0.644	0.582	0.508	0.509	0.492
20	19, Oct, 2014	5.00	0.75	0.027	0.587	0.552	0.602	0.642	0.686	0.759	0.741	0.568	0.469	0.400	0.608	0.585	0.652	0.719	0.590	0.517	0.514	0.519	0.572	0.568	0.627	0.545	0.418	0.397	0.392
21	20, Oct, 2014	5.50	0.78	0.028	0.587	0.552	0.602	0.642	0.686	0.759	0.741	0.568	0.469	0.400	0.608	0.585	0.652	0.719	0.590	0.517	0.514	0.519	0.572	0.568	0.627	0.545	0.418	0.397	0.392
22	02, Nov, 2014	3.50	0.68	0.024	0.587	0.552	0.602	0.642	0.686	0.759	0.741	0.568	0.469	0.400	0.608	0.585	0.652	0.719	0.590	0.517	0.514	0.519	0.572	0.568	0.627	0.545	0.418	0.397	0.392
23	16, Nov, 2014	4.00	0.70	0.025	0.587	0.552	0.602	0.642	0.686	0.759	0.741	0.568	0.469	0.400	0.608	0.585	0.652	0.719	0.590	0.517	0.514	0.519	0.572	0.568	0.627	0.545	0.418	0.397	0.392
24	22, Nov, 2014	6.30	0.82	0.029	0.587	0.552	0.602	0.642	0.686	0.759	0.741	0.568	0.469	0.400	0.608	0.585	0.652	0.719	0.590	0.517	0.514	0.519	0.572	0.568	0.627	0.545	0.418	0.397	0.392
25	13, Dec, 2014	8.00	0.90	0.032	0.587	0.552	0.602	0.642	0.686	0.759	0.741	0.568	0.469	0.400	0.608	0.585	0.652	0.719	0.590	0.517	0.514	0.519	0.572	0.568	0.627	0.545	0.418	0.397	0.392
26	17, Feb, 2018	4.90	0.75	0.028	0.549	0.531	0.576	0.624	0.668	0.748	0.731	0.541	0.446	0.412	0.572	0.571	0.627	0.677	0.558	0.487	0.490	0.496	0.532	0.541	0.626	0.548	0.436	0.419	0.422
27	22, Feb, 2018	13.00	1.15	0.042	0.549	0.531	0.576	0.624	0.668	0.748	0.731	0.541	0.446	0.412	0.572	0.571	0.627	0.677	0.558	0.487	0.490	0.496	0.532	0.541	0.626	0.548	0.436	0.419	0.422
28	09, Mar, 2018	11.00	0.85	0.031	0.549	0.531	0.576	0.624	0.668	0.748	0.731	0.541	0.446	0.412	0.572	0.571	0.627	0.677	0.558	0.487	0.490	0.496	0.532	0.541	0.626	0.548	0.436	0.419	0.422
29	29, Mar, 2018	7.00	0.96	0.035	0.549	0.531	0.576	0.624	0.668	0.748	0.731	0.541	0.446	0.412	0.572	0.571	0.627	0.677	0.558	0.487	0.490	0.496	0.532	0.541	0.626	0.548	0.436	0.419	0.422
30	11, Apr, 2018	9.20	0.81	0.030	0.549	0.531	0.576	0.624	0.668	0.748	0.731	0.541	0.446	0.412	0.572	0.571	0.627	0.677	0.558	0.487	0.490	0.496	0.532	0.541	0.626	0.548	0.436	0.419	0.422
31	12, Apr, 2018	6.23	0.94	0.035	0.549	0.531	0.576	0.624	0.668	0.748	0.731	0.541	0.446	0.412	0.572	0.571	0.627	0.677	0.558	0.487	0.490	0.496	0.532	0.541	0.626	0.548	0.436	0.419	0.422
32	15, Apr, 2018	8.80	0.80	0.030	0.549	0.531	0.576	0.624	0.668	0.748	0.731	0.541	0.446	0.412	0.572	0.571	0.627	0.677	0.558	0.487	0.490	0.496	0.532	0.541	0.626	0.548	0.436	0.419	0.422
33	27, Apr, 2018	6.00	0.78	0.029	0.549	0.531	0.576	0.624	0.668	0.748	0.731	0.541	0.446	0.412	0.572	0.571	0.627	0.677	0.558	0.487	0.490	0.496	0.532	0.541	0.626	0.548	0.436	0.419	0.422
34	08, May, 2018	5.50	1.05	0.039	0.549	0.531	0.576	0.624	0.668	0.748	0.731	0.541	0.446	0.412	0.572	0.571	0.627	0.677	0.558	0.487	0.490	0.496	0.532	0.541	0.626	0.548	0.436	0.419	0.422
35	26, Oct, 2018	8.00	0.90	0.029	0.570	0.545	0.588	0.620	0.657	0.727	0.724	0.565	0.521	0.504	0.586	0.579	0.641	0.688	0.571	0.510	0.512	0.526	0.583	0.595	0.652	0.591	0.513	0.516	0.507
36	31, Oct, 2018	12.00	1.10	0.036	0.570	0.545	0.588	0.620	0.657	0.727	0.724	0.565	0.521	0.504	0.586	0.579	0.641	0.688	0.571	0.510	0.512	0.526	0.583	0.595	0.652	0.591	0.513	0.516	0.507
37	25, Mar, 2019	5.50	0.78	0.032	0.587	0.542	0.549	0.549	0.564	0.672	0.660	0.451	0.402	0.401	0.591	0.576	0.609	0.589	0.482	0.416	0.418	0.418	0.467	0.492	0.561	0.490	0.402	0.407	0.410
38	31, Mar, 2019	13.00	1.15	0.047	0.587	0.542	0.549	0.549	0.564	0.672	0.660	0.451	0.402	0.401	0.591	0.576	0.609	0.589	0.482	0.416	0.418	0.418	0.467	0.492	0.561	0.490	0.402	0.407	0.410

Appendix Table 3. Comparison between principle components of observed and estimated sediment graphs from the channel longitudinal profile method and Hadley et al. (1985) method for calibration stage for the Galazchai Watershed, Iran

NO.	Date	Time to peak (h)		RE (%)	AE (%)	Peak Value (ton)		RE (%)	AE (%)	Base Time (h)		RE (%)	AE (%)	Total Sediment (ton)		RE (%)	AE (%)
		Obs.	Est.			Obs.	Est.			Obs.	Est.			Obs.	Est.		
1	29, Oct 2011	4.5	2.5	44.44	44.44	6.94	153.54	-2112.4	2112.43	10.5	2.5	76.19	76.19	52.26	59.45	-13.76	13.76
2	30, Oct 2011	7	2.5	64.29	64.29	4.33	5007.4	-115546.1	115546.1	19.0	2.5	86.84	86.84	80.84	1938.8	-2298.4	2298.4
3	04, Nov 2011	9	2.5	72.22	72.22	16.23	1938.8	-11846.1	11846.09	20.0	2.5	87.50	87.50	241.01	1330.9	-452.23	452.23
4	05, Nov 2011	6.5	2.5	61.54	61.54	6.89	589.41	-8454.5	8454.5	13.5	2.5	81.48	81.48	82.73	228.21	-175.85	175.85
5	11, Apr 2012	7	2.5	64.29	64.29	49.26	12481.5	-25238.1	25238.1	14.5	2.5	82.76	82.76	773.08	4832.7	-525.13	525.13
6	03, Nov 2012	2.5	2.5	0.00	0.00	2.42	3912.9	-161588.7	161588.7	12.5	2.5	80.00	80.00	23.77	1515.0	-6273.7	6273.7
7	11, Nov 2012	6.5	2.5	61.54	61.54	112.3	8430.0	-7404.67	7404.67	11.5	2.5	78.26	78.26	1075.97	3264.0	-203.36	203.36
8	12, Nov 2012	4.5	2.5	44.44	44.44	205.7	4636.0	-2153.77	2153.77	14.5	2.5	82.76	82.76	2455.41	1795.0	26.90	26.90
9	13, Nov 2012	6.5	2.5	61.54	61.54	324.4	4650.9	-1333.55	1333.55	22.0	2.5	88.64	88.64	7094.69	1800.8	74.62	74.62
10	14, Nov 2012	5	2.5	50.00	50.00	34.20	1079.7	-3057.17	3057.17	23.5	2.5	89.36	89.36	936.46	418.07	55.36	55.36
11	19, Nov 2012	7	2.5	64.29	64.29	20.37	3105.5	-15145.60	15145.60	16.5	2.5	84.85	84.85	291.52	1202.4	-312.47	312.47
12	20, Nov 2012	4.5	2.5	44.44	44.44	3.59	287.27	-7902.05	7902.05	12.5	2.5	80.00	80.00	48.90	111.23	-127.46	127.46
13	25, Nov 2012	3	2.5	16.67	16.67	6.56	1768.2	-26854.56	26854.56	8.5	2.5	70.59	70.59	59.90	684.64	-1042.9	1042.9
14	10, Mar 2014	7	2.5	64.29	64.29	26.62	353.91	-1229.47	1229.47	7.0	2.5	64.29	64.29	75.72	140.44	-85.47	85.47
15	17, Mar 2014	6	2.5	58.33	58.33	20.92	344.47	-1546.61	1546.61	7.0	2.5	64.29	64.29	93.75	136.69	-45.80	45.80
16	18, Mar 2014	7	2.5	64.29	64.29	23.82	533.22	-2138.54	2138.54	18.0	2.5	86.11	86.11	216.52	211.59	2.28	2.28
17	30, Mar 2014	6	2.5	58.33	58.33	32.52	401.09	-1133.36	1133.36	17.0	2.5	85.29	85.29	239.30	159.16	33.49	33.49
18	13, Apr 2014	6	2.5	58.33	58.33	2.66	330.31	-12317.7	12317.7	9.0	2.5	72.22	72.22	20.82	131.07	-529.55	529.55
19	18, Apr 2014	9	2.5	72.22	72.22	14.04	368.06	-2521.51	2521.5	10.0	2.5	75.00	75.00	75.01	146.05	-94.71	94.71
20	19, Oct 2014	23	2.5	89.13	89.13	3652.5	437.49	88.02	88.02	36.0	2.5	93.06	93.06	10028.3	151.32	98.49	98.49
21	20, Oct 2014	11	2.5	77.27	77.27	3652.5	454.99	87.54	87.54	24.0	2.5	89.58	89.58	8788.75	157.37	98.21	98.21
22	02, Nov 2014	3	2.5	16.67	16.67	28.09	396.66	-1312.10	1312.1	5.0	2.5	50.00	50.00	137.19	79.95	41.72	41.72
23	16, Nov 2014	4	2.5	37.50	37.50	21.79	408.32	-1773.9	1773.9	12.0	2.5	79.17	79.17	82.08	141.23	-72.06	72.06
24	22, Nov 2014	4	2.5	37.50	37.50	23.52	478.32	-1933.67	1933.67	12.0	2.5	79.17	79.17	112.89	165.44	-46.55	46.55
25	13, Dec 2014	10	2.5	75.00	75.00	228.08	524.99	-130.18	130.18	12.0	2.5	79.17	79.17	861.39	181.58	78.92	78.92
Mean		6.78	2.50	54.34	54.34	340.8	2122.9	-16579.95	16594.00	14.7	2.5	79.46	79.46	1357.93	839.33	-471.58	512.38
Standard Deviation		3.92	0.00	20.17	20.17	979.8	2952.9	37257.35	37251.10	6.6	0.00	9.41	9.41	2769.67	1151.1	1283.4	1267.7
Coefficient of Variations (%)		57.85	0.00	37.12	37.12	287.5	139.10	-224.71	224.49	45.1	0.00	11.84	11.84	203.96	137.15	-272.16	247.42

Appendix Table 4. Comparison between principle components of observed and estimated sediment graphs from the spatially distributed travel time method and the Hadley et al. (1985) method for calibration stage for the Galazchai Watershed, Iran

NO.	Date	Time to peak (h)		RE (%)	AE (%)	Peak Value (ton)		RE (%)	AE (%)	Base Time (h)		RE (%)	AE (%)	Total sediment (ton)		RE (%)	AE (%)
		Obs.	Est.			Obs.	Est.			Obs.	Est.			Obs.	Est.		
1	29, Oct 2011	4.5	2	55.6	55.6	6.94	49.02	-606.35	606.35	10.50	3.75	64.29	64.29	52.26	66.47	-27.2	27.2
2	30, Oct 2011	7	2	71.4	71.4	4.33	1598.7	-36821.4	36821.4	19.00	3.75	80.26	80.26	80.84	2167.7	-2581.5	2581.5
3	04, Nov 2011	9	2	77.8	77.8	16.23	1097.4	-6661.71	6661.71	20.00	3.75	81.25	81.25	241.01	1488.0	-517.4	517.4
4	05, Nov 2011	6.5	2	69.2	69.2	6.89	188.18	-2631.13	2631.13	13.50	3.75	72.22	72.22	82.73	255.15	-208.4	208.4
5	11, Apr 2012	7	2	71.4	71.4	49.26	3984.9	-7989.50	7989.50	14.50	3.75	74.14	74.14	773.08	5403.2	-598.9	598.9
6	03, Nov 2012	2.5	2	20.0	20.0	2.42	1249.2	-51521.1	51521.1	12.50	3.75	70.00	70.00	23.77	1693.9	-7026.1	7026.1
7	11, Nov 2012	6.5	2	69.2	69.2	112.3	2691.4	-2295.96	2295.96	11.50	3.75	67.39	67.39	1075.97	3606.0	-235.1	235.1
8	12, Nov 2012	4.5	2	55.6	55.6	205.7	1480.1	-619.54	619.54	14.50	3.75	74.14	74.14	2455.41	2006.9	18.3	18.3
9	13, Nov 2012	6.5	2	69.2	69.2	324.4	1484.8	-357.68	357.68	22.00	3.75	82.95	82.95	7094.69	2013.4	71.6	71.6
10	14, Nov 2012	5	2	60.0	60.0	34.20	344.72	-907.97	907.97	23.50	3.75	84.04	84.04	936.46	467.42	50.1	50.1
11	19, Nov 2012	7	2	71.4	71.4	20.37	991.48	-4767.34	4767.34	16.50	3.75	77.27	77.27	291.52	1344.4	-361.2	361.2
12	20, Nov 2012	4.5	2	55.6	55.6	3.59	91.72	-2454.75	2454.75	12.50	3.75	70.00	70.00	48.90	124.36	-154.3	154.3
13	25, Nov 2012	3	2	33.3	33.3	6.56	564.53	-8505.57	8505.57	8.50	3.75	55.88	55.88	59.90	765.46	-1177.9	1177.9
14	10, Mar 2014	7	2	71.4	71.4	26.62	115.26	-332.98	332.98	7.00	3.75	46.43	46.43	75.72	156.74	-106.9	106.9
15	17, Mar 2014	6	2	66.7	66.7	20.92	112.19	-436.28	436.28	7.00	3.75	46.43	46.43	93.75	152.56	-62.7	62.7
16	18, Mar 2014	7	2	71.4	71.4	23.82	173.66	-629.05	629.05	18.00	3.75	79.17	79.17	216.52	236.15	-9.1	9.1
17	30, Mar 2014	6	2	66.7	66.7	32.52	130.63	-301.69	301.69	17.00	3.75	77.94	77.94	239.30	177.63	25.8	25.8
18	13, Apr 2014	6	2	66.7	66.7	2.66	107.58	-3944.4	3944.4	9.00	3.75	58.33	58.33	20.82	146.29	-602.6	602.6
19	18, Apr 2014	9	2	77.8	77.8	14.04	119.87	-753.77	753.77	10.00	3.75	62.50	62.50	75.01	163.01	-117.3	117.3
20	19, Oct 2014	23	3	86.9	86.9	3652.5	126.25	96.54	96.54	36.00	3.75	89.58	89.58	10028.3	168.96	98.3	98.3
21	20, Oct 2014	11	3	72.7	72.7	3652.5	131.30	96.41	96.41	24.00	3.75	84.38	84.38	8788.75	175.72	98.0	98.0
22	02, Nov 2014	3	3	0.0	0.0	28.09	114.46	-307.48	307.48	5.00	3.75	25.00	25.00	137.19	153.19	-11.7	11.7
23	16, Nov 2014	4	3	25.0	25.0	21.79	117.83	-440.75	440.75	12.00	3.75	68.75	68.75	82.08	157.70	-92.1	92.1
24	22, Nov 2014	4	3	25.0	25.0	23.52	138.03	-486.86	486.86	12.00	3.75	68.75	68.75	112.89	184.73	-63.6	63.6
25	13, Dec 2014	10	3	70.0	70.0	228.1	151.50	33.58	33.58	12.00	3.75	68.75	68.75	861.39	202.76	76.5	76.5
Mean		6.78	2.24	59.2	59.20	340.81	694.19	-5341.87	5359.99	14.72	3.75	69.19	69.19	1357.93	939.12	-540.6	575.71
Standard Deviation		3.92	0.43	21.0	21.04	979.77	947.83	11895.41	11887.2	6.64	0.00	14.12	14.12	2769.67	1281.8	1434.3	1420.6
Coefficient of Variations (%)		57.8	19.1	35.5	35.54	287.48	136.54	-222.68	221.78	45.14	0.00	20.40	20.40	203.96	136.49	-265.3	246.75

Appendix Table 5. Comparison between principle components of observed and estimated sediment graphs from the channel longitudinal profile method and WaTEM/SEDEM method for calibration stage for the Galazchai Watershed, Iran

NO.	Date	Time to peak (h)		RE (%)	AE (%)	Peak Value (ton)		RE (%)	AE (%)	Base Time (h)		RE (%)	AE (%)	Total sediment (ton)		RE (%)	AE (%)
		Obs.	Est.			Obs.	Est.			Obs.	Est.			Obs.	Est.		
1	29, Oct 2011	4.5	2.5	44.44	44.44	6.94	146.91	-2016.8	2016.8	10.5	2.50	76.19	76.19	52.26	6.15	88.23	88.23
2	30, Oct 2011	7	2.5	64.29	64.29	4.33	274.42	-6237.6	6237.6	19.0	2.50	86.84	86.84	80.84	11.5	85.79	85.79
3	04, Nov 2011	9	2.5	72.22	72.22	16.23	279.15	-1619.9	1619.9	20.0	2.50	87.50	87.50	241.01	11.7	95.15	95.15
4	05, Nov 2011	6.5	2.5	61.54	61.54	6.89	172.93	-2409.8	2409.8	13.5	2.50	81.48	81.48	82.73	7.24	91.25	91.25
5	11, Apr 2012	7	2.5	64.29	64.29	49.26	287.43	-483.5	483.5	14.5	2.50	82.76	82.76	773.08	12.0	98.44	98.44
6	03, Nov 2012	2.5	2.5	0.00	0.00	2.42	215.99	-8825.0	8825.0	12.5	2.50	80.00	80.00	23.77	9.04	61.96	61.96
7	11, Nov 2012	6.5	2.5	61.54	61.54	112.33	277.97	-147.45	147.45	11.5	2.50	78.26	78.26	1075.9	11.6	98.92	98.92
8	12, Nov 2012	4.5	2.5	44.44	44.44	205.70	221.19	-7.53	7.53	14.5	2.50	82.76	82.76	2455.4	9.26	99.62	99.62
9	13, Nov 2012	6.5	2.5	61.54	61.54	324.43	292.16	9.95	9.95	22.0	2.50	88.64	88.64	7094.7	12.2	99.83	99.83
10	14, Nov 2012	5	2.5	50.00	50.00	34.20	179.55	-425.01	425.01	23.5	2.50	89.36	89.36	936.46	7.52	99.20	99.20
11	19, Nov 2012	7	2.5	64.29	64.29	20.37	239.64	-1076.4	1076.4	16.5	2.50	84.85	84.85	291.52	10.0	96.56	96.56
12	20, Nov 2012	4.5	2.5	44.44	44.44	3.59	158.74	-4321.6	4321.6	12.5	2.50	80.00	80.00	48.90	6.64	86.41	86.41
13	25, Nov 2012	3	2.5	16.67	16.67	6.56	193.98	-2857.1	2857.1	8.5	2.50	70.59	70.59	59.90	8.12	86.44	86.44
14	10, Mar 2014	7	2.5	64.29	64.29	26.62	176.62	-563.5	563.5	7.0	2.50	64.29	64.29	75.72	7.67	89.87	89.87
15	17, Mar 2014	6	2.5	58.33	58.33	20.92	171.91	-721.8	721.8	7.0	2.50	64.29	64.2	93.75	7.47	92.03	92.03
16	18, Mar 2014	7	2.5	64.29	64.29	23.82	266.11	-1017.2	1017.2	18.0	2.50	86.11	86.11	216.52	11.6	94.66	94.66
17	30, Mar 2014	6	2.5	58.33	58.33	32.52	200.17	-515.53	515.53	17.0	2.50	85.29	85.29	239.30	8.70	96.37	96.37
18	13, Apr 2014	6	2.5	58.33	58.33	2.66	164.85	-6097.3	6097.3	9.0	2.50	72.22	72.22	20.82	7.16	65.60	65.60
19	18, Apr 2014	9	2.5	72.22	72.22	14.04	183.69	-1208.3	1208.3	10.0	2.50	75.00	75.00	75.01	7.98	89.36	89.36
20	19, Oct 2014	23	2.5	89.13	89.13	3652.5	174.98	95.21	95.21	36.0	2.50	93.06	93.06	10028	9.48	99.91	99.91
21	20, Oct 2014	11	2.5	77.27	77.27	3652.5	181.98	95.02	95.02	24.0	2.50	89.58	89.58	8788.7	9.86	99.89	99.89
22	02, Nov 2014	3	2.5	16.67	16.67	28.09	158.65	-464.78	464.78	5.0	2.50	50.00	50.00	137.19	8.59	93.74	93.74
23	16, Nov 2014	4	2.5	37.50	37.50	21.79	163.31	-649.49	649.49	12.0	2.50	79.17	79.17	82.08	8.85	89.22	89.22
24	22, Nov 2014	4	2.5	37.50	37.50	23.52	191.31	-713.39	713.39	12.0	2.50	79.17	79.17	112.9	10.4	90.82	90.82
25	13, Dec 2014	10	2.5	75.00	75.00	228.08	209.97	7.94	7.94	12.0	2.50	79.17	79.17	861.4	11.4	98.68	98.68
Mean		6.78	2.50	54.34	54.34	340.81	207.34	-1686.8	1703.5	14.7	2.50	79.46	79.46	1357.9	9.29	91.52	91.52
Standard Deviation		3.92	0.00	20.17	20.17	979.77	45.63	2267.40	2254.9	6.6	0.00	9.41	9.41	2769.7	1.82	9.42	9.42
Coefficient of Variations (%)		57.8	0.00	37.12	37.12	287.48	22.01	-134.42	132.37	45.1	0.00	11.84	11.84	203.96	19.6	10.29	10.29

Appendix Table 6. Comparison between principle components of observed and estimated sediment graphs from the spatially distributed travel time method and WaTEM/SEDEM method for calibration stage for the Galazchai Watershed, Iran

NO.	Date	Time to peak (h)		RE (%)	AE (%)	Peak Value (ton)		RE (%)	AE (%)	Base Time (h)		RE (%)	AE (%)	Total sediment (ton)		RE (%)	AE (%)
		Obs.	Est.			Obs.	Est.			Obs.	Est.			Obs.	Est.		
1	29, Oct 2011	4.5	2	55.56	55.56	6.94	51.17	-637.37	637.37	10.5	3.75	64.29	64.29	52.26	21.24	59.35	59.35
2	30, Oct 2011	7	2	71.43	71.43	4.33	95.59	-2107.6	2107.6	19.0	3.75	80.26	80.26	80.84	39.68	50.91	50.91
3	04, Nov 2011	9	2	77.78	77.78	16.23	97.24	-499.13	499.13	20.0	3.75	81.25	81.25	241.01	40.35	83.26	83.26
4	05, Nov 2011	6.5	2	69.23	69.23	6.89	60.24	-774.28	774.28	13.5	3.75	72.22	72.22	82.73	25.01	69.77	69.77
5	11, Apr 2012	7	2	71.43	71.43	49.26	100.1	-103.25	103.25	14.5	3.75	74.14	74.14	773.08	41.56	94.62	94.62
6	03, Nov 2012	2.5	2	20.00	20.00	2.42	75.24	-3008.9	3008.9	12.5	3.75	70.00	70.00	23.77	31.23	-31.4	31.4
7	11, Nov 2012	6.5	2	69.23	69.23	112.33	96.83	13.80	13.80	11.5	3.75	67.39	67.39	1075.9	40.53	96.23	96.23
8	12, Nov 2012	4.5	2	55.56	55.56	205.70	77.05	62.54	62.54	14.5	3.75	74.14	74.14	2455.4	31.98	98.70	98.70
9	13, Nov 2012	6.5	2	69.23	69.23	324.43	101.8	68.63	68.63	22.0	3.75	82.95	82.95	7094.7	42.25	99.40	99.40
10	14, Nov 2012	5	2	60.00	60.00	34.20	62.55	-82.88	82.88	23.5	3.75	84.04	84.04	936.46	25.96	97.23	97.23
11	19, Nov 2012	7	2	71.43	71.43	20.37	83.48	-309.80	309.80	16.5	3.75	77.27	77.27	291.52	34.65	88.11	88.11
12	20, Nov 2012	4.5	2	55.56	55.56	3.59	55.29	-1440.2	1440.2	12.5	3.75	70.00	70.00	48.90	22.95	53.06	53.06
13	25, Nov 2012	3	2	33.33	33.33	6.56	67.57	-930.06	930.06	8.5	3.75	55.88	55.88	59.90	28.05	53.17	53.17
14	10, Mar 2014	7	2	71.43	71.43	26.62	61.35	-130.47	130.47	7.0	3.75	46.43	46.43	75.72	25.06	66.91	66.91
15	17, Mar 2014	6	2	66.67	66.67	20.92	59.72	-185.45	185.45	7.0	3.75	46.43	46.43	93.75	24.39	73.99	73.99
16	18, Mar 2014	7	2	71.43	71.43	23.82	37.75	-58.49	58.49	18.0	3.75	79.17	79.17	216.52	37.75	82.56	82.56
17	30, Mar 2014	6	2	66.67	66.67	32.52	28.40	12.68	12.68	17.0	3.75	77.94	77.94	239.30	28.40	88.13	88.13
18	13, Apr 2014	6	2	66.67	66.67	2.66	23.39	-779.17	779.17	9.0	3.75	58.33	58.33	20.82	23.39	-12.3	12.3
19	18, Apr 2014	9	2	77.78	77.78	14.04	26.06	-85.60	85.60	10.0	3.75	62.50	62.50	75.01	26.06	65.26	65.26
20	19, Oct 2014	23	3	86.96	86.96	3652.4	30.84	99.16	99.16	36.0	3.75	89.58	89.58	10028	30.84	99.69	99.69
21	20, Oct 2014	11	3	72.73	72.73	3652.4	32.07	99.12	99.12	24.0	3.75	84.38	84.38	8788.7	32.07	99.64	99.64
22	02, Nov 2014	3	3	0.00	0.00	28.09	27.96	0.45	0.45	5.0	3.75	25.00	25.00	137.19	27.96	79.62	79.62
23	16, Nov 2014	4	3	25.00	25.00	21.79	28.79	-32.10	32.10	12.0	3.75	68.75	68.75	82.08	28.79	64.93	64.93
24	22, Nov 2014	4	3	25.00	25.00	23.52	33.72	-43.37	43.37	12.0	3.75	68.75	68.75	112.89	33.72	70.13	70.13
25	13, Dec 2014	10	3	70.00	70.00	228.08	37.01	83.77	83.77	12.0	3.75	68.75	68.75	861.39	37.01	95.70	95.70
Mean		6.78	2.24	59.20	59.20	340.81	58.05	-430.72	465.93	14.72	3.75	69.19	69.19	1357.9	31.24	71.47	74.96
Standard Deviation		3.92	0.43	21.04	21.04	979.77	26.34	744.93	723.43	6.64	0.00	14.12	14.12	2769.7	6.35	31.85	22.41
Coefficient of Variations (%)		57.85	19.1	35.54	35.54	287.48	45.38	-172.95	155.26	45.14	0.00	20.40	20.40	203.96	20.32	44.56	29.89

Appendix Table 7. Comparison between principle components of observed and estimated sediment graphs from the channel longitudinal profile method and the Hadley et al. (1985) method for validation stage for the Galazchai Watershed, Iran

NO.	Date	Time to peak (h)		RE (%)	AE (%)	Peak Value (ton)		RE (%)	AE (%)	Base Time (h)		RE (%)	AE (%)	Total sediment (ton)		RE (%)	AE (%)
		Obs.	Est.			Obs.	Est.			Obs.	Est.			Obs.	Est.		
1	17, Feb 2018	8	2.5	68.75	68.75	13.2	426.91	-3129.27	3129.27	13	2.5	80.77	80.77	21.96	155.3	-607.4	607.4
2	22, Feb 2018	7	2.5	64.29	64.29	56.7	654.6	-1054.50	1054.50	16	2.5	84.38	84.38	89.62	238.2	-165.8	165.8
3	09, Mar 2018	6	2.5	58.33	58.33	30.2	483.84	-1503.71	1503.71	11	2.5	77.27	77.27	158.1	176.1	-11.3	11.3
4	29, Mar 2018	18	2.5	86.11	86.11	78.5	546.45	-595.85	595.85	37	2.5	93.24	93.24	922.7	198.8	78.4	78.4
5	11, Apr 2018	17	2.5	85.29	85.29	18.2	461.07	-2431.96	2431.96	20	2.5	87.50	87.50	166.9	167.8	-0.5	0.5
6	12, Apr 2018	6	2.5	58.33	58.33	3.5	535.07	-15187.7	15187.7	13	2.5	80.77	80.77	33.66	194.7	-478.4	478.4
7	15, Apr 2018	5	2.5	50.00	50.00	20.9	455.38	-2079.89	2079.89	13	2.5	80.77	80.77	112.9	165.7	-46.8	46.8
8	27, Apr 2018	16	2.5	84.38	84.38	62.7	443.99	-608.34	608.34	18	2.5	86.11	86.11	261.4	161.6	38.2	38.2
9	08, May 2018	4	2.5	37.50	37.50	194.9	597.68	-206.69	206.69	11	2.5	77.27	77.27	772.9	217.5	71.9	71.9
10	26, Oct 2018	3	2.5	16.67	16.67	105.8	420.95	-297.84	297.84	19	2.5	86.84	86.84	679.9	165.3	75.7	75.7
11	31, Oct 2018	21	2.5	88.10	88.10	131.4	514.5	-291.67	291.67	33	2.5	92.42	92.42	966.3	202.0	79.1	79.1
12	25, Mar 2019	6	2.5	58.33	58.33	55.5	453.79	-717.64	717.64	16	2.5	84.38	84.38	373.7	178.6	52.21	52.21
13	31, Mar 2019	8	2.5	68.75	68.75	39.9	669.09	-1575.24	1575.24	17	2.5	85.29	85.29	264.2	263.3	0.35	0.35
Mean		9.62	2.5	63.4	63.4	62.4	512.6	-2283.1	2283.1	18.2	2.5	84.4	84.4	371.1	191.1	-70.35	131.2
Standard Deviation		5.84	0.0	20.03	20.03	52.5	80.5	3825.5	3825.5	7.7	0.0	4.8	4.8	329.0	31.3	213.2	182.1
Coefficient of Variations (%)		60.72	0.0	31.6	31.6	83.9	15.7	-167.6	167.6	42.3	0.0	5.7	5.7	88.7	16.4	-303.0	138.8

Appendix Table 8. Comparison between principle components of observed and estimated sediment graphs from the spatially distributed travel time method and the Hadley et al. (1985) method for validation stage for Galazchai Watershed, Iran

NO.	Date	Time to peak (h)		RE (%)	AE (%)	Peak Value (ton)		RE (%)	AE (%)	Base Time (h)		RE (%)	AE (%)	Total sediment (ton)		RE	AE
		Obs.	Est.			Obs.	Est.			Obs.	Est.			Obs.	Est.	(%)	(%)
1	17, Feb 2018	8	2	75.0	75.0	13.22	127.93	-867.70	867.70	13	3.75	71.15	71.15	21.96	173.604	-690.5	690.5
2	22, Feb 2018	7	2	71.4	71.4	56.7	196.16	-245.96	245.96	16	3.75	76.56	76.56	89.62	266.193	-197.0	197.0
3	09, Mar 2018	6	2	66.7	66.7	30.17	144.99	-380.58	380.58	11	3.75	65.91	65.91	158.13	196.752	-24.42	24.42
4	29, Mar 2018	18	2	88.9	88.9	78.53	163.75	-108.52	108.52	37	3.75	89.86	89.86	922.73	222.214	75.92	75.92
5	11, Apr 2018	17	2	88.2	88.2	18.21	138.16	-658.70	658.70	20	3.75	81.25	81.25	166.89	187.493	-12.35	12.35
6	12, Apr 2018	6	2	66.7	66.7	3.5	160.34	-4481.1	4481.1	13	3.75	71.15	71.15	33.66	217.584	-546.4	546.4
7	15, Apr 2018	5	2	60.0	60.0	20.89	136.46	-553.22	553.22	13	3.75	71.15	71.15	112.89	185.178	-64.03	64.03
8	27, Apr 2018	16	2	87.5	87.5	62.68	133.05	-112.26	112.26	18	3.75	79.17	79.17	261.37	180.549	30.92	30.92
9	08, May 2018	4	2	50.0	50.0	194.88	179.10	8.10	8.10	11	3.75	65.91	65.91	772.9	243.046	68.55	68.55
10	26, Oct 2018	3	2	33.3	33.3	105.81	138.09	-30.51	30.51	19	3.75	80.26	80.26	679.89	184.531	72.86	72.86
11	31, Oct 2018	21	2	90.5	90.5	131.36	168.79	-28.49	28.49	33	3.75	88.64	88.64	966.26	219.883	77.24	77.24
12	25, Mar 2019	6	2	66.7	66.7	55.5	152.20	-174.23	174.23	16	3.75	76.56	76.56	373.71	199.478	46.62	46.62
13	31, Mar 2019	8	2	75.0	75.0	39.94	224.40	-461.84	461.84	17	3.75	77.94	77.94	264.23	294.102	-11.31	11.31
Mean		9.6	2.0	70.8	70.8	62.4	158.7	-622.7	623.9	18.2	3.75	76.6	76.6	371.1	213.1	-90.3	147.6
Standard Deviation		5.8	0.0	16.0	16.0	52.4	26.9	1143.8	1143.1	7.7	0.00	7.2	7.2	329.04	34.8	238.3	207.7
Coefficient of Variations (%)		60.7	0.0	22.6	22.6	83.8	16.9	-183.7	183.2	42.3	0.00	9.5	9.5	88.7	16.3	-263.8	140.8

Appendix Table 9. Comparison between principle components of observed and estimated sediment graphs from the channel longitudinal profile method and WaTEM/SEDEM method for validation stage for the Galazchai Watershed, Iran

NO.	Date	Time to peak (h)		RE (%)	AE (%)	Peak Value (ton)		RE (%)	AE (%)	Base Time (h)		RE (%)	AE (%)	Total sediment (ton)		RE (%)	AE (%)
		Obs.	Est.			Obs.	Est.			Obs.	Est.			Obs.	Est.		
1	17, Feb 2018	8	2.5	68.75	68.75	13.22	176.04	-1231.6	1231.6	13	2.50	80.77	80.77	21.96	8.18	62.74	62.74
2	22, Feb 2018	7	2.5	64.29	64.29	56.7	269.93	-376.06	376.06	16	2.50	84.38	84.38	89.62	12.54	86.00	86.00
3	09, Mar 2018	6	2.5	58.33	58.33	30.17	199.51	-561.29	561.29	11	2.50	77.27	77.27	158.13	9.27	94.14	94.14
4	29, Mar 2018	18	2.5	86.11	86.11	78.53	225.33	-186.94	186.94	37	2.50	93.24	93.24	922.73	10.47	98.87	98.87
5	11, Apr 2018	17	2.5	85.29	85.29	18.21	190.12	-944.06	944.06	20	2.50	87.50	87.50	166.89	8.84	94.71	94.71
6	12, Apr 2018	6	2.5	58.33	58.33	3.5	220.64	-6203.9	6203.9	13	2.50	80.77	80.77	33.66	10.25	69.54	69.54
7	15, Apr 2018	5	2.5	50.00	50.00	20.89	187.78	-798.88	798.88	13	2.50	80.77	80.77	112.89	8.73	92.27	92.27
8	27, Apr 2018	16	2.5	84.38	84.38	62.68	183.08	-192.09	192.09	18	2.50	86.11	86.11	261.37	8.51	96.74	96.74
9	08, May 2018	4	2.5	37.50	37.50	194.88	246.46	-26.47	26.47	11	2.50	77.27	77.27	772.9	11.45	98.52	98.52
10	26, Oct 2018	3	2.5	16.67	16.67	105.81	212.22	-100.57	100.57	19	2.50	86.84	86.84	679.89	10.25	98.49	98.49
11	31, Oct 2018	21	2.5	88.10	88.10	131.36	259.38	-97.46	97.46	33	2.50	92.42	92.42	966.26	12.52	98.70	98.70
12	25, Mar 2019	6	2.5	58.33	58.33	55.5	181.80	-227.56	227.56	16	2.50	84.38	84.38	373.71	7.50	97.99	97.99
13	31, Mar 2019	8	2.5	68.75	68.75	39.94	268.04	-571.10	571.10	17	2.50	85.29	85.29	264.23	11.05	95.82	95.82
Mean		9.62	2.50	63.45	63.45	62.41	216.95	-886.00	886.00	18.2	2.50	84.39	84.39	371.10	9.97	91.12	91.12
Standard Deviation		5.84	0.00	20.03	20.03	52.36	32.96	1575.2	1575.2	7.7	0.00	4.83	4.83	329.04	1.56	11.26	11.26
Coefficient of Variations (%)		60.72	0.00	31.57	31.57	83.89	15.19	-177.79	177.79	42.3	0.00	5.72	5.72	88.67	15.67	12.36	12.36

Appendix Table 10. Comparison between principle components of observed and estimated sediment graphs from the spatially distributed travel time method and WaTEM/SEDEM method for validation stage for the Galazchai Watershed, Iran

NO.	Date	Time to peak (h)		RE (%)	AE (%)	Peak Value (ton)		RE (%)	AE (%)	Base Time (h)		RE (%)	AE (%)	Total sediment (ton)		RE (%)	AE (%)
		Obs.	Est.			Obs.	Est.			Obs.	Est.			Obs.	Est.		
1	17, Feb 2018	8	2	75.00	75.00	13.22	64.75	-389.82	389.82	13	3.75	71.15	71.15	21.96	28.37	-29.17	29.17
2	22, Feb 2018	7	2	71.43	71.43	56.7	99.29	-75.12	75.12	16	3.75	76.56	76.56	89.62	43.49	51.47	51.47
3	09, Mar 2018	6	2	66.67	66.67	30.17	73.39	-143.25	143.25	11	3.75	65.91	65.91	158.13	32.15	79.67	79.67
4	29, Mar 2018	18	2	88.89	88.89	78.53	82.89	-5.55	5.55	37	3.75	89.86	89.86	922.73	36.31	96.07	96.07
5	11, Apr 2018	17	2	88.24	88.24	18.21	69.93	-284.05	284.05	20	3.75	81.25	81.25	166.89	30.63	81.64	81.64
6	12, Apr 2018	6	2	66.67	66.67	3.5	81.16	-2218.8	2218.8	13	3.75	71.15	71.15	33.66	35.55	-5.62	5.62
7	15, Apr 2018	5	2	60.00	60.00	20.89	69.07	-230.64	230.64	13	3.75	71.15	71.15	112.89	30.26	73.20	73.20
8	27, Apr 2018	16	2	87.50	87.50	62.68	67.34	-7.44	7.44	18	3.75	79.17	79.17	261.37	29.50	88.71	88.71
9	08, May 2018	4	2	50.00	50.00	194.88	90.66	53.48	53.48	11	3.75	65.91	65.91	772.9	39.71	94.86	94.86
10	26, Oct 2018	3	2	33.33	33.33	105.81	74.19	29.89	29.89	19	3.75	80.26	80.26	679.89	30.22	95.56	95.56
11	31, Oct 2018	21	2	90.48	90.48	131.36	90.67	30.97	30.97	33	3.75	88.64	88.64	966.26	36.93	96.18	96.18
12	25, Mar 2019	6	2	66.67	66.67	55.5	64.95	-17.02	17.02	16	3.75	76.56	76.56	373.71	29.23	92.18	92.18
13	31, Mar 2019	8	2	75.00	75.00	39.94	95.75	-139.75	139.75	17	3.75	77.94	77.94	264.23	43.09	83.69	83.69
Mean		9.62	2.00	70.76	70.76	62.41	78.77	-261.32	278.91	18.23	3.75	76.58	76.58	371.10	34.26	69.11	74.46
Standard Deviation		5.84	0.00	16.02	16.02	52.36	11.62	579.93	571.68	7.71	0.00	7.24	7.24	329.04	5.10	39.02	27.46
Coefficient of Variations (%)		60.72	0.00	22.64	22.64	83.89	14.75	-221.92	204.97	42.28	0.00	9.46	9.46	88.67	14.90	56.46	36.87

RESEARCH PAPER

SPATIOTEMPORAL VARIATIONS OF SOIL MOISTURE AND GROUNDWATER LEVEL IN A SOUTH SUMATRA PEATLAND, INDONESIA DURING 2015–2018

Mokhamad Y. N. Khakim[1*], Akhmad A. Bama[1], Takeshi Tsuji[2,3]
[1]Universitas Sriwijaya, Jl. Raya Palembang-Prabumulih Km. 32, 30662, Indralaya, Indonesia
[2]Kyushu University, 744 Motooka, Nishi-ku, Fukuoka 819-0395, Japan
[3]University of Tokyo, 7-3-1 Hongo, Bunkyo-ku, Tokyo 113-8656, Japan
***Corresponding author:** myusup_nkh@mipa.unsri.ac.id
Received: December 21st, 2021 / Accepted: April 24th, 2022 / Published: June 30th, 2022
https://DOI-10.24057/2071-9388-2021-137

ABSTRACT. The peat hydrological unit of the Air Sugihan River – Air Saleh River, South Sumatra, Indonesia, experienced extreme fires during the 2015 El Niño event. Restoration of 2.0 Mha degraded peatlands has been conducted since 2016. This study aims to analyze spatiotemporal variations of soil moisture content and groundwater level in this site from 2015 to 2018. The soil moisture was estimated using a multiple regression analysis method based on the Sentinel-1A and the European Center for Medium-Range Weather Forecast dataset. The groundwater level model was calculated by using linear regression between the estimated soil moisture and water level observed from field measurements. A minimum moisture content of ~0.78 m^3m^{-3} and a minimum groundwater depth of ~0.50 m below the peat surface were estimated to cause smoldering combustion. A sharp decline in the water table depth (around 1.53 m) led to a decrease in moisture content in October 2015. This month, peat fires severely burned both cultivation and protected areas having dense drainage canals and near rivers. Although there was an increasing trend in the groundwater level and moisture content in 2016, between 2017 to 2018 the water table declined to a depth of ~0.7 m with a corresponding moisture content of ~0.25 m^3m^{-3}. Such decline may have led to a few peat fires which occurred in the dry season of both 2017 and 2018. We recommended that law enforcement efforts should be conducted to raise the mean annual water table to shallower depths than 0.40 m

KEY WORDS: peatland fire, soil moisture, groundwater level, restoration, remote sensing

CITATION: Khakim M.Y.N., Bama A.A., Tsuji T. (2022). Spatiotemporal Variations of Soil Moisture and Groundwater Level in a South Sumatra Peatland, Indonesia During 2015–2018. Geography, Environment, Sustainability, 2(15), p. 58-70
https://DOI-10.24057/2071-9388-2021-137

ACKNOWLEDGEMENTS: We would like to acknowledge the Ministry of Research, Technology, and Higher Education of the Republic of Indonesia for financial support through «Penelitian Dasar Unggulan Perguruan Tinggi (PDUPT)», 054/E4.1/AK.04. PT/2021 and the JSPS KAKENHI grants JP20H01997. We also thank the European Space Agency (ESA) for providing Sentinel-1 data. The authors would also like to thank the Peatland Restoration Agency for providing SESAME data. We would like to thank the two anonymous reviewers and the academic editor.

Conflict of interests: The authors reported no potential conflict of interest.

INTRODUCTION

Peatlands, a habitat for many local unique and protected species, play an essential role in ecosystem services, including carbon balance, hydrological cycle regulation, flood control, and water quality protection (Evers et al. 2017; Page et al. 2009; Wösten et al. 2006). Indonesia is home to the largest tropical peatlands (approximately 22.5 Mha) globally (A. Hooijer et al. 2010), with a thickness of up to about 12 meters and 42% of the area is covered by a peat thickness of 2 meters (A Hooijer et al. 2006). These areas act as a significant carbon sink, storing 77% of total peat and carbon deposits (Aljosja Hooijer et al. 2006).

Peatland fires are closely related to the hydrological regime as well as other factors such as human activities and the local climate. Human activity is a factor related to land use without paying attention to environmental sustainability, including logging, canal construction, and plantation development (Miettinen et al. 2013; Page et al. 2009). In addition, the main climatic factor of the peatland fires is the amount of rainfall (Leng et al. 2019). The extreme climate due to the 2015 El Niño burnt about 850,000 ha of peatland in Sumatra and Kalimantan (Giesen and Sari 2018). Thus, a hydrological issue is an important key to restore the degraded peatland. Soil moisture and water level are important hydrological parameters to characterize peat fires caused by climate extremes.

Peatlands in Indonesia are usually located in remote and inaccessible areas with large spatial coverage. Field measurement has a limitation in spatial coverage to map peatland. Therefore, remote sensing has become a useful complementary method for monitoring and mapping the dynamics of peatland hydrology. A remote sensing technique was applied to estimate subsidence and map vegetation degradation in the study area using the Sentinel-1 dataset (Khakim et al. 2020).

The behavior of the radar backscattering signals as a function of soil moisture has been analyzed based on empirical or physical models (Baghdadi et al. 2016; Dabrowska-Zielinska et al. 2018; Dubois et al. 1995; Oh et al. 1992). The soil moisture estimation

relying on the co-polarized channels is more robust to the presence of vegetation than relying on both the cross and the co-polarized channels (Dubois et al. 1995). When the vegetation is sparse, the radar scattering is dominated by interactions with the underlying surface (Dubois et al. 1995). Several studies utilized the radar backscattering from Sentinel-1 to estimate soil moisture with reasonable accuracy, such as over wetlands using regression models (Dabrowska-Zielinska et al. 2016; Gangat et al. 2020) and a water cloud model (Dabrowska-Zielinska et al. 2018). Meanwhile, a low correlation between water levels and radar backscattering was investigated (Asmuß et al. 2019). Other studies on the estimation of water levels were performed by using the coherence data (Chen et al. 2020; Kim et al. 2017). However, the interferometric coherence was mainly dependent on the temporal baseline and landcover types for Sentinel-1. The coherence is commonly low for wetlands; thus, it is more difficult to map water levels with reasonably spatial distribution.

This study aims to analyze spatiotemporal variations of (1) soil moisture content and (2) groundwater level at the peat hydrological unit of the Air Sugihan River – Air Saleh River, namely the Kesatuan Hidrologi Gambut Sugihan Saleh (KHGSS), South Sumatra, Indonesia, using a multiple regression analysis (MRA) method based on Sentinel-1 and ECMWF datasets. Moreover, this study aims to provide a better understanding of the variation of these two hydrological parameters during the 2015 El Niño event and three years after, during which rewetting measures were in place.

MATERIALS AND METHODS

Study area

The peat hydrological unit of the Air Sugihan River – Air Saleh River (KHGSS) is one of the tropical peatlands in South Sumatra, Indonesia (Fig. 1). This area is located between Air Sugihan River in the East and Air Saleh River in the West. This site area experienced severe fires, large subsidence, and high vegetation degradation from the 2015 El Niño phenomenon (Khakim et al. 2020).

For restoring the degraded peatland due to the 2015 peatland fires, the National Peatland Restoration Agency (BRG) was established by Presidential Decree in January 2016 (President of Republic of Indonesia 2016a). The decree mandated BRG to coordinate and facilitate the restoration of 2.0 Mha of the degraded peatland in 5 years (2016–2021). The restoration was applied in this study area through three approaches (3R), i.e., Rewetting, Revegetation, and Revitalization of livelihoods in the peatland restoration efforts (Giesen and Sari 2018).

A main purpose of rewetting is to restore hydrological properties of drained peatlands. In the study area rewetting has been conducted by blocking canals to raise groundwater levels. Besides preventing peat soil oxidation and reducing carbon emission, the rewetting has been also intended to minimize further subsidence and to prevent peat fire.

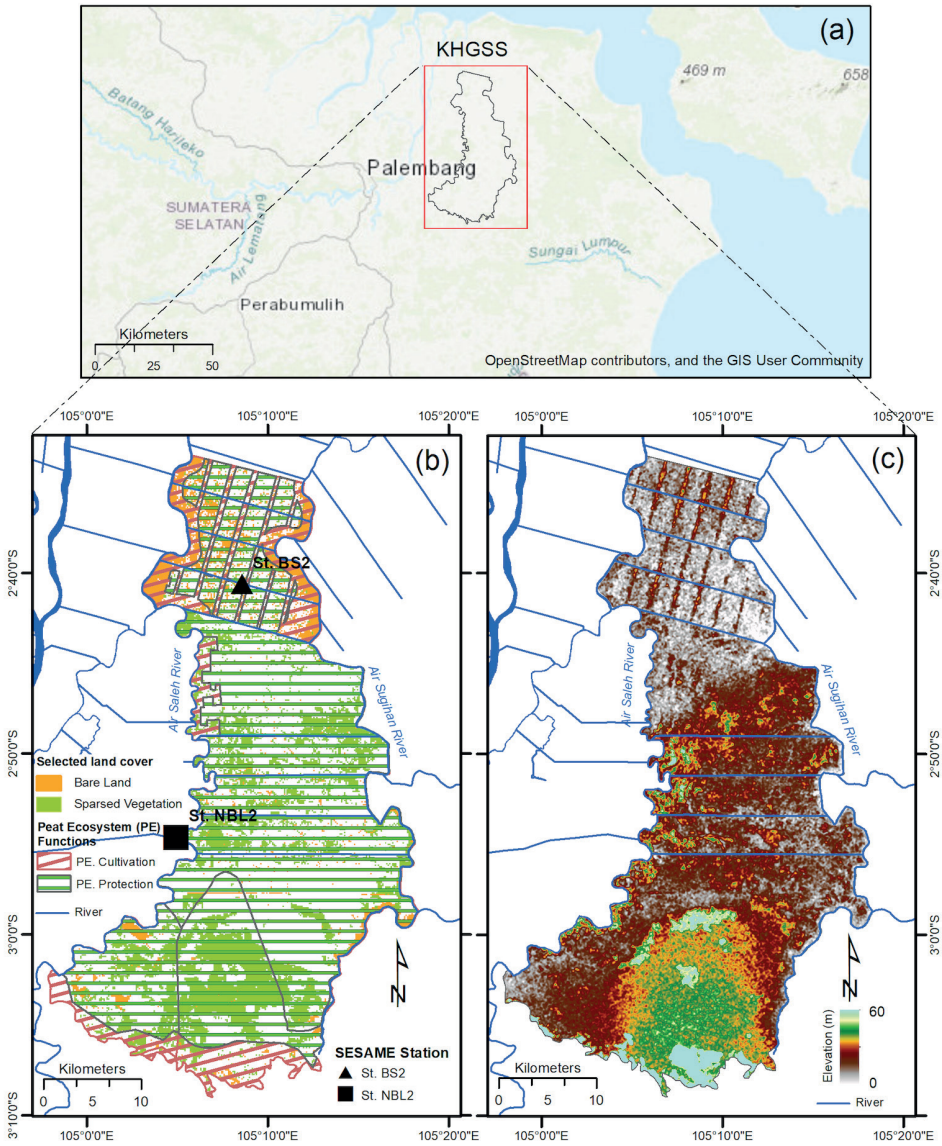

Fig. 1. (a) Location of the study area with (b) peat ecosystem functions (Peat Restoration Agency 2017) and (c) topography of the study area downloaded from http://tides.big.go.id/DEMNAS/

In addition, revegetation, which is the second approach of the restoration, has been intended to restore degraded peat swamp vegetation cover and improve peat forest habitat quality (Dohong 2019). The revegetation in the study area was conducted by replanting indigenous local tree species such as Jelutung (*Dyera lowii* Hook.F), Meranti Bunga (*Shorea leprosula* Miq), Meranti Batu (*Shorea platycarpa* Heim), Tanaman Sagu (*Metroxylon rumphii*), and Gelam (*Melaleuca spp*) (Sodikin et al. 2017). These local trees have been combined with pineapple in an Agroforestry pattern.

The revitalization of local livelihoods, which is the third approach, provides livelihood alternatives for local communities. Therefore, it can create various livelihood alternatives for increasing their income and welfare. Moreover, the local people can be involved in operating and maintaining canal blocking built in their respective sites (Dohong 2019). The fishery canal was made to provide their additional economic benefit. This fishery aims to cultivate species of local fish.

Data

Sentinel-1A GRD data. The European Space Agency's (ESA) Sentinel-1 constellation provides continuous global all-weather, day-and-night radar imaging with a C-band Synthetic Aperture Radar (SAR) instrument operating at a center frequency of 5.405 GHz in support of Global Monitoring for Environment and Security (GMES) applications (Attema et al. 2008). The Sentinel-1 satellite constellations have a revisit time of six days for the SAR data acquisition (Filipponi 2019). This study utilized Level 1 Interferometric Wide Swath (IW) multi-looked Ground Range Detected (GRD) products in high resolution of 20 x 22 m and a pixel spacing of 10 x 10 m (Hornácek et al. 2012). These GRD images are multi-looked with the number of looks of 5 and 1 in range and azimuth, respectively. To cover an area of interest from 2015 to 2018, we selected four datasets with different paths and frames that were downloaded from Alaska Satellite Facility (ASF), as presented in Table 1.

Table 1. The IW GRDH Sentinel-1A images used in this study

No.	Date (yyyy/mm/dd)	Path/Frame	Polarization
1	2015/01/04	98/1171	VV
2	2015/02/21	98/1171	VV
3	2015/03/17	98/1171	VV
4	2015/04/10	98/1171	VV
5	2015/05/17	120/604; 120/598	VV+VH
6	2015/07/15	98/1171	VV
7	2015/08/08	98/1171	VV
8	2015/10/19	98/1171	VV
9	2015/11/25	120/604; 120/598	VV+VH
10	2015/12/19	120/604; 120/598	VV+VH
11	2016/01/12	120/604; 120/598	VV+VH
12	2016/02/05	120/604; 120/598	VV+VH
13	2016/03/24	120/604; 120/598	VV+VH
14	2016/04/17	120/604; 120/598	VV+VH
15	2016/05/11	120/604; 120/598	VV+VH
16	2016/07/22	120/604; 120/598	VV+VH
17	2016/08/15	120/604; 120/598	VV+VH
18	2016/10/02	120/604; 120/598	VV+VH
19	2016/11/19	120/604; 120/598	VV+VH
20	2016/12/13	120/604; 120/598	VV+VH
21	2017/02/22	98/1170	VV+VH
22	2017/03/06	98/1170	VV+VH
23	2017/03/18	98/1170	VV+VH
24	2017/04/23	98/1170	VV+VH
25	2017/05/29	98/1170	VV+VH

26	2017/06/22	98/1170	VV+VH
27	2017/07/04*	98/1170	VV+VH
28	2017/08/21*	98/1170	VV+VH
29	2017/09/14*	98/1170	VV+VH
30	2017/10/20*	98/1170	VV+VH
31	2017/11/13*	98/1170	VV+VH
32	2017/12/31*	98/1170	VV+VH
33	2018/01/12*	98/1170	VV+VH
34	2018/02/17*	98/1170	VV+VH
35	2018/03/13*	98/1170	VV+VH
36	2018/04/18*	98/1170	VV+VH
37	2018/05/12*	98/1170	VV+VH
38	2018/06/17*	98/1170	VV+VH
39	2018/07/11*	98/1170	VV+VH
40	2018/08/16*	98/1170	VV+VH
41	2018/09/09*	98/1170	VV+VH
42	2018/10/03*	98/1170	VV+VH
43	2018/11/20*	98/1170	VV+VH
44	2018/12/26*	98/1170	VV+VH

*used for MRA analysis

ECMWF dataset. ERA-Interim is a global atmospheric reanalysis product from the European Centre for Medium-Range Weather Forecasts (ECMWF) that has been available since 1 January 1979 (Dee et al. 2011). This study utilized the ERA interim-daily datasets of soil moisture level-1 (0 – 7 cm), total precipitation, soil temperature level-1 (0 – 7 cm), and surface roughness in a NetCDF format downloaded from the ECMWF Data Server. We used these data with a spatial resolution of 0.125 x 0.125 degrees.

SESAME's field data. SEnsory data transmission Service Assisted by Midori Engineering (SESAME), a real-time telemetry technology that records precipitation, air temperature, and groundwater level every 10 minutes, was installed in this area to monitor the effectiveness of rewetting activities (Republic of Indonesia 2018). Two stations were installed in this area, namely St. NBL2 and St. BS2. A moisture sensor was installed at a depth of 10 cm from the peat surface. While a waterproof, immersion-type sensor for water level (WL) measurement was placed in a plastic pipe installed vertically from the peat surface to the depth of the mineral soil (Republic of Indonesia 2018; Sulaiman et al. 2017).

Fire hotspot data. This study used the NASA Near Real-Time VNP14IMGTDL_NRT VIIRS 375 m Active Fire Detections in the shapefile format from January 2015 to December 2018 downloaded from the NASA earth data website https://earthdata.nasa.gov/earth-observation-data/near-real-time/firms/. The hotspot data from the VIIRS product has a higher resolution (375 m with nominal temporal resolutions every 12 h) than MODIS data (1 km) so it provides a more reliable estimate of fire perimeters. With this data, the spatiotemporal distribution of burnt areas can be identified. The VIIRS 375 m data are comprised of five distinct single-gain channels extending from the visible to thermal infrared spectral region. The fire detection algorithms were based on the differential radiometric response of high-temperature targets imaged in those two spectral regions (Schroeder et al. 2014). This study used the fires with nominal and high confidence levels.

METHODOLOGY

Backscattering coefficient processing

The co-polarization (VV) GRD images from Sentinel-1 were processed into backscatter coefficients, σ^0, in decibels. This GRD image data processing to obtain the backscatter coefficient in each pixel was implemented using the Sentinel-1 Toolbox. Workflow for processing Copernicus Sentinel-1 GRD products included orbit metadata updates, thermal and image border noise removal, radiometric calibration, as well as range-Doppler and terrain correction (Aukema and Wilson 2019; Filipponi 2019).

Orbital metadata, generally inaccurate within the SAR product, was updated using a precise orbit downloaded automatically on Sentinel Application Platform (SNAP) software version 7.0 to provide accurate information on satellite position and speed. After applying a precise orbit, thermal noise was removed to reduce the effect of noise in the image between sub-swaths; particularly, normalizing the backscatter signal in all Sentinel-1 scenes and reducing discontinuity between sub-plots for scenes in multi-swath acquisition mode. Radiometric artifacts at the image border are produced by azimuth and range compression when generating level-1 products. We then converted digital pixel values to radiometrically calibrated SAR backscatter.

This calibration also converted image intensity values into sigma naught values. The information required to apply the calibration equation is included within the Sentinel-1 GRD product; specifically, a calibration vector included as an annotation in the product allows simple conversion of image intensity values into sigma naught values.

Interference of waves reflected from many elementary scatters resulted in speckles in SAR images. We multilooked the images by a factor of 6 in range and azimuth and applied multitemporal speckle filtering to reduce speckles. Our study required multiple SAR data for temporal analysis. Therefore, we stacked these SAR data before applying the multitemporal speckle filtering with the type of Lee filter (Lee 1981). Some distortions related to side-looking geometry in the SAR data were compensated for representing the image as close as possible to the real world by using range doppler terrain correction. This correction used the one arcsec NASA's Shuttle Radar Topography Mission – Digital Elevation Model (SRTM – DEM) to derive the precise geolocation information and obtain local incidence angles. The target coordinate reference system is the UTM zone 48S. Finally, the backscatter coefficient was converted to dB using a logarithmic transformation (Filipponi 2019; Xianlong Zhang et al. 2021).

Soil moisture and water level estimation

To obtain soil moisture (SM), this study applied an empirical method by using multiple linear regression analysis between backscatter coefficient, σ_{vv}, (BS), local incidence angle, θ, (LIA), soil moisture level-1, 0 – 7 cm, (SM), total precipitation (TP), soil temperature level-1, 0 – 7 cm, (ST), and surface roughness (SR). The backscattering coefficient and local incidence angle are variables derived from the Sentinel-1 IW level-1 GRD products, while SM, TP, ST, and SR are variables obtained from ECMWF with a spatial resolution of 0.125 x 0.125 degrees. The ERA interim-daily SM (layer 1: 0 – 7 cm), TP, ST, and SR from ECMWF were on the same date as those of the BS and LIA from Sentinel-1.

The multiple linear regression analysis refers to a technique for studying the linear relationship among two or more variables. We assumed a linear relationship between SM and independent variables (BS, LIA, TP, ST, and SR). This analysis estimated weighting factors (a-e) and the intercept (f) from Equation (1).

$$SM = a.BS + b.LIA + c.TP + d.ST + e.SR + f \quad (1)$$

For MRA analysis, values of these variables were extracted from the images located at the St. NBL2 point of the SESAME measurement station. Therefore, the predicted SM was validated using the SM measured by the SESAME station. Because SESAME data was available at this site starting around early 2017, SM from this measurement for July 2017 - December 2018 was applied to validate the predicted SM. Another SESAME station (namely St.BS2) was used to validate the predicted results in another place from the derived empirical model.

The predicted soil moisture derived from the multiple linear regression can be written as in Equation (2).

$$SM = 0.009 * BS + 0.010 * LIA + 0.206 * TP - 0.014 * ST + \\ + 0.002 * SR + 0.424 \quad (2)$$

The images of BS, LIA, TP, ST, and SR were resampled into 150 x 150-m pixel sizes to the derived spatial distribution of SM maps. Fig. 2a-e shows the correlation between variables where the highest coefficient of determination (R^2) (0.925) is the relationship between SM and TP. The result shows that the SM increased with an increase in TP. In contrast, SM linearly decreased by increasing the surface roughness with a coefficient of determination of 0.739. A normal probability plot of sample percentiles versus predicted value (Fig. 2f) showed that the model met the assumption of normality.

The predicted soil moisture was compared with the observed soil moisture using the coefficient of determination (R^2), and unbiased root mean squared error (ubRMSE). This ubRMSE was calculated using Equation (3) (Li et al. 2018; Xuefei Zhang et al. 2017). The coefficient of determination and ubRMSE are 0.83 and 0.148 m^3m^{-3}, respectively (Fig. 2g).

$$ubRMSE = \sqrt{\frac{\sum_{i=1}^{n}(Obs_i - Pre_i)^2}{n} - \left(\frac{\sum_{i=1}^{n}(Obs_i - Pre_i)}{n}\right)^2} \quad (3)$$

As the level of soil moisture values from ECMWF data and SESAME measurements are different, the SM obtained from Equation (2) was adjusted by using the linear equation relationship between the ECMWF's SM and the SESAME's SM shown in Fig. 3a resulting in an adjusted SM as expressed in Equation (4).

$$Adj\ SM = 9.168 * SM - 2.191 \quad (4)$$

Furthermore, the linear relationship between SM and WL from SESAME measurements in the KHGSS, as shown in Fig. 3b was applied to estimate WL relative to the ground surface using Equation (5) from the adjusted SM.

$$WL = 1.497 * Adj\ SM - 1.676 \quad (5)$$

RESULTS AND INTERPRETATION

Groundwater level validation

For validation, the estimation results for groundwater level are compared to in-situ SESAME's measurement at BL2, and the level profiles are shown in Fig. 4a. The coefficient of determination and unbiased root mean squared error for the predicted water levels are 0.6119 and 0.1551 m, respectively (Fig. 4b). Based on the coefficient and error calculation, the soil moisture and groundwater level could be predicted for this study.

Relationship between fire hotspots and volumetric moisture contents

Fig. 5 shows spatial and temporal variations in soil moisture contents estimated by using Sentinel-1 and ECMWF data. These maps are overlaid with drainage networks that were created by the Indonesian Peat Restoration Agency (Peat Restoration Agency 2017). The networks were made using Lidar-derived DEM and aerial photographs with a density of 4 points/m^2 and accuracy of less than 10 cm. In addition, Indonesian Center for Agricultural Land Resources Research and Development has created a peat thickness map with 4 classes, i.e., very thin (< 50 cm), thin (50 – 100 cm), medium (100 – 200 cm), and thick (200 – 300 cm) (BBSDLP 2019). Distributions of fire hotspots were correlated with soil moisture contents. The highest moisture was detected over the site area in May 2015. The soil moisture sharply dropped up to 0.02 m^3m^{-3} starting from July to October 2015. Fire hotspots were generally associated with areas of low moisture. The lower the soil moisture, the higher the vulnerability of peatlands to fires. In 2015, the lowest moisture content of soil occurred in October. Therefore, the highest number of fire hotspots were observed this month. It indicates that the El Niño caused dry spells which in turn led to a lack of soil moisture and that in turn increased the number of fire hotspots.

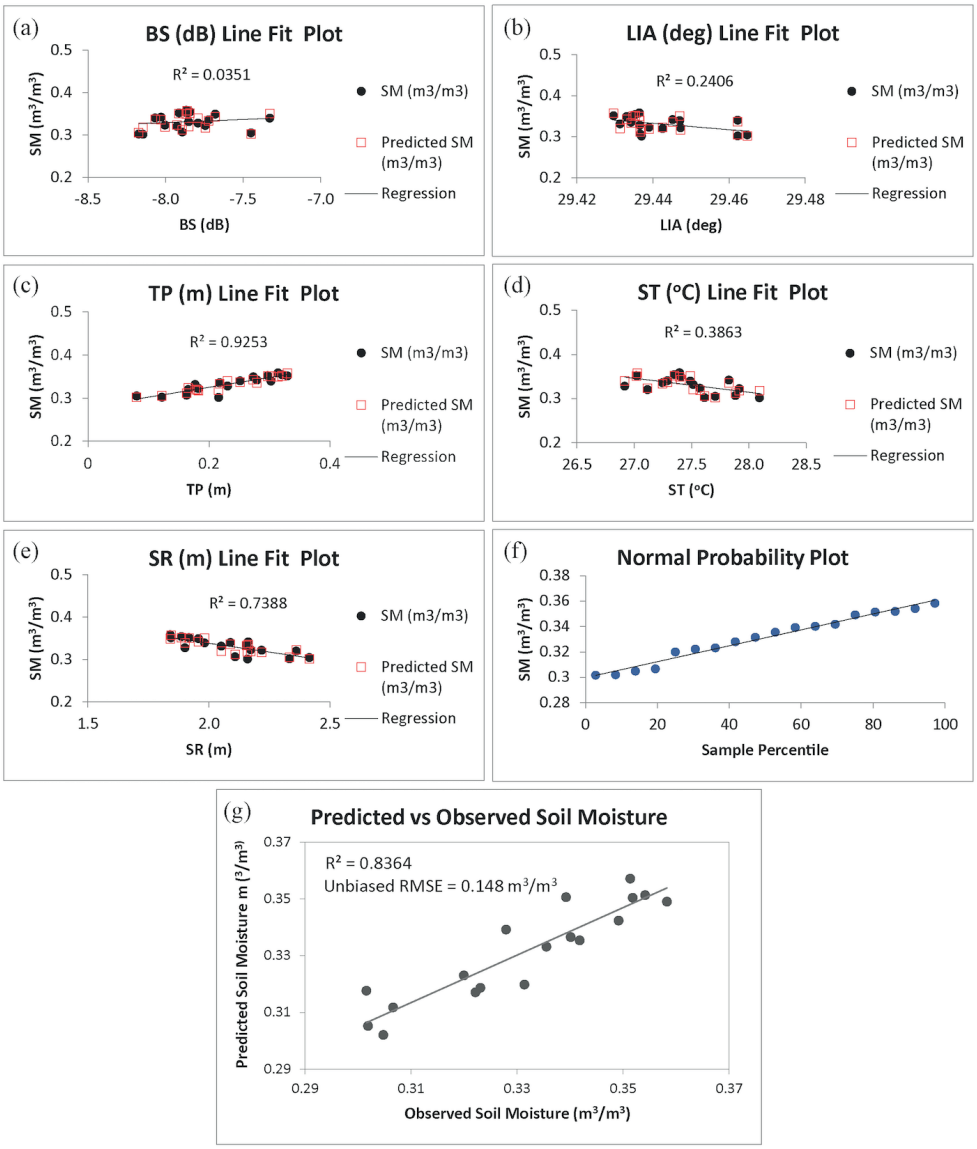

Fig. 2. (a-e) Linear regression fit plot among soil moisture and several variables used to derive a soil moisture equation; (f) Normal probability plot; (g) Correlation between predicted and observed soil moisture

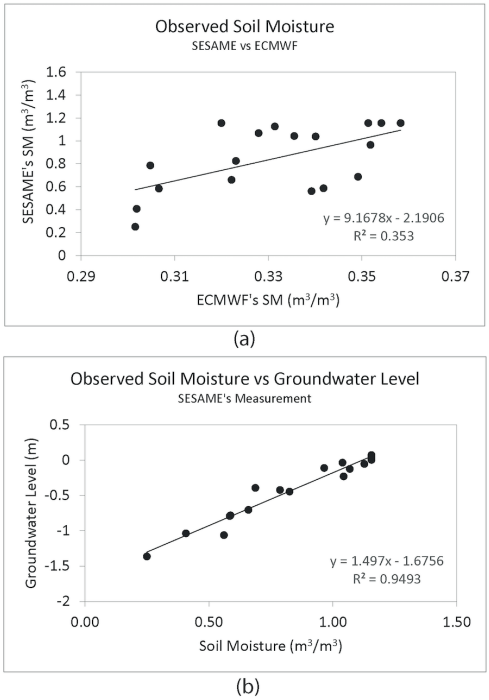

Fig. 3. Linear regression (a) between SESAME's and ECMWF soil moisture; (b) between SESAME's soil moisture and water level measurements

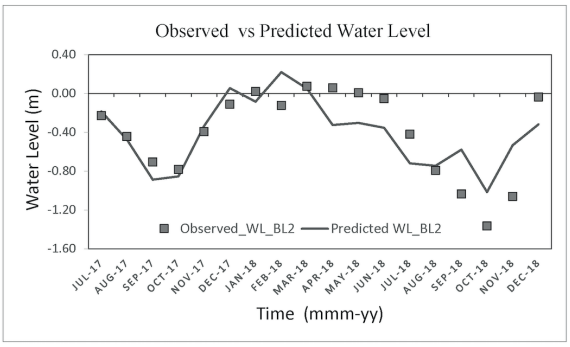

(a)

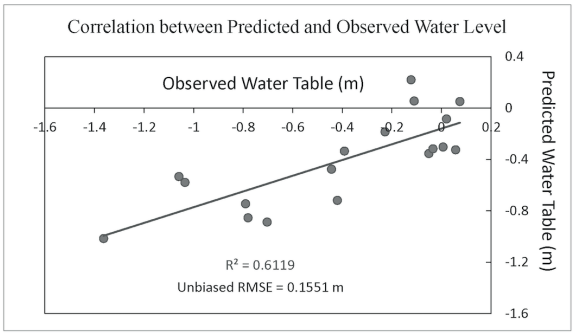

(b)

Fig. 4. Comparison between observed and predicted water levels at NBL2

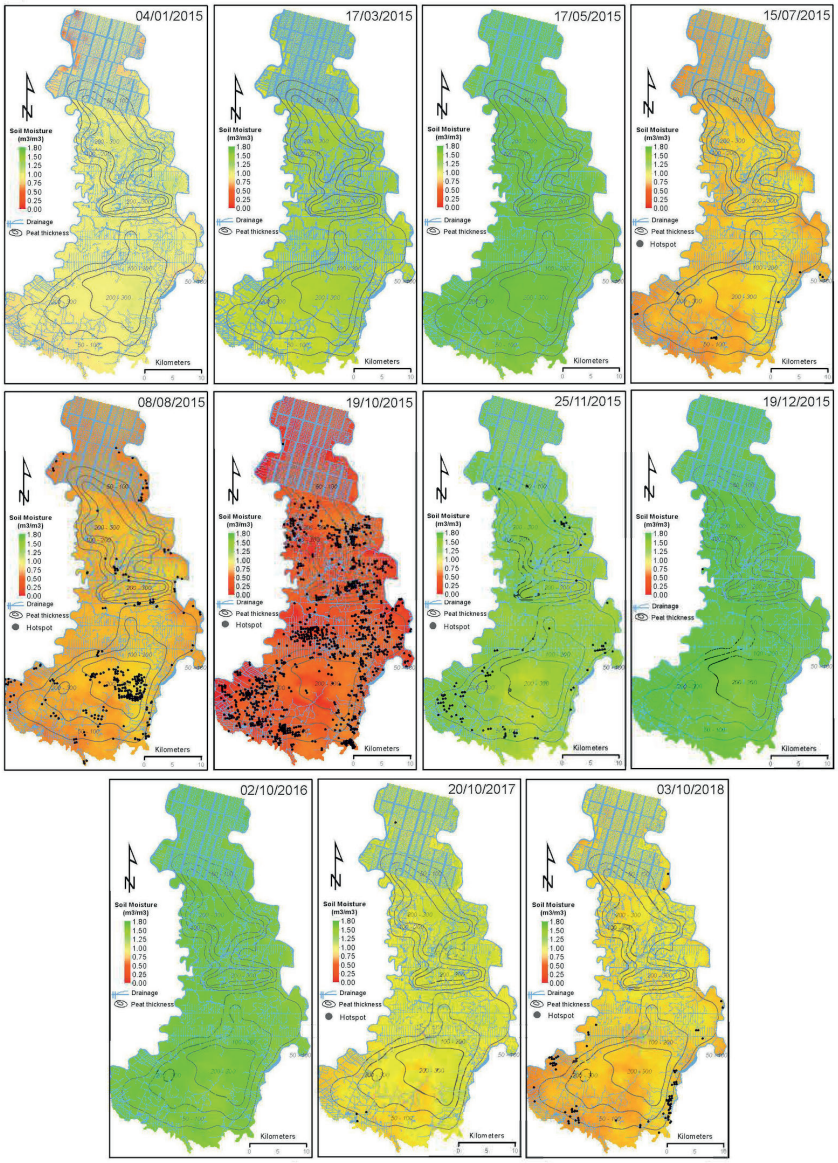

Fig. 5. Peat thickness (BBSDLP 2019) and drainage networks (Peat Restoration Agency 2017) overlaid on selected maps of spatiotemporal soil moisture from January 2015 to October 2018

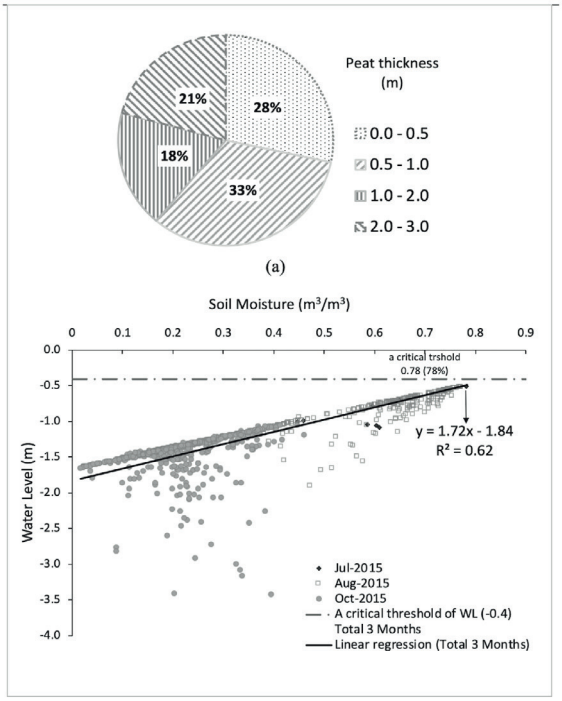

Fig. 6. Percentages of the number of hotspots associated with certain peat thickness; (b) relation between soil moisture and water levels at fire hotspot locations over the KHGSS site for July, August, and October 2015

Furthermore, the moisture content during 2016 – 2018 was generally higher than that in 2015. However, the moisture content continuously declined up to ~0.25 m^3m^{-3} during the dry season (around from July – October) for three consecutive years, 2016 - 2018. The lower soil moisture was associated with dense canal networks and around the edges of the KHGSS site, where two major rivers exist along its boundaries (Fig. 5). In addition, the spatial distribution of fire hotspots generally occurred in areas around these drainage networks, where most people living near the boundaries depend on the peatland for their livelihood including rice cultivation and oil palm plantation. Most of these areas have peat thickness in a range of 0 – 1 m with 61% of total hotspots, as shown in Fig. 6a.

Fig. 6b shows a relationship between variations of the soil moisture and water levels extracted from the point locations of the fire hotspots for July, August, and October 2015. Soil moisture was closely related to water levels, with a correlation of 0.65. Earlier fires, in July 2015, took place at higher moisture and shallower depth of groundwater level. Fig. 6b also indicates that moisture content of 0.78 m^3m^{-3} (78%) and a groundwater level of ~0.50 m below peat surface represent the critical threshold for peat fires in the KHGSS.

Spatiotemporal groundwater level related to the critical threshold value

Fig. 7 shows that spatial variations of the groundwater levels tend to rise from January to May 2015, and most of the KHGSS area was flooding. In contrast, the groundwater levels had dropped to ~5.0 m below the peat surface from July to October 2015. These levels significantly exceeded the critical threshold of 0.4 m below the peat surface (President of Republic of Indonesia 2016b; Usup et al. 2004; Wösten et al. 2008).

Lower levels of groundwater occurred not only in the cultivation areas but also in the conservation area. In addition, the low amount of precipitation during these months was also responsible for large declines in the water level and soil moisture content. As a consequence, the peat became more susceptible to severe fires during the dry season. Moreover, the peat surface elevation may also be lowering by several meters during this season (Khakim et al. 2020). Therefore, when the rainy season with large precipitation events, flooding occurred over this site area.

Although flooding of more than 1 m occurred over only a small area, 0.46% of this site in January 2016, the groundwater levels declined up to less than 0.4 m below the peat surface in the rainy season of the year 2017 and 2018 (Fig. 8). On the other hand, during the dry season from June to October, the groundwater levels over 30.5 – 99.0% of the site area dropped down to ~0.7 m below the peat surface.

Variations of groundwater levels with topographic features and drainage networks

Fig. 9 shows the profiles illustrating trends of estimated water levels varying with topographic elevations along transects 1 and 2 in 2015. The water levels were above the surface along transects 1 and 2 in the wet season (May and November), except in a peat dome area at the distance of ~18 km in transect 1. In contrast, they were below the surface in the dry season (July, August, and October).

Besides the seasons, topographic profiles influenced spatial variations of water level trends. The trends of the water level between these seasons were in opposite slope gradients. During the dry season, the groundwater trends varied relatively following the topographic profiles for lines 1 and 2. As the topography along line 2 has relatively flatter features and a narrower dome than that along line 1, the profiles of the water levels are relatively lower slope gradient along line 2 in May. Otherwise, slight downslope trends from the left to the right side of the profiles in November.

Furthermore, local trends of the fluctuations of the groundwater levels depended on the drainage systems, such as rivers and anthropogenic canals. The depth water table drawdown proximal to drainage and sensitive to local topography was performed in the study as presented in other areas of the shallow degraded peatland in the southwest of England (Luscombe et al. 2016) and of a fen

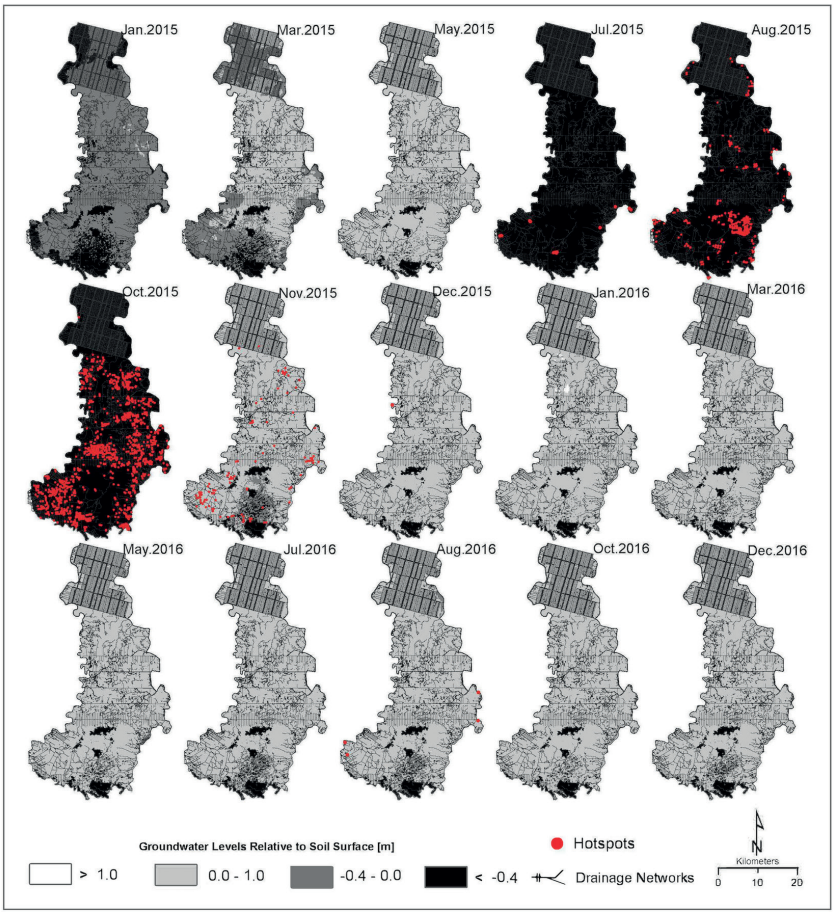

Fig. 7. Spatiotemporal variation of groundwater levels related to the critical threshold values for the year 2015–2016

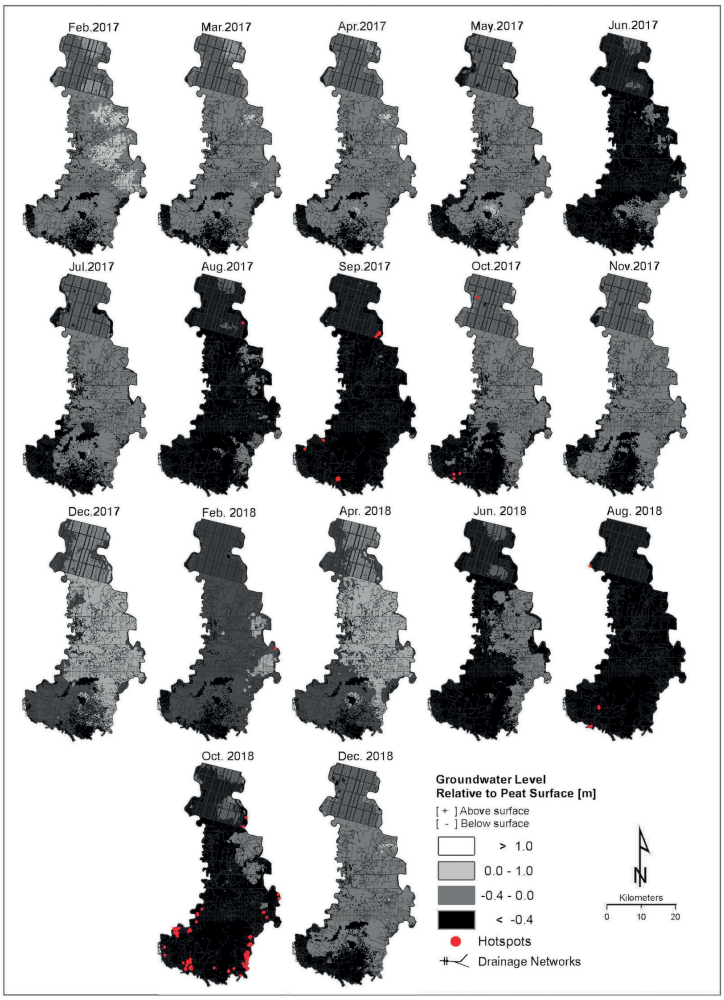

Fig. 8. Spatiotemporal variation of groundwater levels related to the critical threshold values for the year 2017–2018

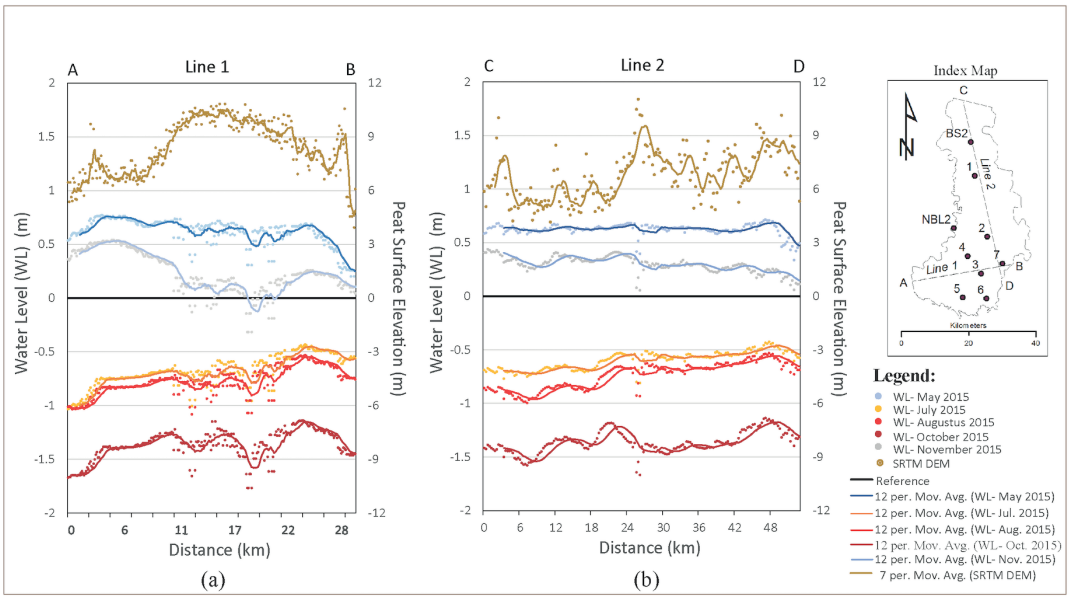

Fig. 9. Profiles of water level variations with topographic features along lines 1 (A-B) and 2 (C-D)

peatland near Quebec City (Whittington and Price 2006). The steepest gradient of the trends occurred on both sides of profile 1 and the right side of profile 2 due to the main rivers, i.e., Air Sugihan river and Air Saleh river. Therefore, higher variability of the groundwater levels between two seasons occurred in areas close to the main rivers. The trends due to drainage systems led to much amount of water discharged fast from a peatland in dry season (Khakim et al. 2020). Small fluctuations of the profiles may be associated with the anthropogenic canals.

Cause and effect relationship on groundwater level variations

Fig. 10 presents an interrelationship on several variables, including monthly precipitation, groundwater level, soil moisture, hotspots at nine points over the site area, and percentages of the areal extent of groundwater depths from 2015 to 2018. The predicted groundwater levels and moisture contents are commonly correlated to those from SESAME measurements.

The variations among the three first variables at all points during this period are highly correlated. The groundwater level and soil moisture also varied with monthly precipitation for seven selected locations from January 2015 to December 2018. Dramatical declines in monthly precipitations led to sharp decreases in groundwater levels from July to October 2015. Areal extent associated with the groundwater level less than the critical threshold of 0.4 m reached a maximum this month during the study period. This led to the much lower moisture content of the peat. Therefore, severe fires indicated by the number of hotspots occurred in October 2015.

In contrast, monthly precipitation increased after October 2015 and reached a peak in January 2016. Therefore, the groundwater levels, as well as the soil moisture content, increased. However, after this month, the groundwater level and soil moisture content gradually decreased and reached a minimum value in September 2017 and August 2018. The peat fires mostly occurred in cultivation and agriculture areas in October 2018. The number of hotspots in these months was much less than those in October 2015. This indicates that the fire hotspots did not occur when the groundwater levels were shallower than the threshold of 0.4 m. The fires occurred when the groundwater levels were deeper than the threshold.

DISCUSSION

The degraded peatland of KHGSS in South Sumatra is a restoration target area in Indonesia. Extensive drainage networks of the peatland area increased their vulnerability to fire, which was further enhanced by prolonged drought periods induced by the 2015 El Niño event. The amount of rainfall and the speed of water runoff influence the peatland catchment hydrology. Under natural conditions, the water table is close to or above the surface (Page et al. 2009). However, activities of illegal logging and land clearing for cultivation significantly impair the peatland holding water capacity in the site area. This condition led to dramatically decline in the water levels from July to October 2015. As a consequence, the peat was decomposed, and the groundwater level and moisture content were reduced. Furthermore, the moisture reduction had initiated subsurface fire to the self-heating and spontaneous combustion of dry peat. Therefore, a large number of hotspots were observed in 2015.

A minimum moisture content of the peat surface in the study area was predicted as much as ~0.78 m^3m^{-3} to preserve peat smoldering and it was corresponding to the groundwater depth of ~0.5 m. It means 0.1 m deeper than the threshold that the Indonesia Government applies through Regulation No 57 of 2016 Concerning Amendment to Government Regulation No 71 of 2014 Concerning Peatland Ecosystem Protection and Management (President of Republic of Indonesia 2014, 2016b). This critical moisture content for peat smoldering varies according to peat types, such as 57-102% moisture for the National Park Service's Whiskeytown National Recreation Area, California, USA (Garlough and Keyes 2011). Peat with a bulk density of 150 kg m^{-3} could self-sustain smoldering propagation up to a critical moisture content of 115% (Prat-Guitart et al. 2016).

Rewetting is a hydrological restoration approach to maintain the groundwater level close to the peat surface. Groundwater is important in preserving the peat from carbon mineralization, peat degradation, and dehydration. The BRG has implemented restoration by blocking canals to rewet peatland over the study area in order to restore the pre-existing hydrological regime. Monitoring both the soil moisture and groundwater levels is the most important role in assessing the restoration efforts of the hydrological functions developed by the BRG based on rewetting activities.

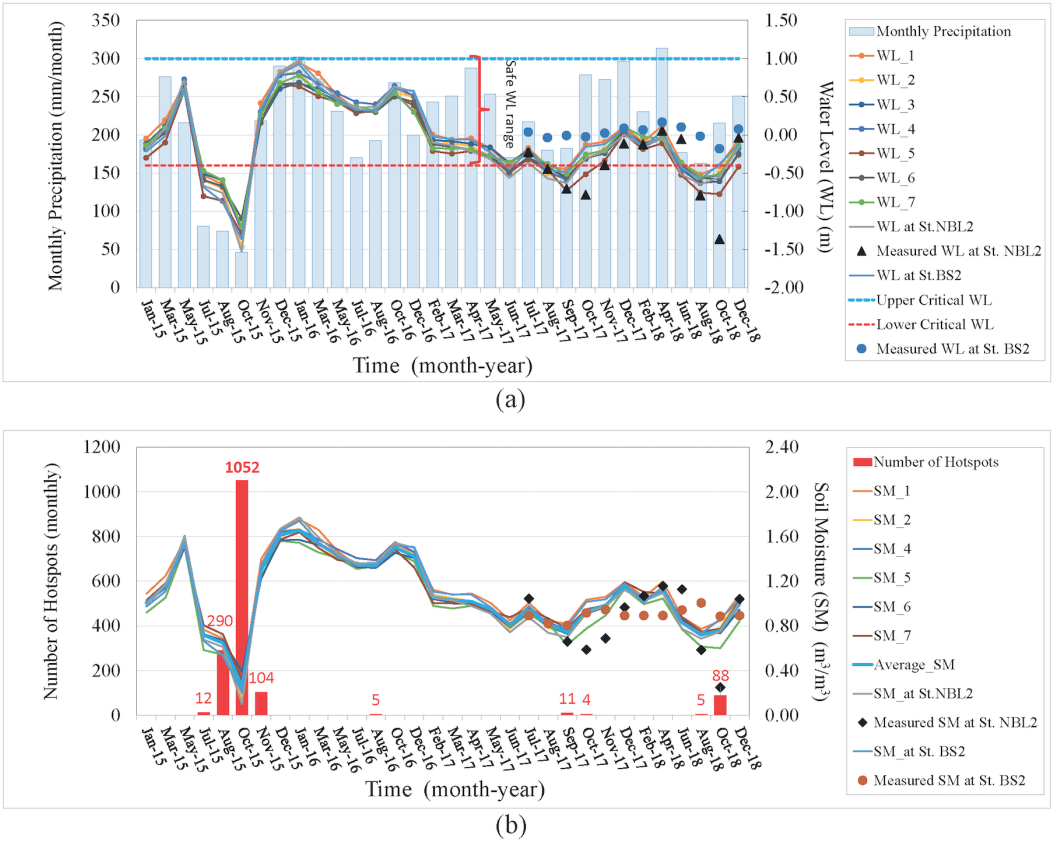

Fig. 10. Profiles of temporal variations of predicted and measured: (a) water levels with monthly precipitation and (b) soil moisture with a number of hotspots for 7 selected locations and 2 SESAME stations from January 2015 to December 2018

As rainfall was high in early 2016, the groundwater level and soil moisture content increased over the study area. However, combustion can create sub-surface hollows at several places within the peatlands (Roy et al. 2014). Thus, volume reduction associated with peat fires and water table depletion led to peatland subsidence (Khakim et al. 2020). The subsidence, in turn, induced flooding in the site area in January 2016. Nevertheless, the groundwater levels significantly dropped more than the critical threshold during the dry season (June–October) of the years 2017 and 2018. Thus, a few fires still occurred at the edge of the southern study area especially in October 2017 and 2018. Human activity is indicated as a main factor of these fires. Land use without regard to environmental sustainability, including illegal logging, canal construction, and plantation and agricultural development are activities that are still frequently carried out by people living near peatlands. Therefore, the restoration efforts became ineffectively in preventing the peat fires.

Furthermore, although the hydrological restoration by blocking canals has an advantage, which remains waterways passable for small boats for transportation of local communities, the canal blocking requires lots of large timber, easily damaged by persons wanting to re-open waterways, and not leading to full rewetting because of the spillways. For restoration to be more effective, comprehensive efforts need to be made to create other types of peatland rewetting and consistent law enforcement.

CONCLUSIONS

Soil moisture and water level dynamics in the KHGSS site have been successfully characterized using MRA analysis based on Sentinel-1 and ECMWF datasets. The estimated moisture contents and water levels agreed well with SESAME measurements. A minimum moisture content of peat smoldering combustion for this site can be indicated as much as ~0.78 m^3m^{-3} (78%), corresponding with a minimum water level of ~0.50 m below peat. The 2015 extreme drought and human activities such as illegal logging, land clearing, and canal construction impaired the water capacity of the peatland. Thus, the peatland ineffectively maintained the groundwater levels shallower than the threshold value (i.e., 0.4 m deep from the peat surface) in the dry season. The peat fires severely burned both cultivation and protected areas having dense catastrophic canals and closing to rivers. Furthermore, trends in groundwater levels and moisture contents increased in 2016. However, they gradually declined to reach ~0.70 m and ~0.25 m^3m^{-3}, respectively, during the period of 2017 – 2018. Consequently, a few fires occurred during the dry season these years. We suggest that this area needs efforts to restore groundwater levels shallower than the threshold of 0.40 m along with law enforcement.

REFERENCES

Asmuß T., Bechtold M. and Tiemeyer B. (2019). On the Potential of Sentinel-1 for High Resolution Monitoring of Water Table Dynamics in Grasslands on Organic Soils. Remote Sensing, 11(14), 1659, DOI: 10.3390/rs11141659.

Attema E., Davidson M., Floury N., Levrini G., Rosich B., Rommen B. and Snoeij P. (2008). Sentinel-1 ESA's new European radar observatory. Proceedings of the European Conference on Synthetic Aperture Radar, EUSAR, 1-4, 2-4.

Aukema J. and Wilson S. (2019). THE SAR HANDBOOK: Comprehensive Methodologies for Forest Monitoring and Biomass Estimation, A.I. Flores-Anderson, K.E. Herndon, R.B. Thapa & E. Cherrington eds.; First, DOI: 10.25966/nr2c-s697.

Baghdadi N., Choker M., Zribi M., El Hajj M., Paloscia S., Verhoest N.E.C., Lievens H., Baup F. and Mattia F. (2016). A new empirical model for radar scattering from bare soil surfaces. Remote Sensing, 8(11), 1-14, DOI: 10.3390/rs8110920.

BBSDLP. (2019). Map of Peatland of Sumatra Island, Scale 1:50,000.

Chen Y., Qiao S., Zhang G., Xu Y.J., Chen L. and Wu L. (2020). Investigating the potential use of Sentinel-1 data for monitoring wetland water level changes in China's Momoge National Nature Reserve. PeerJ, 2020(2), 1–24, DOI: 10.7717/peerj.8616.

Dabrowska-Zielinska K., Budzynska M., Tomaszewska M., Malinska A., Gatkowska M., Bartold M. and Malek I. (2016). Assessment of carbon flux and soil moisture in wetlands applying Sentinel-1 data. Remote Sensing, 8(9), DOI: 10.3390/rs8090756.

Dabrowska-Zielinska K., Musial J., Malinska A., Budzynska M., Gurdak R., Kiryla W., Bartold M. and Grzybowski P. (2018). Soil moisture in the Biebrza Wetlands retrieved from Sentinel-1 imagery. Remote Sensing, 10(12), DOI: 10.3390/rs10121979.

Dee D.P., Uppala S.M., Simmons A.J., Berrisford P., Poli P., Kobayashi S., Andrae U., Balmaseda M.A., Balsamo G., Bauer P., Bechtold P., Beljaars A.C.M., van de Berg L., Bidlot J., Bormann N., Delsol C., Dragani R., Fuentes M., Geer A.J., … Vitart F. (2011). The ERA-Interim reanalysis: Configuration and performance of the data assimilation system. Quarterly Journal of the Royal Meteorological Society, 137(656), 553-597, DOI: 10.1002/qj.828.

Dohong A. (2019). Restoring Degraded Peatland in Indonesia: the 3R Approach. PARISH F., YAN L.S., ZAINUDDIN M.F. & GIESEN W. (Eds.) RSPO Manual on Best Management Practices (BMPs) for Management and Rehabilitation of Peatlands. 2 Ed. Kuala Lumpur: RSPO., 57, 2016–2017.

Dubois P.C., Zyl J. V and Engman T. (1995). Measuring soil moisture with imaging radars. IEEE Transactions on Geoscience and Remote Sensing, 33(4), 915-926, DOI: 10.1155/2015/610307.

Evers S., Yule C.M., Padfield R., O'Reilly P. and Varkkey H. (2017). Keep wetlands wet: the myth of sustainable development of tropical peatlands – implications for policies and management. Global Change Biology, 23(2), 534-549, DOI: 10.1111/gcb.13422.

Filipponi F. (2019). Sentinel-1 GRD Preprocessing Workflow. Proceedings, 18(1), 11, DOI: 10.3390/ecrs-3-06201.

Gangat R., van Deventer H., Naidoo L. and Adam E. (2020). Estimating soil moisture using Sentinel-1 and Sentinel-2 sensors for dryland and palustrine wetland areas. South African Journal of Science, 116(8), 1-9, DOI: 10.17159/sajs.2020/6535.

Garlough E.C. and Keyes C.R. (2011). Influences of moisture content, mineral content and bulk density on smouldering combustion of ponderosa pine duff mounds. International Journal of Wildland Fire, 20(4), 589-596, DOI: 10.1071/WF10048.

Giesen W. and Sari E.N.N. (2018). Tropical Peatland Restoration Report : the Indonesian case Tropical Peatland Restoration Report : The Indonesian Case Berbak Green Prosperity Partnership/Kemitraan Kesejatheraan Hijau (Kehijau Berbak), Issue March, DOI: 10.13140/RG.2.2.30049.40808.

Hooijer A., Page S., Canadell J.G., Silvius M., Kwadijk J., Wösten H. and Jauhiainen J. (2010). Current and future CO 2 emissions from drained peatlands in Southeast Asia. Biogeosciences, 7(5), 1505–1514, DOI: 10.5194/bg-7-1505-2010.

Hooijer A, Silvius M., Wosten H. and Page S. (2006). PEAT-CO2, Assessment of CO2 Emissions From Drained Peatland in SE Asia. http://www.wetlands.org/Portals/0/publications/Report/Peat CO2 report.pdf

Hooijer Aljosja, Silvius M., Wösten H., Page S., Hooijer A., Silvius M., Wösten H. and Page S. (2006). PEAT-CO2, Assessment of CO2 emissions from drained peatlands in SE Asia. Delft Hydraulics Report Q3943, 36.

Hornácek M., Wagner W., Sabel D., Truong H., Snoeij P., Hahmann T., Diedrich E. and Doubkova M. (2012). Potencial for high resolution systematic global surface soil moisture retrieval via change detection using Sentinel-1. IEEE Journal of Selected Topics in Applied Earth Observations and Remote Sensing, 5(4), 1303-1311, DOI: 10.1109/JSTARS.2012.2190136.

Khakim M.Y.N., Bama A.A., Yustian I., Poerwono P., Tsuji T. and Matsuoka T. (2020). Peatland subsidence and vegetation cover degradation as impacts of the 2015 El niño event revealed by Sentinel-1A SAR data. International Journal of Applied Earth Observation and Geoinformation, 84(August 2019), DOI: 10.1016/j.jag.2019.101953.

Kim J.W., Lu Z., Gutenberg L. and Zhu Z. (2017). Characterizing hydrologic changes of the Great Dismal Swamp using SAR/InSAR. Remote Sensing of Environment, 198, 187-202, DOI: 10.1016/j.rse.2017.06.009.

Lee J. Sen. (1981). Speckle analysis and smoothing of synthetic aperture radar images. Computer Graphics and Image Processing, 17(1), 24-32, DOI: 10.1016/S0146-664X(81)80005-6.

Leng L.Y., Ahmed O.H. and Jalloh M.B. (2019). Brief review on climate change and tropical peatlands. Geoscience Frontiers, 10(2), 373-380, DOI: 10.1016/j.gsf.2017.12.018.

Li J., Wang S., Gunn G., Joosse P. and Russell H.A.J. (2018). A model for downscaling SMOS soil moisture using Sentinel-1 SAR data. International Journal of Applied Earth Observation and Geoinformation, 72(May), 109-121, DOI: 10.1016/j.jag.2018.07.012.

Luscombe D.J., Anderson K., Grand-Clement E., Gatis N., Ashe J., Benaud P., Smith D. and Brazier R.E. (2016). How does drainage alter the hydrology of shallow degraded peatlands across multiple spatial scales? Journal of Hydrology, 541, 1329-1339, DOI: 10.1016/j.jhydrol.2016.08.037.

Miettinen J., Wang J., Hooijer A. and Liew S. (2013). Peatland Conversion and Degradation Processes in Insular Southeast Asia: a Case Study in Jambi, Indonesia. Land Degradation & Development, 24(4), 334-341, DOI: 10.1002/ldr.1130.

Oh Y., Sarabandi K. and Ulaby F.T. (1992). An empirical model and an inversion technique for radar scattering from bare soil surface. IEEE Transactions on Geoscience and Remote Sensing, 30(2), 370-381.

Page S., Hosciło A., Wösten H., Jauhiainen J., Silvius M., Rieley J., Ritzema H., Tansey K., Graham L., Vasander H. and Limin S. (2009). Restoration ecology of lowland tropical peatlands in Southeast Asia: Current knowledge and future research directions. Ecosystems, 12(6), 888–905, DOI: 10.1007/s10021-008-9216-2.

Peat Restoration Agency. (2017). Final Report: Data Acquisition and Thematic Mapping in KHG Area of Cawang - Lalang River and KHG of Sugihan - Saleh River.

Prat-Guitart N., Rein G., Hadden R.M., Belcher C.M. and Yearsley J.M. (2016). Propagation probability and spread rates of self-sustained smouldering fires under controlled moisture content and bulk density conditions. International Journal of Wildland Fire, 25(4), 456-465, DOI: 10.1071/WF15103.

Protection and management of the peat ecosystem, Pub. L.., 71 (2014).

Amendment to Government Regulation Number 71 of 2014 concerning peatland ecosystem protection and management, Pub. L. No. 57 (2016).

Peat Restoration Agency, Pub. L., 1 (2016).

Republic of Indonesia. (2018). Project final report between JICA (Japan International Cooperation Agency) and BRG (Peatland Restoration Agency in Indonesia).

Roy P.D., Rivero-Navarrete A., Sánchez-Zavala J.L. and López-Balbiaux N. (2014). Subsurface fire and subsidence at Valle del Potosí (Nuevo León, Mexico): Preliminary observations. Boletin de La Sociedad Geologica Mexicana, 66(3), 553-557, DOI: 10.18268/BSGM2014v66n3a10.

Schroeder W., Oliva P., Giglio L. and Csiszar I.A. (2014). The New VIIRS 375m active fire detection data product: Algorithm description and initial assessment. Remote Sensing of Environment, 143, 85-96, DOI: 10.1016/j.rse.2013.12.008.

Sodikin E., Munandar M., Setiawan A., Prayitno M.B. and Suwandi S. (2017). Pilot project implementasi paludikultur dan agroforestry lahan APL di Desa Perigi, Pangkalan Lampam, KHG Sungai Sugihan - Saleh Lumpur Ogan Komering Ilir, Sumatera Selatan.

Sulaiman A., Sari E.N.N. and Saad A. (2017). Panduan teknis pemantuan tinggi muka air lahan gambut sistem telemetri. The Republic of Indonesia Peat Restoration Agency.

Usup A., Hashimoto Y., Takahashi H. and Hayasaka H. (2004). The principal types of vegetation in the. Tropics, 14(1), 1-19. https://www.jstage.jst.go.jp/article/tropics/14/1/14_1_1/_pdf

Whittington P.N. and Price J.S. (2006). Advanced Bash-Scripting Guide An in-depth exploration of the art of shell scripting Table of Contents. Hydrological Processes, 20, 3589-3600, DOI: 10.1002/hyp.6376.

Wösten J.H.M., Clymans E., Page S.E., Rieley J.O. and Limin S.H. (2008). Peat-water interrelationships in a tropical peatland ecosystem in Southeast Asia. Catena, 73(2), 212-224, DOI: 10.1016/j.catena.2007.07.010.

Wösten J.H.M., Van Den Berg J., Van Eijk P., Gevers G.J.M., Giesen W.B.J.T., Hooijer A., Idris A., Leenman P.H., Rais D.S., Siderius C., Silvius M.J., Suryadiputra N. and Wibisono I.T. (2006). Interrelationships between hydrology and ecology in fire degraded tropical peat swamp forests. International Journal of Water Resources Development, 22(1), 157-174, DOI: 10.1080/07900620500405973.

Zhang Xianlong, Chan N.W., Pan B., Ge X. and Yang H. (2021). Mapping flood by the object-based method using backscattering coefficient and interference coherence of Sentinel-1 time series. Science of the Total Environment, 794, 148388, DOI: 10.1016/j.scitotenv.2021.148388

Zhang Xuefei, Zhang T., Zhou P., Shao Y. and Gao S. (2017). Validation analysis of SMAP and AMSR2 soil moisture products over the United States using ground-based measurements. Remote Sensing, 9(2), DOI: 10.3390/rs9020104.

RESEARCH PAPER

SPATIAL MODELLING OF KEY REGIONAL-LEVEL FACTORS OF COVID-19 MORTALITY IN RUSSIA

Egor A. Kotov[1*], Ruslan R. Goncharov[1], Yuri V. Kulchitsky[1], Varvara A. Molodtsova[1], Boris V. Nikitin[2,3]
[1]Faculty of Urban and Regional Development, HSE University, Myasnitskaya str. 13-4, Moscow 101000, Russia
[2]Institute of Regional Consulting, office 903, Nakhimovsky prosp. 32, Moscow 117218, Russia
[3]Faculty of Geography, Moscow State University, Leninskie Gory 1, Moscow 119899, Russia
***Corresponding author:** kotov.egor@gmail.com
Received: June 30th, 2021 / Accepted: April 24th, 2022 / Published: June 30th, 2022
https://DOI-10.24057/2071-9388-2021-076

ABSTRACT. Intensive socio-economic interactions are a prerequisite for the innovative development of the economy, but at the same time, they may lead to increased epidemiological risks. Persistent migration patterns, the socio-demographic composition of the population, income level, and employment structure by type of economic activity determine the intensity of socio-economic interactions and, therefore, the spread of COVID-19.
We used the excess mortality (mortality from April 2020 to February 2021 compared to the five-year mean) as an indicator of deaths caused directly and indirectly by COVID-19. Similar to some other countries, due to irregularities and discrepancies in the reported infection rates, excess mortality is currently the only available and reliable indicator of the impact of the COVID-19 pandemic in Russia.
We used the regional level data and fit regression models to identify the socio-economic factors that determined the impact of the pandemic. We used ordinary least squares as a baseline model and a selection of spatial models to account for spatial autocorrelation of dependent and independent variables as well as the error terms.
Based on the comparison of AICc (corrected Akaike information criterion) and standard error values, it was found that SEM (spatial error model) is the best option with reliably significant coefficients. Our results show that the most critical factors that increase the excess mortality are the share of the elderly population and the employment structure represented by the share of employees in manufacturing (C economic activity according to European Skills, Competences, and Occupations (ESCO) v1 classification). High humidity as a proxy for temperature and a high number of retail locations per capita reduce the excess mortality. Except for the share of the elderly, most identified factors influence the opportunities and necessities of human interaction and the associated excess mortality.

KEYWORDS: COVID-19, spatial models, socio-economic factors, climatic factors, excess mortality, Russian regions

CITATION: Kotov E.A., Goncharov R.R., Kulchitsky Y.V., Molodsova V.A., Nikitin B.V. (2022). Spatial Modelling of Key Regional-Level Factors of Covid-19 Mortality In Russia. Geography, Environment, Sustainability, 2(15), p. 71-83
https://DOI-10.24057/2071-9388-2021-076

ACKNOWLEDGEMENTS: The reported study was funded by RFBR according to the research project № 20-04-60490 «Ensuring balanced regional development during a pandemic with spatially differentiated regulation of socio-economic interaction, sectoral composition of the economy and local labour markets».

Conflict of interests: The authors reported no potential conflict of interest.

INTRODUCTION

Intensive socio-economic interactions are a prerequisite for the innovative development of the economy, but at the same time, they may lead to increased epidemiological risks. Persistent migration patterns, socio-demographic composition of the population, income level, and employment structure by type of economic activity determine the intensity of socio-economic interactions and, therefore, the spread of COVID-19.

Most research on COVID-19 focuses on factors affecting COVID-19 infection rates and the resulting mortality. Many papers employ spatial regression models to achieve a better model fit and more trustworthy estimates of the effects. With this paper we aim to add to the existing body of research by revealing various factors for the case of Russian regions with a specific focus on physical human interaction using models that could be compared between countries. Below we provide an in-depth review of previous research along with the variable selection process.

MATERIALS AND METHODS

Data

The full data set and analysis code for this paper is available on GitHub, so the findings are fully reproducible and auditable: https://github.com/e-kotov/ru-covid19-regional-excess-mortality (doi: 10.5281/zenodo.6515455).

The dependent variable

A meta-analysis of 63 research papers (Franch-Pardo et al. 2020) showed that the most frequently used indicators for COVID-19 analysis are COVID-19 infection and mortality rates.

However, the use of these parameters relies heavily on the quality of data collection and reporting. When there is little trust in the collected data, it cannot be used, which is why the data on infection rates should be avoided even when it is available. Therefore, in this study, we used excess mortality as our target variable. The downside of using excess mortality is that this data becomes available much later than COVID-19 infection rates and reported deaths. However, recently published infection and death rates seem to correlate well with the excess mortality, so analysis for more recent periods can be performed on the data similar to what most researchers use.

Another reason to use excess mortality is that apart from deaths caused directly by the COVID-19 infection, it also takes into account deaths caused by the interruption of the regular healthcare provision. Excess mortality is also helpful for comparing data between different counties as it compensates for the possible differences in the mortality statistics collection (Rodríguez-Pose and Burlina 2021; Yarmol-Matusiak et al. 2021).

Our excess mortality variable is the ratio of per capita mortality for April 2020 - February 2021 to the mean over the previous five years.

The independent variables

We used the existing research to guide the selection of variables. A review of recent studies allowed us to divide the variables into several groups. Additionally, we also used our own Human Interaction group, which was a primary focus of this research. The final list of examined variables is presented in Appendix A.

Human Interaction

Under this group, we summarised multiple variables that fall under different groups in other studies but indicate how much physical human contact is required (or is possible, if there is a choice) for day-to-day activities, even during lockdowns.

Although the type of economic activity suggests a certain income level, we think it is an excellent indicator of how much physical human contact with clients or co-workers a particular job requires. For example, the share of the population working in retail influences the number of physical contacts. A higher number of retail outlets per capita may indicate a larger number of people working in retail, leading to more opportunities for violating the lockdown or distancing measures for both workers and consumers.

However, a higher area of retail per capita may allow better social distancing. Similarly, the mobility-related variables such as airport density, road and rail-road density, and the number of buses per capita may be regarded as indicators of how many people may be in direct contact and at what distance.

Some researchers (Andersen et al. 2021; Chakraborti et al. 2021; Desmet and Wacziarg 2021; Hass and Jokar Arsanjani 2021; Henning et al. 2021; Mollalo et al. 2020; Rahman et al. 2020; Scarpone et al. 2020) include very similar variables (retail outlets provision, big retail provision and road densities) as so-called environment factors.

Demographic

This group includes age structure with a specific focus on the share of population past working age, urbanisation and ethnic mix (Agnoletti et al. 2020; Amdaoud et al. 2021; Andersen et al. 2021; Ascani et al. 2021; Bański et al. 2021; Chakraborti et al. 2021; Desmet and Wacziarg 2021; Ehlert 2021; Hass and Jokar Arsanjani 2021; Henning et al. 2021; Konstantinoudis et al. 2021; Luo et al. 2021; Maiti et al. 2021; Mogi et al. 2020; Mollalo et al. 2020; Oto-Peralías 2020; Perone 2021; Rahman et al. 2020; Raymundo et al. 2021; Rodríguez-Pose and Burlina 2021; Sannigrahi et al. 2020; Scarpone et al. 2020; Sun et al. 2020; Zemtsov and Baburin 2020). We were primarily concerned with the age structure due to the higher COVID-19 fatality risks for the older population, using the share of post-, under- and working-age population in the analysis.

This group also includes migration flows at intra- and inter-regional levels, as well as international level (Chakraborti et al. 2021; Chen et al. 2021; Maiti et al. 2021; Wang et al. 2021). Even though international travel was heavily restricted at the beginning of the pandemic, it was not restricted early enough. Therefore, past international migration flows might be indicative of the international travel at the beginning of 2020, which influenced the spread of the virus and the excess mortality early on. The inter- and intra-regional travel within Russia were not as restricted and were even encouraged at some point to stimulate internal tourism.

Socio-economic

These indicators include unemployment rate, poverty rate, real income, salary, and employment across different economic activities (Agnoletti et al. 2020; Amdaoud et al. 2021; Andersen et al. 2021; Ascani et al. 2021; Bański et al. 2021; Chakraborti et al. 2021; Desmet and Wacziarg 2021; Ehlert 2021; Konstantinoudis et al. 2021; Luo et al. 2021; Maiti et al. 2021; Mogi et al. 2020; Mollalo et al. 2020; Oto-Peralías 2020 p.; Rahman et al. 2020; Raymundo et al. 2021; Rodríguez-Pose and Burlina 2021; Sannigrahi et al. 2020; Scarpone et al. 2020; Sun et al. 2020; Zemtsov and Baburin 2020). We included income-related variables in the analysis (see Appendix A) as we expected them to reveal the regions where the population cannot afford to obey the lockdowns and cease work or cannot afford extra medical care due to low income. However, employment by economic activities was regarded as part of a different group of variables - human interaction.

Mobility

These indicators include mobility patterns, passenger flows on public transport, mean travel time and more (Andersen et al. 2021; Ascani et al. 2021; Luo et al. 2021; Maiti et al. 2021; Rodríguez-Pose and Burlina 2021; Zemtsov and Baburin 2020). We included some mobility-related variables in the human interaction group above.

Healthcare provision and population health

In this category, other researchers note healthcare expenses per capita, the number of ventilators per capita, medical personnel per capita (Amdaoud et al. 2021; Bański et al. 2021; Konstantinoudis et al. 2021; Luo et al. 2021; Maiti et al. 2021; Mollalo et al. 2020; Perone 2021; Rahman et al. 2020; Raymundo et al. 2021; Rodríguez-Pose and Burlina 2021; Sannigrahi et al. 2020; Scarpone et al. 2020;

Sun et al. 2020; Zemtsov and Baburin 2020). Others also include indicators of public health, such as the number of smokers, the number of people with diabetes, the share of the overweight population (Andersen et al. 2021; Desmet and Wacziarg 2021; Ehlert 2021; Konstantinoudis et al. 2021; Luo et al. 2021; Mogi et al. 2020; Mollalo et al. 2020; Zemtsov and Baburin 2020). Even though a meta-analysis by Kolosov et. al (2021) suggests that there is no significant influence of the level of healthcare provision on mortality, we still tested this hypothesis for Russia on a regional level. Since healthcare indicators are usually highly correlated, we used the number of doctors per capita as an indicator of the current level of healthcare and its variation over five years as an indicator of how the healthcare provision had changed recently.

Climate and Environment

Many researchers also considered climate factors. Most of them used mean temperature and humidity, as well as precipitation and UV exposure (Hass and Jokar Arsanjani 2021; Konstantinoudis et al. 2021; Luo et al. 2021; Maiti et al. 2021; Oto-Peralías 2020; Perone 2021; Qi et al. 2020; Rahman et al. 2020; Wang et al. 2021). Some papers also used data on droughts and floods (Luo et al. 2021) as well as air quality via CO2 levels and other emissions (Agnoletti et al. 2020; Chakraborti et al. 2021; Hass and Jokar Arsanjani 2021; Luo et al. 2021; Maiti et al. 2021; Oto-Peralías 2020; Perone 2021; Rodríguez-Pose and Burlina 2021; Wang et al. 2021). We argue that temperature and humidity, apart from possibly affecting the survival of the virus, may also influence the willingness and opportunities of the population for outdoor vs indoor social gatherings.

Indices

Various indices may be regarded as a separate group, as they usually combine multiple indicators. A self-isolation index published by Yandex was used by Russian researchers (Zemtsov and Baburin 2020). Some indices are more focused on a particular topic, such as the healthcare quality index (Perone 2021), social trust index (Amdaoud et al. 2021), and economic diversity index (Ascani et al. 2021). Some indices are more comprehensive, for example, Community Need Index which covers income, culture, education, living conditions and healthcare (Henning et al. 2021) and the infection risk index (only available as a pre-print at the moment[1]). Due to the underlying data and methodology, it is often hard to calculate similar indices for different countries. We considered using the Herfindahl-Hirschman Index (HHI) for employment structure, which was applied in the study of Ascani et al. (2021). However, it was found that the shares of employment across different economic activities are a much better predictor of the excess mortality.

As we demonstrate in Fig. 1 below, most variables are subject to spatial autocorrelation. Therefore, we used spatial regression models to achieve the best results.

Clusters of the Excess mortality variable in Fig. 1 seem to provide limited support for the hypothesis that a pandemic should follow the pattern of the spatial diffusion of innovations (Hägerstrand 1973). During the first year, we can see that high excess mortality clustered in the regions of the Central Federal District while low mortality was observed in relatively remote regions that do not have intensive communication with the Central Federal District. However, we do not see high-value clustering in

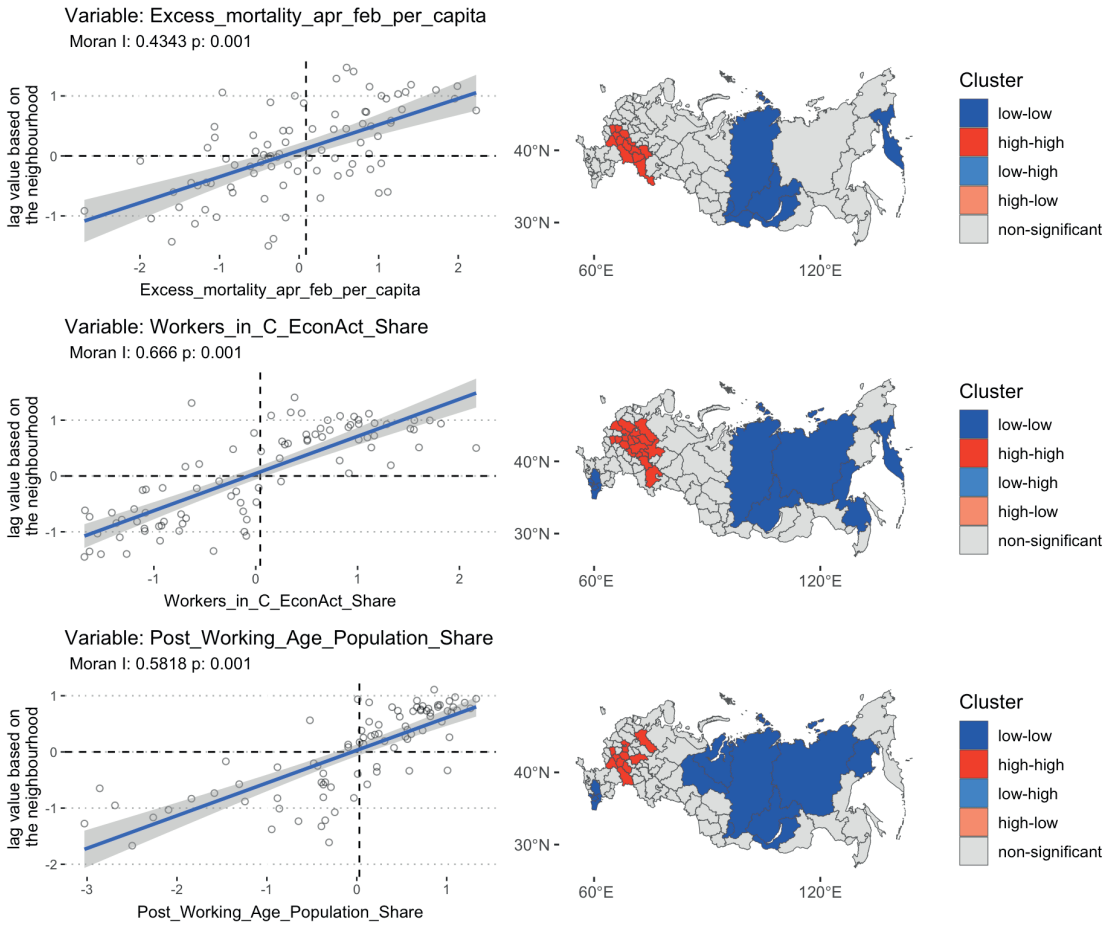

Fig. 1. Spatial autocorrelation tests for excess mortality and some explanatory variables

[1]Baum C.F. and Henry M. (2020). Socioeconomic Factors influencing the Spatial Spread of COVID-19 in the United States [SSRN Scholarly Paper]. DOI: 10.2139/ssrn.3614877

the Far Eastern Federal District and around The Republic of Tatarstan. The absence of such clustering may be due to the large size of the regions. We would expect the clustering to be present at the municipal level, confirming that the virus spread from the most populated cities to the least populated ones, which is in line with the spatial diffusion of innovations theory.

Clustering of other variables is given in Fig. 1 for illustrative purposes only. Clustering is different for different variables which justifies the incorporation of spatial effects into the regression analysis to compensate for these variations. Since the spatial clustering of excess mortality has diverging patterns, we can assume that it cannot be explained only by spatial autocorrelation of explanatory variables. Therefore, a model that compensates for the unobserved spatially correlated model errors should be used.

Method

We performed exploratory data analysis for all variables listed in Appendix A. Some variables were log-transformed for a better fit in linear models.

The selection of variables for the models was performed in the following way. For all the dependent variables we calculated Pearson correlation coefficients. We also fitted an ordinary least squares model for every independent variable against the excess mortality and calculated the R^2 and the p-value of the model (see the LM R2 and LM p-value columns in Table 1). After that, independent variables were ranked by descending R^2 and correlation (see Table 1). Using the list of top-ranked independent variables we eliminated the ones with the highest correlation (with a correlation coefficient of more than 0.7) to avoid potential multicollinearity in the models.

Then we constructed a series of baseline ordinary least squares (OLS) regression models following the basic equation:

$$y_i = \beta_0 + X_i\beta + \varepsilon_i \quad (1)$$

where y_i is excess mortality in the region i, β_0 is the intercept, X_i is a vector of selected explanatory variables, β is a vector of regression coefficients, and ε_i is a random error term.

We tried various combinations of factors in OLS regressions based on exploratory data analysis and corresponding model interpretation. After obtaining the best OLS model (1) we tested the independent variable, explanatory variables, and the OLS model residuals for spatial autocorrelation. The matrix of spatial neighbours for the spatial autocorrelation test and the resulting spatial models were created based on region boundary polygons from OpenStreetMap (OpenStreetMap contributors 2017) with GeoDa software[2] (Anselin et. al 2006) using first-order queen contiguity. Regions without neighbours (such as Kaliningrad Region and Sakhalin Region) were manually connected to 2-3 closest regions[3].

Based on the results of spatial autocorrelation tests we applied a selection of spatial models (LeSage and Pace 2009).

Spatially Lagged-X Model (SLX) was used to compensate for spatial autocorrelation of the explanatory variables:

$$y_i = \beta_0 + X_i\beta + W_iX_i\theta + \varepsilon_i \quad (2)$$

where, in addition to the OLS (1), W_i is a vector of spatial weights (a corresponding row of the spatial weights matrix), θ is the $k\times1$ coefficient vector for the exogenous spatially lagged independent variables.

Spatial Lag Model (SLM, also referred to as SAR – spatial autoregressive model) was used to compensate for spatial autocorrelation of the dependent variable:

$$y_i = \beta_0 + X_i\beta + \rho W_iy_i + \varepsilon_i \quad (3)$$

where p is the spatial lag parameter.

Spatial Error Model (SEM) was used to compensate for spatial autocorrelation of the error terms:

Table 1. Explanatory variables ranked by the highest correlation with excess mortality

Variable Name	Correlation	LM R2	LM p-value
Workers_in_C_EconAct_Share	0.5820	0.3387	0.0000000
Workers_in_G_EconAct_Share	0.5387	0.2902	0.0000001
Population_log	0.5344	0.2856	0.0000001
Floor_Area_per_capita	0.5007	0.2507	0.0000011
Workers_in_O_EconAct_Share	-0.4971	0.2471	0.0000013
Road_Density_log	0.4732	0.2239	0.0000048
Workers_in_P_EconAct_Share	-0.4722	0.2230	0.0000051
Population_Density_log	0.4573	0.2091	0.0000108
Workers_in_B_EconAct_Share_log	-0.4223	0.1783	0.0000569
Population_Below_Living_Wage_Share	-0.4081	0.1666	0.0001056
SME_in_GRDP_Share	0.3890	0.1513	0.0002335
Workers_in_R_EconAct_Share	-0.3839	0.1473	0.0002873
GRDP_in_GDP_Share_log	0.3780	0.1429	0.0003618
Migr_Outflow_InterReg_3Y_mean_per_capita_x10000	-0.3592	0.1290	0.0007364
Buses_per_capita_log	-0.3502	0.1226	0.0010187

[2]https://geodacenter.github.io

[3]The specific neighbours for those regions can be viewed by downloading the provided data and code.

$$y_i = \beta_0 + X_i\beta + u_i,\ u_i = \lambda W_i u_i + \varepsilon_i \quad (4)$$

where λ is a spatial lag parameter for the spatially correlated errors, u_i is a spatial component of the error, and ε_i is a spatially uncorrelated error.

Spatial Durbin Model (SDM) was used to compensate for spatial autocorrelation of the explanatory and the dependent variables:

$$y_i = \beta_0 + \rho W_i y_i + X_i\beta + W_i X_i\theta + \varepsilon_i \quad (5)$$

Spatial Durbin Error Model (SDEM) was used to compensate for spatial autocorrelation of the explanatory variables and the error terms:

$$y_i = \beta_0 + X_i\beta + W_i X_i\theta + u_i,\ u_i = \lambda W_i u_i + \varepsilon_i \quad (6)$$

SARAR (spatial autoregressive model with spatially autocorrelated disturbances, also referred to as SAC – spatial autoregressive combined model) was used to compensate for spatial autocorrelation of the independent variable and the error terms (Kelejian and Prucha 1998):

$$y_i = \beta_0 + X_i\beta + \rho W_i y_i + u_i,\ u_i = \lambda W_i u_i + \varepsilon_i \quad (7)$$

General Nesting Spatial Model (GNS, also referred to as mixed spatial autoregressive combined model) was applied as the final model that combines all the models above and tries to compensate for spatial autocorrelation of all components:

$$y_i = \beta_0 + X_i\beta + \rho W_i y_i + W_i X_i\theta + u_i,\ u_i = \lambda W_i u_i + \varepsilon_i \quad (8)$$

The code for all plots and tables was written in R language. The data, code and weights matrix are available in the supplementary materials on GitHub (Kotov 2022).

RESULTS AND DISCUSSION

Baseline OLS selection

We analysed a series of OLS models (see Fig. 2 and Fig. 3 below) by looking at the coefficients of the variables and their 95% confidence intervals. All coefficients are robust and z-standardised, which makes their effect on excess mortality comparable regardless of the unit size of any individual variable. If the confidence interval of a coefficient is entirely located to the right or to the left of the center at the 0 mark in Fig. 2 and Fig. 3, it means that there is a statistically significant negative or positive effect on the excess mortality.

We started with the model M0, which takes into account population density (using population density and residential floor per capita variables), employment in economic sectors that require close human interaction (B – mining, C – manufacturing, G – retail and services, P – education, and in small and medium enterprises in general), and local transportation opportunities and constraints (number of buses and cars per capita). M0 clearly showed that population density and transportation constraints have no effect on mortality. The only two significant variables are the share of employees in manufacturing (C) and retail & services (G), as these are the only variables with confidence intervals that do not cross the zero-line. The proximity of the confidence interval to zero may be due to the inclusion of insignificant variables in the model, therefore we removed some of these variables starting with the model M4 below.

M1 is an extension of M0 with climate variables (temperature and humidity). It was found that temperature does not affect mortality, while the effect of humidity is uncertain and should be tried in further models.

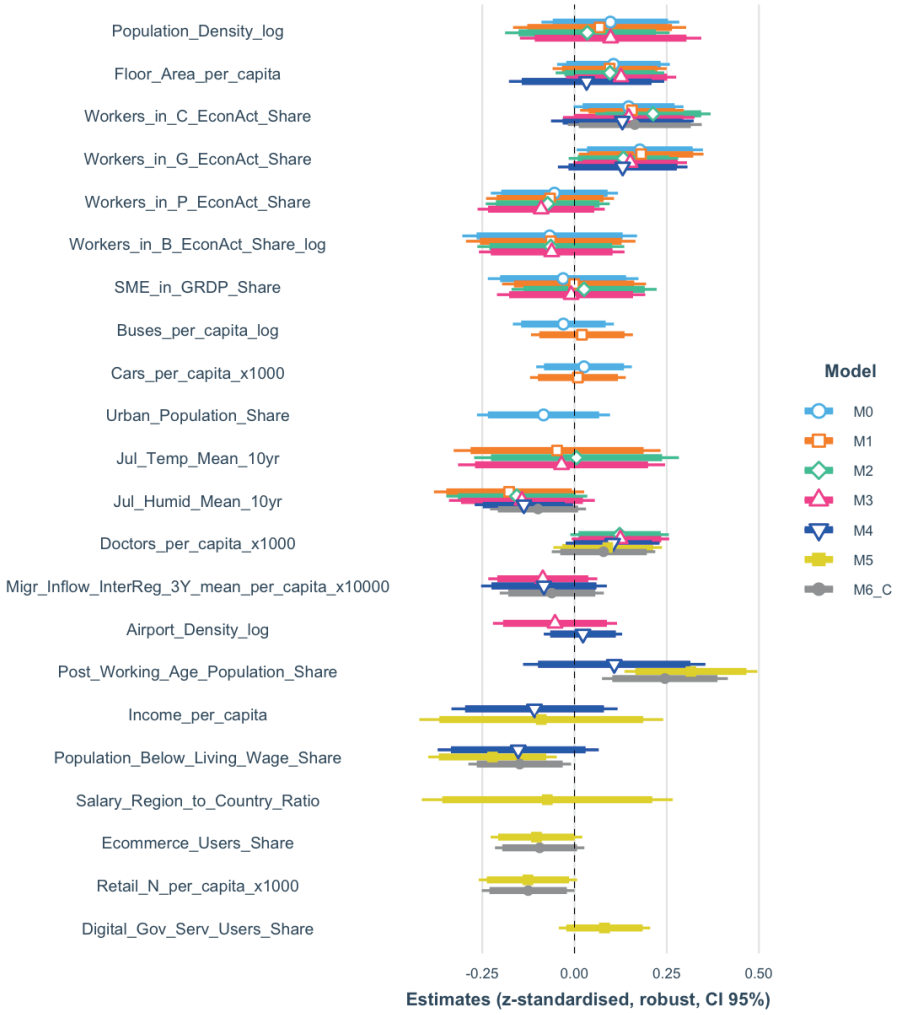

Fig. 2. Comparison of the coefficients of the models M0-M6_C

M2 adds the healthcare component (number of doctors per capita). It was found that, depending on the model, the confidence interval may touch the zero mark, but this factor is still worth considering in further models.

M3 adds interregional migration flow and opportunity for the spread of COVID-19 following the Hägerstrand's (1973) spatial diffusion of innovation (via the airport density). It was found that airports have no detectable effect, which suggests that air travel between regions was likely not a significant factor in the COVID-19 spread across Russia, while inter-regional migration is worth considering.

With the next model M4, we eliminated the non-significant variables from previous models and added age (as the elderly are the most affected by both the virus and the deterioration of regular medical care) and income (following the hypothesis that in poorer regions the population will ignore the restrictions more frequently as they must provide money for their families). It was found that on its own M4 has almost no significant coefficients, however, it provides information on the potential of individual variables. Population density expressed as residential floor area per capita proved to be insignificant, as its coefficient in M4 falls almost to zero. The coefficients for the share of workers in manufacturing (C) and retail & services (G), the number of doctors per capita, and humidity in M4 and previous models vary slightly but mostly remain significant, suggesting that these two economic domains with intensive and close human interaction are important negative factors of the excess mortality.

M5 builds on M4 by adding digital skills, the share of e-commerce users and the overall provision of retail businesses. In M5 we can see that income expressed as the share of the population with income below the living wage has a high negative impact on excess mortality. This is counterintuitive but may suggest that those households interacted less, as they had no money to spend. The higher share of e-commerce users, as well as the higher number of retail locations per capita, also had a negative effect, as the reliance on face-to-face contact was lower in regions with high values for these variables. Interestingly, M5 also suggests that a higher share of the population using government services over the Internet somehow negatively affects mortality.

Finally, models M6_C, M6_G and M6_CG are the ultimate models with the most significant variables that demonstrate a noticeable and explainable effect. The difference is that M6_C uses the share of employees in manufacturing (C), while M6_G replaces it with the share in retail and services (G). M6_CG uses the shares in both C and G economic activities. We can see the comparison of these M6 models in Fig. 3. Clearly, the share of employees in C and G is almost equally important, both according to the models and the logic behind the variables, however with the M6_C model we are able to capture the effect of retail with the number of retail locations per capita and e-commerce. M6_G and M6_CG, despite their overall similarity to M6_C, do not reproduce the same effects reliably. M6 models also suggest that the number of doctors is irrelevant, which makes sense compared to the previous models as this variable had a positive effect on excess mortality, which could only be explained by assuming that contacts through doctors were stimulating additional infections. The insignificance of the healthcare provision is also in line with previous findings (Kolosov et al. 2021).

A statistical summary of all OLS models is provided in Fig. 4 below. It shows that models M6_CG and M6_C are the best according to most model quality metrics. They have the lowest AICc (corrected Akaike information criterion), highest R-squared and adjusted R-squared, and lowest RMSE (root-mean-square error). Therefore, we used these models and their variables as the best baseline for the spatial extension of the model.

Extension of the best OLS with a spatial component

We used M6_CG as the baseline OLS model and extended it with spatial specifications as described in the methodology in equations (2) through (8). As we can see from Fig. 5, the best models are SEM (Spatial Error Model), LAG (Spatial Lag Model) and OLS. These models have the lowest corrected Akaike Information Criterion (AICc), but the values are very close and not significantly different. However, SEM helps to compensate for the spatial autocorrelation of some unobserved and unaccounted spatially autocorrelated factors. The LAG model corrects for the spatial autocorrelation of the excess mortality (as seen at the top of Fig. 1) and the fact that the spread of COVID-19 is indeed quite likely to occur between the neighbouring regions, which is also observed on the global scale. Other models (all models below OLS in Fig. 5) do produce lower model errors, however, they add very little in terms of interpretability of the results in general and the model coefficients.

Fig. 6 provides a comparison of the OLS model coefficients with and without its spatial extensions. The graph suggests that compensating for spatial autocorrelation increases confidence in the significance of several variables, including the number of retail locations per capita, the share of post-working age population and

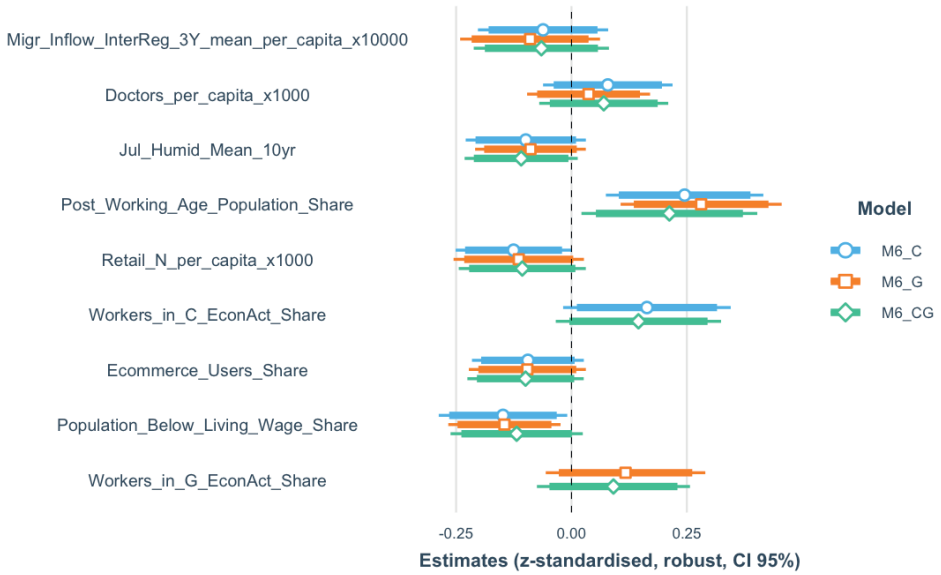

Fig. 3. Comparison of the coefficients of the model M6 variants

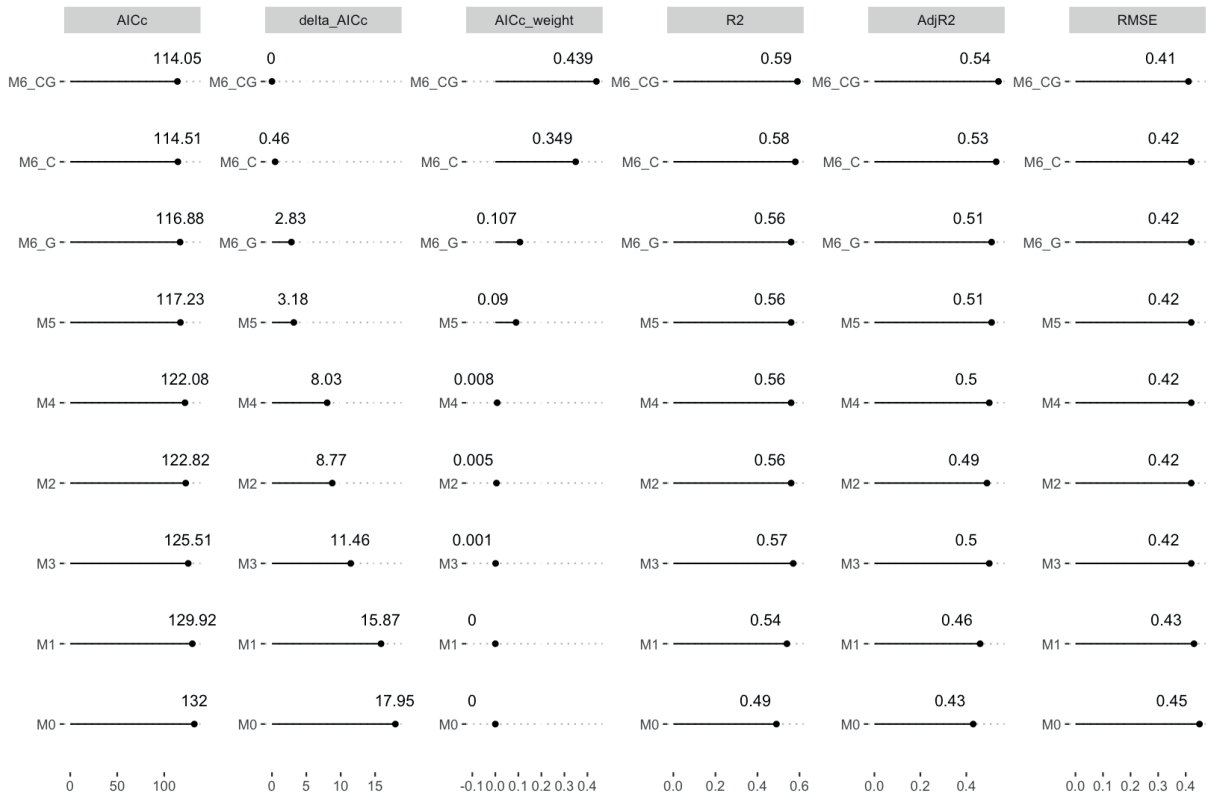

Fig. 4. Summary of baseline OLS models

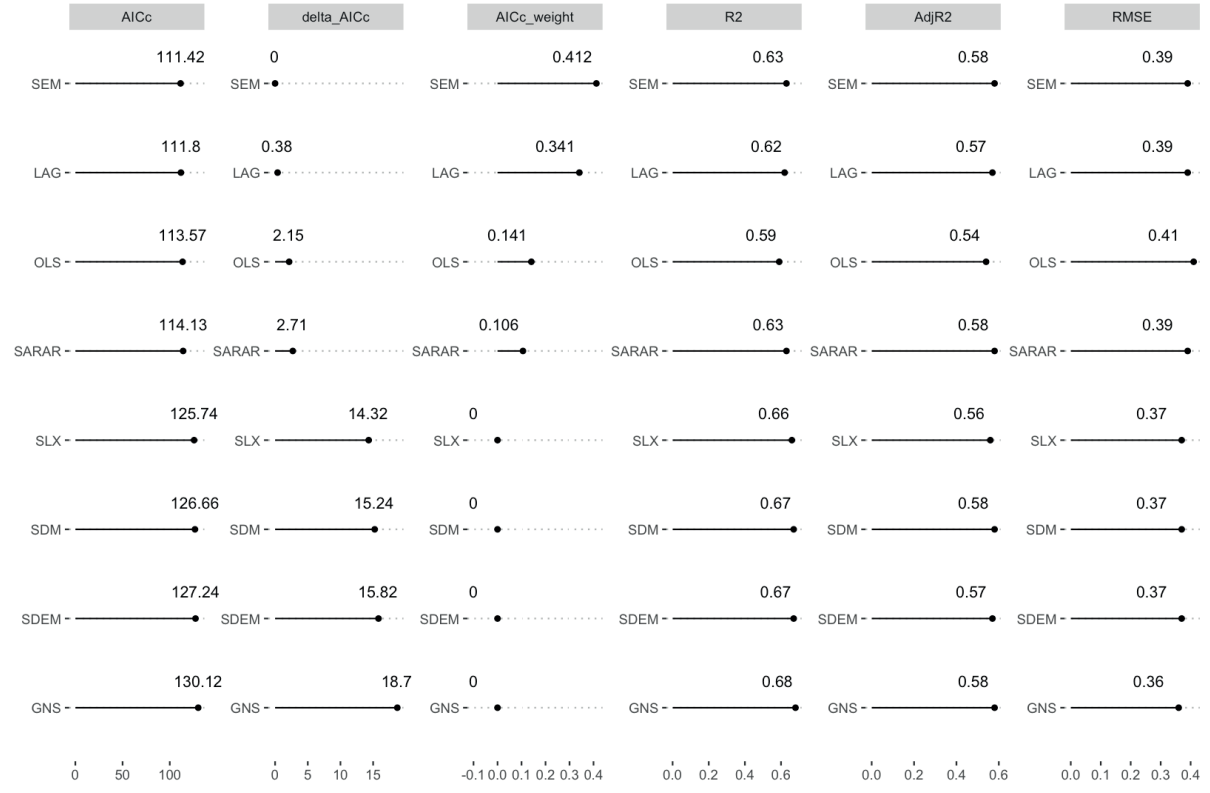

Fig. 5. Comparison of the OLS model performance with and without spatial extensions for the final set of variables

the share of employees in manufacturing (C), but not the share of workers in retail (G) and the number of doctors per capita. The effect of the share of e-commerce users on excess mortality is still insignificant, which might be due to the use of old data as Rosstat has not yet published the 2020 data, and pre-2020 the share of consumers who shop online was lower.

We can also observe that most variables do not show any external effects on neighbouring regions («lag.» variables at the bottom of Fig. 6). That is, the values of these variables in the neighbours of any given region do not affect the excess mortality in the region of interest. The only exception is the number of doctors per capita, which increases the excess mortality in neighbouring regions without any logical explanation.

Lambda and rho are significant in the corresponding SEM and LAG models, but not in their derivatives. SEM and LAG models are almost equivalent in all other aspects (model quality based on AICc, R-squared and RMSE, as well as model coefficients). This reinforces the statement

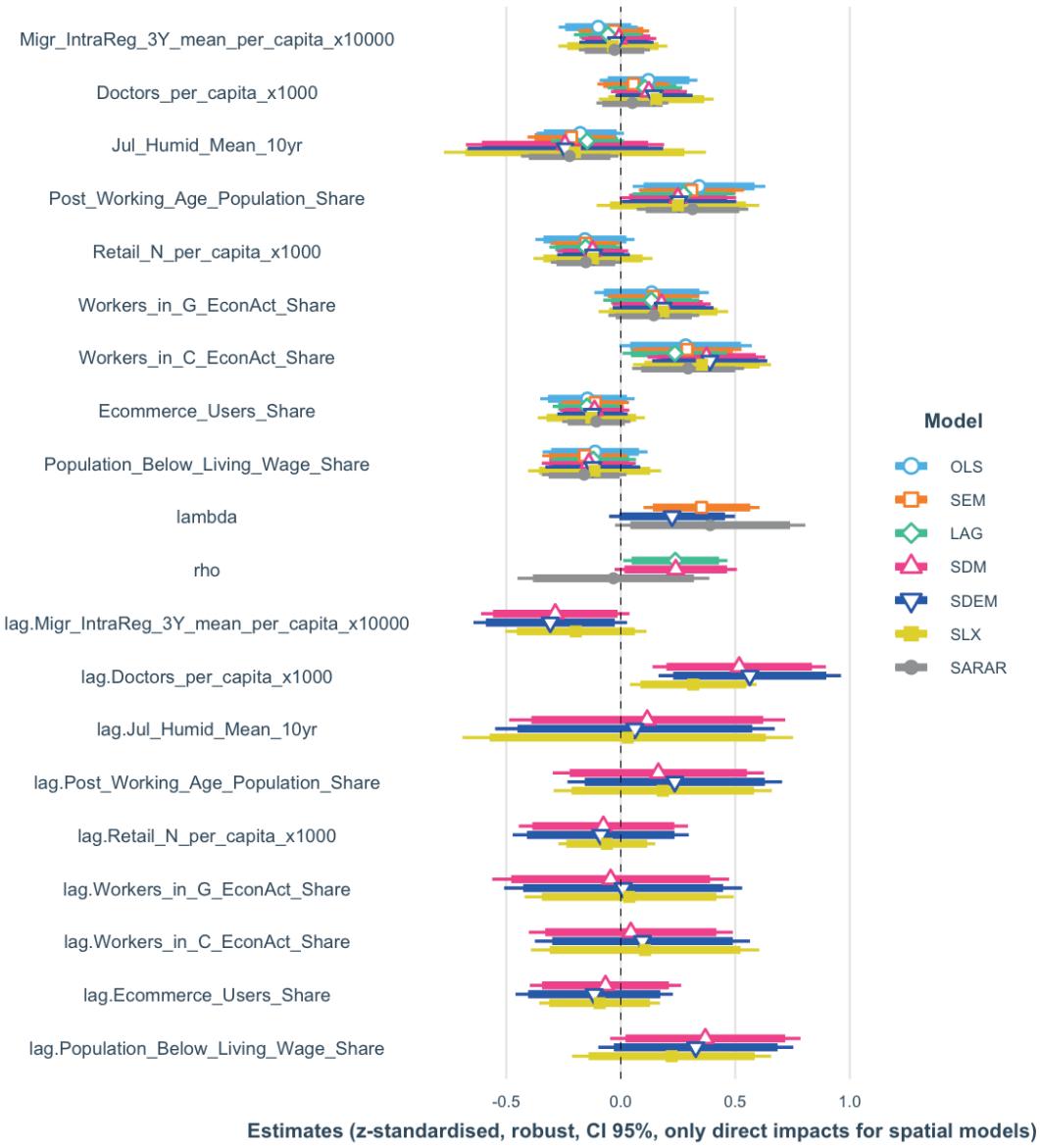

Fig. 6. Comparison of the OLS model coefficients with and without spatial extensions

that there are some unobserved spatially autocorrelated components missing from the model. However, their absence is partially compensated by the spatial extension of the OLS. Given that in the SARAR model both lambda and rho are insignificant and demonstrate an opposite effect, we can conclude that only LAG (compensates for the autocorrelation of excess mortality) or SEM (compensates for unobserved spatially autocorrelated variables) models can be considered as the best fit.

In Table 2 we directly compare the z-standardised coefficients and the number of significant variables in all models. It can be seen that the LAG extension of the OLS model results in more robust estimates for a larger number of variables.

As we can see from Table 2, the most important factor for excess mortality according to the best SEM model is the share of the post-working age population. It has the highest value of the standardised coefficient (0.31), which confirms the well-known fact that the early COVID-19 wave largely affected the elderly. Almost equally important (0.29) is the share of workers in manufacturing, where very close contact is common and social distancing is sometimes impossible. What is more, in manufacturing jobs workers often reside together in communal accommodation.

High humidity has a negative (-0.22) effect on excess mortality. In fact, humidity is highly correlated with temperature, and even though the temperature did not make it into the final model, we can assume humidity as a proxy for temperature. Climate conditions might explain not only the specifics of the COVID-19 virus related to humidity and temperature but also differences in the behaviour of the population, for example, the propensity to spend more or less time outdoors.

We manually marked the number of retail locations per capita as significant as it only formally misses the 5% significance level with a p-value of 0.0506. The negative coefficient (-0.15) confirms that a larger number of shops per capita in a given region leads to a lower density of customers in those shops, and therefore increases the opportunities for social distancing and reduces interaction. The share of employees in retail (G) is not significant, however, we expect it to be a proxy for a similar effect.

The last parameter that is significant and highly important in terms of its effect is the lambda of the SEM model. This suggests that there are one or more unobserved spatially autocorrelated factors, that neither we nor other researchers have considered. The effect of other variables is not significant. From the literature review, we have not seen high R^2 values and therefore full models even in studies concerning much smaller spatial units than Russian regions. We expect that a more complete model would be able to capture more individual effects at the municipal level.

Table 2. Comparison of the OLS, SEM and LAG estimates

	OLS	SEM	LAG
(Intercept)	0.00	-0.02	-0.02
	(0.08)	(0.10)	(0.07)
Migr_IntraReg_3Y_mean_per_capita_x10000	-0.10	-0.03	-0.06
	(0.09)	(0.08)	(0.08)
Doctors_per_capita_x1000	0.12	0.06	0.11
	(0.11)	(0.08)	(0.08)
Jul_Humid_Mean_10yr	-0.18	-0.22 *	-0.15
	(0.10)	(0.10)	(0.08)
Post_Working_Age_Population_Share	0.34 *	0.31 **	0.27 *
	(0.15)	(0.12)	(0.11)
Retail_N_per_capita_x1000	-0.16	-0.15*	-0.15
	(0.11)	(0.08)	(0.08)
Workers_in_G_EconAct_Share	0.13	0.14	0.13
	(0.13)	(0.10)	(0.11)
Workers_in_C_EconAct_Share	0.28	0.29 *	0.24 *
	(0.15)	(0.12)	(0.12)
Ecommerce_Users_Share	-0.15	-0.11	-0.15
	(0.10)	(0.08)	(0.08)
Population_Below_Living_Wage_Share	-0.11	-0.16	-0.12
	(0.11)	(0.09)	(0.10)
Lambda λ		0.35 **	
		(0.13)	
Rho p			0.24 *
			(0.12)
N	85	85	85
Pseudo-R2	0.59	0.63	0.62
Adjusted pseudo-R2	0.54	0.58	0.57
AICc	113.57	111.42	111.80

All continuous predictors are mean-centered and scaled by 1 standard deviation. Standard errors are heteroskedasticity robust.
*** $p < 0.001$; ** $p < 0.01$; * $p < 0.05$.

As we can see from Fig. 7 below, the shares of employment in many economic activities are highly correlated with each other, as well as with the excess mortality. So hypothetically a model for excess mortality could be composed completely based on employment rates. We explored this option and can conclude that using just one of the economic activity types, either G (trade) or C (manufacturing), is the best option. Fitting the same set of spatial models using A, D, G and R economic activities results in similar R^2 and model error and even lower AICc values, however, it unnecessarily limits the model to just economic activities, which cannot be the only explanation for the excess mortality.

The employment in C (manufacturing) does not necessarily capture the whole employment and interaction structure, but it is just enough to explain the excess mortality without relying on other economic activities. Employment in G (retail) is just as important but was pushed out from the final model by the employment in C (mining) variable. The large workforce in retail leads to more opportunities and more necessity for close physical interaction between co-workers and with the customers. As a result, even though it was not found to be significant in the model, the overall correlation of the share in G with the excess mortality suggests that it does have an effect, which is not captured at the regional level.

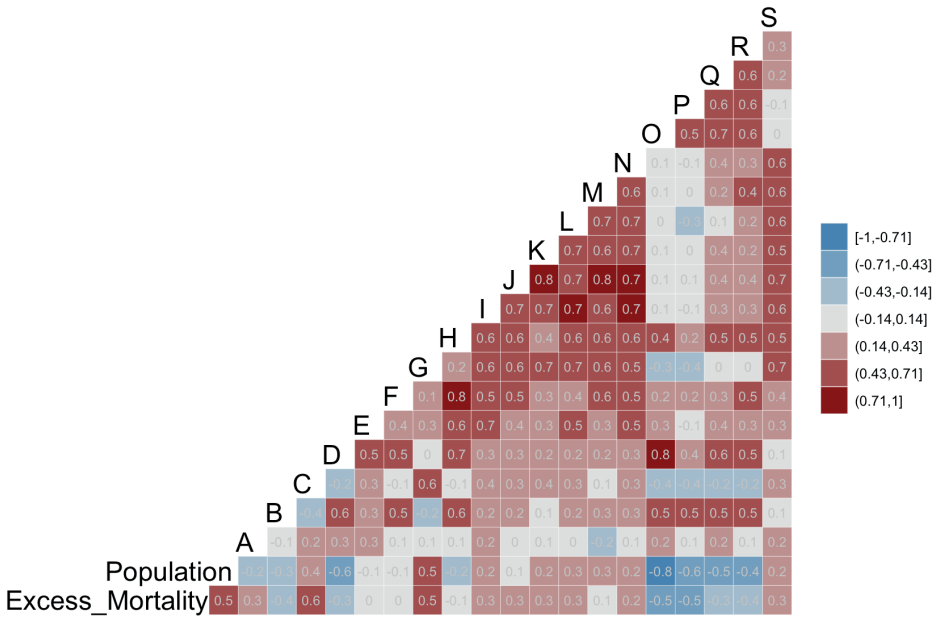

Fig. 7. Correlation matrix for the shares of employment in different economic activities

CONCLUSIONS

We identified the most important factors that caused the excess mortality between April 2020 and February 2021. The share of the elderly population was confirmed by our model as the obvious reason for excess deaths, followed closely by the share of employees in manufacturing (C economic activity according to European Skills, Competences, and Occupations (ESCO) v1 classificaiton). On the other hand, higher humidity, and a higher number of retail locations per capita reduce the excess mortality with a comparable impact.

Our final model is not complete and mostly focuses on a few factors, however, it is reliable in terms of the selection of these factors, which were identified based on the significance of their effect, as well as accounting for spatial autocorrelation. Still, there is room for improvement of the model.

Queen-type contiguity neighbourhood matrix is too simplified, so the spatial extensions of the baseline OLS model can potentially be improved by using a different type of spatial weights. For example, spatial weights based on the air-and rail-passenger flows for the year 2020 could be a better fit, as they would probably explain the pandemic transmission paths and intensity following the Hägerstrand's (1973) model of the spatial diffusion of innovations. Currently, we focused heavily on human interaction and possibly failed to take into account other factors, while compensating for spatial autocorrelation was not enough.

Due to data limitations, the current best model was built for the regional level. Because of the modifiable area unit problem, which is manifested in the excessive averaging of mortality and other variables over irregularly sized and populated regions, it might not be possible to improve the obtained results. We expect the same model to provide better results at a municipal level when the mortality data becomes available.

REFERENCES

Agnoletti M., Manganelli S. and Piras F. (2020). Covid-19 and rural landscape: The case of Italy. Landscape and Urban Planning, 204, 103955, DOI: 10.1016/j.landurbplan.2020.103955.

Amdaoud M., Arcuri G. and Levratto N. (2021). Are regions equal in adversity? A spatial analysis of spread and dynamics of COVID-19 in Europe. The European Journal of Health Economics, 22(4), 629-642, DOI: 10.1007/s10198-021-01280-6.

Andersen L.M., Harden S.R., Sugg M.M., Runkle J.D. and Lundquist T.E. (2021). Analyzing the spatial determinants of local Covid-19 transmission in the United States. Science of The Total Environment, 754, 142396, DOI: 10.1016/j.scitotenv.2020.142396.

Anselin L., Ibnu S. and Youngihn K. (2006). GeoDa: An Introduction to Spatial Data Analysis. Geographical Analysis 38(1), 5-22, DOI: 10.1111/j.0016-7363.2005.00671.x.

Ascani A., Faggian A. and Montresor S. (2021). The geography of COVID-19 and the structure of local economies: The case of Italy. Journal of Regional Science, 61(2), 407-441, DOI: 10.1111/jors.12510.

Bański J., Mazur M. and Kamińska W. (2021). Socioeconomic Conditioning of the Development of the COVID-19 Pandemic and Its Global Spatial Differentiation. International Journal of Environmental Research and Public Health, 18(9), 4802, DOI: 10.3390/ijerph18094802.

Chakraborti S., Maiti A., Pramanik S., Sannigrahi S., Pilla F., Banerjee A. and Das D.N. (2021). Evaluating the plausible application of advanced machine learnings in exploring determinant factors of present pandemic: A case for continent specific COVID-19 analysis. Science of The Total Environment, 765, 142723, DOI: 10.1016/j.scitotenv.2020.142723.

Chen Y., Chen M., Huang B., Wu C. and Shi W. (2021). Modeling the Spatiotemporal Association Between COVID-19 Transmission and Population Mobility Using Geographically and Temporally Weighted Regression. GeoHealth, 5, e2021GH000402, DOI: 10.1029/2021gh000402.

Desmet K. and Wacziarg R. (2021). JUE Insight: Understanding spatial variation in COVID-19 across the United States. Journal of Urban Economics, 103332, DOI: 10.1016/j.jue.2021.103332.

Ehlert A. (2021). The socio-economic determinants of COVID-19: A spatial analysis of German county level data. Socio-Economic Planning Sciences, 101083, DOI: 10.1016/j.seps.2021.101083.

Franch-Pardo I., Napoletano B.M., Rosete-Verges F. and Billa L. (2020). Spatial analysis and GIS in the study of COVID-19. A review. Science of The Total Environment, 739, 140033, DOI: 10.1016/j.scitotenv.2020.140033.

Hägerstrand T. (1973). Innovation diffusion as a spatial process. University of Chicago press.

Hass F.S. and Jokar Arsanjani J. (2021). The Geography of the Covid-19 Pandemic: A Data-Driven Approach to Exploring Geographical Driving Forces. International Journal of Environmental Research and Public Health, 18(6), 2803, DOI: 10.3390/ijerph18062803.

Henning A., McLaughlin C., Armen S. and Allen S. (2021). Socio-spatial influences on the prevalence of COVID-19 in central Pennsylvania. Spatial and Spatio-Temporal Epidemiology, 37, 100411, DOI: 10.1016/j.sste.2021.100411.

Kelejian H.H. and Prucha I.R. (1998). A Generalized Spatial Two-Stage Least Squares Procedure for Estimating a Spatial Autoregressive Model with Autoregressive Disturbances. The Journal of Real Estate Finance and Economics, 17(1), 99-121, DOI: 10/bxvhm4.

Kolosov V.A., Tikunov V.S. and Eremchenko E.N. (2021). Areas Of Socio-Geographical Study Of The Covid-19 Pandemic In Russia And The World. GEOGRAPHY, ENVIRONMENT, SUSTAINABILITY, 14(4), 109-116, DOI: 10.24057/2071-9388-2021-091.

Konstantinoudis G., Padellini T., Bennett J., Davies B., Ezzati M. and Blangiardo M. (2021). Long-term exposure to air-pollution and COVID-19 mortality in England: A hierarchical spatial analysis. Environment International, 146, 106316, DOI: 10.1016/j.envint.2020.106316.

Kotov E. (2022). e-kotov/ru-covid19-regional-excess-mortality article data and code. URL: https://github.com/e-kotov/ru-covid19-regional-excess-mortality. Zenodo, DOI: 10.5281/zenodo.6515455.

LeSage J. and Pace R.K. (2009). Introduction to Spatial Econometrics. CRC Press.

Luo Y., Yan J. and McClure S. (2021). Distribution of the environmental and socioeconomic risk factors on COVID-19 death rate across continental USA: a spatial nonlinear analysis. Environmental Science and Pollution Research, 28(6), 6587-6599, DOI: 10.1007/s11356-020-10962-2.

Maiti A., Zhang Q., Sannigrahi S., Pramanik S., Chakraborti S., Cerda A. and Pilla F. (2021). Exploring spatiotemporal effects of the driving factors on COVID-19 incidences in the contiguous United States. Sustainable Cities and Society, 68, 102784, DOI: 10.1016/j.scs.2021.102784.

Mogi R., Kato G. and Annaka S. (2020). Socioeconomic inequality and COVID-19 prevalence across municipalities in Catalonia, Spain [Preprint], DOI: 10.31235/osf.io/5jgzy.

Mollalo A., Vahedi B. and Rivera K.M. (2020). GIS-based spatial modeling of COVID-19 incidence rate in the continental United States. Science of The Total Environment, 728, 138884, DOI: 10.1016/j.scitotenv.2020.138884.

OpenStreetMap contributors (2017). OpenStreetMap. [online] Available at: https://www.openstreetmap.org [Accessed 01 Jul. 2021]

Oto-Peralías D. (2020). Regional correlations of COVID-19 in Spain [Preprint], DOI: 10.31219/osf.io/tjdgw.

Perone G. (2021). The determinants of COVID-19 case fatality rate (CFR) in the Italian regions and provinces: An analysis of environmental, demographic, and healthcare factors. Science of The Total Environment, 755, 142523, DOI: 10.1016/j.scitotenv.2020.142523.

Qi H., Xiao S., Shi R., Ward M.P., Chen Y., Tu W., Su Q., Wang W., Wang X. and Zhang Z. (2020). COVID-19 transmission in Mainland China is associated with temperature and humidity: A time-series analysis. Science of The Total Environment, 728, 138778, DOI: 10.1016/j.scitotenv.2020.138778.

Rahman M.H., Zafri N.M., Ashik F. and Waliullah M. (2020). Gis-Based Spatial Modeling to Identify Factors Affecting COVID-19 Incidence Rates in Bangladesh [SSRN Scholarly Paper], DOI: 10.2139/ssrn.3674984.

Raymundo C.E., Oliveira M.C., Eleuterio T. de A., André S.R., da Silva M.G., Queiroz E.R. da S. and Medronho R. de A. (2021). Spatial analysis of COVID-19 incidence and the sociodemographic context in Brazil. PLOS ONE, 16(3), e0247794, DOI: 10.1371/journal.pone.0247794.

Rodríguez-Pose A. and Burlina C. (2021). Institutions and the uneven geography of the first wave of the COVID-19 pandemic. Journal of Regional Science, 61(4), 728-752, DOI: 10.1111/jors.12541.

Sannigrahi S., Pilla F., Basu B. and Sarkar Basu A. (2020). The overall mortality caused by COVID-19 in the European region is highly associated with demographic composition: A spatial regression-based approach. https://ui.adsabs.harvard.edu/abs/2020arXiv200504029S.

Scarpone C., Brinkmann S.T., Große T., Sonnenwald D., Fuchs M. and Walker B.B. (2020). A multimethod approach for county-scale geospatial analysis of emerging infectious diseases: a cross-sectional case study of COVID-19 incidence in Germany. International Journal of Health Geographics, 19(1), 32, DOI: 10.1186/s12942-020-00225-1.

Sun F., Matthews S.A., Yang T.-C. and Hu M.-H. (2020). A spatial analysis of the COVID-19 period prevalence in U.S. counties through June 28, 2020: where geography matters? Annals of Epidemiology, 52, 54-59.e1, DOI: 10.1016/j.annepidem.2020.07.014.

Wang Q., Dong W., Yang K., Ren Z., Huang D., Zhang P. and Wang J. (2021). Temporal and spatial analysis of COVID-19 transmission in China and its influencing factors. International Journal of Infectious Diseases, 105, 675-685, DOI: 10.1016/j.ijid.2021.03.014.

Yarmol-Matusiak E.A., Cipriano L.E. and Stranges S. (2021). A comparison of COVID-19 epidemiological indicators in Sweden, Norway, Denmark, and Finland. Scandinavian Journal of Public Health, 49(1), 69-78, DOI: 10.1177/1403494820980264.

Zemtsov S.P. and Baburin V.L. (2020). Risks of morbidity and mortality during the COVID-19 pandemic in Russian regions. Population and Economics, 4(2), 158-181, DOI: 10.3897/popecon.4.e54055.

Appendix A. Variables used in the study

Group	Variable Name	Description	Source*
Dependent variable	Excess_mortality_apr_feb_per_capita	Excess per capita mortality over a period from April 2020 to February 2021 compared to the mean over previous 5 years	1
Demographic	Population	Mean population during a calendar year	1
Demographic	Urban_Population_Share	Share of urban population	1
Demographic	Migr_IntraReg_3Y_mean_per_capita_x10000	3-year mean intraregional migrants per 10 000 inhabitants	1
Demographic	Migr_Inflow_InterReg_3Y_mean_per_capita_x10000	3-year mean interregional arriving migrants per 10 000 inhabitants	1
Demographic	Migr_Inflow_International_3Y_mean_per_capita_x10000	3-year mean international arriving migrants per 10 000 inhabitants	1
Demographic	Migr_Outflow_InterReg_3Y_mean_per_capita_x10000	3-year mean interregional departing migrants per 10 000 inhabitants	1
Demographic	Migr_Outflow_International_3Y_mean_per_capita_x10000	3-year mean international departing migrants per 10 000 inhabitants	1
Demographic	Employees_in_Working_Age_Population_Share	Share of employed people in total working-age population	1
Demographic	Working_Age_Population_Share	Share of working-age population in total population	1
Demographic	Under_Working_Age_Population_Share	Share of under working-age population in total population	1
Demographic	Post_Working_Age_Population_Share	Share of post-working-age population in total population	1
Environment	Jan_Temp_Mean_10yr	10-year mean of temparature in January (2010-2020)	2
Environment	Jul_Temp_Mean_10yr	10-year mean of temparature in July (2010-2020)	2
Environment	Jan_Humid_Mean_10yr	10-year mean of humidity in January (2010-2020)	2
Environment	Jul_Humid_Mean_10yr	10-year mean of humidity in January (2010-2020)	2
Human Interaction	Road_Density	Total length of federal and regional level roads / area of the region	3
Human Interaction	Rail_Road_Density	Total length of standard width rail roads / area of the region	3
Human Interaction	Airport_Density	Total number of airports / area of the region	3, 4
Human Interaction	Buses_per_capita	Number of buses per person	1
Healthcare	Doctors_per_capita_x1000	Number of doctors per 1 000 inhabitants	1
Healthcare	Change_over_5yrs_Doctors_per_capita_x1000	Ratio of the number of doctors per 1 000 inhabitants, 2019 to 2015	1
Human Interaction	Modern_Retail_Area_per_capita_x1000	Total area of large retail (600+ square meters) per 1000 inhabitants	1
Human Interaction	Floor_Area_per_capita	Residential floor area per person	1
Human Interaction	Retail_N_per_capita_x1000	Total number of all retail stores per 1000 inhabitants	1
Human Interaction	Retail_Area_per_capita_x1000	Total area of all retail retail per 1000 inhabitants	1
Human Interaction	Cars_per_capita_x1000	Number of private passanger cars per 1 000 inhabitants	1
Human Interaction	Ecommerce_Users_Share	Share of people using ecommerce for shopping	1

Human Interaction	Digital_Gov_Serv_Users_Share	Share of people using digital government services	1
Human Interaction	Workers_in_A_EconAct_Share	Share of working-age population working in A - Agriculture	1
Human Interaction	Workers_in_B_EconAct_Share	Share of working-age population working in B - Mining	1
Human Interaction	Workers_in_C_EconAct_Share	Share of working-age population working in C - Manufacturing	1
Human Interaction	Workers_in_D_EconAct_Share	Share of working-age population working in D - Electricity, Gas, etc.	1
Human Interaction	Workers_in_E_EconAct_Share	Share of working-age population working in E - Water Supply	1
Human Interaction	Workers_in_F_EconAct_Share	Share of working-age population working in F - Construction	1
Human Interaction	Workers_in_G_EconAct_Share	Share of working-age population working in G - Wholesale and Retail Trade	1
Human Interaction	Workers_in_H_EconAct_Share	Share of working-age population working in H - Transportation and Storage	1
Human Interaction	Workers_in_I_EconAct_Share	Share of working-age population working in I - Accomodation and Food	1
Human Interaction	Workers_in_J_EconAct_Share	Share of working-age population working in J - IT and Communication	1
Human Interaction	Workers_in_K_EconAct_Share	Share of working-age population working in K - Finance and Insurance	1
Human Interaction	Workers_in_L_EconAct_Share	Share of working-age population working in L - Real Estate	1
Human Interaction	Workers_in_M_EconAct_Share	Share of working-age population working in M - Professional, Scientific, Technical	1
Human Interaction	Workers_in_N_EconAct_Share	Share of working-age population working in N - Administrative and Support	1
Human Interaction	Workers_in_O_EconAct_Share	Share of working-age population working in O - Public Administration and Defence	1
Human Interaction	Workers_in_P_EconAct_Share	Share of working-age population working in P - Education	1
Human Interaction	Workers_in_Q_EconAct_Share	Share of working-age population working in Q - Healthcare and Social Work	1
Human Interaction	Workers_in_R_EconAct_Share	Share of working-age population working in R - Arts, Entertainment and Recreation	1
Human Interaction	Workers_in_S_EconAct_Share	Share of working-age population working in S - Other Services	1
Socioeconomic	Salary_Region_to_Country_Ratio	Ratio of mean regional salary to mean national salary	1
Socioeconomic	Population_Below_Living_Wage_Share	Share of population with income below the living wage	1
Socioeconomic	Mean_Real_Wage	Mean Real Wage	1
Socioeconomic	Income_per_capita	Income per person	1
Socioeconomic	SME_in_GRDP_Share	Share of Small and Medium Enterprise output in Gross regional domestic product	1
Socioeconomic	GRDP_in_GDP_Share	Share of Gross regional domestic product in Gross Domestic Product	1
Socioeconomic	Patents_per_capita_x10000	Number of patents per 10 000 inhabitants	1

*1 – Federal State Statistics Service – Rosstat, 2 – All-Russia Research Institute of Hydrometeorological Information - World Data Center (RIHMI-WDC), Roshydromet, 3 – OpenStreetMap, 4 – Aircraft owners and pilots association of Russia

RESEARCH PAPER

OPTIMAL BANDWIDTH FOR GEOGRAPHICALLY WEIGHTED REGRESSION TO MODEL THE SPATIAL DEPENDENCY OF LAND PRICES IN MANADO, NORTH SULAWESI PROVINCE, INDONESIA

Winsy Weku[1,2*], Henny Pramoedyo[1], Agus Widodo[1], Rahma Fitriani[1]
[1]Brawijaya University, Malang, Indonesia
[2]Sam Ratulangi University, Manado, Indonesia
***Corresponding author:** winsyweku@gmail.com
Received: November 27th, 2021 / Accepted: April 24th, 2022 / Published: June 30th, 2022
https://DOI-10.24057/2071-9388-2019-154

ABSTRACT. Bandwidth plays a crucial role in the Geographically Weighted Regression modelas it affects the model's ability to describe spatial dependencies. If the bandwidth is too large, the model will be similar to a normal regression model. Conversely, if it is too small, the model will be too rough. Bandwidth can be selected in several ways, e.g. manually determined by experts or using Akaike Information Criteria, Cross-Validation, and Lagrange Multiplier methods. This study offers an alternative approach to choosing bandwidth based on the covariance function representing a linear combination between the Bessel and Gaussian-Type functions. We applied this function to analyze the land price in Manado with four infrastructure accessibility variables, such as accessibility to government offices, education facilities, shopping centers, and healthcare facilities. Therefore, the proposed method is different from the index methods (AIC and CV) which have been used by other researchers. The results showed that the non-parametric covariance function provides a smaller bandwidth than conventional methods, specifically Akaike Information Criteria and Cross-Validation. In addition, the value of R^2(adjusted) given by the covariance function is greater than the one given by the proportional method. This means that the optimal bandwidth obtained using the covariance function is more suitable to explain the land price in the city of Manado.

KEY WORDS: bandwidth, covariance function, land price, infrastructure

CITATION: Weku W., Pramoedyo H., Widodo A., Fitriani R. (2022). Optimal Bandwidth for Geographically Weighted Regression to Model the Spatial Dependency of Land Prices in Manado, North Sulawesi Province, Indonesia. Geography, Environment, Sustainability, 2(15), p. 84-90
https://DOI-10.24057/2071-9388-2019-154

Conflict of interests: The authors reported no potential conflict of interest.

INTRODUCTION

The modelling capabilities of Geographically Weighted Regression (GWR) are greatly influenced by the choice of bandwidth (geographical distance) and kernel function. The selected bandwidth limits the data (in this case, the location) to be within the bandwidth range. If the bandwidth is large, more data will be included in the analysis. The obtained GWR model will be smooth and closer to a simple regression model. Conversely, a small bandwidth will limit the data to a small sample, which in its turn will result in a roughmodel. Therefore, choosing the suitable bandwidth is an open problem which is very interesting to study. Bandwidth selection is usually done through several methods, e.g., manually by field experts or using Akaike Information Criteria (AIC), Cross-Validation (CV), and Lagrange Multiplier (LM) methods. The resulting bandwidth also varies, which makes determining bandwidth a challenging problem.

Because of the high use of GWR, several advanced studies have been carried out focusing onthe bandwidth selection, particularly using AICc and CV, which are very common data-driven methods that are sensitive to outliers. Leung et al. (2000) proposed to use the goodness of fit test and stated that bandwidth represents the degree of freedom of the GWR residue. Brunsdon et al. (2000) formed a bandwidth vector using the backfitting algorithm. Farber and Paez (2007) reduced bias by modifying the CV procedure. Meanwhile, Leong and Jue (2017) performed iteration procedures as well as solved numerical iteration problems. The use of correlograms to determine the geographical distance (bandwidth) was also implemented by some researchers, for example, spatial correlograms with index morans were used by Abebe et al. (2015) to measure wheat field landscapes in Ethiopia, or by Hetmanski et al. (2010) who measured the effects of pigeon habitat in 33 cities in the Pomeranian province, Poland. In addition, a spline correlogram was also used by Liu and Wemberly (2015) to measure the influence of climate and landscape on the spread of fires in the western United States from 1984 to 2010, and by Bjornstad et al. (1999) to measure the dynamics of tree mice and field mice in northern Japan during 1962-1992. However, correlograms are indexes that do not have the form of a covariance function as a condition of validity. Weku et al. (2019b) used a correlogram with a covariance function that appropriates the validity of definite positive to determine geographic distance.

In practice, bandwidth is a measure that determines the geographical distance between one location and other locations. For example, the fluctuation of land prices is influenced by the proximity of the studied location to urban centers that have a complete infrastructure. The closer a location is to the infrastructure center, the higher will be the land price, and, on the other hand, the land price will be lower when it is located far from the infrastructure. According to Manganelli et al. (2013),the land price can be significantly influenced by many factors. Apart from several general aspects (e.g. macroeconomic conditions, profit security, taxation), it is also affected by intrinsic and extrinsic factors. Extrinsic factors in urban areas are closely related to the spatial distribution of goods and needs. Because of that, the existence of infrastructure (access to public services and transportation, the existence of basic commercial services, etc.) and the environment (social context, noise level, clean water, etc.) in the spatial context become very important for marketing experts. As a result, extrinsic factors play a very large role in determining the geographical distribution of land prices. Land prices in Indonesia are not set by the government, the market price of land adheres to a closed market and is only known to the seller and the buyer. The determination of land prices carried out by the government depends on the Tax Object Sales Value (Nilai Jual Objek Pajak-NJOP) which is a reference for assessing land prices. However, this NJOP often does not reflect the actual land price.

The land price in Manado is considered very attractive because in recent years there has been an upward trend along with the development of the city's public service infrastructure. In particular, public facilities and infrastructure in the downtown Central Business District (CBD) include government offices, education and health services, several crowd centers, etc. The economic theory of classical urban land states that distance is one of the most important factors that determine the land price. Along with the increasing land prices inside the CBD where workers and business people gather, land prices around the CBD also increase as the distance to the destination decreases, resulting in higher accessibility and reduced travel costs. So, it is not surprising that the land price in the vicinity of Manado's CBD has increased due to the accessibility of public service infrastructure. To explore the idea of land prices, it is very important to understand their relationship with the accessibility of public service infrastructure.

Some studies on land prices and external factors have been done before, for example, Cellmer et al. (2014) used 5 variables (land use, ownership status, infrastructure, geometric configuration, and noise level), Du and Mulley (2012) used 3 variables (property data, transportation access-infrastructure, and socio-economic data), while Jiao and Liu (2012) used 3 variables (economic index, location, and infrastructure). In general, extrinsic variables that influence land prices were used in these studies, including the proximity of infrastructure locations. Manganelli et al. (2013) stated that extrinsic factors in the form of infrastructure, accessibility of specificpublic services, and availability of basic commercial services are very important in determining land prices. Grace and Saberi (2018) measured the accessibility of infrastructure for a certain location using spatial autocorrelation (Moran's I) followed by an Ordinary Least Square model. Chen (2018) studied land price differentiation and its factors in Guangdong, China using Exploratory Spatial Data Analysis (ESDA) and GWR methods. Apart from the mentioned factors, topography (e.g. valleys, slopes, earthquake traces, etc.) also has a significant influence on land prices (Kok 2011). However, it was not considered in this study.

Because determining bandwidth is very important to analyze the geographical distance correlation of land prices, bandwidth optimization became the main objective of the study. After that, the obtained bandwidth wasused to model the land price in Manado. This means that the GWR model is based on a correlogram matrix (covariance function) which is not the same as the matrix used so far.

MATERIALS AND METHODS

The use of accurate samples and data is very important for carrying out statistical analysis and interpreting the results. Inthis study, land prices in the city of Manado are expected to correspond to extrinsic factors, particularly to the accessibility of infrastructure from the observation sites. This land price model was developed using 150 sample locations.

RESEARCH AREA

This research was carried out in Manado city which is the capital of North Sulawesi province (Indonesia). Geographically, Manado is located on Manado Bay and surrounded by mountainous terrain. Based on BPS (Central Bureau of Statistics) data (Statistics of Manado Municipality, 2018), in 2017 the city had a population of430133 in habitants. The large population in Manado leads to a high population density. With an area of 157.26 km^2, the population density reaches 2736 people/km^2. The city of Manado is located at the edge of the northern peninsula of the island of Sulawesi, at 124°40' - 124°50' East and 1°30' - 1°40' North.

Fig. 1. Location of the study area in Manado City, North Sulawesi Province, Indonesia

ACCESSIBILITY

Location accessibility is a very important element of external factors that affect land prices. In a very general sense, the word accessibility refers to the ease of reaching potential destinations from certain locations using certain transportation systems. There are various approaches to measure accessibility depending on the objectives of the research. Continuous measurement (Hansen/Gravity Accessibility Measurement) is known as a robust approach to measure general accessibility for a particular service. For example,for education accessibility,the closest distance can be usedas a potential approach to measure accessibility because each student generally wants to live in areas that are near educational facilities.

Because of this, four accessibility variables that are expected to affect land prices in the city of Manado were used, i.e. the accessibility of government offices, educational accessibility, shopping center accessibility and hospital accessibility. The locations for the four variables are shown in Figure 2 (b). For the Government Office Accessibility, there were two locations of government offices used in this study, i.e. the Governor's office and the Mayor's office (red). For Education Accessibility, there are three major tertiary education locations in the city of Manado, including two public and one private institution (blue). For the Accessibility to Shopping Centers, there are 8 shopping center locations divided into modern shopping centers and traditional shopping centers (green). For Hospital Accessibility, there are 7 hospitals where 4 hospitals are owned by the government and 3 hospitals are owned by private parties (yellow). All 150 studied land locations are close to the highway, as well as the locations of infrastructure corresponding to the four variables that are considered to affect land prices.

GWR MODEL

GWR is a technique that brings the framework from a simple regression model to a weighted regression model (Fotheringham, et al. 2002). As a result, it produces a local linear regression model that generates a local parameter estimator model for each point or location where the data is collected. In a GWR model, the dependent variable is predicted by an independent variable whose respective regression parameter values depend on the location where the data is observed. AGWR model can be written as follows:

$$y_i = \beta_0(u_i, v_i) + \sum_{k=1}^{P} \beta_k(u_i, v_i) x_{ik} + \varepsilon_i \quad (1)$$

Where y is the estimated value of the dependent variable for observation i, x_{ik} is the value of the k^{th} variable for i, (u_i,v_i) is the coordinate location of i, β_0 is the intercept, $\beta_k(u_i,v_i)$ is the regression parameter of i, ε_i is the error term with iid assumption.

The purpose of GWR is to estimate these parameters for each independent variable X and for each geographical location i. The GWR estimation procedure is as follows: (i) drawing a circle of a given bandwidthh around one particular location i (center), (ii) calculating the weight for each neighboring observation according to its distance to the center, and (iii) estimating the model coefficient using the least-squares regression. As a result,the estimation of each row uses the equation:

$$\hat{\beta}(i) = (X^T W(i) X)^{-1} X^T W(i) Y \quad (2)$$

where X is the data matrix of the independent variable, Y is the vector of the dependent variable, $W(i)$ is the geographical weight matrix for the center $i = diag\,[w_{i1}, w_{i2}, \ldots, w_{in}]$.

W_i can be written as $W_i = f(d_i, h)$, where $f(.)$ is a spatial kernel function, d_i is a vector of the distance between the center i and all neighbors, and h is the bandwidth or decay parameter. The fixed spatial kernel function that was used in this study to describe the geographical weight matrix W is the Gaussian descending distance kernel function:

$$[K(r)] = exp(-0.5(d_{ij}/r)^2) \quad (3)$$

The fixed kernel function assumes that the bandwidth in each centre i is constant in all observation areas. If locations i and j intersect, then $w_{ij}=1$, where w_{ij} is decreasing following the Gaussian curve along with the increasing d_{ij}. The weight is not zero for all data points, no matter how far all the points are from the center i (Fotheringham et al., 2002).

BANDWIDTH SELECTION: COVARIANCE FUNCTION

To estimate bandwidth, we propose using a covariance function. The used covariance function must be valid, meaning that it should have positive definite characteristics (Golinski, 2018). Weku et al.(2019a) showed that the exponential and Bessel functions are valid and positive definite. The Gaussian-type covariance function is given by:

$$C_{Gau-type}(h) = \exp\left(-\frac{h}{r}\right)^m \quad (4)$$

for m=1, the equation becomes an exponential function and can be rewritten as

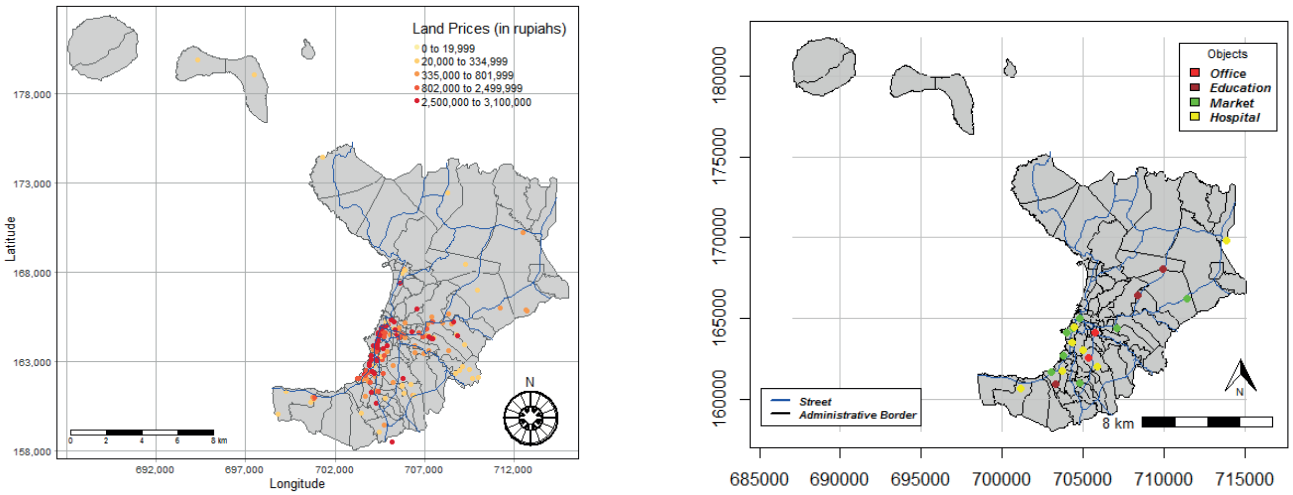

Fig. 2. (a) The distribution of land prices in the study area, (b) The locations of government offices, universities, shopping centers and hospitalsas independent variables

$$C_{\exp}(h) = \exp\left(-\frac{h}{r}\right)^1 \quad (5)$$

The Bessel covariance function can be written as

$$C_{bessel}(h) = \sum_{k=0}^{\infty} J_0\left(\frac{kbh}{\omega}\right)^1 \quad (6)$$

Based on the principle of linear combination, the Bessel-Gaussian type covariance function can be written as follows:

$$CF = \sum_{k=1}^{2} J_0\left(\frac{kbh}{\omega}\right) exp\left(-\left(\frac{h}{\omega}\right)^1\right) \quad (7)$$

where J_0 is a Bessel function, k is a base, scalar b represents nodes of the wave, h is the longest distance of locations, while ω is a parameter related to the distance (i.e. 1/3.h).

The following steps will show that both functions are valid. We will show that the exponential function is definite positive(valid) as shown by Schoenberg (only the first proof).

Proof. Taking corollary in Schoenberg (1937), it is stated that if $\Phi(x)$ is homogeneous and such that $e^{-\phi}$ is positive definite then $e^{-\phi\gamma}$ is also positive definite for $0<\gamma<1$.

Furthermore, we know that e^{-x^2} is a positive definite by virtue of its formula and properties. Consequently $e^{-|x|^{2\gamma}}$ is positive definite for $0<\gamma<1$.

As we know, valid positive definite functions are finite. Weku (2019b) makes it clearer by showing that the Bessel function is positive definite (valid) because it has an exponential upper bound. Based on the Weierstrass principle, because the exponential function is positive definite, the Bessel function is also positive definite.The relationship between the Bessel functions bounded by the exponential function can be written as follows:

$$|J_v(x)| \le \frac{1}{v!}\left(\frac{|x|^v}{2}\right) exp\left(\frac{|x|}{2}\right)^2$$

It is known that the exponential and Bessel covariance functions are valid and meet definite positive conditions. This means that the covariance function can be used as a correlogram to determine spatial geographic distances of land prices in Manado.

RESULTS AND DISCUSSION

The results and discussion section can be divided into two parts, the first part focuses on selecting bandwidth from several existing methods and in the second part, the optimal bandwidth is used in GWR modeling. Three methods for determining bandwidth were considered in this study, i.e. AICc, CV and Covariance Function (proposed method). The equations for calculating bandwidth with the AICc and CV methods can be written as follows (Mennis, 2006):

$$AIC_c = 2n\log_e(\hat{\sigma}) + n\log_e(2\varphi) + n\left\{\frac{n+tr(S)}{n-2-tr(S)}\right\}$$

$$CV = \sum_{i=1}^{n}\left(y_i - \hat{y}_i\right)^2$$

The results of calculations using the Covariance Function are displayed in Figure 3, where the value of covariance is plotted against distance. The intersection between the covariance curve and the distance axis represents geographical distance.The first intersection with the distance axis is the optimal bandwidth because it illustrates the strength of the correlation around the origin. After that, the correlation weakens which does not reflect the strength of the correlation.

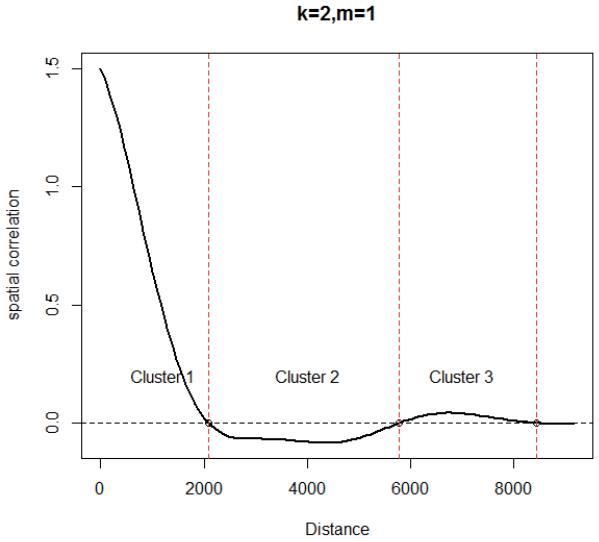

Fig. 3. The Optimal Geographical Distance of land prices in Manado

The three methods for calculating bandwidth were implemented using R software. The results of the bandwidth calculation are presented in Table 1. The largest bandwidth was found by AICc while the smallest one was found by the Covariance Function. Three parameters were calculated to determine the appropriate bandwidth for spatial dependence of land prices, namely R2 (adjusted), R2 and AIC. The appropriate model was then selected based on the largest R2 (adjusted) and R2 values as well as the smallest AIC value.

Table 1 presents three different bandwidth estimates, where the bandwidth of the covariance function is the smallest while the bandwidth of AICc is the largest. The bandwidth of 2091.351 meters obtained from the Covariance Function calculation is the optimal bandwidth because it has the largest coefficient of determination R2 (adjusted), which is equal to 0.5022. Conversely, the bandwidth values provided by AICc and CV with low coefficients of determination (0.2571 and 0.2614, respectively) have a low ability to explain the land prices. Even though the AIC values are almost the same for the

Table 1. The assessment of various bandwidth selection methods

Assessment	Bandwidth Selection Methods		
	Covariance Function	AICc	CV
	2091.351 meters	5452.273 meters	4736.107 meters
R2(adjusted)	0.5022	0.2571	0.2614
R2	0.3786	0.3033	0.3130
AIC	4579.152	4554.265	4554.101

three bandwidths, we can state that the model that uses the bandwidth of the covariance function reproducesthe actual land price dataand out performs AICc and CV methods. As a result, we chose a bandwidth of 2091.351 meters to model land prices using GWR.

ESTIMATED COEFFICIENT OF THE GWR MODEL

GWR software provides results in the form of information on spatial variation. Table 2 illustrates descriptive statistics generated by GWR with a bandwidth of 2091.351 meters. The values calculated for quartiles represent the variability of land prices witheach variable.

SPATIAL CHARACTERISTICS OF THEESTIMATED COEFFICIENT

The results of the GWR model forthe four variables (accessibility to government offices, universities, market centers, and hospitals) were mapped as shown in Figure 4 to see spatial variation and analyse the effects of infrastructure accessibility factors on land prices. The coefficients of the GWR model estimated using the fixed kernel function are concentrated in the downtown area.

Figure 4(a-d) shows the results of parameter estimation using different colors and gaps between variables. Values of local parameters are colored in such a way that positive values are represented in red, negative values are represented in white and yellow corresponds to values around zero. It is very clear from the map that all parameters indicate spatial variation, especially the government variable.

In Figure 4a, which shows local parameter estimates for the Government Office variable, it is very clear that there is spatial variation in land prices throughout the area. The coefficient will be positive in most areas that are centralized and negative in some of the outermost observation areas. This means that land prices are strongly influenced by the accessibility of the governor's and mayor's government offices. The geographical center shows that local parameters

Table 2. Results ofGWR coefficient estimation with a bandwidth of 2091.351 meters

	Min.	1st Qu.	Median	3rd Qu.	Max.
Intercept	-178403	1942007	2032163	2300653	2585733
Gov	-1024.790	229.355	428.058	491.648	516.030
Univ	-270.658	-140.124	-86.586	-43.555	164.040
Market	-618.881	-531.782	-464.042	-424.350	1413.650
Hospital	-558.326	-443.590	-409.258	-361.990	772.020

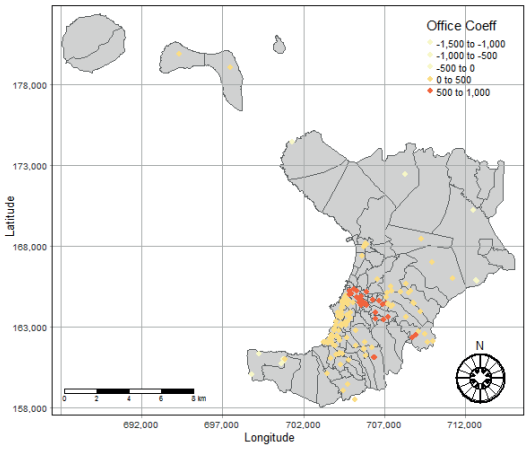

a. map of parameter estimates with variable Office

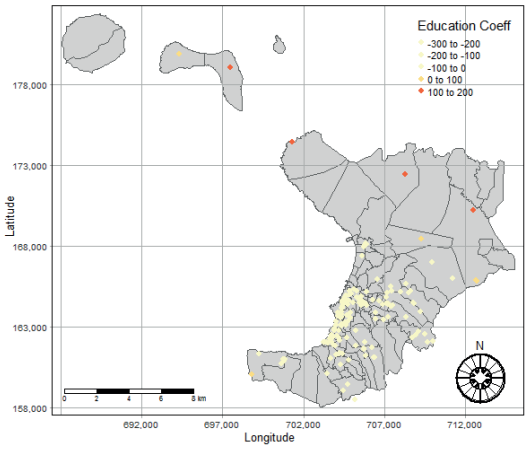

b. map of parameter estimates with variable Education

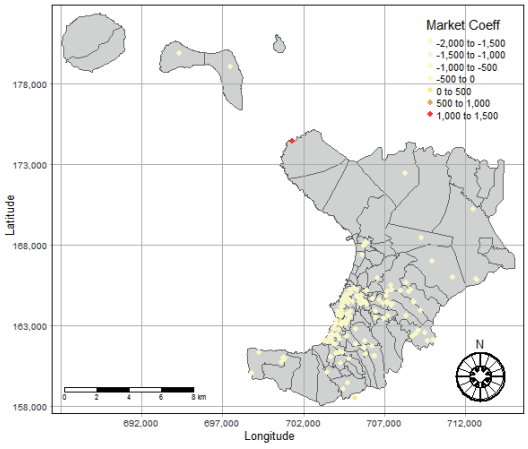

c. map of parameter estimates with variable Market

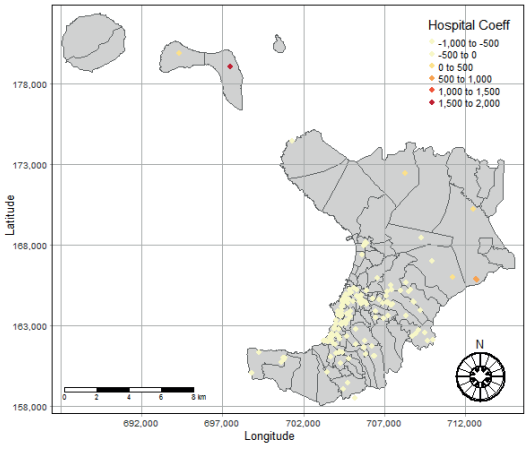

d. map of parameter estimates with variable Hospital

Fig. 4. Map of parameter estimates for each variable (Government Office, Universities, Market Centers and Hospitals)

are significant positive indicating that proximity to the Government Office will increase the price of land in urban centers. In the outermost region, parameters are significant negative even in small amounts. The negative parameter value meansthat the low accessibility of the Government Office leads to a negative increase in land prices in these locations.

This means that land prices in each location are strongly influenced by the presence of the governor's and mayor's government offices. The land that is closer to the office is more expensive, while the price of the land located far from the office center is lower due to the lack of government facilities.

Meanwhile, Figures 4b, 4c, and 4d show that there are clear spatial variations in local parameter estimates for the Education, Shopping, and Hospitals variables through out the observation area. The general pattern is the same, higher access to these facilities (resulting in decreasing travel time due to shorter distances) will result in increased land prices. However, there is a large area that is shown in Figures 4b, 4c, and 4d where local parameters are significant negative. This area covers a large part of Manado city and approaches the city center. All regions with a negative relationship between the three distance variables andland prices are inverse to the regions that have access to Government Office facilities shownin Figure 4a.

In this study, it was shown that bandwidth estimated using the covariance function gives very good results and outperforms the traditional methods (AICc and CV). It was found that the location of government offices, in this case, the governor's office and the mayor's office, has a significant influence on the increase in land prices. This suggests that residents of Manado city are still dependent on government services. On the other hand, land prices are not too dependent on education, health, and market service facilities because there is a variety of options that are spread evenly through out the city.

As explained earlier, the government does not perform open regulation of land prices, resulting in the sale and purchase of land carried out in a closed manner between the seller and the buyer. Research on land price prediction using the GWR model has provided a new approach that can assist the government in determining land prices based on the proximity of the observed land locations to various facilities. In this approach, land prices can be adjusted at any time depending on the variables used in the model. As a result, the government and community will have the same understanding in determining the land price so that people willno longer need to make closed sales. The results of predictive mapping using contour maps present land prices that can be used as an open reference for the community in addition to the NJOP provided by the government. Currently, the land price in a location varies according to the assessment of each person as everyone can sell their land based on their assumptions. As a result, land prices become uncertain because they are not set openly by the government, which can lead to the practice of selling land in discriminately by speculators.

CONCLUSIONS

Determination of optimal bandwidth is fundamental and crucial formodeling the spatial dependence of land prices using GWR. This study has shown that using the Covariance Function to determine bandwidth provides a large coefficient of determination R2 (adjusted) when compared to the bandwidth calculated using the AICc and CV methods.This means that the bandwidth produced by the Covariance Function is suitable for modeling land prices in Manado.

Determining land prices without taking into account their spatial dependence can cause errors. The development of spatial statistical techniques based on Geographically Weighted Regression can help to overcome these errors and provide a better analysis of land prices. In this study, the GWR technique was applied to analyze land prices in the city of Manado and determine the homogeneous locations.The results provided by the local GWR model revealed the relationship between thespatial variation ofland prices and the variables usedin the model. Mapping of the results showed that accessibility of Universities, Market Centers and Hospitals affect land prices with negative parameter estimates, while Government Office accessibility has positive parameter estimates. Determination of the appropriate model to describe land prices can also be done using the AICc assessment, which shows that the Hospital variable has the greatest influence on the price of land in the city of Manado. This selection is based on the smallest AICc value, which is followed by the Government Offices, Universities and Market Centers variables.

REFERENCES

Abebe T.D., Naz A.A., and L´eon J. (2015). Landscape genomics reveal signatures of local adaptation in barley (Hordeum vulgare L .). Frontiers in PlantScience, October.

Bidanset P.E., Lombard J.R. (2014a). Evaluating Spatial Model Accuracy in Mass Real Estate Appraisal: A Comparison of Geographicaly Weighted Regression and the Spatial Lag Model. Cityscape: A Journal of Policy Development and Research, 169-182.

Bidanset P.E., Lombard J.R. (2014b). The Effect of Kernel and Bandwidth Spesification in Geographicaly Weighted Regression Models on the Accuracy and Uniformity of Mass Real Estate Appraisal. Journal of Property Tax Assessment & Administration, 5-16.

Bjørnstad O.N., Chr.Stenseth N., and Saitoh T. (1999). Synchrony And Scaling In Dynamics Of Voles And Mice In Northern Japan. Ecology 80, 2, 622-637.

Brundson C., Fotheringham A.S., Charlton M. (1999). Some Notes on Parametric Significance Testa for Geographically Weighted Regression. England: John Wiley & Sons Ltd.

Cellmer R., Belej M., Zrobek S., Kovac M.S. (2014). Urban Land Value Map - A Methodological Approach. Geodetski Vestnik, 535-551.

Du H., & Mulley C. (2006). The Relationship Between Transport Accessibility and Land Value: A Local Model Approach with Geographically Weighted Regression. Transportation Research Record: Journal of the Transportation Research Board, 197-205.

Du H., Mulley C. (2012). Understanding spatial variations in the impact of accessibility on land value using geographically weighted regression. The Journal of Transport and Land Use, 46-59.

Farber S. and Paez A. (2007). A systematic investigation of cross-validationin GWR model estimation: empirical analysisand Monte Carlo simulations, J. Geograph Syst., DOI: 10.1007/s10109-007-0051-3.

Fotheringham A.S., Brundson C., Charlton M. (2002). Geographically Weighted Regression: the analysis of spatially varying relationships. England: John Wiley & Sons Ltd.

Golinskii L., Malamud M., Oridoroga L. (2018). Radial Positive Definite Functions and Schoenberg Matrices with Negative Eigenvalues, Transactions of the American Mathematical Society, 370.

Grace R., and Saberi M. (2018). The value of accessibility in residential property.In Australasian Transport Research Forum 2018 Proceeding, 1-17.

Hetmanski T., Bochenski M., Tryjanowski P., and Sk´orka P. (2010). The effect of habitat and number of inhabitants on the population sizes ofFeral Pigeons around towns in Northern Poland. European Journal of WildlifeResearch, 421-428.

Kok N., Monkkonen P., Quigley J.M., (2011). Economic Geography, Jobs, and Regulations: The Value of Land and Housing, Journal of Urban Economics.

Leong Y.Y., Yue J.C. (2017). A modification to geographically weighted regression, International Journal of Health Geographics, 16(11), DOI: 10.1186/s12942-017-0085-9.

Leung Y., Me C-L., Zhang W-X. (1999). Statistical tests for spatial nonstationarity based on thegeographically weighted regression model, Environment and Planning A, (32) 9-32, DOI:10.1068/a3162.

Liu Z., and Wimberly M.C. (2015). Climatic and Landscape Influences on Fire Regimes from 1984 to 2010 in the Western United States. PLOS ONE.

Manganelli B., Pontrandolfi P., Azzato A., Murgante B. (2013). Urban Residential Land Values Analysis: The Case of Potenza. ICCSA 2013, Part IV, LNCS 7974 (304-314). Springer-Verlag Berlin Heidelberg.

Mennis J. (2006). Mapping the Results of Geographically Weighted Regression, The Cartography Journal, 171-179.

Schoenberg I.J., (1937). Metric Spaces and Positive Definite Functions, Trans. Amer. Math. Soc. 522-536.

Weku W., Pramoedyo H., Widodo A., Fitriani R. (2019a). Positive Definite Functions of Non MonotonVariogram to Define the Spatial Dependency of Correlogram, AIP Proceedings,The 8th SEAMS-UGM Conference.

Weku W., Pramoedyo H., Widodo A., Fitriani R. (2019b). Non MonotonCorrelogramTo Identify The Radius Of Spatial Dependence On Land Prices, Journal of Urban and Regional Analysis.

RESEARCH PAPER

CHANGE DETECTION OF VEGETATION COVER USING REMOTE SENSING AND GIS – A CASE STUDY OF THE WEST COAST REGION OF SOUTH AFRICA

Clive Coetzee[1]
[1]Faculty of Military Science, University of Stellenbosch, Private Bag X2, Saldanha, 7396, South Africa
***Corresponding author:** clivecoetzee@sun.ac.za
Received: June 14th, 2021 / Accepted: April 24th, 2022 / Published: June 30th, 2022
https://DOI-10.24057/2071-9388-2021-067

ABSTRACT. This article investigates the possible permanent vegetation cover (VC) change over an extended time for five municipal regions in South Africa by applying satellite-acquired remote sensed normalized difference vegetation index (NDVI) values within a geographic information system (GIS), spatial (West Coast District) and time (1981 to 2019 and 2000 to 2020) context. The NDVI index measures surface reflectance and give a quantitative estimation of vegetation growth and biomass. The study found relevance in its application since VC change detection has taken prominence over the past number of years in terms of sustainable development. Methods of analysis include image mapping, temporal image differencing, Moran I statistic, and the Mann-Kendall trend test. In the main areas that recorded significant changes in their NDVI values (plus or minus 0.4 difference on their original NDVI value) over time, in general, have experienced substantial and permanent VC change. These areas are also spatially clustered and concentrated within specific areas within the wider district. However, these areas constitute only a minority of areas (less than 20%), whereas most of the areas within the district did not experience such significant and permanent change in VC. Instead, the changes that did occur in these majority of areas were related to seasonal variation, i.e., temporal changes.

KEYWORDS: NDVI, NOAA, MODIS, vegetation cover, change detection

CITATION: Coetzee C. (2022). Change Detection of Vegetation Cover Using Remote Sensing and GIS – A Case Study of the West Coast Region of South Africa. Geography, Environment, Sustainability, 2(15), p. 91-102
https://DOI-10.24057/2071-9388-2021-067

Conflict of interests: The authors reported no potential conflict of interest.

INTRODUCTION

Vegetation Cover (VC) is most probably not a stable or constant phenomenon and presumably ebbs and flows over time. These changes could purely be seasonal or could be more permanent, i.e., the changes in VC may be short to medium term or could be long lasting. To this end, Alawamy et al. (2020) state that a great many of studies reveal that hardly any terrains on earth, in outlying places and isolated regions, are enduring in their unaffected environment.

VC change detection becomes very relevant when given the significance and relevance of VC change for economic development and planning and policy formulation. As Das and Angadi (2021) put it, "Exact statistics on how fast or slow VC transform and urban growth is crucial for the sustainable development and management of natural resources". This view is echoed by Alawamy et al. (2020) stating that our appreciation and mapping of VC change have preoccupied a relevant and significant bearing in policy-making in terms of the management of the world's natural resources as well as the monitoring of environmental changes.

It, therefore, seems plausible that the monitoring of VC change dynamics should be instrumental in the effectual planning and sustainable development of expanding economies. To this end, the NDVI is one of the more appropriate classification methods commonly adopted in exploring VC change (Aburas et al., 2015; Lunetta et al., 2006). Given that vegetation and, in particular, vegetation growth and biomass are in general regarded as the principal proxy of VC (Di Gregorio and Jansen 2000), the quantitative analysis regarding changes in its composition, biomass and vigour based on multispectral remote sensing assist in land cover change detection.

Remotely sensed NDVI features came to be extensively applied for VC change detection (for example, Mbatha and Xulu, 2018; Alphan and Derse, 2011; Cihlar, 2000). Rogan and Chen (2004) and Deng et al. (2008) described digital change detection as "the process of determining and/or describing changes in VC properties based on co-registered multi-temporal remote sensing data." Ayele et al. (2018) and Zhao et al. (2004) elaborate on the above statement proposing that the main focus of the change detection process based on digital images is to mathematicise the VC change for divergent features of interest for different time resolutions.

Gandhi et al. (2015) and Aburas et al. (2015) also note that the assessment of change detection is a desirable method of representing the changes detected in the various land use categories. The studies employed the NDVI technique with different threshold values for features extraction by calculating the percentage of land use per land cover and the associated change over time. Sahebjalal and Dashtekian (2013) detected the locations where the land cover has changed by subtracting the 2006 NDVI

image values from the 1990 NDVI image values. The derived 10% change threshold image, i.e., image displaying only the 10% decrease or increase in NDVI values, were presented.

According to Meneses-Tovar (2012), the NDVI can be used as a proxy for computing the difference between the energy received and emitted by earth phenomenon. The NDVI can be estimated by incorporating the Red and Near Infra-Red (NIR) bands of a sensor system, typically from Landsat satellites. The NDVI approach is based on the proposition that healthy/unhealthy vegetation has low/high reflectance rates of the electromagnetic spectrum's visible side. This is true because of the presence of high levels of chlorophyll. In addition to the above, Firl and Carter (2011) published a detailed tutorial on deriving Vegetation Indices (VI) from Landsat 5 Thematic Mapper and Landsat 7 Enhanced Thematic Mapper.

Given the fact that the NDVI index can be viewed as a dominant indicator that can be used in detecting the physical material at the surface of the earth over time intervals and in defined locations utilizing the remote sensing technique, the purpose (aim) of this study is to utilize the remote sensed NDVI over two periods (1982 to 2019 and 2000 to 2020) for five municipal regions located on the West Coast of South Africa as a change detection function to differentiate whether or not such changes have been permanent (long-lasting) in nature or not.

The article has been structured in the following way: Section 2 puts forward a brief background to calculating the NDVI, the study approach, the data generation process, and the study area. Section 3 focuses on the geographical information system (GIS), spatial, time, and trend analysis using the NDVI in point pattern methodology. Reconciling the findings of the vegetation temporal change analysis is the focus of Section 4. In the final section, a summary and conclusion are provided.

MATERIALS AND METHODS

Study Area

Five municipal regions were chosen for this study. There are no particular reasons for this choice, and it is purely by default. These five municipal regions are:

Swartland (size = 3 700 km^2)
Bergriver (size = 2 015 km^2)
Saldanha Bay (size = 4 407 km^2)
Cederberg (size = 8 007 km^2)
Matzikama (size = 12 981 km^2)

The municipal regions (right panel) within the South African context (left panel) are displayed in Figure 1. The district (municipalities as a collective) are located on the West Coast of South Africa within the Western Cape Province (red boundary).

The district is bordered by the Atlantic Ocean on the west and the Swartland region on the east. As such, the district is characterised by a low winter rainfall which decreases rapidly northwards, from 400 mm in the Swartland region to less than 100 mm in the Matzikama region. Because of dry summers, the Region has a distinct vegetation of grasses, shrubs, and trees. As part of the Cape Floral Kingdom, the Region is home to thousands of species of plants, including fynbos which is indigenous to the Region and found nowhere else in the world.

Overall, the Regional climate is typically Mediterranean, with warm, dry summers and mild, wet winters and low summer rainfall prevail. Near the coast, summer's temperature rises from a pleasant low of 15° C to a heart warming 27° C. Inland temperatures are some 3-5° C higher. Coastal winters see the mercury dropping to a mild 7° C at night and rising to a comfortable 18° C by day. Away from the beach, morning wakens to an invigorating 5° C and midday peaks at 22° C. Because of the Indian and Atlantic oceans' influence, inland and coastal temperatures differ over short distances, and macro- and micro climates are created.

Methods

According to Wu et al. (2016) and Zhang et al. (2013), NDVI can be used as a measure or proxy of surface reflectance and offer a quantitative estimation of vegetation health, i.e., vegetation growth and biomass. In general, healthy vegetation (greater levels of chlorophyll) reflects greater levels of near-infrared (NIR) and green light in relation to other wavelengths. However, greater levels

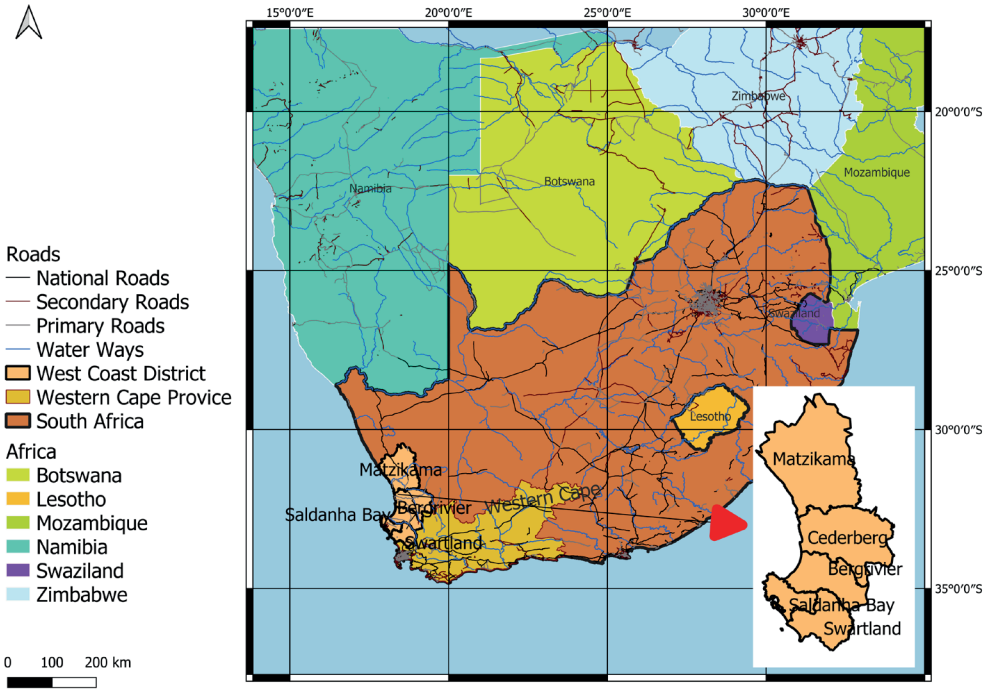

Fig. 1. Regions with the South African Context

of red and blue light (RED) are absorbed. A plant is green as observed by the human eye, since the chlorophyll pigment in it reflects the green waves and absorbs the red waves. Consequently, a healthy/unhealthy plant - one with many/few chlorophyll and cell structures - actively absorbs/reflects red light and reflects/absorbs NIR. The exact opposite will be true for an unhealthy plant. To this end space-based satellite sensors measure wavelengths of light absorbed and reflected by green plants.

The index defined values ranges from -1.0 to 1.0, portraying greens, where negative values are mainly formed from clouds, water and snow, and values close to zero are primarily formed from rocks and bare soil. Values 0.1 or less match empty areas of rocks, sand or snow. Values between 0.2 to 0.4 represent shrubs and meadows, while values ranging from 0.6 to 0.8 represent temperate and tropical forests (Wu et al., 2016; Zhang et al., 2013).

The NDVI derived values per location will be presented analyzed in a Geographical Information System (GIS) context. Visualizing the NDVI values gives a perspective of the state of vegetation cover in the Region and notably the historical trend and changes thereof at a very decentralized level. In the main, the analysis was performed in Excel, EVIEWS, and QGIS.

To test or assess the possible prevalence of spatial autocorrelation the study employed the Global Moran I index. According to Sowunmi et al. (2012), the global spatial autocorrelation (Moran I) analysis supply applicable statistics to capture the sequence of NDVI values in the Region of interest. Homogeneity of the Region of interest (the locations displays the same NDVI patterns) were assumed. Spatial clustering of similar values across geo-space are associated with positive Moran I values. Negative and significant values proposes that neighbouring values are more distinct than expected by chance. This suggest that high values are often found near low values. An advantage of using the Moran I is that its maximum and minimum possible values are not forced within the (–1, 1) range, unlike the Pearson product-moment correlation coefficient, for example. The Moran's I can be calculated as follows(Viton, 2010);

$$I = \left(S / \sum ijwij\right)\left(\frac{\sum ujwij(b_1 - b)(b_j - b)}{\sum i(bi - b)^2}\right) \quad (1)$$

where
S = number of observations
Σijwij= sum over all *i* and *j* of *ωij*
wij = spatial weight between *i* and *j*.
ωij bibj = weight * cross product terms.

To further explore the possible spatial autocorrelation nature of the locations, the study made use of a local indicator of spatial association (LISA) suggested in Anselin (1995). A LISA is seen as having two important characteristics. First, it provides a statistic for each location with an assessment of significance. Second, it establishes a proportional relationship between the sum of the local statistics and a corresponding global statistic. These statistics and relationships are then presented in the form of a cluster map and a significance map. The significance map shows the locations with a significant local statistic, with the degree of significance reflected in increasingly darker shades of green. The cluster map augments the significant locations with an indication of the type of spatial association, based on the location of the value and its spatial lag in the Moran scatter plot.

Following on the possible spatial autocorrelation nature of the locations, the study tested the NDVI behaviour of each location for the existence of possible structural breaks. A structural break occurs when a time series abruptly changes at a point in time and, as such, proposes a fundamental change in the underlying vegetation cover. In time series analysis, the detection of structural breaks can be performed using the cross-section independent and cross-section dependent unit root testing methods. The Dickey-Fuller test has been widely used to detect possible structural breaks and, as such, has been used as well. The presence of a unit root (structural break) in the NDVI of a location or locations suggests that the vegetation cover has indeed fundamentally changed at that location or locations. The testing procedure for the Dickey-Fuller test is applied to the model, i.e.,

$$\Delta y_t = a + \beta_t + \gamma y_{t-1} + \delta_1 \Delta y_{t-1} + \ldots + \delta_{p-1} \Delta y_{t-p+1} + \varepsilon_t \quad (2)$$

where
α = constant term
β = the coefficient on a time trend
ρ = the lag order of the autoregressive process
y = variable under consideration
ε = error term

Supplementing the structural break analysis, the study also employed a trend assessment of the NDVI behaviour of each location. In this regard, the Mann Kendall Trend Test was used to analyze the NDVI behaviour of each location for consistently increasing or decreasing trends. The Mann-Kendall test is used to determine whether a time series has a monotonic upward or downward trend. A mean-reverting NDVI series (irrespective of location) suggest very little, if any, change in the underlying vegetation cover over the period under consideration. However, a mean-reverting series excludes the presence of any significant trend (either upward or downward). Thus, the presence of a trend proposes that the underlying vegetation cover has indeed changed over the period under consideration. The Mann Kendall Trend Test is applied to the model, i.e.,

$$s = \sum_{k=1}^{n-1} \sum_{j=k+1}^{n} \operatorname{sgn}\left(x_j - x_k\right) \quad (3)$$

where
Time Series = *x1, .., xn*
n = length of the sample
xk and *xj* are from k=1, 2, …, *n-1* and *j= k+1*, …, n

$$sgn\left(xj - xk\right) = \begin{cases} +1, if\,(xj - xk) \rangle 0 \\ 0, if\,(xj - xk) = 0 \\ -1, if\,(xj - xk) \langle 0 \end{cases} \quad (4)$$

Data

This study used two remote sensing datasets in both the general and specific approaches. The first dataset is the NOAA CDR AVHRR NDVI: Normalized Difference Vegetation Index, Version 5 dataset (NOAA, 2021 and Vermote et al., 2014). The dataset is available from 1981-06-24 to 2021-03-04 on a daily basis, gridded at a resolution of 0.05°, computed globally over land surfaces and provided by NOAA (NOAA, 2020). The data is generated using the Google Earth Engine Code Editor.

The second dataset is the MOD13Q1.006 Terra Vegetation Indices 16-Day Global 250 m dataset (MODIS, 2021). The data is available from 2000-02-18 to 2021-02-18, twice monthly, gridded at 250 m spatial resolution (pixel size), and provided by NASA LP DAAC at the USGS EROS Centre (USGS, 2020 The data is also generated using the Google Earth Engine Code Editor.

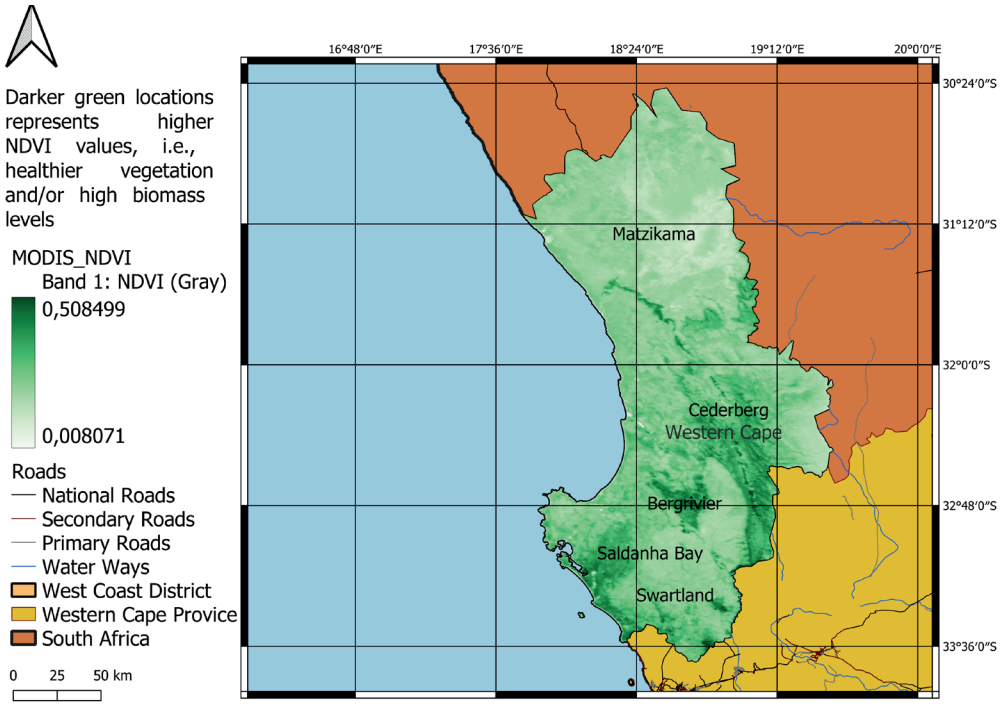

Fig. 2. NOAA and MODIS NDVI Map

The results of the data generation process (both datasets) can be presented as shown in Figure 2. The figure to the left represents the daily average (1981 to 2019) NOAA NDVI value for the district (five regions collective) per granular location, whilst the right figure represents the daily average (2000 to 2020) USGS MODIS NDVI value for the district also per granular level. In both cases, dark green coloured locations represent NDVI values closer to 1, whilst very light green (almost white) coloured locations represent NDVI values closer to 0. As referenced, locations with high NDVI values portray healthy vegetation and/or high biomass levels and vice versa.

Given the size of the district, the study will also make use of point pattern analysis. Therefore, it was necessary to generate random points within each of the regions. The random points in the polygons function in QGIS were used to generate 100 random point-locations in each Region of interest, i.e., 500 point-locations in total. These randomly generated 500 point-locations are displayed in Figure 3. It is relevant to note that some areas were not covered with random points suggesting that the included random points may not be fully representative of the Region as a collective. However, it is worth noting that these areas are mostly nature reserves or high elevation areas, which should, in theory, be relatively immune to significant and permanent vegetation change.

These 500 point-locations were populated with monthly NDVI data from 1981 to 2019 using the NOAA dataset and from 2000 to 2020 using the MODIS dataset using the Google Earth Engine Code Editor. In terms of the two datasets, the following general statistics were presented:

NOAA dataset, 500 point-locations and 448 months (224 000 observations)

MODIS dataset, 500 point-locations and 251 months (125 500 observations)

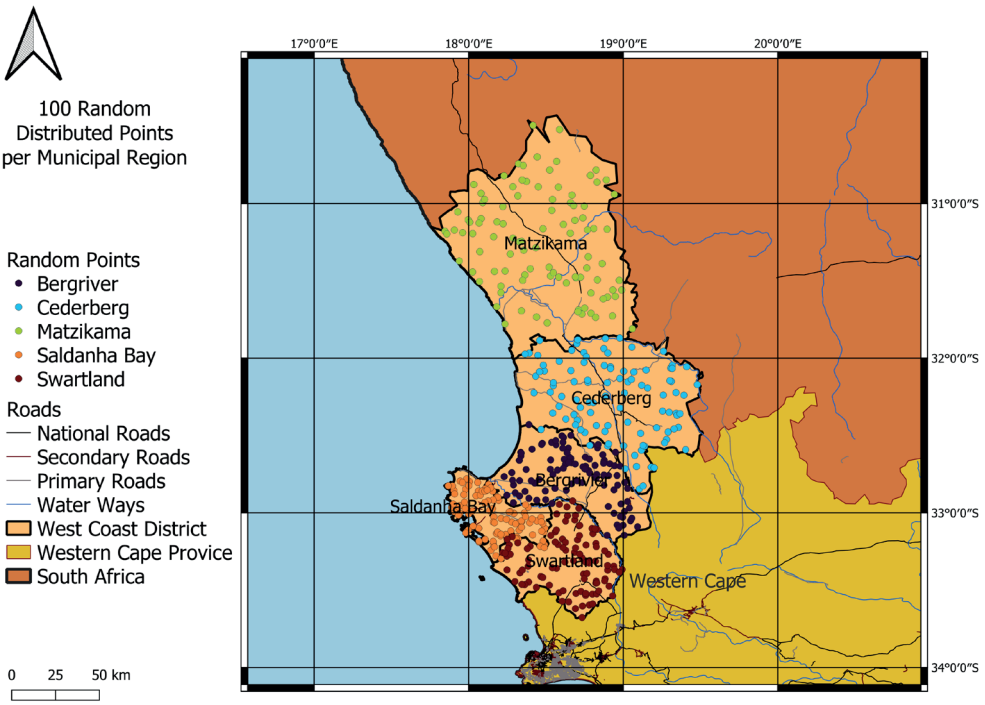

Fig. 3. Random Point-locations

Results - NDVI GIS Analysis

The NOAA and MODIS datasets for the 500 point-locations for the stated periods is presented in panel format in Figure 4 and Figure 5. The mean regional (RegionDemean) and mean district (Regionmean) NDVI values for the NOAA and MODIS datasets are illustrated with the red and green lines, respectively. Point-locations 0 to 44 802, 44 903 to 89 601, 89 602 to 134 401, 134 402 to 179201 and 179 201 to 224 000, represent the Bergriver, Cederberg, Matzikama, Saldanha Bay and Swartland regions with regards to the NOAA dataset, respectively. Point-locations 0 to 25 101, 25 102 to 50 201, 50 202 to 75 301, 75 302 to 100 401 and 100 402 to 125 500, represent the Bergriver, Cederberg, Matzikama, Saldanha Bay and Swartland regions with regards to the MODIS dataset, respectively.

From a time perspective, the two datasets can be presented as set out in Figure 6 and Figure 7. The datasets indicate the monthly NDVI value per point-location (500 point-locations) for the respective periods. The colored lines represenstthe various point locations and given the number of the locations it is not possible to present them in a legend. The seasonal nature of the NDVI values is clearly visible. In general, the datasets seem to contain no significant structural breaks, i.e., fairly constant mean values following a seasonal trend.

Figure 8 displays the temporal difference image (in absolute format) between the average February 2019, 2018, and 2017 and February 1982, 1983, and 1984 NDVI values in terms of the NOAA dataset (left panel) and the temporal difference image (in absolute format) between the average February 2020,2019 and 2018 and February 2000, 2001 and 2002 NDVI values in terms of the MODIS dataset (right panel). Dark green represents significant positive change (increase in NDVI values). In contrast, white represents significant negative change (decrease in NDVI values), suggesting that many locations within the Swartland, Saldanha Bay, and Bergriver regions experienced positive change while most locations with the Cederberg and Matzikama regions experienced negative change.

The global spatial autocorrelation (Moran I) analysis results for the February 1982 and February 2018 periods regarding the NOAA dataset and February 2000 and February 2020 periods concerning the MODIS dataset are displayed in Figure 9 and Figure 10. The Moral I statistics are displayed in the first column showing a value of 0.74

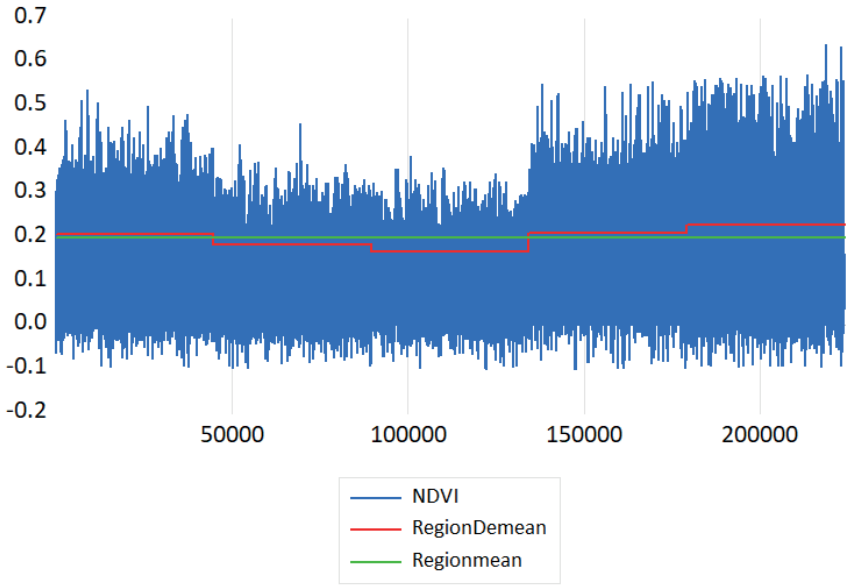

Fig. 4. NOAA NDVI per Point-Location, January 1982 to April 2019

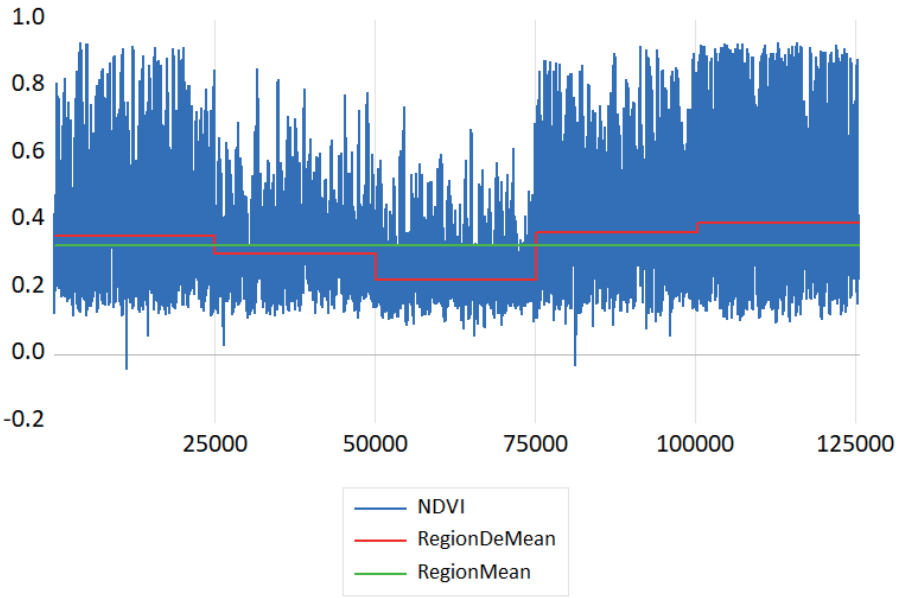

Fig. 5. MODIS NDVI per Point-Location, January 2000 to December 2020

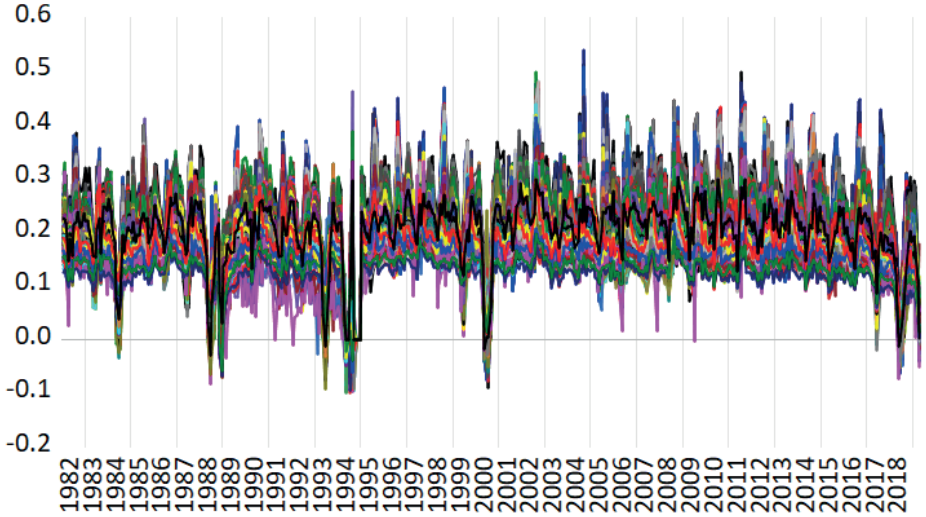

Fig. 6. NOAA NDVI per Month, January 1982 to April 2019

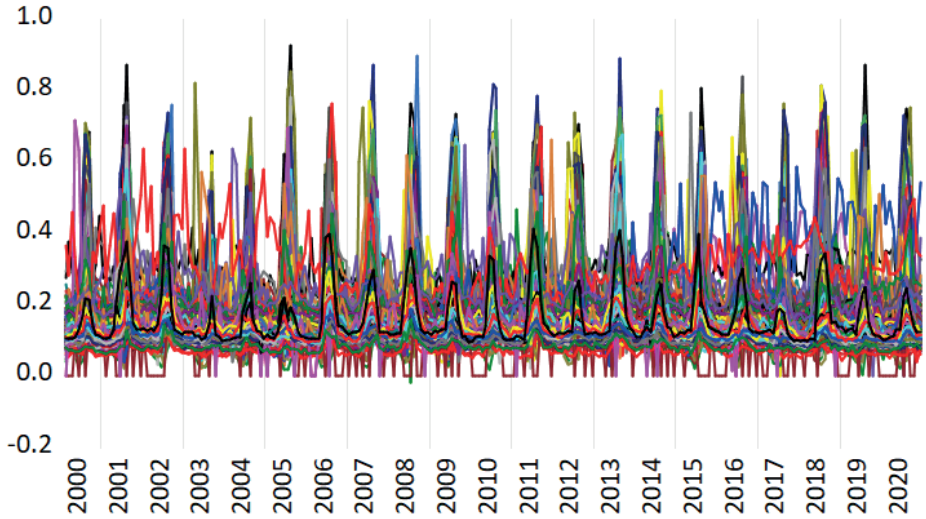

Fig. 7. MODIS NDVI per Month, January 2000 to December 2020

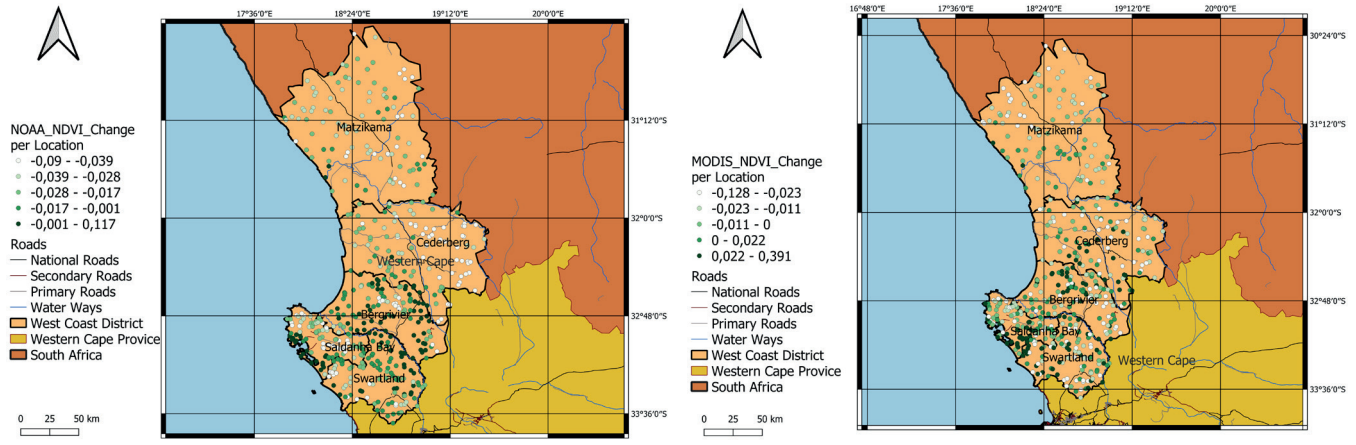

Fig. 8. NOAA and MODIS NDVI Change Visualization

and 0.73 in February 1982 and February 2018, respectively, regarding the NOAA dataset, compared to 0.39 and 0.51 in February 2000 and February 2020 regarding the MODIS dataset. The associated z-values (not indicated) for the four periods suggest a strong acceptance of the alternative hypothesis of spatial clustering. The second column (cluster map) shows that the high NDVI locations bordered by high NDVI locations (high-high clusters in red) are concentrated in the six sub-point-locations (representing around 24 percent of the 500 point-locations). The low-low NDVI point-locations (low-low clusters in blue) are concentrated in the four sub-point-locations (representing about 20 percent of the 500 point-locations). The results (as per the third column = significance map) also show that the NDVI point-locations have not changed much over the two respective periods, irrespective of the dataset, i.e., the point-locations with significant clusters (in green) have not changed over the two periods, regardless of any dataset.

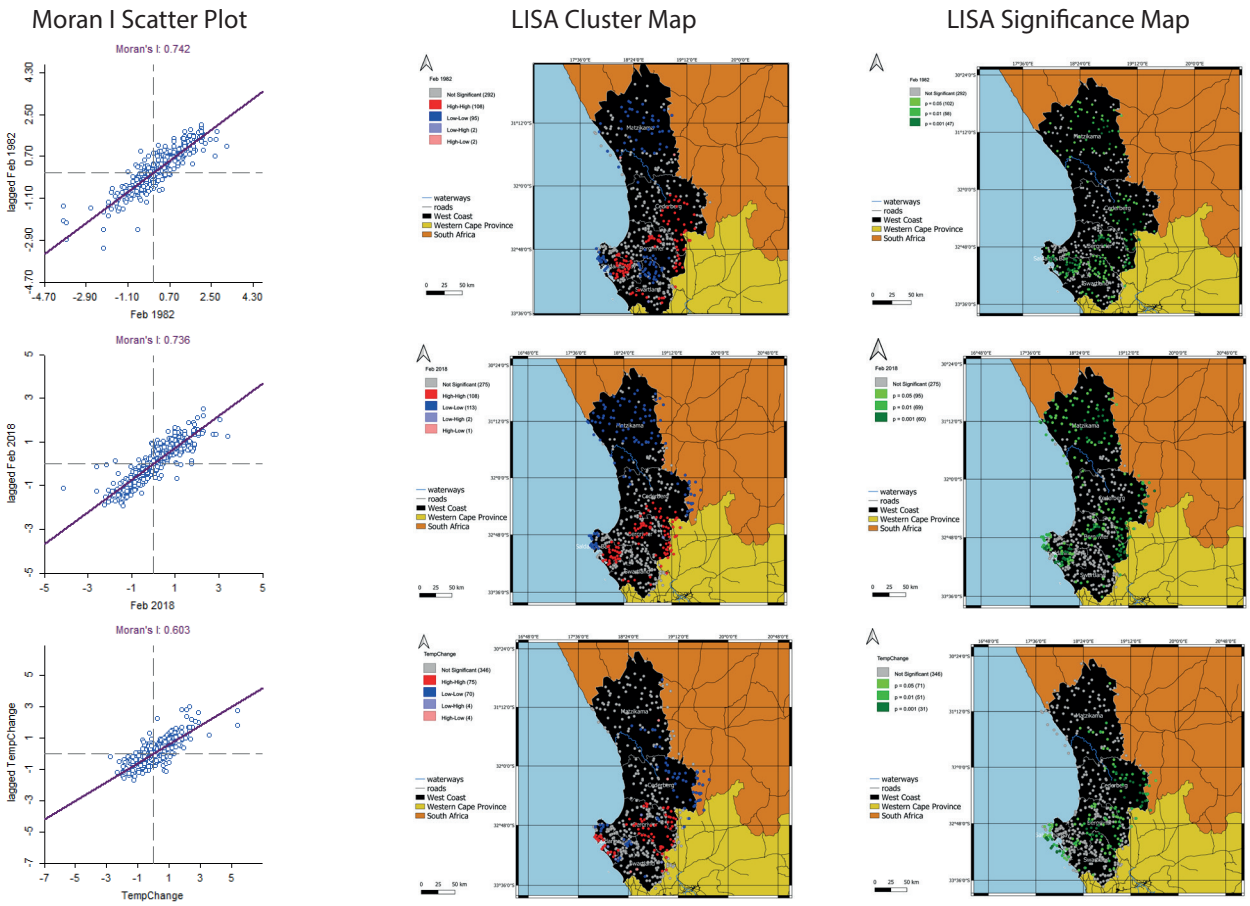

Fig. 9. Moran I, Cluster and Significance Map, February 1982 and 2018 and February 1982 to 2018 (change) NDVI values, NOAA dataset

Note: top row = February 1982, Middle row = February 2018 and Bottom row = February 2018 minus February 1982 (change)

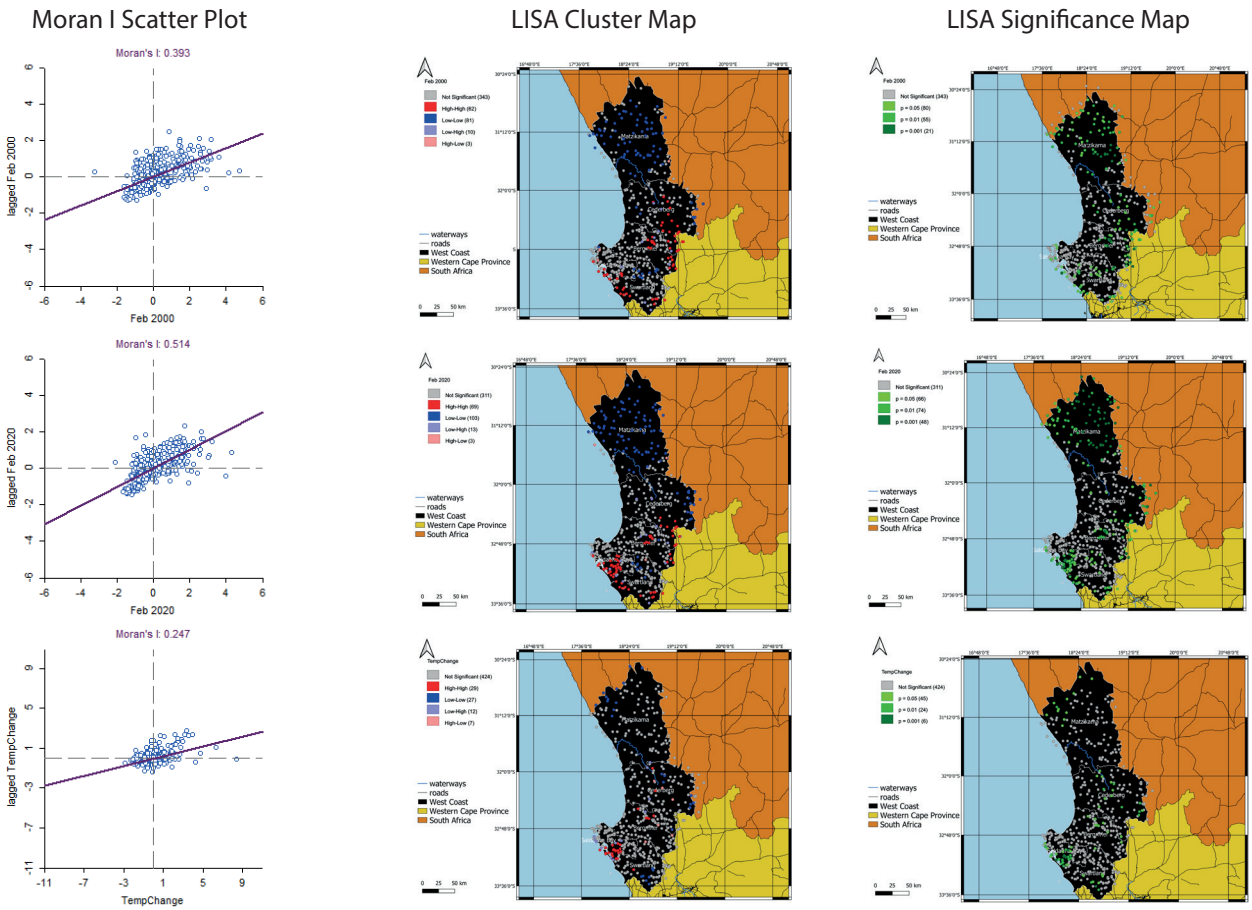

Fig. 10. Moran I, Cluster and Significance Map, February 2000 and 2020 and February 2000 to 2020 (change) NDVI values, NOAA dataset

Note: top row = February 2000, Middle row = February 2020 and Bottom row = February 2020 minus February 2000 (change)

Additionally, the Moran I analysis (Figure 11) displays the average monthly Moran I statistics for the year 1982 (grey line) and 2018 (yellow line) using the NOAA dataset and the average monthly Moran I statistics for the year 2000 (orange line) and 2020 (blue line) using the MODIS dataset. It is noticeable that the Moran I statistics significantly increases during the winter (rain) months irrespective of the dataset. In each case the Moran I statistics doubles during the winter months. The spatial autocorrelation of the 500 point-locations, therefore, displays significant seasonal patterns.

The Moran I derived results suggest strong spatial relationships, especially during the winter months (May to August). Testing for the presence of time relationships (figures 6 and 7) also seems warranted (structural break analysis) utilizing both the cross-section independent and cross-section dependent unit root testing procedures in EViews (Chang and Song 2002). The results (not presented) for both datasets strongly support the stationarity hypothesis in that the various test statistics' (Levin, Lin & Chu, Pesaran, and Shin, ADF – Fisher, PP – Fisher, Bai and Ng, Pooled statistic, CIPS, and Truncated CIPS) probability values indicate the acceptance of the alternative hypothesis, i.e., the absence of unit-roots. This suggests that the NDVI values of the 500 point-locations are mean-reverting over time, and therefore no significant structural change has occurred.

However, on closer inspection of the results, there are indeed point-locations that experienced structural breaks over the period. Thus, although the vast majority of point-locations have experienced no significant change (mean-reverting), there are indeed several point-locations that have (contain unit-roots). Regarding the NOAA (left panel) and MODIS (right panel) datasets, there are 197 and 139 point-locations (of the 500 point-locations) where the null hypothesis, i.e., the presence of unit roots, could not be rejected. These point-locations (unit root point-locations) are displayed in Figure 12 below (red colour).

Identifying a trend in a series, albeit including a seasonal component, can be done by applying a nonparametric test such as the Mann-Kendall trend test (Mbatha and Xulu, 2018; Drapela and Drapelova, 2011). Meals et al. (2011) further state that the Mann-Kendall trend test is especially appropriate for non-normal distribution data, which is the case for both datasets (applying the Jarque-Bera and Shapiro-Wilk tests to both datasets reveal that none of the point- locations or months are normally distributed, test results not included). Meals et al. (2011) further argue that the Mann-Kendall test explores whether increases or decreases in the y-values over time can be found. This can be done through what is essentially a nonparametric form of monotonic-trend regression analysis. The Mann-Kendall test assesses the sign of the post-measured and pre-measured data difference. Each post-measured value is compared to all values measured earlier; resulting in a total of n(n-1)/2 possible pairs of data. In this case, the aggregate observations are represented by n. This argument is supported by Ahmad et al. (2015) that further argue that the Mann-Kendall test is also not affected by outliers.

There has been no trend over time accounts for the null hypothesis (H0), while there has been a trend (increasing or decreasing) over time accounts for the alternate hypothesis (H1) (Motiee and McBean, 2009). Measuring the significance of the trend is done through the test statistic Zs. In other words, if | Zs| is greater than Zα/2, then the alternative hypothesis is valid, implying that the trend is not significant. The chosen level of significance (e.g. 5% with Z 0.025 = 1.96) is represented by α. An additional statistic obtained performing the Mann-Kendall test is Kendall's tau. Kendall's tau measures correlation and hence accounts for the significance of the association between the two variables. Kendall's tau is performed on the data ranks, i.e., the values are put in order and numbered, 1 for the lowest value, etc. Like other correlation measures, Kendall's tau assumes values between ±1 and +1, with a positive correlation indicating that the ranks of both variables increase or decrease together and vice versa (Yue and Wan 2004).

Concerning the NOAA and MODIS datasets, there were on average 367 and 171 point-locations (of the 500 point-locations) where the alternative hypothesis could not be rejected. These point-locations (trend point-locations) are displayed in Figure 13 below (red colour). Within the NOAA dataset (left panel), most trend point-locations are within the Bergriver and Swartland regions. Within the MODIS dataset (right panel), most trend point-locations are within the Cederberg and Bergiver regions. Again, it is evident that the two types of point-locations (non-trend in green and trend in red) follow a spatial clustering pattern. Therefore, the trend point-locations are characterized by spatial and time autocorrelation, while the non-trend point-locations are represented by only spatial autocorrelation.

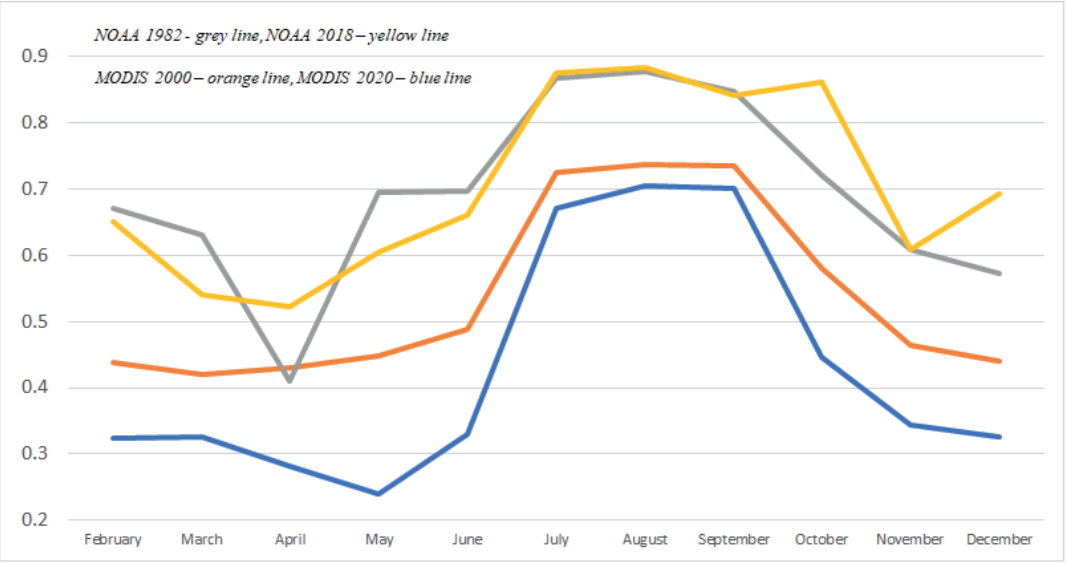

Fig. 11. Average Monthly Moran I statistics for the selected years using the NOOA and MODIS datasets

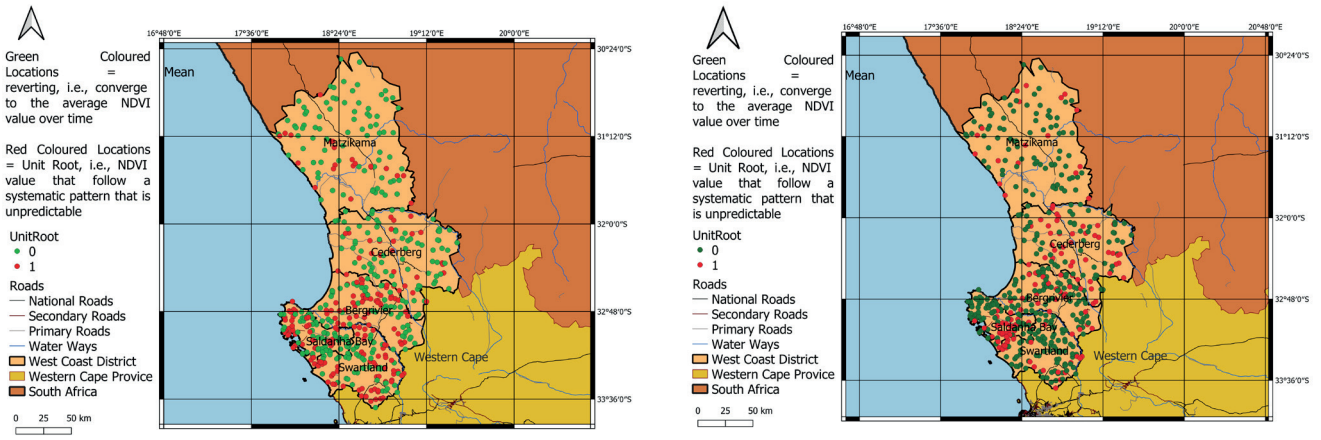

Fig. 12. Mean Reverting and Unit Root Point-locations

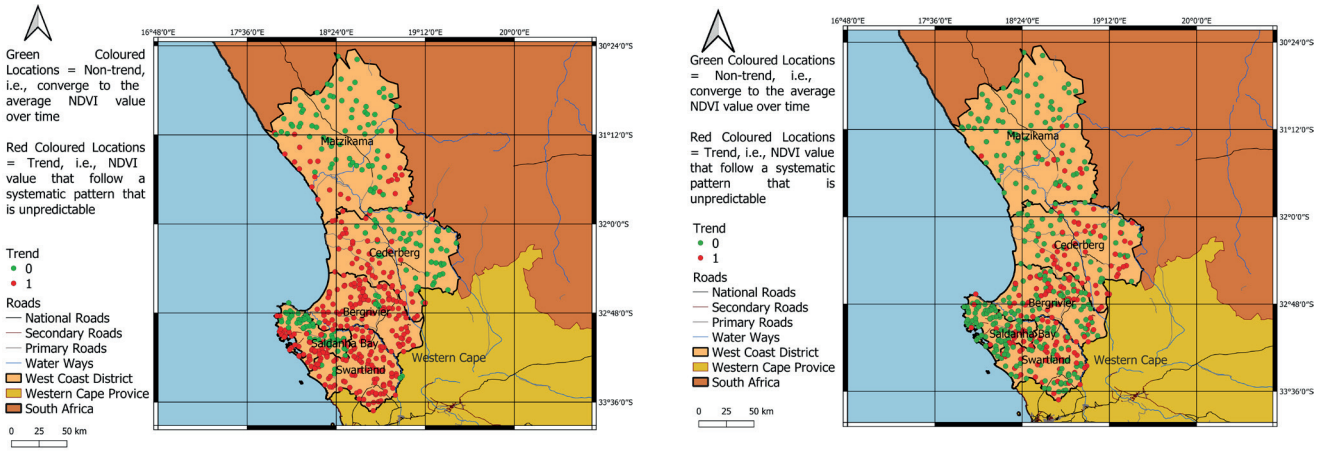

Fig. 13. Non-trend and Trend Point-locations

DISCUSSION

Aligning the findings of the time autocorrelation analysis (Figure 12) and the trend analysis (Figure 13) yields the results as presented in Figure 14. The results were derived from averaging the NOAA and MODIS structural break and trend images. The point-locations with structural breaks and trends are shown in red, while the mean-reverting and non-trend point-locations are shown in green. The spatial autocorrelation or spatial clustering is again very evident. It is also apparent that most areas or point-locations within the district did not experience any significant trend/structural change in vegetation over the 40- or 20-year periods. Thus, it can be argued that the majority of the vegetation change was most probably because of seasonal variation and changes thereof. Locating the structural break and trend -point-locations, i.e., point-locations that experienced statistically significant vegetation change over time within the NOAA and MODIS temporal differencing images (Figure 3.5), yields the results in Figure 15. Within the average NOAA and MODIS temporal differencing image, only point-locations that recorded significant NDVI change (increase or decrease of more than 0.4 in the original NDVI value) have been highlighted, i.e., blue coloured point-locations (left image) and bright coloured point-locations (right image). In the main areas that recorded significant changes in their NDVI values (plus or minus 0.4 difference on their original NDVI value) over time, in general, have experienced significant and permanent vegetation change. These areas are also spatially clustered and concentrated within specific areas within the wider district. However, these areas constitute only a minority of areas (less than 20%), whereas most of the areas within the district did not experience such significant and permanent change in vegetation. Instead, the changes that did occur in these majority of areas were related to seasonal variation, i.e., temporal changes. It is, therefore, possible to argue that most of the point-locations within the district have not experienced any significant and permanent change since the 1980'

In the main areas that recorded significant changes in their NDVI values (plus or minus 0.4 difference on their original NDVI value) over time, in general, have experienced significant and permanent VC change. These areas are also spatially clustered and concentrated within specific areas within the wider district. These areas constitute, however, only a minority of areas (less than 20%), whereas most of the areas within the district did not experience such significant and permanent change in VC. Rather, the changes that did occur in these majority of areas were related to seasonal variation, i.e., temporal changes. It is, therefore, possible to argue that most of the point-locations within the district have not experienced any significant and permanent change since the 1980s.

For the purpose of this article, no inference will be made as to the causes for the significant and permanent VC change. For such an inference, further work will be required, which falls outside the scope of this article. Nevertheless, various hypothetical causes can be put forward, such as Agricultural expansion, Urban expansion, Surface water change, and change in weather patterns. Le Roux, Cooper, and Mans (2016) argued that proximate causes for Land Use Land Cover Change in the Western Cape Province (the West Coast Region falls within the Western Cape Province, see Figure 2.1) were identified as infrastructure, agriculture and forestry changes and underlying causes as political, demographic, economic, technological and cultural factors.

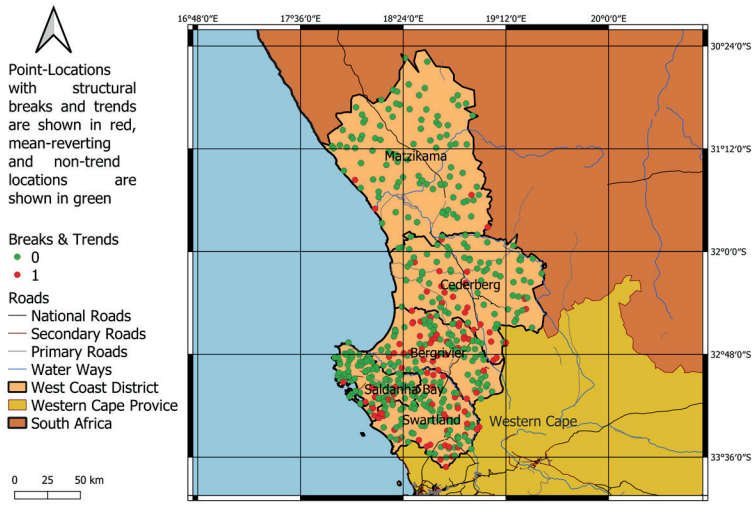

Fig. 14. Non-Change vs Change Vegetation Cover Point-locations

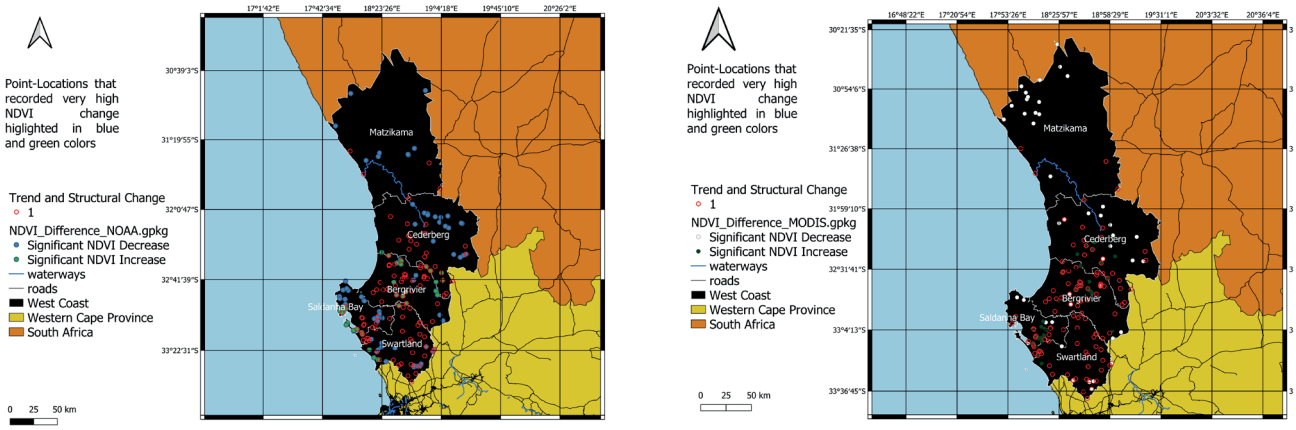

Fig. 15. Point locations that Experienced Significant Land Cover Change over Time

Summary and Conclusions

Land use and land cover (VC) is most probably not a stable or constant phenomenon and ebbs and flows over time. Given the significance and relevance of land use change for economic development and planning and policy formulation, VC change detection becomes very relevant. It therefore seems plausible that the monitoring of VC change dynamics should be instrumental in the effectual planning and sustainable development of expanding economies. To this end, the normalized difference vegetation index (NDVI) is one of the widely accepted methods of classification applied in VC change detection.

The study mainly followed a general to specific approach, specifically with regard to the method of analysis. In terms of the general approach, the focus was on raster and vector (area) analysis applied to the five regions covering the regions as a collective (i.e., the district). The specific approach, on the other hand, focused on point pattern (point-locations) analysis applied to a sample of 100 random points within each Region of interest, i.e., reducing the size of the regions to 100 point-locations each, assuming these point-locations are representative of the regions as a whole.

Two remote sensing datasets were used for this study in both the general and specific approaches. The first dataset was the NOAA CDR AVHRR NDVI: Normalized Difference Vegetation Index, Version 5 dataset. The second dataset was the MOD13Q1.006 Terra Vegetation Indices 16-Day Global 250m dataset. Five municipal areas (regions of interest) were chosen for the study. The regions (district as a collective) are located on the West Coast of South Africa within the Western Cape Province (red boundary). The district accounts for about 2.6 percent and 24 percent of the total land surface of South Africa and the Western Cape Province, respectively.

Temporal differencing the 1981 to 1985, 2015 to 2019, 2000 to 2004, and 2015 to 2020 NOAA and MODIS images respectively yielded images that suggested that the areas that experienced large changes in NDVI values have been random in spatial terms. In general, most of these areas (large change areas) experienced decreases (deterioration) in NDVI values. On the other hand, most areas within each Region only experienced modest decreases (deterioration) in NDVI values. The 500 point-location analysis proposed that many locations within the Swartland, Saldanha Bay and Bergriver regions experienced positive change whilst most locations within the Cederberg and Matzikama regions experienced negative change.

In order to test the NDVI spatial autocorrelation hypothesis the study employed the Global Moran I index. The associated z-values suggested a strong acceptance of the alternative hypothesis of spatial clustering, i.e., presence of spatial autocorrelation. It was noticeable that the Moran I statistics significantly increased during the winter (rain) months irrespective of the dataset. In each case, the Moran I statistics doubled during the winter months. The spatial autocorrelation of the 500 point-locations, therefore, displayed significant seasonal patterns.

Testing for the presence of time relationships utilizing both the cross section independent and cross section dependent unit root testing procedures strongly supported the stationarity hypothesis in that the various

test statistics probability values indicated the acceptance of the alternative hypothesis, i.e., the absence of unit roots. This suggested that the NDVI values of the 500 point-locations were mean reverting over time and therefore no significant structural change has occurred. Applying the Mann-Kendall trend test indicated that the majority of point-locations based on the NOAA time series, MODIS time series and MODIS trend series had not experienced a trend over time.

In the main, areas that recorded significant changes in their NDVI values (plus or minus 0.4 difference on their original NDVI value) over time, in general, have experienced significant and permanent VC change. These areas are also spatially clustered and concentrated within specific areas within the wider district. These areas constitute, however, only a minority of areas (less than 20%), whereas most of the areas within the district did not experience such significant and permanent change in VC. Rather, the changes that did occur in these majority of areas were related to seasonal variation, i.e., temporal changes. It is therefore possible to argue that most of the locations within the district have not experienced any significant and permanent change since the 1980s.

REFERENCES

Anselin L. (1996). The Moran Scatterplot as an ESDA Tool to Assess Local Instability in Spatial Association, in: M. Fischer, H. J. Scholten, D. Unwin (Eds.), Spatial analytical perspectives on GIS. Taylor & Frances, London, England, p. 111–125.

Aburas M.M., Abdullah S.H., Ramli M.F. & Ash'aari Z.H. (2015). Measuring land cover change in Seremban, Malaysia using NDVI index. Procedia Environmental Sciences. 30, 238 – 243.

Alawamy J.S., Balasundram S.K., Mohd. Hanif A.H. & Sung C.T.B. (2020). Detecting and Analyzing Land Use and Land Cover Changes in the Region of Al-Jabal Al-Akhdar, Libya Using Time-Series Landsat Data from 1985 to 2017. Sustainability 2020, 12, 4490 DOI:10.3390/su12114490.

Ahmad I., Tang D., Wang T., Wang M. & Wagan B. (2015). Precipitation trends over time using Mann-Kendall and Spearman's rho tests in Swat River basin, Pakistan. Adv. Meteorol.

Ayele G.T., Tebeje A.M., Demissie S.S., Belete A.M., Jemberrie M.A., Teshome W.M., Mengistu D.T. & Teshale E.Z. (2018). Time Series Land Cover Mapping and Change Detection Analysis Using Geographic Information System and Remote Sensing, Northern Ethiopia. Air, Soil and Water Research, 11, 1–18.

Cihlar J. (2000). Land cover mapping of large areas from satellites: status and research priorities. International Journal of Remote Sensing. 21(6), 1093–1114.

Campos J., Ericsson N.R. & Hendry D.F. (2005). General-to-specific Modeling: An Overview and Selected Bibliography. Board of Governors of the Federal Reserve System, International Finance Discussion Papers, Number 838.

Chang Y. & Song W. (2002). Panel Unit Root Tests in the Presence of Cross-Sectional Dependency and Heterogeneity. Presentation at the 2002 ASSA Meeting held in Atlanta.

Das S. & Angadi D.P. (2020). Land use land cover change detection and monitoring of urban growth using remote sensing and GIS techniques: a micro-level study. GeoJournal, DOI: 10.1007/s10708-020-10359-1.

Deng J., Wang K., Deng Y. & Qi G. (2008). PCA-based landuse change detection and analysis using multispectral and multisensor satellite data. International Journal of Remote Sensing, 29(16), 4823–4838.

Di Gregorio A. & Jansen L.J.M. (2000). Land Cover Classification System (LCCS): Classification Concepts and User Manual. Food and Agriculture Organization of the United Nations, Rome, 1998.

Drapela K. & Drapelova I. (2011). Application of Mann-Kendall test and the Sen's slope estimates for trend detection in deposition data from Bílý Kříž (Beskydy Mts., the Czech Republic) 1997–2010. Beskdy Mendel University in Brno, 4 (2), 133–146.

Firl G.J. & Carter F. (2011). Lesson 10: Calculating Vegetation Indices from Landsat 5 TM and Landsat 7 ETM+ Data. [online] Available at: http://ibis.colostate.edu/webcontent/ws/coloradoview/tutorialsdownloads/co_rs_tutorial10.pdf. [Accessed 15 May 2021]

Google Earth Engine, Gorelick N., Hancher M., Dixon M., Ilyushchenko S., Thau D., & Moore R. (2017). Google Earth Engine: Planetary-scale geospatial analysis for everyone. Remote Sensing of Environment.

Herwartz H. (2007). A note on model selection in (time series) regression models - General-to-specific or specific-to-general?. Economics Working Paper, 2007-09.

De Jong R. & Sakarya H. (2016). The Econometrics of the Hodrick-Prescott Filter. The Review of Economics and Statistics. 98(2), 310–317.

Le Roux A., Cooper A.K. & Mans G. (2016). Land Use and Land Cover Change in the Western Cape Province: Quantification of Changes & Understanding of Driving Factors. Conference: 7th Planning Africa Conference 2016 – Making Sense of the Future: Disruption and Reinvention At: Johannesburg, South Africa

Meals D.W., Spooner J., Dressing S.A. & Harcum J.B. (2011). Statistical analysis for monotonic trends. Tech Notes 6, November 2011. Developed for U.S. Environmental Protection Agency by Tetra Tech, Inc., Fairfax, VA, 23.

Meneses-Tovar C. (2012). NDVI as indicator of degradation. Unasylva (FAO).

MODIS (2021). Images and data from 2000 was retrieved on 2021/01/10 from https://lpdaac.usgs.gov, maintained by the NASA EOSDIS Land Processes Distributed Active Archive Center (LP DAAC) at the USGS Earth Resources Observation and Science (EROS) Center, Sioux Falls, South Dakota. 2018.

Mucina L., Knevel I.C., Adams J.B. & Rutherford M.C. (2006). Coastal Vegetation of South Africa. Strelitzia 19(2006)

Mbatha N. & Xulu S. (2018). Time Series Analysis of MODIS-Derived NDVI for the Hluhluwe-Imfolozi Park, South Africa: Impact of Recent Intense Drought. Climate, 6, 95, DOI:10.3390/cli6040095.

NOAA (2021). NOAA Climate Data Record (CDR) of AVHRR Normalized Difference Vegetation Index (NDVI), v5. [online] Available at: https://data.noaa.gov/dataset/dataset/noaa-climate-data-record-cdr-of-avhrr-normalized-difference-vegetation-index-ndvi-version-5. [Accessed 15 May 2021]

Motiee H. & McBean E. (2009). An Assessment of Long Term Trends in Hydrologic

Components and Implications for Water Levels in Lake Superior. Hydrology Research, 40(6), 564-579.

Rogan J. & Chen D. (2004). Remote sensing technology for mapping and monitoring land-cover and land-use change. Progress in Planning. 61(4), 301-325.

Rouse J. W., Haas R. H., Schell J. A. & Deering D. W. (1974). Monitoring vegetation systems in the Great Plains with ERTS. NASA. Goddard Space Flight Center 3d ERTS-1 Symp., 1, Sect. A

Sahebjalal E. & Dashtekian K. (2013). Analysis of land use-land covers changes using normalized difference vegetation index (NDVI) differencing and classification methods. African Journal of Agricultural Research, 8(37), 4614-4622.

Sowunmi F. A., Akinyosoye V. O., Okoruwa V.O. & Omonona B. T. (2012). The Landscape of Poverty in Nigeria: A Spatial Analysis Using Senatorial Districts- level Data. American Journal of Economics. 2(5), 61–74.

Vermote E., Justice C., Csiszar I., Eidenshink J., Myneni R., Baret F., Masuoka E., Wolfe R., Claverie M. & NOAA CDR Program (2014): NOAA Climate Data Record (CDR) of Normalized Difference Vegetation Index (NDVI), v4. [indicate subset used]. NOAA National Climatic Data Center. DOI:10.7289/V5PZ56R6.

Viton P. A. (2010). Notes on Spatial Econometric Models. City and Regional Planning, 870(3):2-17.

Wade T.G., Wickham J.D., Nash M. & Neale A.C. (2003). A Comparison of Vector and Raster GIS Methods for Calculating Landscape Metrics Used in Environmental Assessments. Photogrammetric Engineering and Remote Sensing. 69(12), 1399–1405.

Wu D.H., Zhao X., Liang S.L., Zhou T., Huang K.C., Tang B.J. & Zhao W.Q. (2015). Time-lag effects of global vegetation responses to climate change. Global Chang. Biol, DOI:10.1111/gcb.12945.

Yue S. & Wang C. (2004). The Mann-Kendall Test Modified by Effective Sample Size to Detect Trend in Serially Correlated Hydrological Series. Water Resources Management, 18, 201–218.

Zhang B.Q., Wu P., Zhao X.N., Wang Y.B. & Gao X.D. (2013). Changes in vegetation condition in areas with different gradients (1980–2010) on the Loess Plateau, China. Environ. Earth Sci, 68, 2427–2438.

Zhao G., Lin G., & Warner T. (2004). Thematic mapper data for change detection and sustainable use of cultivated land: A case study in the Yellow River delta. China. International Journal of Remote Sensing, 25(13), 2509–2522.

RESEARCH PAPER

INFLUENCE OF WATERSHED LAND USE ON WATER QUALITY IN THE STATE OF SANTA CATARINA, BRAZIL

Isabel C.B. Vieira[1*], Eduardo A.W. Ribeiro[2]

[1]Master's Program in Environmental Technologies, Catarinense Federal Institute (IFC), Rodovia BR 280, Km 27, Araquari, SC 89245-000, Santa Catarina, Brazil.

[2]Doctor of Geography, Professor at the Catarinense Federal Institute (IFC), Rodovia BR 280, Km 27, Araquari, SC 89245-000, Santa Catarina, Brazil.

***Corresponding author:** isabelbohnvieira@gmail.com

Received: February 16th, 2021 / Accepted: April 24th, 2022 / Published: June 30th, 2022

https://DOI-10.24057/2071-9388-2021-015

ABSTRACT. The inappropriate use of water resources by human actions compromises the balance between natural and anthropogenic factors. In this study, exploratory and field research were conducted with a scope of quantifying, based on satellite imaging, the use and occupation of land on the banks of the Itajaí-Açu River, the largest watercourse in the Itajaí River Basin, located in the State of Santa Catarina, Brazil. Five sampling points were allocated along the river at different times of the year to analyze water quality using chemical and biological indicators. The characterization of land use and occupation was carried out with Sentinel-2B satellite images at 10m resolution and QGIS software. Version 3.6.3 of the R Software was used to consolidate the data. The land use was categorized into several classes, the most representative of which was vegetation, which presented coverage of 34.42%, followed by the pastures and open fields class, with 27.83%, agriculture, with 18.18%, and urban areas, with 16.59% coverage. Our study showed that 62.6% of the river's base was affected by anthropogenic influence, characterizing an environment severely altered from its normal state. The results obtained in the statistical analysis revealed a directional correlation between land use and water quality, thus indicating that cities on the banks of watercourses are major sources of potential contaminants. Among the classes of land use, the presence of vegetation along the riverside territory attenuated part of the load of pollutants launched into the Itajaí-Açu River. This finding highlights the importance of conserving the vegetation alongside the river to maintain water quality and, consequently, preserve the ecosystem's biota.

KEYWORDS: land use; water quality, watershed, thermotolerant coliform indicators

CITATION: Isabel C.B. Vieira, Eduardo A.W. Ribeiro (2022). Influence of watershed land use on water quality in the state of Santa Catarina, Brazil. Geography, Environment, Sustainability, 2(15), p. 103-110
https://DOI-10.24057/2071-9388-2021-015

Conflict of interests: The authors reported no potential conflict of interest.

INTRODUCTION

The inadequate use of water resources by anthropogenic processes endangers the ecosystem's biota and, consequently, damages collective health. According to Costa Santos et al. (2019), the expansion of agricultural areas, the increase in urban agglomeration, and the exploitation of natural resources are examples of anthropogenic actions that cause rapid changes in the land cover, generating environmental repercussions.

River basins are areas drained by a river or a river system that flows into a common location where rainwater flows superficially or seeps into the soil, forming springs and watercourses and recharging the groundwater (Furlan et al. 2016). Since the beginning, as human life settled on the banks of rivers and developed their urban and industrial agglomerations, the river basins began to serve as containers for pollutants derived from land and the atmosphere (Martins et al. 2015).

Water resources are indispensable for the growth of a territory's economy and the maintenance of essential activities for human survival. However, the human actions carried out in the water resources' surroundings modify the physical, chemical, and biological environment, which, in turn, causes a significant decrease in water quality and water body biodiversity (Okumura et al. 2020).

In 1997, Brazil created a water resources policy (Law No. 9.433/97) to ensure current and future generations' necessary water availability at quality standards appropriate for the respective uses (*Lei No 9.433. Institui a Política Nacional de Recursos Hídricos 1997*). The chemical, physical, and biological parameters measured in a water body can indicate the degree of contamination and provide a basis for managing this resource. Such indication helps to assist in decision-making, focusing on the maintenance, remeasurement, and protection of water bodies.

According to Susanti and Wahyuningrum (2020), watershed management is inseparable from land use and management. The inappropriate use of land, disregarding soil and water conservation, causes damage to the watershed ecosystems. The mapping of land use and land cover emerges as a tool to quantify biodiversity losses. It can also measure the environmental impacts caused by territory urbanization. The interpretation of satellite images associated with water quality parameters in a river enables researchers to diagnose the river's current condition, identify the most relevant water quality issues (Silva 2015), and establish correlations regarding the compromised use and occupation of the land (Vieira 2019).

Considering this overview, several studies have shown a direct relationship between land use, maintenance of

the vegetation cover, and changes in the water quality of watercourses. According to the study carried out by Freire and Castro (2014) in a hydrographic basin in the state of Espírito Santo (Brazil), there was a strong positive correlation (0.87) between the Water Degradation Index (associated with low oxygen content and high nitrate levels) and the Soil Human Activity Index (associated with soil exposure and pastures). Pereira (2016), while conducting a study in the Alto Tietê Hydrographic Basin (São Paulo, Brazil), evidenced the importance of analyzing the influence of soil use and occupation on the quality of water bodies after obtaining a high correlation with the concentrations of nutrients in the water that derived from human occupation around the basin. Cornelli et al. (2016) found that the native forest located in the sub-basins of the city of Caxias do Sul (Rio Grande do Sul, Brazil) attenuated the release of pollutants into the watercourses, thereby improving water quality.

According to Yang et al. (2018), analyzing and predicting spatiotemporal changes and exploring the corresponding impacts on water quality are essential for controlling and improving the ecological environment of water in watersheds. This monitoring can substantiate the importance of preserving natural resources and the consequent quality of life and health of the population living along the riverside or in nearby areas. In this context, the development of policies and guidelines aimed at territorial planning to improve the water quality in hydrographic basins is necessary, providing sustainable development and the identification of land use and occupation (Asciutti et al. 2019). It is crucial that studies like this be conducted since water quality can affect the health and welfare of the community in the long run (Ifabiyi et al. 2020).

Nunes et al. (2019) showed the advantages of using total and thermotolerant coliform indicators as bacteriological markers in aquatic environments; however, their study did not correlate with the satellite images. On the other hand, Costa Santos et al. (2019) demonstrated that Landsat images are reliable for assessing land use and occupation dynamics in areas protected by law regarding river preservation. Zhang et al. (2019) showed how the correlation between land use and chemical indicators proved vital for assessing water quality in the tributaries of a reservoir in China. In addition to the type of margin occupation and sample size analysis, the authors also drew attention to the seasonal variations that influenced the results; however, their study did not address the bacterial variables. Abdo and Prakash (2020) revealed that changes brought about by urbanization are highly correlated with several environmental problems that require attention, mainly concerning geotechnological resources.

There is a promising way of integrating data collected in the field with satellite images for environmental analysis. In this small review, it can be noted that, although there are countless technological instruments and geoprocessing methodologies available, it is encouraged that these methods be revised in order to contribute to this discussion. In addition, only a few systematic records show the correlation of chemical and biological indicators with land use and occupation.

The present study resulted from a research project aimed at quantifying, based on satellite imaging, the use and occupation of land on the banks of the Itajaí-Açu River, the largest watercourse in the Itajaí River Basin, located in the State of Santa Catarina, Brazil. Here, the land quantification was correlated with water quality, as determined by chemical and biological indicators at different selected points of the river.

MATERIALS AND METHODS

This section addresses the step-by-step approach used in this field and exploratory study and comprises the following subtopics: study area, characterization of land use and occupation, and chemical and biological monitoring of the water.

Study area

In Santa Catarina, the Itajaí River Basin has a total area of 15,000 km^2, which corresponds to 16.15% of the state territory. Approximately 20% of the population lives in the river territory. The Itajaí-Açu River is the longest watercourse in the basin, measuring 188.0 km in length and occupying an area of 2,780.0 km^2. It is formed by the confluence of the *Itajaí do Oeste and Itajaí do Sul* rivers, and originates in the municipality of Rio do Sul (*Fundação Agência de Água do Vale do Itajaí 2010*). The location of the Itajaí-Açu River is shown in Figure 1.

Five water sampling points were allocated along the Itajaí-Açu River; the first one was established at the source of the river, in the municipality of Rio do Sul, while the last one was located at the river's mouth, in the municipality of Navegantes. The choice of the other collection points took place in order from the first to the last point and consisted of vegetation area, urban areas, and open fields/areas (Fig. 1).

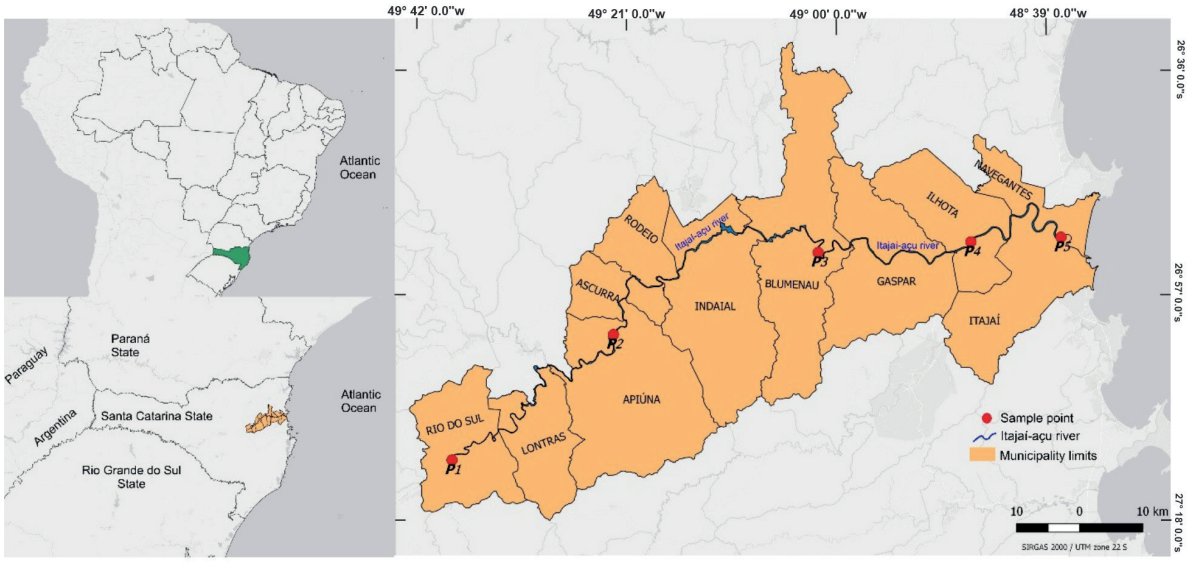

Fig. 1. Location and position of the sampling points along the Itajaí-Açu River

Characterization of soil use and occupation

In order to obtain images of the banks of the Itajaí-Açu River, files were freely downloaded from the Copernicus Open Access Hub website, which is managed by the European Space Agency (ESA). Images were taken by the Sentinel-2 satellite, at 10m resolution (Bottom of Atmosphere), with pictures obtained from the orbit areas T22JGR, T22JFQ, and T22JFR, dated August 2019. With the QGIS software - version 2.18, it was possible to determine the composition of the false-color bands using B08, B03, B04, and subsequent mosaic with B04, B03, B02, thus delimiting an area of 300 meters parallel to the margins of the buffer.

Land use/occupation was classified according to the *Dzetsaka* automatic classification tool into five classes: urban areas, pastures and open fields, agriculture, lakes and bodies of water, and vegetation, as shown in Table 1.

With the *Dzetsaka* plugin, a method of supervised classification developed by Nicolas Karasiak that uses a GMM (Gaussian Mixture Model) classifier, the automatic raster classification process in false color was carried out for the sample areas (Karasiak 2021). Using the classified raster image, the features identified by the algorithm were validated with true image color. Subsequently, the classified image was transformed into *shapefile* format, generating polygons for the specified classes, in which the area of each class was quantified.

Chemical and biological monitoring of the water

The parameters used as variables to correlate the use and occupation of the soil with water quality were selected according to Resolution No. 357/2005 of the Brazilian National Environment Council (CONAMA), according to their use classes, classified as fresh water. Nitrite and nitrate were used as chemical indicators, whereas thermotolerant coliforms and total coliforms were used as biological markers (Resolução CONAMA No 357 2005); the analyzed periods were the spring and summer seasons, with a water sample being collected per point/per station, totaling 40 analyzes throughout the territory. All samples were analyzed at the Central Laboratory of Analytical Tests, UNIVALI – CLEAn, in the municipality of Itajaí - SC, which followed the normative references of the Standard Methods for the Examination of Water and Wastewater, considering the following potability limits: nitrite, up to 1 mg/L; nitrate up to 10 mg/L for all water use classes; thermotolerant coliforms, class 1 up to 200 thermotolerant coliforms per 100 ml, class 2 up to 1000 thermotolerant coliforms per 100 ml, classes 3 and 4 without exceeding 4000 thermotolerant coliforms per 100 ml; total coliforms, unspecified, just an indicator of biological contamination.

In order to consolidate the objective proposed in this partial research, i.e., to correlate the use and occupation of land and water quality, the R Software, version 3.6.3, was used. For the Pearson correlation analysis, descriptive statistics were applied to extract the average variation coefficients.

RESULTS AND DISCUSSION

From sampling station 1 (P1) to sampling station 5 (P5), a total of 109.16 km² of land use were classified. The values obtained by coverage area has been shown in table 2.

This land-use classification had a buffer of 300 meters from the river bank to both sides, as shown in the map in Fig. 2. Among all the classes, the most representative of land use was the vegetation class, which presented coverage of 34.42%. Next came the pastures and open fields class, with 27.83%, agriculture with 18.18%, and urban areas with 16.59% coverage. When the sampling points on the map were analyzed individually (table 2), point 2 (P2) was the region that presented the highest vegetation occupancy. In contrast, point 1 (P1) stood out as being occupied mainly by agriculture, point 4 (P4) by pastures and open fields, and, finally, points 3 (P3) and 5 (P5) showed to be highly occupied by urban areas.

Table 1. Classes used for training the algorithm in supervised classification

Feature Code	Class Name	Interpretation Example
1	Urban areas	residential areas, infrastructure, highways, isolated buildings, and industrial areas.
2	Pastures and Open Fields	animal grazing, open fields without animals, soccer fields, and vacant lots.
3	Agriculture	rice, banana, and other identified crops.
4	Lakes and Bodies of Water	artificial weirs, wetlands, and river entry.
5	Vegetation	remnants of Ombrophilous Dense Forest, capoeirão forests, shrubs, and reforestation.

Source: Primary data, 2020

Table 2. Classification of the use and occupation of soil and their respective areas and percentages of coverage

Class Name	Area [km²]	% of coverage
Urban areas	18,11	16,59
Pastures and Open Fields	30,38	27,83
Agriculture	19,85	18,18
Lakes and Bodies of Water	3,25	2,98
Vegetation	37,57	34,42
Total	109,16	100

Source: Primary data, 2020

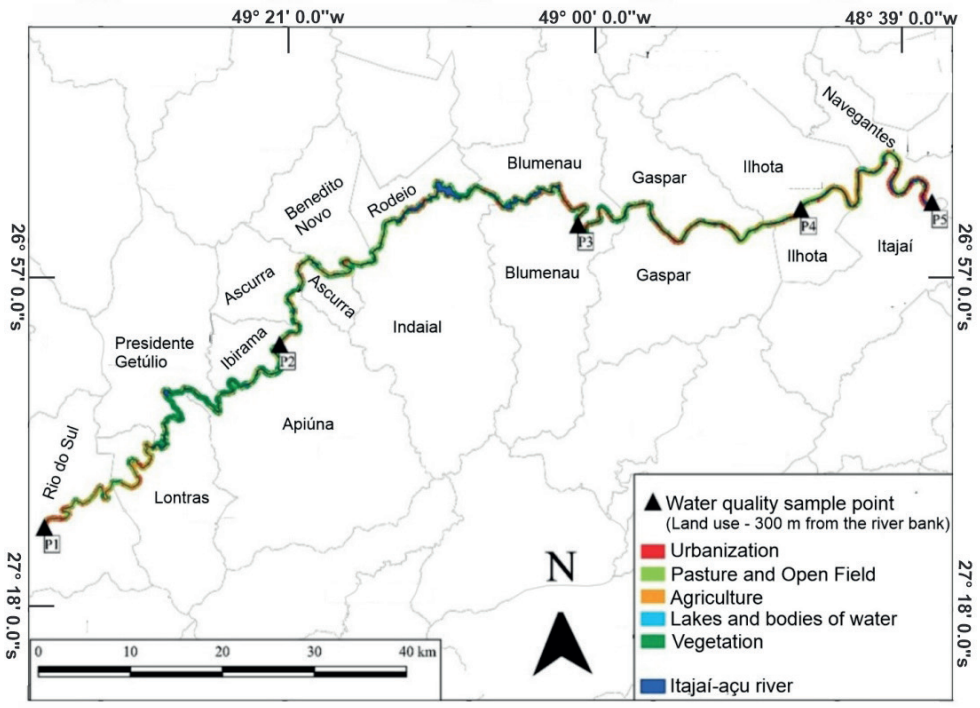

Fig. 2. Classification of the use and occupation of soil on the banks of the Itajaí-Açu River

According to the obtained results, it was possible to note that 62.6% of the analyzed territory was under anthropogenic influence, thus characterizing a severely altered environment. Experts claim that urbanization is one of the main changes in land cover that is highly correlated with many environmental problems, with constant effects on the atmosphere, water and soil (Abdo and Prakash 2020). Similar results were reported by Almeida et al. (2016) while studying a watershed in Tocantins, Brazil. Also, Sulistyo et al. (2020), who explored the Air Bengkulu River watershed in Indonesia, showed that land erosion can be caused by several factors, such as the loss of vegetation cover due to deforestation, agricultural practices, and the construction of residential areas. These alleged attacks are related to the hydrographic basin under study, because it has 62.6% of its territory under anthropogenic influence.

Corroborating with the aforementioned authors, the present study, which analyzed land use and occupation activities, confirmed that several environmental weaknesses may enhance some natural processes, with the intensification of soil loss through erosion and consequent silting, leading to reduced water quality. Barbosa and da Silva Filho (2018), signaled the occupation of the land, promoted by intense urbanization and agricultural activities from the 1980s and 1990s, as an aggravating factor of soil sealing, generating the increase of sediments for the rivers, impairing the quality of the waters. Irregular human actions are also pointed out by Paula et al.(2021), inferring the processes of the physical environment such as erosion and silting as the destruction of waterways.

The primary data gathered in the water quality assessment during the two analyzed seasons and at the five sampling points are shown in Table 3. In addition, the reports can be ratified by accessing the following link: encurtador.com.br/fnuER.

Based on the results, it can be noted that the nitrite indicator showed consistency in value during the spring season, which influenced the subsequent correlation with the data on land use and occupation. At sampling points P1, P2, P3 and P4, nitrate levels are within the standard established by CONAMA resolution No. 357/05, being less than 10 mg/L of nitrate (-NO3), in both stations. However, in the spring, point P5 exceeded that allowed by the same resolution, presenting 24.61 mg/L (Table 3). It is necessary to note that nitrates are toxic to humans, causing a disease called infantile methemoglobinemia, which is lethal for children (Xavier et al. 2018) . If this water is ingested, the nitrate is reduced to nitrite in the bloodstream and competes with free oxygen, leading to asphyxia. Therefore, nitrate is the standard for water potability, with its maximum value allowed at 10 mg/L also by Ordinance No. 518 of the Ministry of Health (BRASIL, 2004).

The nitrite indicator was found within the established parameters of water potability, at all sampling points in both stations, according to CONAMA Resolution No. 357/05, which establishes the maximum value of 1 mg/L of nitrite (–NO2). Betio et al. (2016), point out that one of the hypotheses for not detecting high values of this indicator in the water can be explained by the rapid transformation of nitrite to nitrate by bacteria of the genus Nitrobacter, present in the soil of the river, causing it to move quickly for groundwater.

Regarding biological indicators (Table 3), when categorized according to water use classes by CONAMA Resolution No. 357/05, point 1 showed 16,000 (MPN - most likely number) thermotolerant coliforms per milliliter (ml) of water, in both seasons , fitting as fresh water class 4, having its use only for navigation and landscape harmony. Point 2, for the same indicator, presented 330 and 790 MPN/ml in the spring and summer seasons respectively, fitting as class 2 fresh water, which allows up to 1000 thermotolerant coliforms/100ml, where its use is intended for human consumption after conventional treatment, primary contact recreation and vegetable irrigation. The Point 3 was classified as freshwater class 4 in spring and class 3 in summer. This class establishes up to 2500 thermotolerant coliforms/100ml, intended for human consumption only after advanced treatment and for secondary contact recreation (sporadic or accidental). Point 4 showed 2200 MPN/ml; 330 MPN/ml of thermotolerant coliforms respectively in the spring and summer seasons, attributing themselves as classes 3 and 2. Finally, the point 5, with results that attributed the classes of water use, the point 3 in spring and class 4 in summer. The abovementioned values, when compared to the Brazilian legislation, point to biological contamination throughout the sampled territorial extension. According to Lima et al. (2018), the presence of thermotolerant coliforms in water samples may indicate contamination by intestinal pathogens, harmful to health, arising exclusively from human fecal origin.

Table 3. Primary water collection data results

Primary Laboratory Data										
	P1		P2		P3		P4		P5	
Parameter (Unite)	Spring	Summer	Spring	Summer	Spring	Summer	Spring	Summer	Spring	Summer
Nitrite (mg/mL)	0.01	0.12	0.01	0.12	0.01	0.13	0.01	0.44	0.01	0.25
Nitrate (mg/mL)	3.81	0.58	5.66	0.31	5.29	0.92	5.29	1.06	24.61	1.44
Thermo. Coliforms (MPN/100mL)	16000	9200	330	790	16000	2200	2200	330	1700	16000
Total Coliforms (MPN/100mL)	16000	16000	2200	1300	16000	5400	16000	3500	16000	16000

Source: Primary data, 2020

After correlating the classes of land use and occupation with the chemical and biological indexes found in the water sample analysis, conducted in the spring and summer, using the R Statistical Software, for Sperman correlation, we obtained the data shown in Fig. 3. According to Freire and Castro (2014), correlations equal to or greater than 0.7 (r = 0.7) are considered strong correlations, which become even stronger when the value approaches 1.0 (r = 1.0). Positive values indicate that the two variables move together in the same direction; similarly, negative values were obtained when the two variables move in opposite directions in the hypothesis. Based on Table 3, it is noted that, during the spring, the urbanization class showed a negative correlation with the chemical indicator nitrate (r = -0.95) and a positive correlation with thermotolerant coliforms (r = 0.8), the agriculture class showed a positive correlation with nitrate and a negative correlation with total and thermotolerant coliforms (r = 0.74; -0.77; -0.88, respectively). In summer, the classes pasture and vegetation showed a negative correlation with nitrate (r = -0.8; 1, respectively) and the classes agriculture and vegetation showed a negative correlation with the chemical indicator nitrite (both, r = -0.8). In this season there was no strong positive correlations for the land use classes.

During the spring season, the thermotolerant coliform content in the water increased due to the impact of urbanization on water quality, as shown in Figure 3. This can be explained by the influence of climatic factors. However, the same indicator decreased significantly during the summer season, owing to the increase in precipitation, which led to its dilution in the river. Our data corroborate with the study conducted by Cheng et al. (2018) on the Haihe River Basin in China, where the authors stated that dilution by precipitation became a dominant factor that affected water quality and resulted in relatively better indexes than in the pre-rainy season. Centeno et al. (2016), in the state of Rio Grande do Sul, also observed that increases in precipitation led to an improvement in water quality. Additionaly, Nunes et al. (2019) reported that the presence of thermotolerant coliforms in the aquatic environment of the Salgadinho River (Ceará, Brazil) was indicative of contamination by human feces, which resulted from the lack of basic sanitation in the region. In this sense, Amorim et al. (2020), in their study of a hydrographic basin in the state of Alagoas, found that the impaired quality of surface water in water bodies, resulting from the negative influence of anthropogenic actions, mainly arises from the inadequate disposal of effluents.

Considering the agriculture class, a positive correlation of nitrate in the spring and a negative correlation of nitrite in the summer were identified. The decrease in the indicator's presence in the river was due to nitrification (a process that follows fertilization in the panicle stage of rice cultivation from September to October). Nitrification is the term used to describe the first step of the biological nitrogen removal process, in which ammonia (chemical fertilizer) is oxidized into nitrite, which, in turn, is oxidized into nitrate (Streck et al. 2006). When plants reach a certain degree of development, they reduce nitrate content in their roots and transport the compound to different parts of the plant in the form of amino acids. This result was pointed out in the study by Cristina et al. (2013) on nitrate reductase in rice cultivars. During the spring, the indicator nitrite showed constant values (due to the nitrification process mentioned previously) in all five sampling locations, making it impossible to calculate the correlation.

Fernandes et al. (2017), in their study on the impact of nitrogen fertilization on pastures, also reported a reduction

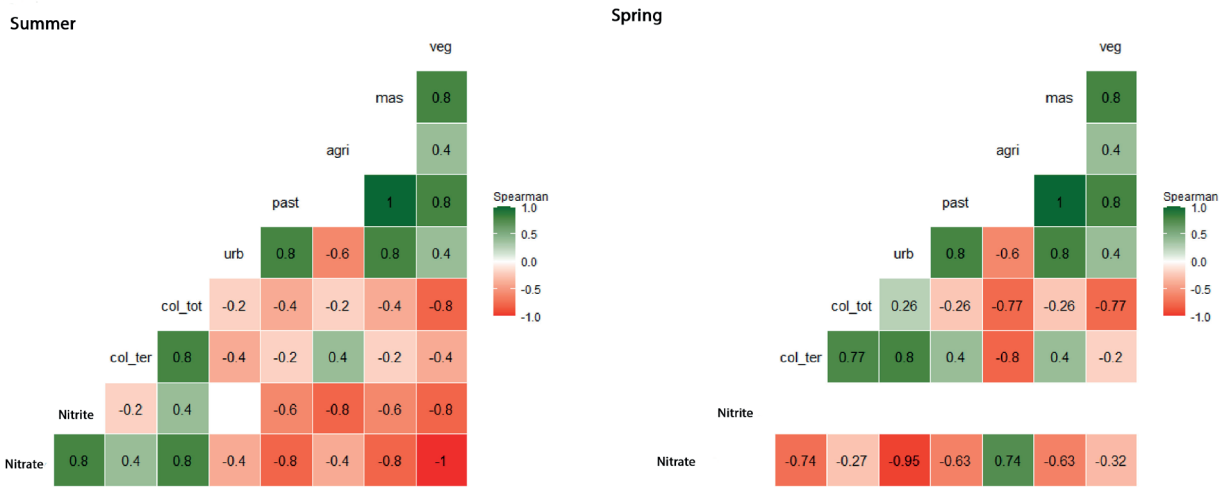

Fig. 3. Correlations between chemical and biological indicators and the classes of land use and occupation

of the indicator in the soil during the development cycle of grasses; this can be explained since they absorb differentiated amounts of nitrogen in the form of nitrate (NO3-) and ammonium (NH4+). Also, Zhang et al. (2019) revealed that farmland and urban areas promoted unfavorable impacts on water quality; in contrast, forest and grasslands presented a favorable influence on water quality. These findings are consistent with the correlations obtained from both the chemical and biological indicators in the present study.

Santos et al. (2020) stated that agriculture is the form of land use that most contributes to the generation of surface runoff into sub-basins. The mineral and organic fertilizers applied to crops for enhanced agricultural production can be carried out to watercourses through surface runoff, compromising water quality. According to Mello et al. (2018), agricultural and urban areas are responsible for water quality degradation. The sewage derived from residential areas, sediments, and nutrients from short-cycle crops lead to nonpoint source pollution into rivers.

Finally, it can be noted that vegetation plays a crucial role in the reduction of nitrite and nitrate indicators in water, as well as total and thermotolerant coliforms. It acts as a natural filter in the ecosystem by minimizing the leaching of these indicators from the soil to the water, contributing to the maintenance of the natural biota. Shang et al. (2018) demonstrated the importance of soil-stream hydrological connectivity, primarily because there is a phase that can be frequently mobilized through water leaching and flushing, evidencing the need for more empirical studies to incorporate a science-based management framework. These studies highlight the relevance of water quality assessments since contaminated or polluted water bodies can become vectors of water-borne diseases, generating serious public health problems, affecting future demand for good quality water (Santos 2020). According to Pessoa et al. (2018), collecting and treating all generated sewage and the supervision of irregular sewer connections could improve the quality of river waters since the release of sewage is one of the leading causes of water body degradation.

Satellite imaging is vital for monitoring land use and occupation (Gonçalves and Ribeiro 2021). The integration of field research with geospatial data provides knowledge to understand new information regarding the impact of humans on nature. Therefore, in the era of information and technology, technological knowledge is essential for environmental management.

CONCLUSION

The way human beings use and occupy the soil is directly associated with water quality in watercourses. Therefore, a directional correlation analysis was performed in the present study, dividing land use into different classes. Depending on the climatic season, each class of land use and occupation positively or negatively influenced water quality.

According to the obtained results, we can conclude that the waters of the Itajaí-Açu River are potentially contaminated by total and thermotolerant coliforms. Anthropogenic influence and inadequate land use regarding the discharge of urban and industrial effluents without suitable treatment into the watercourse were verified.

The values obtained for the biological indicator thermotolerant coliforms at the confluence of the river, in the municipality of Rio do Sul, disqualify the suitability of its waters for consumption and bathing on account of human fecal contamination. The minimum coliform density established in CONAMA Resolution No. 357/2005, used to assess water quality, is 1,000 MPN per 100 mL of water. Our results on water quality transcended the minimum value. Thus, the water of the respective river was classified as class 4, which could only be reserved for purposes of navigation and landscape harmony. Hence, the results indicate that the biological contamination of the Itajaí-Açu River confluence occurs upstream, with subsequent contamination along its course.

Our results also showed that even with the impacts generated by anthropogenic influence on the banks of the Itajaí-Açu River, the vegetation present on the riverside was capable of attenuating part of the pollutant load released through agricultural, industrial, and domestic effluents. Therefore, it can be inferred that cities on the banks of watercourses serve as potential water contaminants.

Based on our findings, it is noteworthy that public actions are essential for developing policies and guidelines aimed at territorial planning to improve water quality in hydrographic basins and their occupation. Access to clean water and adequate sanitary sewage systems constitute an effort that should be continued in order to carry out concrete actions that contribute to the environmental health of the territory of water bodies and their inhabitants.

REFERENCES

Abdo Z.A. and Prakash S. (2020). A Review Paper on Monitoring Environmental Consequences of Land Cover Dynamics with The Help of Geo-informatics Technologies. Geosfera Indonesia, 5(3), 364–389, DOI: 10.19184/GEOSI.V5I3.18284

Almeida R.F.B., Bayer M. and Ferreira Júnior L.G. (2016). Compartimentação morfométrica da bacia do Rio do Coco como subsídio a análise de fragilidade ambienta. Mercator (Fortaleza), 15(4), 83–94. DOI: 10.4215/RM2016.1504.0006

Amorim E., Junior C., Souza V. and Neves M. (2020). Cargas Poluentes em Corpos Hídricos do Município de Maceió/AL. Revista DAE, 222(68), 36–51. DOI: 10.36659/dae.2020.015

Asciutti G.A.M., Stanganini F.N. and Melanda E.A. (2019). Identificação dos diferentes usos e ocupação do solo da bacia hidrográfica do rio do Quilombo, São Carlos/SP utilizando imagem de satélite Sentinel 2 e o complemento SCP do QGIS. Anais Do XIX Simpósio Brasileiro de Sensoriamento Remoto, 2539–2539. https://proceedings.science/sbsr-2019/papers/identificacao-dos-diferentes-usos-e-ocupacao-do-solo-da-bacia-hidrografica-do-rio-do-quilombo--sao-carlos-sp-utilizando-#

Lei no 9.433. Institui a Política Nacional de Recursos Hídricos, (1997) (testimony of Brasil). http://www.planalto.gov.br/ccivil_03/leis/l9433.htm

Ministério da Saúde. Portaria nº 518, de 25 de março de 2004. Brasília: Fundação Nacional de Saúde. https://bvsms.saude.gov.br/bvs/publicacoes/portaria_518_2004.pdf

Barbosa L. S., Da Silva Filho E. P. (2018). Influencia Influência do uso e ocupação na qualidade da água no Rio Pirarara, afluente do Rio Machado, Rondônia/Brasil. Revista Ibero-Americana de Ciências Ambientais, 9(7), 320-332. DOI: 10.6008/CBPC2179-6858.2018.007.0030

Betio M. M., Eiras M. M., Santos M. M. (2016). Contaminação das águas subterrâneas por lixões desativados: avaliação da antiga área de disposição final de resíduos sólidos de Rolândia –PR. Águas Subterrâneas, Anais XIX Congresso Brasileiro de Águas Subterrâneas. DOI: 10.14295/ras.v0i0.28753

Centeno L.N., Cecconello S.T., Moraes P.B., Guedes H.A.S., Centeno A.N. and Cecconello S.T. (2016). Análise temporal da qualidade da água de um arroio no sul do Rio Grande do Sul. Revista Thema, 13(2), 109–119. DOI: 10.15536/THEMA.13.2016.109-119.363

Cheng X., Chen L., Sun R. and Kong P. (2018). Land use changes and socio-economic development strongly deteriorate river ecosystem health in one of the largest basins in China. Science of The Total Environment, 616–617, 376–385. DOI: 10.1016/J.SCITOTENV.2017.10.316

Resolução CONAMA no 357, (2005) (testimony of Conselho Nacional do Meio Ambiente). https://www.icmbio.gov.br/cepsul/images/stories/legislacao/Resolucao/2005/res_conama_357_2005_classificacao_corpos_agua_rtfcda_altrd_res_393_2007_397_2008_410_2009_430_2011.pdf

Cornelli R., Elisabete Schneider V., Anderson Bortolin T., Cemin G. and Macedo dos Santos G. (2016). Análise da Influência do Uso e Ocupação do Solo na Qualidade da Água de Duas Sub-Bacias Hidrográficas do Município de Caxias do Sul. Scientia Cum Industria, 4(1), 1–14. DOI: 10.18226/23185279.V4ISS1P1

Costa Santos L.A., Fernandes Vieira L.M., De Aquino Martins P.T. and Ferreira A.A. (2019). Conflicts of land use and cover for the period 1985 to 2017 in the Caldas River Basin-Go. Fronteiras, 87(2), 189–211. DOI: 10.21664/2238-8869.2019V8I2.P189-211

Cristina A., Milene L., De A. and Carvalho F. (2013). Documentos 280 Empresa Brasileira de Pesquisa Agropecuária Embrapa Arroz e Feijão Ministério da Agricultura, Pecuária e Abastecimento. www.cnpaf.embrapa.br

De Melo A. C. A., Eiras, M. M., Dos Santos M. M. (2018). Sensibilidade ambiental do meio físico para disposição de resíduos sólidos urbanos na Região Metropolitana de Londrina–PR. Geografia (Londrina), 27 (2), 207-224. DOI: 10.5433/2447-1747.2018v27n2p207

Fernandes G., Tiecher T., Piton R., Pellegrini A. and Santos D.R. (2017). Impact of nitrogen fertilization of perennials pastures on the contamination of natural resources. Revista Brasileira de Tecnologia Agropecuária, 1(1), 3–14. http://www.revistas.fw.uri.br/index.php/rbdta/article/view/2482/2259

Freire A. and Castro E. (2014). Análise da Correlação do uso e Ocupação do Solo e da Qualidade da Água. Revista Brasileira de Recursos Hídricos, 19(1), 41–49. DOI: 10.21168/RBRH.V19N1.P41-49

Fundação Agência de Água do Vale do Itajaí. (2010). Planos das Bacias do Rio Itajaí. https://www.aguas.sc.gov.br/index.php?option=com_k2&view=item&layout=item&id=1904&Itemid=248&jsmallfib=1&dir=JSROOT/DHRI/Planos+de+Bacias/Plano+da+Bacia+Hidrografica+do+Rio+Itajai

Furlan A.R., Filipini R.C. and Reis J.T. (2016). Os Diferentes Tipos de Uso e Cobertura da Terra e sua Influência nos Parâmetros de Qualidade da Água. Ciência e Natura, 38(3), 1319–1330. DOI: 10.5902/2179460X22694

Gonçalves V. and Ribeiro E.A.W. (2021). Obtenção de série histórica da evolução da classe Floresta Plantada a partir dos dados de uso e cobertura do solo da Coleção 5 do projeto MapBiomas. Metodologias e Aprendizado , 4, 99–105. DOI: 10.21166/metapre.v4i.1491

Ifabiyi P.I., Oladele B. and Salau W. (2020). Water Poverty Assessment in Olorunsogo Local Government Area of Oyo State, Nigeria. Geosfera Indonesia, 5(1), 92–105. DOI: 10.19184/GEOSI.V5I1.13438

Karasiak N. (2021). Dzetsaka QGIS Plugin. https://plugins.qgis.org/plugins/dzetsaka/

Lima, J. A. de M., Bethonico M. B. de M, Vital M. J. S. (2018) Água e doenças relacionadas a água em comunidades da bacia hidrográfica do rio Uraricoera-Terra Indígena Yanomami-Roraima. Hygeia, 14(27), 136-154. DOI: 10.14393/Hygeia142711

Martins A.L.M., Lopes M.C. and Simedo M.B.L. (2015). Monitoramento de qualidade de água: Suporte para gestão ambiental na microbacia do córrego da Olaria. Periódico Eletrônico Fórum Ambiental Da Alta Paulista, 11(6), 143–157. DOI: 10.17271/1980082711620151253

Mello K. de, Valente R.A., Randhir T.O., dos Santos A.C.A. and Vettorazzi C.A. (2018). Effects of land use and land cover on water quality of low-order streams in Southeastern Brazil: Watershed versus riparian zone. CATENA, 167, 130–138. DOI: 10.1016/J.CATENA.2018.04.027

Nunes L.M., Monteiro M. de F.G., Júnior D.L. de S., Aquino P.E.A. de, Saraiva C.R.N., Leandro M.K. do N.S., Marques A.E.F., Silva R.O.M. da and Leandro L.M.G. (2019). Pesquisa de coliformes totais e termotolerantes no rio Salgadinho no município de Juazeiro do Norte, CE. Revista Eletrônica Acervo Científico, 7, e2243–e2243. DOI: 10.25248/REAC.E2243.2019

Okumura A.T.R., Da Silva A.G., Da Silva N.R.S., Lopes E.R.D.N., Bifano R.B.A. and Quilenato R.V.Q.V. (2020). Water quality assessment of a tropical river from a soil usage and vegetation cover perspective. Revista Brasileira de Geografia Fisica, 13(4), 1835–1850. DOI: 10.26848/rbgf.v13.4.p1835-1850

Paula L. R., Cesar K. F. A., Batista A. K. R., Siqueira F. F. F. S, Da Silva L., Filho D. L., Ferreira M.F. R., Almeida M. A. G., Nunes L. A. G, Soares J. da P., Azevedo C. A. S. Da Silva F. L. (2021). Análise físico-química da qualidade da água do rio Itapecuru no município de Caxias-MA. Research, Society and Development, 10(15), e551101521973-e551101521973. DOI:10.33448/rsd-v10i15.21973

Pereira R.H. de A. (2016). Análise espaço temporal de parâmetros de qualidade de água e sua relação com uso e ocupação na bacia do Alto Tietê. Aleph, 105 f. https://repositorio.unesp.br/handle/11449/144007

Pessoa J.O., Orrico S.R.M. and Lordêlo M.S. (2018). Qualidade da água de rios em cidades do Estado da Bahia. Engenharia Sanitaria e Ambiental, 23(4), 687–696. DOI: 10.1590/S1413-41522018166513

Santos A.C. dos, Martins C.S., Aparecida de Melo N. and Filho J.E.A. (2020). Quantification of nitrogen and phosphorus loads in the Bom Jardim river sub-basin (MG). Revista DAE, 15–33. https://doi.org/10.36659/dae.2020.050

Shang P., Lu Y.H., Du Y.X., Jaffé R., Findlay R.H. and Wynn A. (2018). Climatic and watershed controls of dissolved organic matter variation in streams across a gradient of agricultural land use. Science of The Total Environment, 612, 1442–1453. DOI: 10.1016/J.SCITOTENV.2017.08.322

Silva J.M.O. (2015). Uso do sensoriamento remoto para a estimativa da temperatura de superfície na microbacia do rio granjeiro, crato, ceará | Geosaberes. Geosaberes, 6(1), 130–144. http://www.geosaberes.ufc.br/geosaberes/article/view/418

Streck N.A., Bosco L.C., Michelon S., Walter L.C. and Marcolin E. (2006). Duração do ciclo de desenvolvimento de cultivares de arroz em função da emissão de folhas no colmo principal. Ciência Rural, 36(4), 1086–1093. DOI: 10.1590/S0103-84782006000400007

Sulistyo B., Barchia M.F., Hindarto K.S. and Listyaningrum N. (2020). The Effect of Land Unit Elimination on The Conservation Activity Plan at Air Bengkulu Watershed, Bengkulu Province. Indonesian Journal of Geography, 52(2), 170–180. DOI: 10.22146/IJG.48578

Susanti P.D. and Wahyuningrum N. (2020). Identification of the Main Water Quality Parameters for Monitoring and Evaluating Watershed Health. Indonesian Journal of Geography, 52(2), 227–238. DOI: 10.22146/IJG.47280

Vieira I. (2019). Mapeamento da área de preservação permanente na margem norte do rio Itajaí-Açu em área urbana consolidada. Metodologias e Aprendizado , 1(0), 26–29. DOI: 10.21166/metapre.v1i0.641

Xavier, F. V., Malagutti, W., Silva, R. W. D. C., & Moreira, C. A. (2018). Emprego da sondagem elétrica vertical integrada às análises químicas e microbiológicas no diagnóstico preliminar da contaminação do solo e da água subterrânea no cemitério municipal da cidade de Rio Claro (SP). Engenharia Sanitária e Ambiental, 23 (2), 333-344. DOI:10.1590/S1413-41522018152375

Yang K., Yu Z., Luo Y., Yang Y., Zhao L. and Zhou X. (2018). Spatial and temporal variations in the relationship between lake water surface temperatures and water quality - A case study of Dianchi Lake. Science of The Total Environment, 624, 859–871. DOI: 10.1016/J.SCITOTENV.2017.12.119

Zhang J., Li S., Dong R., Jiang C. and Ni M. (2019). Influences of land use metrics at multi-spatial scales on seasonal water quality: A case study of river systems in the Three Gorges Reservoir Area, China. Journal of Cleaner Production, 206, 76–85. DOI: 10.1016/J.JCLEPRO.2018.09.179

RESEARCH PAPER

SEAGRASS ZOSTERA IN THE RUSSIAN SECTION OF THE BALTIC SEA

Anton A. Iurmanov[1*], Mikhail S. Romanov[1], Marika A. Gerb[2], Alexandra A. Volodina[3], Irina B. Baikova[3], Igor Yu. Popov[4,5], Mikhail Yu. Markovets[6]

[1]Main Botanical Garden named after N. V. Tsitsin RAS, st.Botanicheskaya, 4, Moscow, 127276, Russia
[2]Shirshov Institute of Oceanology, RAS, 36, Nahimovskiy prospect, Moscow, 117997, Russia
[3]Museum of the World Ocean, Petr Velikiy Embankment, 1, Kaliningrad, 236006, Russia
[4]Saint-Petersburg State University, Universitetskaya n. 7/9, Saint-Petersburg, 199034, Russia
[5]Nizhne-Svirsky state reserve, st. K. Marx, 27, Lodeinoe Pole, 1187700, Russia
[6]Biological station «Rybachy», Zoological Institute RAS, Rybachy, Kaliningrad reg., 238535, Russia
***Corresponding author:** yurmanov–anton.ya.ru@yandex.ru
Received: February 1th, 2021 / Accepted: April 24th, 2022 / Published: June 30th, 2022
https://DOI-10.24057/2071-9388-2022-013

ABSTRACT. Information on seagrass in the Russian section of the Baltic Sea – Sambia Peninsula, Curonian Spit, and Gulf of Finland (water area of Kaliningrad and Leningrad regions) is generalized based on a recent survey, literature search, and study of herbarium samples. Seagrasses are found in the emissions of most of the coast of the Kaliningrad region, but they are extremely few. All discovered seagrasses belong to one species – *Zostera marina L.* In the absence of an opportunity to distinguish the emissions of *Zostera marina* brought in by currents from other regions of the Baltic Sea from local emissions, the possibility of the presence of a small number of single individuals of this species in the seawater area of the Sambia Peninsula and the Curonian Spit remains. Specimens of *Zostera marina* brought in by storms from the western part of the Baltic Sea, as well as an individual found during diving studies in 2009, can take root and form small meadows in the future, provided they are protected from surf waves and a stable substrate, settling with the help of vegetative shoots. Poorly rooted seagrasses can also be washed ashore. The mobile sandy ground found in most of the study area may be the reason why seagrass plants do not form stable communities. In the Russian section of the Gulf of Finland, seagrass had not been recorded. Probably, they occur in small numbers in its northern part.

KEYWORDS: seagrasses, Zosteraceae, *Zostera marina*, Baltic Sea

CITATION: Iurmanov A.A., Romanov M.S., Gerb M.A., Volodina A.A., Baikova I.B., Popov I.Y., Markovets M.Y. (2022). Seagrass Zostera In the Russian Section Of the Baltic Sea. Geography, Environment, Sustainability, 2(15), p. 111-115
https://DOI-10.24057/2071-9388-2022-013

ACKNOWLEDGEMENTS: A. Iurmanov and M. Romanov acknowledge the support of the Russian Foundation for basic research, the project No 19–34–90164, and the project of Main Botanical Garden No 18–118021490111–5. The work was carried out by M. Romanov in accordance with institutional research project No 122042700002-6. The work by M. A. Gerb took place in a framework of the project 0128-2021-0012 Shirshov Institute of Oceanology. M. Markovets acknowledges the project AAAA-A19-119021190073-8 by Zoological Institute, RAS.

Conflict of interests: The authors reported no potential conflict of interest.

INTRODUCTION

Seagrasses are a group of monocots (Monocotyledoneae – Alismatales) that live underwater (Hogarth 2015). Their aggregations form «underwater meadows» which are valuable habitats including diverse animal species (Den Hartog 1970). In the Baltic Sea, such meadows are notable for the fact that they can be the habitat of the European eel Anguilla anguilla (Boström et al. 2003), a valuable commercial fish, the number of which is declining catastrophically (Pike et al. 2020). In the Baltic Sea, seagrasses are represented only by the Zosteraceae family (Borum et al. 2004), including *Zostera marina* L., which is widespread in semi-surf-protected conditions throughout the Baltic Sea (Blinova 2007) and Zostera noltii Horneman, a species with a narrower area, the eastern border of which in the Baltic Sea is located in the Vistula Lagoon, in the territorial waters of Poland. There are also reports of findings of Zostera noltii in the waters of Lithuania (Labanauskas 2009). Seagrasses are of economic value since they are used as «straw» – the raw material for the manufacture of packaging materials, paper, compost, etc. (Kardakova 1957; Kulepanov 2005). Moreover, various substances extracted from seagrasses are supposed to be useful in pharmacology and cosmetology (Aminina 2005). Economic activities in the coastal zone directly or indirectly lead to an increase in water turbidity, which harms seagrasses (Duarte 2002; Short et al. 2011; Unsworth et al. 2014). Many species suffer a catastrophic decline (Orth 2006; Waycott and Williams 2006). The peak of seagrass decline in the Baltic Sea occurred in the 1980s, but they have not yet fully recovered (Krause-Jensen et al. 2020). This circumstance determines the need for their research. In the Baltic Sea, seagrass habitats have been identified mainly in

its western part (Boström et al. 2003). The coastal waters of the Russian section of the sea have been little studied in this respect. Information about seagrasses was usually collected along the way in the course of work on other topics (Volodina 2011; Volodina and Gerb 2013; Gerb and Volodina 2020; Gorbunova and Esiukova 2020). The article at hand aimed to summarize all available information about the seagrasses near the Russian coasts of the Baltic Sea. We addressed to the relevant publications and museum collections; generalized the results of our own surveys.

MATERIAL AND METHODS

Using the Russian Science Citation Index, Scopus and Web of Science resources we looked for the publications reporting on seagrasses in the Russian section of the Baltic Sea, that is, the coastal waters of the Kaliningradskaya oblast and Leningradskaya oblast. We also examined the samples of seagrasses in herbarium collections: Immanuel Kant Baltic Federal University, Institute of Living Systems (KLGU), Komarov Botanical Institute (LE), Saint Petersburg State University (LECB), Tsitsin Main Moscow Botanical Garden of Academy of Sciences (MHA), Moscow State University Faculty of Biology (MW) and Faculty of Geography (MWG), Atlantic Branch of the Institute of Oceanology, P.P. Shirshov of the Russian Academy of Sciences (AB IO RAS, Kaliningrad, the acronym of the herbarium is missing), the Museum of the World Ocean (MWO, Kaliningrad, the acronym of the herbarium is missing). Based on the obtained data we identified the coastal areas, where the occurrence of seagrasses could be expected. We observed them from 23 to 29 September 2020; 1 km of the coastline was surveyed at each site. We described, collected, and photographed the beached remains of seagrasses. In June 2021 the surveyed sections were partly explored by snorkeling. Moreover, we summarized the results of our previous studies performed in Kaliningradskaya oblast from 2008 to 2012 (Volodina and Gerb 2013) and Leningradskaya oblast from 2017 to 2021. The latter took place in process of the expedition of the Russian geographic society «Gogland Island»; we observed the shores of the Islands of the Gulf of Finland (Gogland, Bolshoy Tyuters, Sommers, Moshchny, Maly) to register beached seagrasses. To specify the taxonomy we used the guide by N. N. Tsveliov (2000) and the World atlas of seagrasses (Green and Short 2003).

Fig. 1. Beached fragment of *Zostera marina*, Sambia peninsula

RESULTS

The publications and herbarium samples indicate that seagrasses occur only in Kaliningradskaya oblast. Such reports are relatively numerous (table 1). From 1982 to 2021 the remains of seagrasses were registered in Kaliningradskaya oblast in 12 locations (Fig. 1, 2; Table 1). Only one living specimen was noted. It was found in 2009 at a depth of 2 m together with perennial and annual algae (location № 6 in Figure 2). All recorded specimens belong to *Zostera marina* species. In most cases, discarded leaves of seagrasses were found, while the bigger parts of the plants occurred rarely. The largest accumulation of leaves was noted at Cape Gvardeysky (location № 5 in Figure 2) – 244 leaf fragments from 7 to 35 cm long, 211 of them on 50 meters of the route. Underwater surveys showed that there is a rocky bottom in the sections without beached remains of seagrasses; it is covered with an almost continuous layer of filamentous algae. In areas where emissions have been detected, the bottom is sandy.

As for the Russian section of the Gulf of Finland, we failed to find information of seagrasses occurrence, although the relevant studies are rather numerous. Neither herbarium samples, nor reports presented in publications are known. The relevant reports pointed out low salinity at the coasts (e.g. Gubelit 2011), it is hardly suitable for seagrasses. The salinity is enough high at the islands located in the central part of the Gulf, but only algae were registered there among macrophytes so far (Kukk 1988). Our attempts to find the beached remains of seagrasses on the islands were also unsuccessful, only the algae were noted in the wrack.

The seagrasses have been noted at the Russian-Finnish borderline from the Finnish side. Ten samples of beached remains of *Zostera marina* were collected from 1965 to 1989. The nearest congregations of seagrasses in Finland are located at a distance of hundred kilometers westwards (Uotila 2021). No similar records are known for the Russian-Estonian borderline. The nearest site of seagrass registration is far from the state borderline there (Möller and Martin 2007).

DISCUSSION

The beached remains of seagrasses indicate the fact that *Zostera marina* does grow in the coastal waters of the Kaliningrad region. Had the remains been transferred to it in large quantities from afar, then they would be recorded over the whole coastline; moreover, Zostera noltii, would also be encountered as it inhabits the neighboring areas (Labanauskas 2000). However, the small number of remains and the failures to find bottom-growing specimens indicate that seagrasses are scarce; they hardly form big underwater meadows.

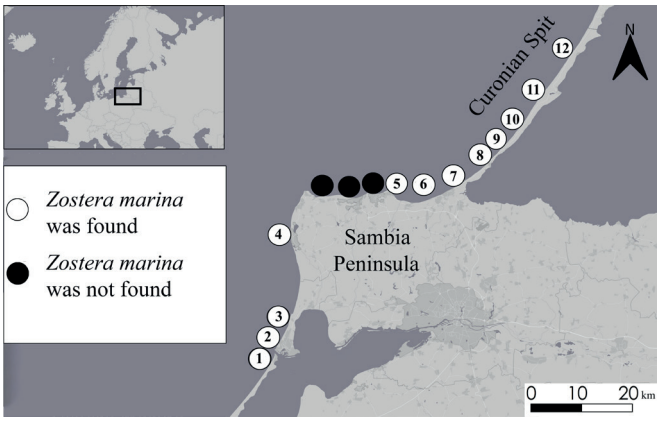

Fig. 2. Locations of the sites under study in Kaliningradskaya oblast, the legend is in Table 1

Table 1. Records of *Zostera marina* in Kaliningradskaya oblast, the numbers correspond to the Figure 2.

№	Coordinates (start/ end of the route for results of a survey performed in 2020)	Date of sampling	Herbarium (* – results of a survey performed in 2020)	Coast survey site	Collected samples	
					Number of leaves	Number of shoots
1	N 54.623689, E 19.866867	12.08.1999	KLGU	Vistula Spit, Kosa village	0	3
	N 54.634332, E 19.876196	01.07.2010	AB IO RAS		0	6
2	N 54.647137, E 19.874504 / N 54.653843, E 19.884376	25.09.2020	IO RAS *	Sambian Peninsula, city of Baltiysk	8	2
3	N 54.680224, E 19.910671	19.08.1995	KLGU	Sambian Peninsula, Mechnikovo village	1	3
4	N 54.867211, E 19.932228 / N 54.876120, E 19.931143	26.09.2020	IO RAS *	Sambian Peninsula, Yantarnyy village	2	4
5	N 54.960471, E 20.258877 / N 54.961471, E 20.271548	29.09.2020	IO RAS *	Sambian Peninsula, Cape Gvardeisky	244	0
6	N 55.046111, E 20.363056	09.09.2009	AB IO RAS	Rooted on the shallows (at a depth of 2 meters, sandy substrate)	0	1
7	N 54.963427, E 20.479510	26.06.2011	AB IO RAS	Sambian Peninsula, Zelenogradsk	0	10
8	N 55.013775, E 20.605672	04.07.2000	KLGU	Curonian Spit, Lesnoye village	1	1
	N 55.016148, E 20.610391 / N 55.023418, E 20.620873	23.09.2020	IO RAS *		42	6
9	N 55.049810, E 20.666673 / N 55.056441, E 20.677567	29.09.2020	IO RAS *	Curonian Spit, Dyuna village	76	12
10	N 55.091755, E 20.727132	20.07.2020	MWO	Curonian Spit, Fringilla Ornithological Station	0	1
	N 55.091141, E 20.726306 / N 55.098690, E 20.735431	27.09.2020	IO RAS *		28	8
11	N 55.134817, E 20.776143	06.08.1982	KLGU	Curonian Spit, campsite Khvoynoye	0	1
12	N 55.223326, E 20.888577 / N 55.230760, E 20.897399	27.09.2020	IO RAS *	Curonian Spit, Dune Efa	10	8

A certain number of seagrasses are regularly brought to the surveyed territory. The transportation of the plant fragments over the sea is one of the dispersion modes of the seagrasses (Den Hartog 1970; Iurmanov 2022). The fragments with shortened vegetative shoots torn off from the maternal rhizome are moved by waves and currents and then root in other suitable places (Vekhov 1992). In the western part of the Baltic Sea, underwater meadows have survived, and therefore they can serve as a source of such planting material. However, it is hardly abundant. In our case, the rooting of such plants is hampered by the fact that most of the bottom of the coastline is covered by moving sands. In a relatively small area at the center of the surveyed coast, the bottom surface is more stable, since it is covered mainly with boulders, pebbles, and gravel; between the rocky substrate, there are areas with

sandy soil (Spiridonov et al. 2010). Seagrasses could exist in some numbers in such plots, but in this very area, there are effluents from treatment facilities of settlements, which leads to an increase in eutrophication and turbidity, i.e. negative impacts on seagrasses.

Since seagrasses have been hardly explored in Kaliningradskaya oblast in the past, it remains unknown whether their numbers have recently declined, or they were not abundant «initially». In neighboring coastal waters of Poland a sharp decline of «underwater meadows» took place since the 1950s (Boström et al. 2003). At present, the aggregations of algae have expanded instead, i. e. the same we observed in a part of the surveyed area. It is possible that seagrasses declined in the same way in Kaliningradskaya oblast.

As for the northern section of the Russian part of the Baltic Sea, the situation seems to be similar there: seagrasses have not been studied in the past, and therefore it is not clear how natural their absence is. Due to strong desalination and the proximity of settlements, the conditions for the seagrasses are unfavorable in most of these waters. However, in its western part the formation of suitable habitats is possible. The coastal waters near the islands located close to the center of the Gulf of Finland are relatively clean and saline. We surveyed only a part of the islands and probably the unexplored islands are promising in this regard.

The decline of seagrasses in the Baltic Sea might have been related to overfishing: it results in the small number of top predatory fishes, the lack of them increases intermediate predatory fishes, the big numbers of these small fishes increase the pressure on small invertebrates; all this contribute the nutrient enrichment of water, the overgrowth of filamentous algae, which influence negatively the seagrasses (Baden et al. 2012). Such data have been obtained for the western side of the Baltic Sea, but similar processes over the studied territory are likely as overfishing has been continuously progressing there over the centuries (Popov 2017). The number of top predatory fishes is insignificant compared to the «initial» or «normal» one. Algae thickets exist in coastal waters. Probably, a part of them replaced the seagrasses beds existing in the past.

The absence of «underwater meadows» is an undesirable phenomenon, since they are a valuable habitat. In such a situation the question of artificial cultivation of seagrasses arises (Meyer and Nehring 2006). Probably some potential habitats have not been lost completely. Moreover the disease of seagrasses which caused their rapid decline several decades ago might have been weakened recently (Brakel et al. 2019) therefore some possibilities to increase the seagrass abundance do exist. A part of the coastal waters of the Russian part of the Baltic Sea may be suitable for such projects.

CONCLUSIONS

In the Russian section of the Baltic Sea the seagrasses *Zostera marina* occur in small numbers only in the southern part, i. e. Kaliningradskaya oblast. They hardly form underwater meadows of noticeable areas. Most of the potential habitats have been lost because of increased water turbidity resulting from anthropogenic pressure on the coastal areas. This situation is an additional illustration of the global decline of seagrasses and the impoverishment of the Baltic Sea ecosystems.

REFERENCES

Aminina N. (2005). Main trends of the studies on algae and sea grasses of Far East. Isvestiya TINRO, 141, 348-354.

Baden S., Emanuelsson A., Pihl L., Svensson C., and Åberg P. (2012). Shift in seagrass food web structure over decades is linked to overfishing. Mar. Ecol. Prog. Ser., 451, 61-73.

Blinova E. (2007). Algae-macrophytes and grasses of the seas of the European part of Russia (flora, distribution, biology, reserves, mariculture). Moscow: VNIRO (In Russian).

Borum J., Duartes C., Krause J. and Greve T. (2004). European seagrasses: an introduction to monitoring and management. London: EU Project Monitoring and Managing of European Seagrasses (M&MS).

Boström C., Baden S. and Krause-Jensen D. (2003). The sea grasses of Scandinavia and Baltic Sea. In: E. Green and F. Short, eds., World Atlas of Seagrasses. Berkeley: University of California Press.

Brakel J., Jakobsson-Thor S., Bockelmann A.-C. and Reusch T. (2019). Modulation of the Eelgrass – Labyrinthula zosterae Interaction Under Predicted Ocean Warming, Salinity Change and Light Limitation. Front. Mar. Sci., 6(268), 1-13.

Den Hartog C. (1970). The seagrasses of the World. Rotterdam: A.A. Balkema.

Duarte C. (2002). The future of seagrass meadows. Environmental Conservation, 29, 192–206.

Gerb M. and Volodina A. (2020). Macrophytes of the south-eastern part of the Baltic Sea and its lagoons. In: Materials of the IX International Scientific and Practical Conference «Marine Research and Education», Moscow, 1, 139-142. (In Russian).

Gorbunova Ju. and Esiukova E. (2020). Emissions of macroalgae and seagrass in the Russian part of the south-east Baltic Sea coast. Izvetiya KGTU, 59, 24-34. (In Russian with English summary).

Green E. and Short F. (2003). World Atlas of Seagrasses. Berkeley: University of California Press.

Gubelit Yu. and Kovalchuk N. (2013). Macroalgal community in conditions of the eastern part of the Gulf of Finland. Proceedings of the Zoological Institute, RAS, 3, 90-97. (In Russian with English summary).

Gubelit Yu. I. (2011). Structure and functioning of coastal algocenosises of the eastern part of the Gulf of Finland. PhD thesis. Saint-Petersburg. Zoological Institite RAS

Hogarth P. (2015). The Biology of Mangroves and Seagrasses. 3rdEd. Oxford etc.: Oxford University Press.

Iurmanov A. (2022). Phylogenetic phytogeography of selected groups of seagrasses (Monocotylendoneae – Alismatales) based on analysing of genes 5.8s rRNA and RuBisCo large subunit. Geography, Environment, Sustainability, 15(1), 61-69.

Kardakova E. and Kizevetter I. (1953). Sea grasses of Far East. Vladivostok: Primorskoye knijnoye izdatelstvo. (In Russian).

Krause-Jensen D., Duarte C., Sand-Jensen K., and Carstensen J. (2021). Century-long records reveal shifting challenges to seagrass recovery. Glob Change Biol., 27, 563-575.

Kukk H. (1988). Long-term changes in the bottom vegetation of Hogland (Suursaari) Island coastal waters). Izv. AN SSSR. Biol. Ser. 37(3), 242-244.

Kulepanov V.N. (2005). Studies of macrofitobenthos at the coasts of Primorie. Izvestiya TINRO, 141, 355-364. (In Russian with English summary).

Labanauskas V. (2000). Benthic macrophyte communities on the Lithuanian coast of the Baltic Sea. Botanica Lithuanica, 6(4), 401-413. (in Lithuanian with English summary).

Meyer Th. and Nehring S. (2006). Anpflanzung von Seegraswiesen (Zostera marina L.) als interne Maßnahme zur Restaurierung der Ostsee. Rostock. Meeresbiolog. Beitr., 15, 105-119. (in German with English summary).

Möller T. and Martin G. (2007). Distribution of the eelgrass Zostera marina L. in the coastal waters of Estonia, NE Baltic Sea. Proc. Estonian Acad. Sci. Biol. Ecol., 56(4), 270-277.

Orth R. (2006). A Global Crisis for Seagrass Ecosystems. BioScience, 56, 987-996.

Pike C., Crook V. and Gollock M. (2020). Anguilla anguilla. The IUCN Red List of Threatened Species. https://dx.doi.org/10.2305/IUCN.UK.2020-2.RLTS.T60344A152845178.en. [Accessed 22 Jul. 2021].

Popov I. (2017). Overfishing in the Baltic Sea Basin in Russia, Its Impact on the Pearl Mussel, and Possibilities for the Conservation of Riverine Ecosystems in Conditions of High Anthropogenic Pressure. Biology Bulletin, 1, 46-51.

Short F., Polidoro B., Livingstone S., Carpenter K., Bandeira S., Bujang J., Calumpong H., Carruthers T., Coles R., Dennison W., Erftemeijer P., Fortes M., Freeman A., Jagtap T., Kamal A., Kendrick G., Kenworthy W., La Nafie Y., Nasution I., Orth R., Prathep A., Sanciangco J., van Tussenbroek B., Vergara S., Waycott M. and Zieman J. (2011). Extinction risk assessment of the world's seagrass species. Biological Conservation, 144, 1961-1971.

Spiridonov M., Zhamoyda V., and Ryabchuk D. (2010). Regional and ecological geology of the Russian Baltic and its coastal zone. Regional'naya geologiya i metallogeniya, 44, 90-103. (In Russian with English summary).

Tsveliov N. (2000). Manual of the vascular plants of North-West Russia. Saint-Petersburg: SPKhFA. (In Russian).

Unsworth R., Keulen van M. and Coles R. (2014). Seagrass meadows in a globally changing environment. Marine Pollution Bulletin, 83, 383-386.

Uotila P. (2021). Zostera marina. Finnish biodiversity Information Facility. https://laji.fi/en/taxon/MX.40159 [Accessed 05 July 2021].

Vekhov V. (1992). Zostera of the White Sea. Moscow: Moscow State University. (In Russian).

Volodina A. (2011). Preliminary results of studies of macrophyte communities in the coastal zone of the southeastern Baltic (Kaliningrad region) In: Materials of the All-Russian Conference: «Domestic Geobotany: Major Milestones and Prospects» SPb, 1, 47-51. (In Russian).

Volodina A. and Gerb M. (2013). Macrophytes of the coastal zone of the Russian sector of the southeastern part of the Baltic Sea (Kaliningrad region). Izvestiya KGTU, 28, 129-135. (In Russian with English summary).

Waycott M. and Williams S. (2006). A global crisis for seagrass ecosystems. Bioscience, 56, 987-996.

RESEARCH PAPER

SHORELINE CHANGE DETECTION USING DSAS IN PARIAMAN CITY, WEST SUMATERA

Widya Prarikeslan[1,3], Dian A. Arif[3], Eri Barlian[2], Nurhasan Syah[2],Yulia Nanda[3],Widia Sutriani[3]
[1]Doctoral Program of Environmental Sciences, – Universitas Negeri Padang, Prof. Dr. Hamka Street, Padang, 25171, Indonesia
[2]Environmental Sciences Department – Universitas Negeri Padang, Prof. Dr. Hamka Street, Padang, 25171, Indonesia
[3]Department of Geography, Faculty of Social Science – Student Universitas Negeri Padang , Prof. Dr. Hamka Street, Padang, 25171, Indonesia
***Corresponding author:** widya_geo@fis.unp.ac.id
Received: August 18th, 2021 / Accepted: April 24th, 2022 / Published: June 30th, 2022
https://DOI-10.24057/2071-9388-2021-097

ABSTRACT. This study was conducted to determine the shoreline change that occurred in the coastal of Pariaman city due to accretion and erosion. The present study of the shoreline changes along Pariaman City was done using DSAS 5.0 vector analysis. Landsat 5 TM 1989, Landsat 7 ETM+1999 and 2011, and Landsat 8 OLI/TIRS 2020 images were interpreted first. The results indicate that during 1989 – 1999 there was abrasion with an average distance of change of 281,60 m. The period from 1999 to 2011 was characterized by accretion with an average distance of change of 15,98 m. The latter period 2011 – 2020 was dominated by accretion with an average distance of change of 53,68 m. The indicated fundamental output of the study is to provide useful scientific information and data for development planning and coastal areas, especially those managing the environment and their ecosystems, as well as for the government and related stakeholders and academics and scientists for the use of resources and space in coastal areas. Stakeholders include the city government office in Padang Pariaman, Ministry of Marine Affairs and Fisheries, Regional Disaster Management Agency and Ministry of Public Works and Public Housing of Republic of Indonesia.

KEY WORDS: Shoreline change, DSAS, abrasion, accretion

CITATION: Prarikeslan W., Arif D.A., Barlian E., Syah N., Nanda Y., Sutriani W. (2022). Shoreline Change Detection Using Dsas in Pariaman City, West Sumatera. Geography, Environment, Sustainability, 2(15), p. 116-123
https://DOI-10.24057/2071-9388-2021-097

ACKNOWLEDGEMENTS: The authors would like to thank Lembaga Penelitian dan Pengabdian Masyarakat Universitas Negeri Padang for funding this research.

Conflict of interests: The authors reported no potential conflict of interest.

INTRODUCTION

The threats that occur in the area are becoming increasingly large and include natural and anthropogenic disturbances in the form of sea-level rise, abrasion, and various activities that overexploit resources. Indeed, over 80% of the world's beaches are experiencing coastal erosion with rates ranging from 1,0 cm/year to 30 m/year, and this presents a serious hazard to many coastal regions (Addo A, Walkden, Mills & T 2008). Shoreline change detection is indispensable for monitoring coastal zoning (Nassar, et al. 2019).

Coastlines are unique features on the Earth's surface. Coastlines are one of 27 features recognized by the International Geographical Data Committee (IGDC). A coastline is generally defined as the meeting line between land and water bodies. A coastline can be interpreted easily, but it is difficult to record because water levels are always changing. To determine and record the line of meetings, a coastline is coordinated with tidal events where the shoreline is drawn based on a certain tide level (Li, Di, & Ma 2001). A coastline becomes the position of the water surface at a certain time, which occurs dynamically and can be an indicator of the occurrence of abrasion and accretion events on a beach (Genz, Fletcher, Dunn, Rooney, & J.J. 2007). The place where the interactions between tides occur is called the coastal zone. Ccoastlines continue to change due to geomorphic processes in the form of abrasion and accretion, periodic storms, flooding, and continuous changes in sea level (Nayak 2002).

The movement of shorelines over time is usually a predictable component of variation that can be regarded as a signal or trend and short-term variation or noise. Long-term phenomena, such as a rise in sea level or a shift in natural sediment supply, occur over periods of decades to centuries and produce torn predictable trends (Dolan, Fenster, & Holme 1991).

The world's population of 45% occupies coastal areas, which results in continued pressure on coastal areas as a result of the development process and exploitation of land resources, and coastal areas only cover 20% of the world's total land area (Mentaschi, Vousdoukas, Voukouvalas, & Feyen 2018). This pressure is caused by the development of the fishing, tourism, and settlement industries, which depend on conditions such as water quality, physical infrastructure, and biodiversity. Coastal residents utilize the diversity of coastal ecosystem resources in various ways, such as agricultural use, developed land, and tourism (Burt & Bartholomew 2019). This can be seen at Pariaman Beach, where dynamic changes in the coastline occur due to geomorphic processes in the form of abrasion, accretion, periodic storms,

floods, and continuous changes in sea level. Pariaman Beach is relatively flat, with a slope of less than 20 degrees and depth variations ranging from 0 meters to 125 meters for distances up ot 20 km to sea. At distances of 0 meters (beach) to 5000 meters to sea, the maximum water depth is 20 meters (Ondara et al. 2018). The current velocity of the water of Kota Pariaman ranges from 0 m/s to 0.03 m/s, with the dominant direction being perpendicular to the coast. In the northern part of the waters, as well as the southern part, the dominant current comes from the north, making the area prone to abrasion and accretion.

Periodic analysis of shorelines is needed to monitor coastal areas, and the use of remote sensing is very efficient in obtaining information on shoreline dynamics (Rajasree, Deo, & Nair, 183.221-234). In addition, temporary analysis of coastal areas is also useful in understanding the distribution of shoreline dynamics and assisting in the formulation of coastal area policies (Zhang 2011).

Data time series with a spatial resolution similar to that of imagery are often needed to unify a process over a long period (Kasim & Salam 2015). Data time series with high resolution are very difficult to obtain, especially in Indonesia, which is a developing country. Therefore, to overcome problems related to data time series availability, multiscale analysis data integration can be considered. Various studies in various cases have been carried out using different spatial and temporal resolution integrations (Armenakis & Savopol 2004) (Zimmermann & Bijker 2004).

Geographic Information System (GIS) based methods are used by utilizing DSAS tools, an extension of ArcGIS developed by the USGS to calculate shoreline changes through temporal data (Qiao et al. 2018). The use of the DSAS is very important in analyzing the rate of shoreline change, as indicated by the rate of erosion and sedimentation, which is very useful in developing coastal areas economically as a basis for policy-making (Raj, Gurugnanam, Sudhakar, & Francis 2019).

The purpose of this study is to analyze multitemporal shoreline changes by utilizing satellite imagery from 1989, 1999, 2011, and 2020. Statistical image processing using DSAS 5.0 tools is useful for measuring the rate of accretion and abrasion at the study site.

MATERIALS AND METHODS

The research was conducted on the coast of Pariaman city as a representative of the west coast of the island of Sumatera, Indonesia (Fig. 1). This location is one of the locations where tourism is growing rapidly in West Sumatra. This study was carried out with GIS (ArcGIS) and image processing tools using MultiMate. This research was conducted using ArcGIS and ENVI software. Both types of software are applications for processing spatial data, Landsat satellite imagery data in this case. After geoprocessing the image data on ENVI, the coastline is extracted each year. The coastline is then converted into a shapefile, which will then be processed in ArcGIS. To see changes in the coastline, one of the tools in ArcGIS is used, namely, the DSAS. The DSAS is an add-on product in ArcGIS that builds transects from predefined baselines to estimate shoreline change. The DSAS is one of the change detection applications developed by the USGS.

Coastal analysis can be performed by utilizing various types of imagery (Fawzi & Iswari 2018). High-resolution imagery is very good for shoreline delineation because it produces detailed information but is very expensive if monitoring is performed regularly (Zhao, Guo, Yan, Wang, & Li 2008). Therefore, Landsat imagery is used, which has a fairly good resolution but at an affordable cost. The main data were obtained from Landsat satellite images at different recording times, namely, in 1989, 1999, 2011, and 2020, which covered 31 years. The selected image has a spatial resolution of 30 meters. Image descriptions are presented in Table 1.

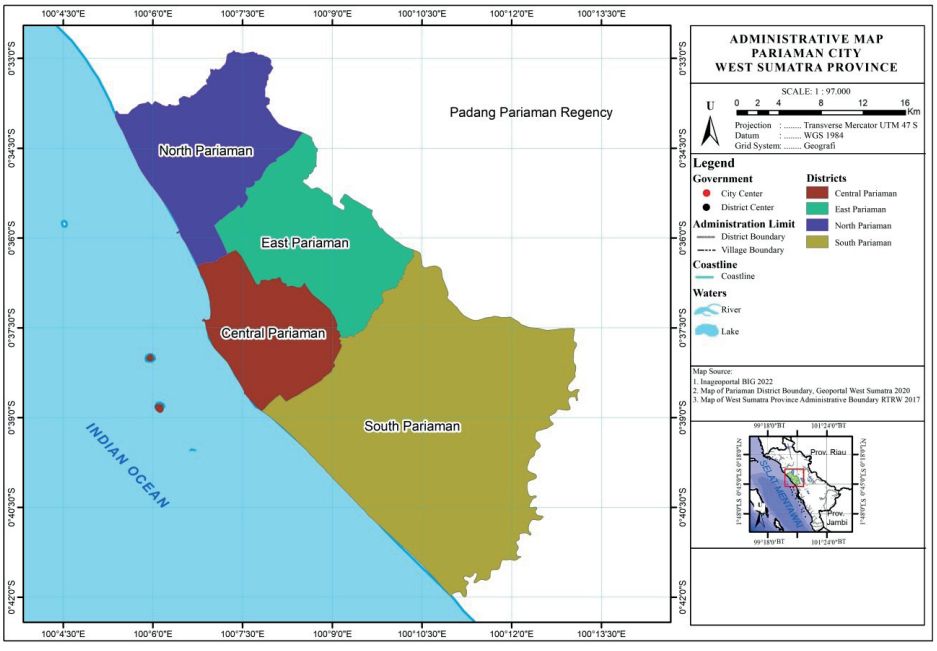

Fig. 1. Landsat image description

Table 1. The assessment of various bandwidth selection methods

Year	Path and Row	Landsat	Spatial Resolution
1989	127 – 60	Landsat 5 TM	30
1999	127 – 60	Landsat 7 ETM+	30
2011	127 – 60	Landsat 7 ETM+	30
2020	127 – 60	Landsat 8 OLI/TIRS	30

Image processing begins with image cutting to focus on the research location. The Image recording quality is different from one another, so radiometric correction is needed to improve the poor quality image caused by image damage and atmospheric noise (Ardiansyah 2015). Image calibration is performed using radiometric calibration and atmospheric correction with Fast Line of Sight Atmospheric Analysis of Spectral Hypercubes (FLSAAH). The final stage in image analysis is overlaid, so geometric correction must be performed to ensure that all images have the same spatial resolution (Darmiati 2020). Coastal extraction is performed by digitizing the on-screen image (Arief 2011). The on-screen digitalization process has the disadvantage of relying on visual ability to identify objects but has a good degree of accuracy (Kasim, Multiple Method Approach in Monitoring Coastline Change using Landsat Remote Sensing Dataset and GIS 2012). To help the shoreline extraction process, spectral analysis was performed. On Landsat 5 and Landsat 7 TM images, ETM+ images were obtained using the -5 band because they can distinguish between soil and rock objects, and shoreline extraction from Landsat 8 OLI/TIRS images was perform by using the combined RGB method (color RGB) (Nugraha 2016). It is the best method for shoreline determination using visual interpretation because it shows a clear boundaries between sea and land (Winarso & Budhiman 2001).

Data Analysis

The shoreline of Pariaman city is 6,52 km long and divided into 4 segments. The shoreline dynamics observed using DSAS 5.0 tools are the net shoreline movement and endpoint rate in 1989–1999, 1999–2011, and 2011–2020. The baseline is based on the shoreline in the topography map obtained by the Geospatial Information Agency (BIG). In the DSAS, net shoreline movement (NSM) analysis is used to determine the magnitude of the distance of temporal shoreline changes. A positive (+) NSM measurement indicates that the beach has accretions, and a negative value (-) indicates that the beach has undergone abrasion. Next, the rate of shoreline change is measured with the end point rate (EPR). The EPR method calculates the rate of shoreline change by comparing the difference between the distances of the oldest shoreline and the most recent shoreline in a predetermined period. Data that are positive (+) indicate that the beach has accretions, and data that have a negative value (-) indicate that the beach has experienced abrasion (Arif, Prarikeslan, & Syaharani 2020).
To understand the movement of the coastline in a certain time interval, it is very important to use shoreline statistics. This movement indicates the direction of change in this region. Abrasion and accretion are two important factors that cause shoreline changes. The previously generated transect lines were used to generate statistics along the coast on each transect to see trends in shoreline changes that occurred (Kallepalli, Kakani, James, & Richardson 2017).

a. Net shoreline movement (NSM). These NSM statistics provide information on the distance between the youngest and oldest shorelines, with negative or positive symbols indicating abrasion or accretion, respectively.

NSM = distance between the oldest and youngest shorelines

b. End point level (EPR). EPR statistics are easy to use to calculate and compare 2 lines.

EPR = NSM distance /time between the oldest and most recent shorelines

RESULTS

In general, the physical components of the beach in the eastern part of the study site include silt, sand, and gravel deposited from the erosion of the Bukit Barisan process. Sandy beaches are highly dynamic places due to the low resistance of materials to dynamics factors (Ward 2010). Physiographically the Pariaman city coast is a coast under wave erosion conditions, and the erosion process of the coastal area has resulted in the decline of the shoreline. The shoreline, as the object of this research, was extracted from three Landsat images. NSM and EPR measurements were performed between 1989 and 1999, 1999 and 2011, and 2011 and 2020.

Shoreline Change from 1989–1999

In 1989–1999, abrasion occurred, with an average abrasion distance of 281,60 m and an average change in the shoreline of 28,16 m/year. The shoreline change map from 1989–1999 is shown in Fig. 2.

Shoreline changes in Pariaman city between 1989 and 1999 indicate the occurrence of abrasion/erosion in the coastal area, which caused the land area to decrease. The land area decreased with an average distance of 281,60 m at a rate of 28,16 m/year. This shows that the changes that occured are very substantial, so coastal management must make decisions so that the land does not continue to experience dangerous abrasion/erosion. The abrasion that occurs is influenced by hydro-oceanographic activities such as wind, which triggers the height of the waves and the strength of the waves that hit the land.

Based on the above matrix for 1989–1999 coastal management decisions must be made so that abrasion does not continue to occur with a very large rate of change. This is in line with structural management decisions, such as decisions to protect coastal buildings, make groins along the coast at a certain length and distance, and plant crops that can protect the coast from the energy of large waves.

Table 2. Shoreline change from 1989-1999

Segment	Net Shoreline Movement (m)		End Point Rate (m/year)		Process
	(+)	(-)	(+)	(-)	
1	-	270,91	-	27,09	Abrasion
2	-	313,51	-	31,35	Abrasion
3	-	272,40	-	27,24	Abrasion
4	-	269,59	-	26,96	Abrasion
Total	-	281,60	-	28,16	Abrasion

Source: Primary data processing

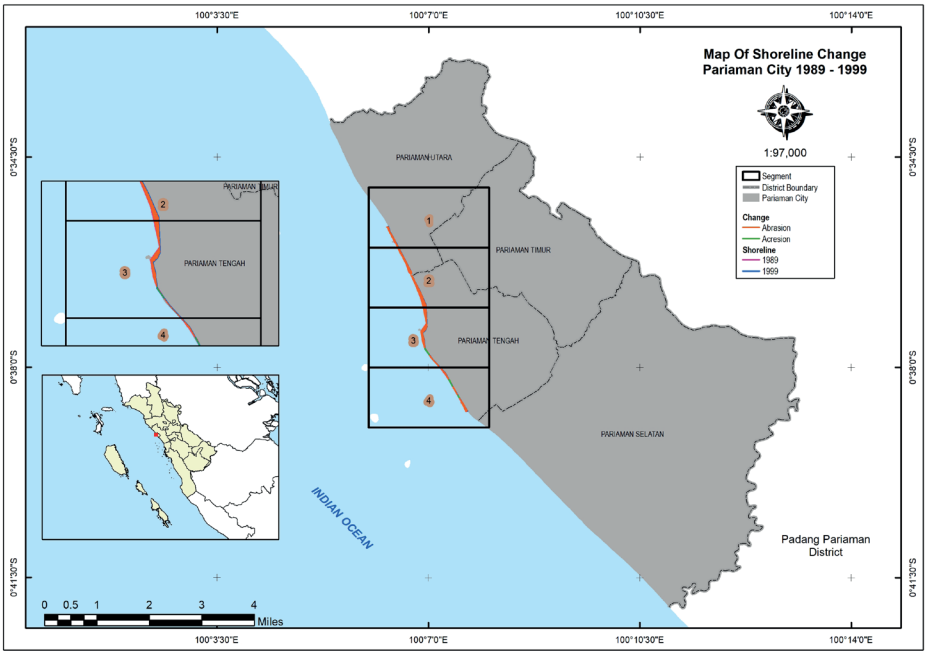

Fig. 2. Shoreline change from 1989-1999

Locations of Zone	Rate of Change, EPR (m/yr)	Segment	ERP (m/yr) [Mean]	Evaluation	Risk Level	Decision
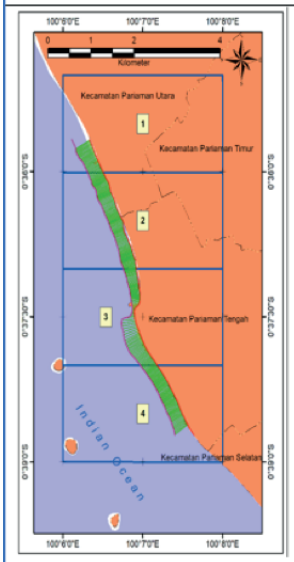	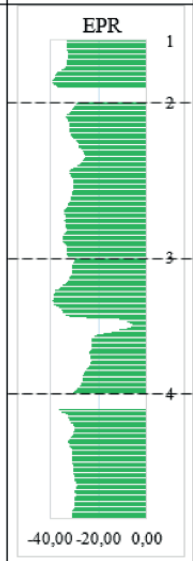	1	-27,09	Very high erosion		Required
		2	-31,35	Very high erosion		Required
		3	-27,24	Very high erosion		Required
		4	-26,96	Very high erosion		Required

Fig. 3. Decision matrix showing shoreline evolution and risk assessment for the EPR zone between 1989 and 1999

Shoreline change in 1999–2011

From 1999–2011 the average abrasion distance was 15,98 m, with an EPR of 1,33 m/year, while the average accretion distance was 17,68 m, with an EPR reaching 1,47 m/year (Fig. 3). The dominant coastal dynamic process that acts on all segments is accretion. The longest average added distance of 29,82 m occurs in segment 3, with an EPR value of 2,48 m/year. Changes in the 1999–2011 shoreline are presented in Table 3.

Table 3. Shoreline change in 1999-2011

Segment	Net Shoreline Movement (m)		End Point Rate (m/year)		Process
	(+)	(-)	(+)	(-)	
1	10,22	-	0,85	-	Accretion
2	16,12	27,84	1,34	2,32	Abrasion
3	29,82	9,52	2,48	0,79	Accretion
4	14,56	10,58	1,21	0,88	Accretion
Total	17,68	15,98	1,47	1,33	Accretion

Source: Primary data processing

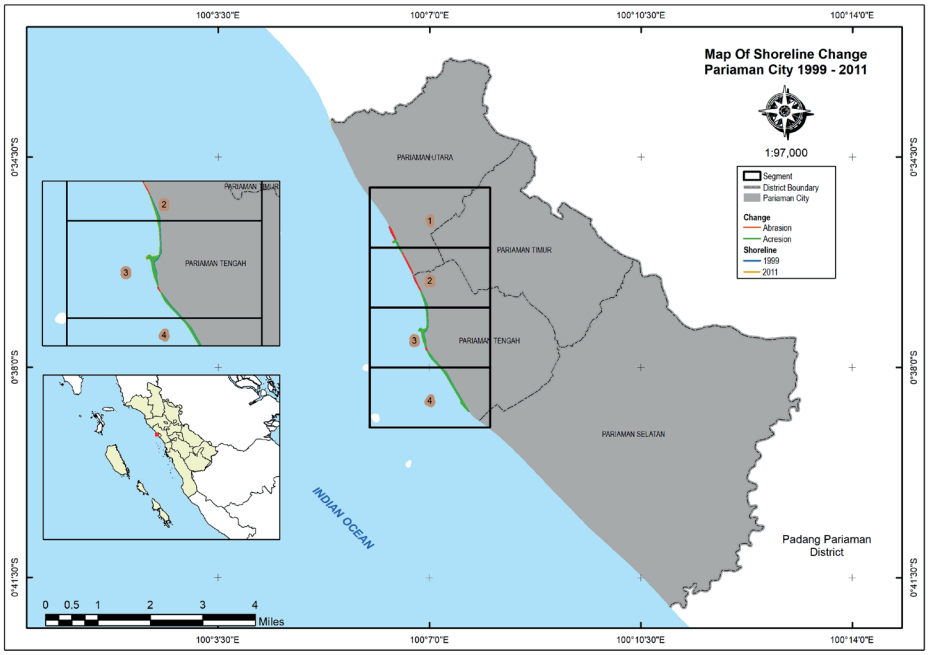

Fig. 4. Shoreline change in 1999–2011

Locations of Zone	Rate of Change, EPR (m/yr)	Segment	ERP (m/yr) [Mean]	Evaluation	Risk Level	Decision
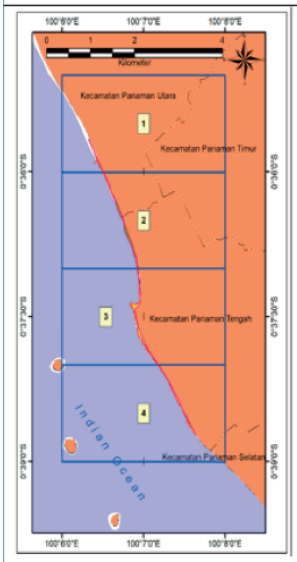	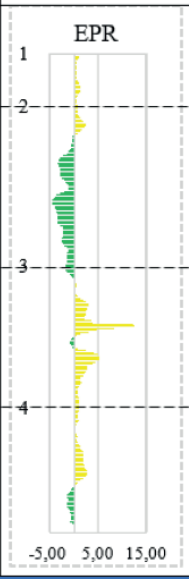	1	0,85	Moderate Accretion		Not - Required
		2	-2,32	Very high erosion		Required
		3	2,48	Very high accretion		Not - Required
		4	1,21	Very high accretion		Not - Required

Fig. 5. Decision matrix showing shoreline evolution and risk assessment for the EPR zone between 1999 and 2011

Changes in the coastline in Pariaman city between 1999 and 2011 indicate the occurrence of abrasion and accretion in the coastal area, which causes changes in the coastline. Land increases with an average rate of change of 1,47 m/year, but along the coast, abrasion also occurs, with an average rate of change of 1,33 m/year. This shows that the changes that occur are very dynamic, so it is necessary to make coastal management decisions so that the land does not continue to experience adverse abrasion/erosion. Fig. 5 shows the shoreline change matrix or dynamics that occurred. Between 1999 and 2011, there were changes in the form of abrasion and accretion, which must be studied so that abrasion does not occur continuously. Structural management of coastal areas in the form of buildings or making groins along the coast is effective in reducing the rate of abrasion that occurs along coasts. In segment 2, it is necessary to build coastal protection structures and groins to reduce abrasion.

Shoreline Change in 2011–2020

From 2011–2020, the average abrasion distance was 5,94 m, with an EPR of 0,44 m/year, while the average accretion distance was 53,68 m, with an EPR reaching 5,96 m/year (Fig. 4). The dominant coastal dynamic process that acts on all segments is accretion. The longest average added distance of 66,52m occurs in segment 3, with an EPR value of 7,39 m/year. Changes in the 2011–2020 shoreline are presented in Table 4.

Changes in the coastline in Pariaman city between 2011 and 2020 indicate the occurrence of abrasion and accretion in the coastal area, which causes changes in the coastline. Land increases with an average rate of change of 5,96 m/yar, but along the coast, abrasion also occurs,with an average rate of change of 0,44 m/year. This shows that the changes that occur are very dynamic; therefore, it is necessary to make coastal management decision so that the land does not continue to experience harmful abrasion/erosion.

Table 4. Shoreline change in 2011-2020

Segment	Net Shoreline Movement (m)		End Point Rate (m/year)		Process
	(+)	(-)	(+)	(-)	
1	58,94	7,69	6,55	0,88	Accretion
2	31,13	-	3,46	-	Accretion
3	66,52	3,93	7,39	0,44	Accretion
4	58,13	-	6,46	-	Accretion
Total	53,68	5,94	5,96	0,44	Accretion

Primary data processing

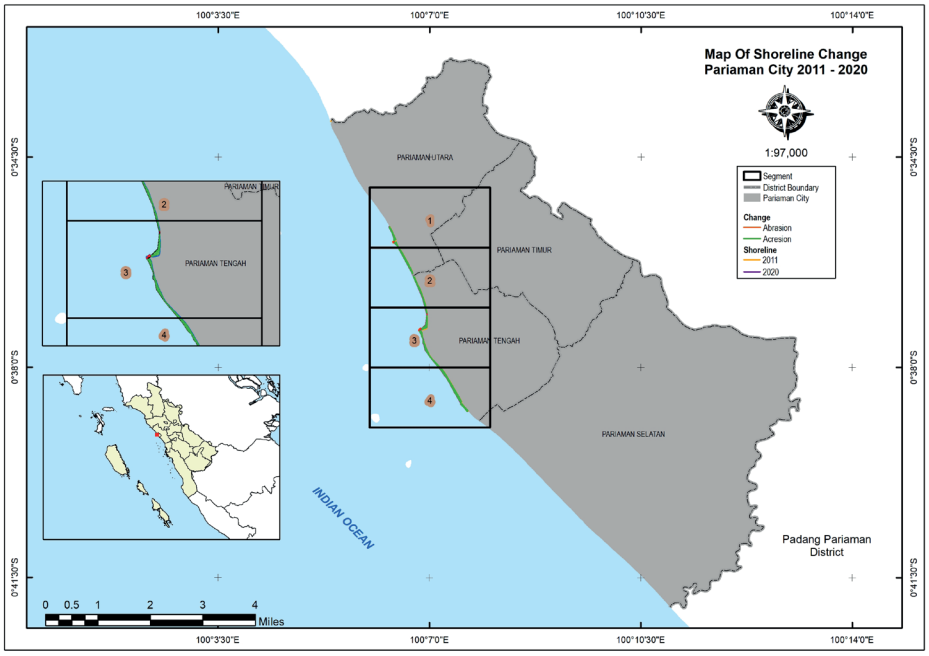

Fig. 6. Shoreline change in 2011–2020

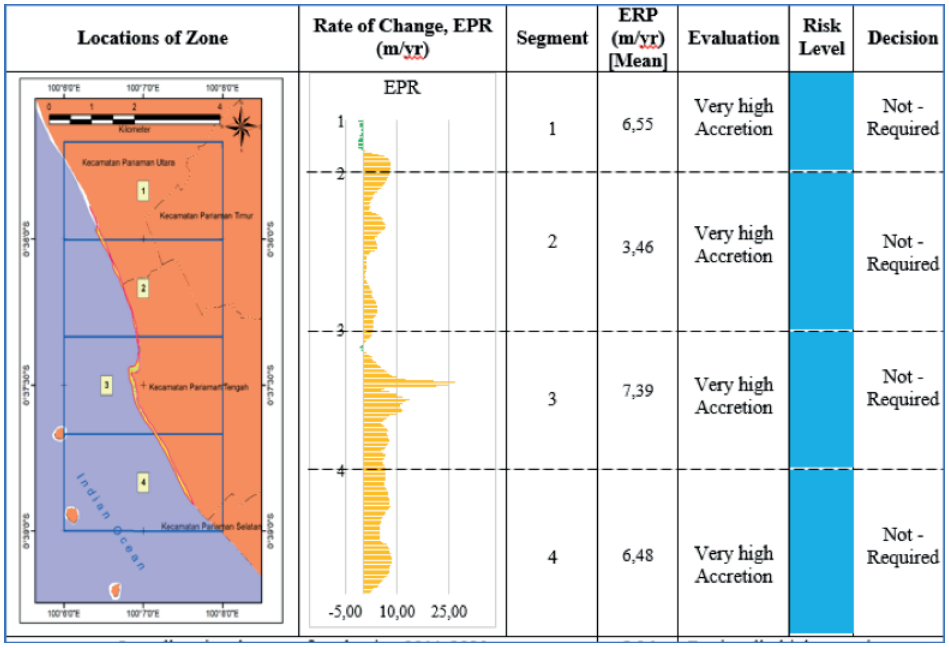

Fig. 7. Decision matrix showing shoreline evolution and risk assessment for the EPR zone between 2011 and 2020

Fig. 7 shows the matrix or the dynamics of shoreline changes that occur. Between 2011 and 2020, there was a change in the form of accretion, which must be studied so that abrasion does not occur continuously. Structural management by making coastal groins along the coast is effective in reducing the rate of abrasion that occurs along the coast. From 2011–2020, the land area continues to increase. This indicates that in the upstream area, there is soil damage or erosion, which causes 30% of the sediment to enter the river and move upstream so that the land area increases or undergoes accretion.

Segment 3 is an area where the accretion process is very dominant. This condition is caused by its position near the river mouth. Sediment input resulting from the erosion process of upper lands gathers in this region. Structural management is also one of the factors in the accretion process. At this location groins were built to protect tourist sites. Based on NSM and EPR measurements, during each observation period, a very dominant accretion process occurred due to hydro-oceanographic factors. This process increases the risk of abrasion due to waves on the beach. Underwater morphological conditions also influence the refraction process and eventually form a longshore current (Bird, 2008). Furthermore, sediments resulting form the erosion of upper lands are carried by longshore currents. The trend of shoreline dynamics also increased, with the erosion rate reaching 281,60 m in 1989-1999, 15,98 m in 1999-2011 and 5,94 m in 2011–2020.

With the characteristics and dynamics of coastal and marine areas, development potentials and problems, and government policies for the marine sector, optimal and sustainable coastal and marine development can only be achieved through integrated coastal and marine management.

DISCUSSION

Coastline changes have an impact on coastal ecosystems. Ecosystem life is disrupted by coastline changes. The erosion of sandy beaches represents a real threat to coastal economies. This is especially the case for those territories that derive their family income from tourist services, being a major factor for the socio-economic development of tourist communities (de paula 2021). This can occur due to the influence of human activities as well as hydro-oceanographic factors. Based on wave data obtained from wind data calculations show that the dominant wave from the direction of west, while based on the beach geomorphology, sand shoal (Sandy Spit) generally trending north-south. This shows that the wave forms an angle when touch the shoreline and the direction of the current parallel to the coast (longshore current) dominant from the north, causing the abrasion process continues to progress towards north along with the construction of groynes in along the coastline of Pariaman (Solihuddin, Tb.2011).Therefore, changes in coastlines must be handled. As a direct result of this finding, there will hopefully be efforts to overcome abrasion naturally (back to nature), such as planting coconut trees and fir trees around coasts to reduce the impact of greater abrasion as well as building breakwater and coastal protection buildings and moving seawards. Government management has also considered the condition of the river mouth, which is the meeting point between upstream activities and marine activities (waves and tides). Optimal management must be continued to reduce the risk of coastal abrasion. By comparison with other coastal areas of the world, the analysis of erosion data shows that in European coastal zones, 1500 km are artificial coasts (Balearic Islands, Gulf of the Lion, Sardinia, Adriatic, Ionian and Aegean coasts) occupied by harbors (1250 km) (Corine 1998). According to the data collected by Corine, approximately 25% of the Italian Adriatic coast and 7.4% of the Aegean coast show an evolutionary tendency toward erosion, whereas approximately 50% of the Euro-Mediterranean coastal zone is considered stable. Coastal states commit themselves to the integrated management and sustainable development of coastal areas and the marine environment under their national jurisdiction. The regional significance of this research is knowing areas with very high erosion and accretion extents so that it is easier to find solutions to solve these problems (Benasa G. 2006).

CONCLUSIONS

The calculated shoreline change statistics are NSM and the EPR. NSM refers to the amount of change over time, and the EPR refers to the rates of change. Therefore, further analysis (trend investigation and hazard line construction) was carried out using the EPR.

Shoreline change is a threat to cities that have coastal areas. Changes in coastlines are an indicator of coastal dynamics due to the iterative reactions between hydro-oceanography and human activities. From 1989–1999 the process of abrasion or a reduction in a land area of 281,60 m dominated the dynamics that occurred in Pariaman city. Then, between 1999 and 2011 and 2011 and 2020, accretion or an increase in land area dominated.

The changes (abrasion and accretion) occurring in this region were investigated using change detection of shorelines extracted from satellite imagery spanning 31 years. The overall change is estimated from 1989–2020. The impact of local phenomena is indicated by short-term trends, while long-term trends are used to calculate the overall change.

REFERENCES

Addo A.K., Walkden Mills M. a., & T.J. (2008). Detection, Measurement, and prediction of shoreline recession in Accra, Ghana. ISPRS Journal of Photogrammetry and Remote Sensing, 63(5).543-558.

Ardiansyah (2015). Remote Sensing Image Processing using ENVI 5.1 and ENVI Lidar (Theory and Practice). South Jakarta: PT. LABSIG INDERAJA ISLIM.

Arief M. (2011). Study of Coastline Change using Landsat Satellite Data in Kendal Regency. Remote Sensing Journal, 8.

Arif D., Prarikeslan W., & Syaharani L. (2020). Analysis of Shoreline Dynamics for Coastal Management Practice in Pariaman, West Sumatera. International Journal, 19(72), 166-172.

Armenakis C., & Savopol F. (2004). Image Processing and GIS Tools for Feature and Change Extraction. International Archives of Photogrammetry, Remote Sensing & Spatial Information Sciences, 35.611-616.

Bird E. (2008). Coastal Geomorphology. England: Wiley.

Benassai ,G.(2006). Introduction Coastal Dynamics and Shorline Protection. WITpress publishes leading books in Science and Technology. University of Naples Parthenope, Italy

Burt J., & Bartholomew A. (2019). Towards More Sustainable Coastal Development In An Urbanized Seascape. Marine Pollution Bulletin, p93-102.

CORINE (1998). COastal eRosIoN databasE. CEC, Luxembourg, 79pp plus maps

Darmiati (2020). Analysis of Coastline Changes in the West Coast Region of Tanah Laut Regency, South Kalimantan. Journal of Tropical Marine Science and Technology, 12(1).

De paula, Davis P., Lima Jailson C., Barros Eduardo L. (2021). Coastal Erosion And Tourism: The Case Of The Distribution Of Tourist Accommodations And Their Daily Rates. Geography, Environment, Sustainability, 14(3), 110-120.

Dolan R., Fenster M., & Holme S. (1991). Temporal Analysis of Shoreline Recession and Accretion. Journal of Coastal Research, 723-744.

Fawzi N., & Iswari M. (2018). Remote Sensing for Coastal Studies. Oceana, XLIII(2).

Genz A., Fletcher C., Dunn R., Rooney L.F., & J.J. (2007). The Predictive Accuracy of Shoreline Change Rate Methods and Alongshore Beach Variation on Maui, Hawaii. Journal of Coastal Research, 23(1 (231)).87-105.

Kallepalli A., Kakani N., James D., & Richardson M. (2017). Digital Shoreline Analysis System-Based Change Detection Along the Highly Eroding Krishna-Godavari Delta Front. Journal of Applied Remote Sensing, 11(3).036018.

Kasim F. (2012). Multiple Method Approach in Monitoring Coastline Change using Landsat Remote Sensing Dataset and GIS. Agropolitan Scientific Journal, 5.

Kasim F., & Salam A. (2015). Identification of Coastline Changes using Satellite Imagery and Their Correlation with Land Cover Along the South Coast of Gorontalo Province. Scientific Journal of Fisheries and Marine Affairs, 3(4).

Li R., Di K., & Ma R. (2001). A Comparative Study of Shoreline Mapping Techniques. GIS for Coastal Zone Management, 53-60.

Mentaschi L., Vousdoukas M., Voukouvalas E., & Feyen L. (2018). Global Long-Term Observations of Coastal Erosion and Accretion. Scientific Reports, 8(1), 1-11.

Nassar K., Mahmod W., Fath H., A, Negm K.N., & A. (2019). Shoreline Change Detection using DSAS Technique: Case of North Sinai Coast, Egypt. Marine Georesources & Geotechnology, 37(1), 81-95.

Nayak S. (2002). Use of Satellite Data in Coastal Mapping. Indian Cartographer, 22, 147-157.

Nugraha I. (2016). Coastline Extraction using Landsat Satellite Imagery on the Southeast Coast of Bali (Case Study of Gianyar and Klungkung Regencies). Proceedings of the National Marine Seminar.

Raj N., Gurugnanam B., Sudhakar V., & Francis P. (2019). Estuarine Shoreline Change Analysis Along with the Ennore River Mouth, South East Coast of India, using Digital Shoreline Analysis System. Geodesy and Geodynamics, 10(3), 205-212.

Rajasree B., Deo M., & Nair L. (2016). Effect of Climate Change on Shoreline Shifts at A Straight and Continuous Coast. Estuarine, Coastal, and Shelf Science, 183, 221-234.

Solihuddin Tb. (2011). Karakteristik Pantai Dan Proses Abrasi Di Pesisir Padang Pariaman, Sumatera Barat. Globë, 13(2), Desember 2011, 112 - 12

Winarso G., & Budhiman S. (2001). The Potential Application of Remote Sensing Data for Coastal Study. . In Proc. 22nd. Asian Conference on Remote Sensing, Singapore, 1-5.

Zhang Y. (2011). Coastal Environmental Monitoring using Remotely Sensed Data and GIS Techniques in The Modern Yellow River Delta, China. Environmental Monitoring and Assessment, 179(1), 15-29.

Zhao B., Guo H., Yan Y., Wang Q., & Li B. (2008). A Simple Waterline Approach for Tidelands using Multi-Temporal Satellite Images; A Case Study in the Yangtze Delta. Estuarine, Coastal and Shelf Science, 77(1), 134-142.

Zimmermann G., & Bijker W. (2004). Monitoring the Amazon with Different Spatial and Temporal Resolution. In The XX ISPRS Congress Proceeding.

ges.rgo.ru/jour/

ISSN 2542-1565 (Online)